Spatial Variability of Particles in Waste Rock Piles

by

David Barsi

A thesis submitted in partial fulfillment of the requirements for the degree of

Master of Science
in
Geoenvironmental Engineering

Department of Civil and Environmental Engineering
University of Alberta

Abstract

Mine waste rock material has the potential to generate acid rock drainage (ARD) through the oxidation of sulphide minerals. Waste rock is one of the most abundant materials at mine sites that must be managed appropriately to limit the generation of ARD and other harmful by-products; therefore, they need to be well characterized. In order to study the spatial variability in material properties of waste rock, a small scale experimental waste rock pile was deconstructed in 2014. The pile was part of the Test Piles Research Program located at the Diavik Diamond Mine in NWT, Canada. During the deconstruction process bulk samples were collected following a three dimensional grid. These samples were used to measure the particle size distribution (PSD) of the material at discrete locations within the pile.

Measurement of the PSD showed that the material was segregated during placement, generally becoming coarser with depth. Further analysis of the PSD showed that the material varied in three dimensional space, creating coarser and finer zones. Therefore spatial distribution of PSD was not just related to elevation. The PSD data represented particles between 0.075 mm and 75 mm, with larger particles not physically measured.

Hydraulic properties were also estimated, using a variety of techniques, to predict saturated and unsaturated behaviour in different material types. The measured and estimated data was used to show how the material properties differed throughout the pile. The waste rock material was also classified into six different groupings based on the amount of material finer than 4.75 mm. This classification system divides materials based on their ability to retain water under suction. Approximately 12% of the sampled materials represented rock like material with no capillarity, and 36% represented soil like material with strong capillarity. Over half of the sampled materials showed characteristics that represented the transition between soil like and rock like materials, displaying weak capillarity.

Estimation of the hydraulic properties produced reasonable results in most cases. Estimated soil water characteristic curves displayed a reasonable trend in the air entry value as the material changed from fine to coarse. However, this method generated residual saturation values that were larger than expected. Hydraulic conductivity and unsaturated permeability values were also predicted satisfactorily. Saturated hydraulic conductivity values were in a similar range to earlier studies at this site.

The classifications allowed for the definition of data ranges for the different material groups. These data sets may be used to improve the understanding of the hydraulic and geochemical behaviour of the material, in previous and ongoing studies at this site. The overall sample and classification methodology may be useful in studying waste rock at other sites as well. Finally, study of the representative elemental volume identified that field sample spacing would need to be much denser in order to recreate a representative model of the pile. Such a sampling program is impractical, and reinforces the need for new data collection techniques that may include remote imaging or geostatistical methods.

Acknowledgements

There are many people who helped in the creation of this thesis. I would first like to thank Dr. Ward Wilson, who gave me such a great opportunity to come and study at the University of Alberta. From there I was able to pursue my research under the supervision of Dr. Dave Sego, and Dr. Nick Beier. Dave has a knack for making the most complicated problems seem simple, and Nick has great enthusiasm for problem solving. Their support and guidance was invaluable.

The administration staff in the department is top notch, and made my time at the U of A so much easier. I would especially like to thank Christine, Sally, Vivian, and Annette, who were of great help at so many points along this journey.

I would like to thank the other professors involved with the Test Piles research for their efforts to provide numerous grad students with a world class research project to be part of. Thank you to Dr. Dave Blowes, Dr. Leslie Smith, and Dr. Rich Amos. The research is made possible through funding provided by the Natural Science and Engineering Research Council of Canada, the International Network for Acid Prevention, the Mine Environment Neutral Drainage program, the Canadian Foundation for Innovation and Rio Tinto (Diavik Diamond Mines Inc). I would also say thanks to all the test-pilers, past and present, who have put in so much time and effort helping out with research efforts beyond their own. The Deconstruction wouldn't have been the same without Steve, Colleen, Jordan, Andrew, David W., Sean, Jeff B, and Jeff L, and the numerous students; those were some long crazy nights we shared digging rocks under a smoky midnight sky. The Diavik Environment Department was also a huge help, so I would thank David Wells, Darcy, Diane, Justin, Kyla, and Tianna.

My time at the U of A has also introduced me to many great friends, who are too many to name here. But I will thank Neeltje, Bereket, Ralph, Paul, and Janeen for their help with lab work (moving rocks around), and support in completing this. Thanks as well to Dan Rothrock, and Nick De Jong for all their help processing the samples in the lab.

I would also like to thank my mentor Dr. Rashid Bashir, who has been a constant source of support since before I returned to university. He has provided advice, and guidance to help me complete this thesis, and find balance in life.

Finally I will thank my family. My parents and brother have always been there for me, with never ending support. I can't thank them enough for helping me to achieve all that I have. And to Kelly, I think the best part of this whole journey was that it brought me to you. You have been such a positive influence in my life, and I thank you for helping me get this done.

Table of Contents

List of Tables

List of Figures

1 Introduction

The mining industry is a major contributor to Canada's economy. In 2014, the industry contributed $57 billion to Canada's gross domestic product, while employing over 375,000 workers. The industry also accounted for 18.2% of Canadian exports in 2014, and remains a top destination for exploration investment by international organizations (Marshall 2015). Mining activities can also pose significant risks to the environment, causing financial liability as well.

One of the most prominent environmental risks associated with mining is acid rock drainage (ARD) and the associated processes that may leach metals, or degrade the underlying permafrost. ARD is a by-product of a natural process that occurs when sulphide minerals, exposed in the mined ore, oxidize by reacting with oxygen and water. The resulting drainage may be neutral to acidic and have the potential to dissolve metals from the waste rock and transport them into the surrounding environment. The mining process enhances the ARD process, by increasing the surface area that is exposed to react, as ore and waste rock are blasted or crushed. In North America alone, the estimated cost of remediating ARD at abandoned mine sites is tens of billions of dollars (The International Network for Acid Prevention (INAP) 2009). While responsible mining companies will clean up their sites, many are abandoned by their operators at the end of mining. These costs will ultimately fall to the taxpayers, as governments will be responsible for remediating these sites. This liability can be reduced through better mining practices, making it easier and more affordable to remediate these sites during operations. This requires a better understanding of the material properties, and the relationships between geochemical, microbial, and physical processes that occur in the fragmented waste rock (Amos et al. 2015).

A study by Amos et al. (2015) examined the results of several field scale waste rock characterization projects. It was concluded that the fundamental mechanisms that drive ARD appear to be well understood. However, the principal mechanisms and their relationships between each other can differ significantly between sites, based on the variability in material properties, as well as climatic conditions. The study highlighted the importance of site specific characterization of material properties, as these properties will drive the ARD reaction mechanisms.

1.1 Research Program and Objectives

The goal of this research is to quantify the spatial variability in material properties of waste rock in a dump, constructed using traditional methods. These material properties will drive the various mechanisms that can create ARD, leach and transport metals, or degrade permafrost. By understanding

the variability in these properties, it will be possible to gain further insight into the physical and geochemical processes that occurred in the waste rock. By quantifying the spatial variability in traditionally constructed waste rock piles, it will be possible to determine the importance of collecting such information, and to develop a methodology for collecting this information effectively. Spatial variability data can increase the resolution of known data within a waste rock pile, allowing for the creation of more complex models that can better represent the factors affecting ARD generation.

A research program was conducted at Diavik Diamond Mines Inc. (DDMI) Diavik mine site in the Canadian Arctic. The research was part of the Diavik Test Piles Research program, a multi university collaborative research initiative, funded by the International Network for Acid Prevention (INAP), Mine Environment Neutral Drainage (MEND), and Canadian National Science and Environment Research Council (NSERC). The test piles research program includes three small scale waste rock piles that were constructed to characterize fluid, gas and thermal transport processes, and the geochemical and microbiological processes in a continuous permafrost environment; and utilize this information to guide the cover design for the full-scale waste rock dump (Smith 2006). The research presented in this thesis includes the deconstruction of one of the test piles in order to collect in situ waste rock samples. Samples were collected on a three dimensional grid, as the pile was deconstructed. Samples were later tested in a laboratory to determine physical properties of the waste rock. This data was used to estimate additional material properties, as well as to examine the spatial variability within the pile.

The specific research objectives were:

1. To design and execute a waste rock pile deconstruction sampling program that will collect a large number of samples using a 3 dimensional grid.
2. To conduct laboratory analysis to determine the particle size distribution (PSD) of the samples.
3. To use the PSD data to estimate saturated and unsaturated hydraulic conductivity parameters. This data will be useful for understanding fluid and gas transport and storage in the pile.
4. To examine the spatial variability of the material properties within the waste rock pile.

1.2 Thesis Organization

This thesis includes six main chapters. Chapter 1 provides an introduction to the research topic, and the methods used in the research program. The case study that was a part of this research program is also introduced. Chapter 2 presents a literature review. Relevant studies were included for the topics of mine waste production and storage, waste rock characterization, as well as a summary of similar studies in the past. Chapter 3 details the case study presented in this research. It includes a description of the site, the research program, and the methodology for data collection. Chapter 4 presents the results of data collected during the research program. Chapter 5 is a discussion of the results presented in Chapter 4. It includes discussion of the various PSD studies from the research site, material segregation, spatial variability, material classification, representative elemental volume, and the collection of PSD data. Chapter 6 summarizes the conclusions of this research, as well as providing recommendations for further research.

2 Literature Review

2.1 Introduction

Mining activities can produce massive amounts of waste material. Waste rock is simply the material that has to be removed in order to access the ore body. Following excavation, this waste material is generally stored in massive dumps, exposed to the environment. All waste materials have the potential to interact with the environment in a harmful way, by adding contaminants to the water cycle. In order to design effective preventative and associated monitoring strategies, the fluid flow processes must be well understood. This requires knowledge of the particle size distribution, and the spatial arrangement of particles that will create matrix supported and matrix free zones (Smith and Beckie 2003). Particle size distributions impact both mineral reaction rates and reaction duration by affecting the reactive surface area, the distances between potentially reactive particles, and the porosity and permeability of a solid. Porosity and permeability of a solid are particularly important with regard to movement and transport of air, water, and reaction products from weathering reactions (INAP, 2009). As the particle size distribution is so important to understanding material behaviour, standards have been developed to allow for accurate data collection. These standards cover sample collection and lab processing techniques. They also attempt to address some of the challenges that may be faced when trying to standardize methods for such heterogeneous materials.

2.2 Waste Rock Production and Storage

2.2.1 Mine Waste Production

Mining operations utilize surface mining, underground mining, or a combination of these two methods. In general surface mining and underground mining both include blasting, excavation, hauling, storing of waste, and milling of ore (The International Network for Acid Prevention (INAP) 2009). While underground mines typically create less waste than surface mines, each method has the potential to create massive stockpiles that can contain up to billions of tonnes of rock, covering areas of 1000 hectares or more (Wilson 2011). Blasting intact rock breaks it apart into manageable sizes, allowing mine equipment to remove it for storage or processing (Price 2009). The blasted material can have particle sizes ranging from clay/silt size to boulders that are many meters in size, as observed in this research study. This new range of particle sizes drastically increases the surface area that is available for reactions compared to the intact rock. Additional steps in the process can also break the material down

into smaller pieces through abrasion including loading material into haul trucks, transportation, and dumping.

2.2.2 Waste Rock Dump Construction

At most mines, the desired commodity is a small volume fraction of what is mined. Most of the material is waste that must be stored on site. Most mine sites are essentially waste storage facilities (Price 2009), and their geotechnical and environmental performance must extend for centuries (Wilson 2011). Waste rock is generally transported by haul trucks to the disposal site. Typical waste rock dumps are built up into piles as waste material is repeatedly dumped down the slopes that form at the angle of repose (Neuner 2009). This process may include direct dumping by the haul truck (end-dumping), or with the haul truck dumping its load and having a dozer push the material over the edge (push-dump), or a combination of the two (Darling 2011).

These construction methods lead to down slope material segregation by gravity, with larger particles moving further down the slope creating a coarse rubble zone at the base of the pile. Variability in the PSD of material being dumped can create coarser and finer inter fingered dipping beds of material (Herasymuik 1996). Activity by heavy equipment can create horizontal traffic surfaces, where material is packed tightly together (The International Network for Acid Prevention (INAP) 2009). In general, the waste rock consists of matrix material (particles < 1 cm) that is located in the voids between larger clasts (cobbles and boulders) (Neuner 2009). The waste rock can be clast supported with large grains in direct contact, or matrix supported with large grains suspended in the finer matrix. Figure 1 illustrates the typical structure that is formed using these construction techniques.

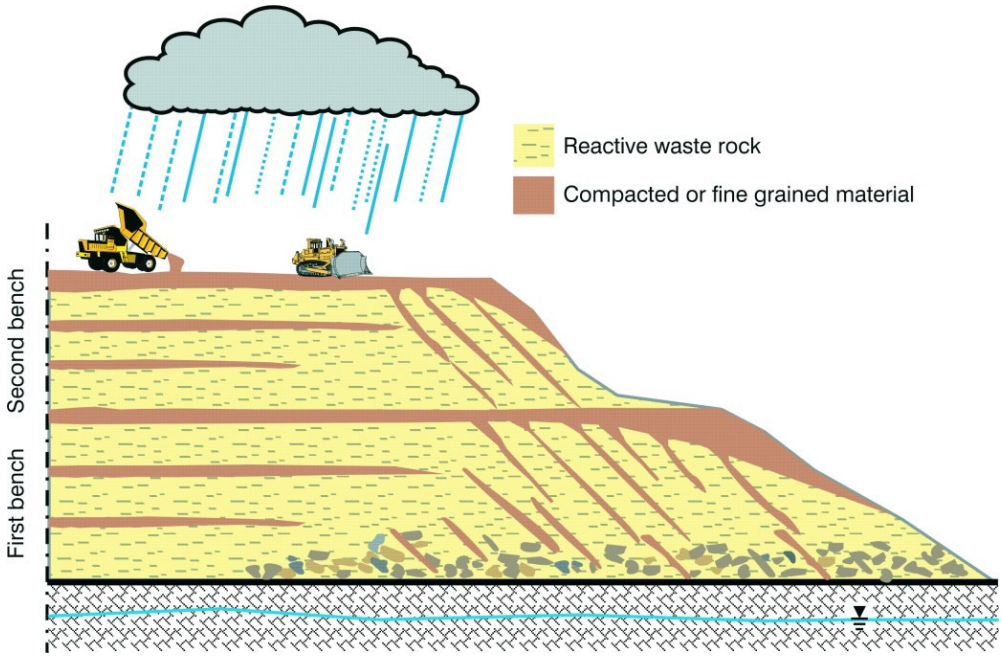

Figure 1 - Conceptual Model for Waste Rock (Bussiere 2007)

2.2.3 Environmental Issues

This type of waste rock dump construction has been used for over a century, at mine sites all over the world. It is completely appropriate when designing for geotechnical stability, however, where the materials are reactive, this type of dump may promote future oxidation and the generation of ARD (The International Network for Acid Prevention (INAP) 2009). The GARD Guide explains how ARD is generated by the oxidation of sulphide minerals, as follows. The most common mineral of concern is pyrite (FeS_2), though many other sulphide minerals may cause problems as well. The initial reaction between pyrite, oxygen, and water is represented as:

$$FeS_2 + {}^{7}/_{2}O_2 + H_2O = Fe^{2+} + 2SO_4^{2-} + 2H^+ \quad [1]$$

Ferric iron rapidly accelerates the oxidation of pyrite by producing large amounts of protons, and hence, very acidic water. This can be seen in the following reaction:

$$FeS_2 + 14Fe^{3+} + 8H_2O = 15Fe^{2+} + 2SO_4^{2-} + 16H^+ \quad [2]$$

With a continued supply of oxygen the generation of ferric iron can proceed via the reaction:

$$Fe^{2+} + {}^{1}/_{2}O_2 + H^+ = Fe^{3+} + {}^{1}/_{2}H_2O \quad [3]$$

These reactions summarize how pyrite oxidation can generate ARD. The initial reaction generates ferrous iron, and some acidity. With a sustained oxygen supply this ferrous iron can react into ferric iron. The ferric iron will then contribute to reaction [2], and accelerate the production of protons. This process is represented in figure 2.

Oxygen and water are key components in the ARD reaction, and the supply of both is readily available due to the structures created when constructing waste rock dumps using traditional methods. The coarse rubble zone at the base allows oxygen to enter the dump and move upward due to buoyancy and thermal advection. The unsaturated nature of the material allows upward movement of oxygen, while allowing water flow and storage in the finer matrix material (Wilson 2011). Preferential water flow through voids and coarser material may happen during conditions of high infiltration, but will ultimately drain into the finer material in unsaturated conditions (Herasymuik 1996). The finer material has the greatest surface area, allowing for more sulphide minerals to react. Once the process begins, oxidation and the production of ARD may continue for centuries, as low pH water and oxygen continue to drive the reactions.

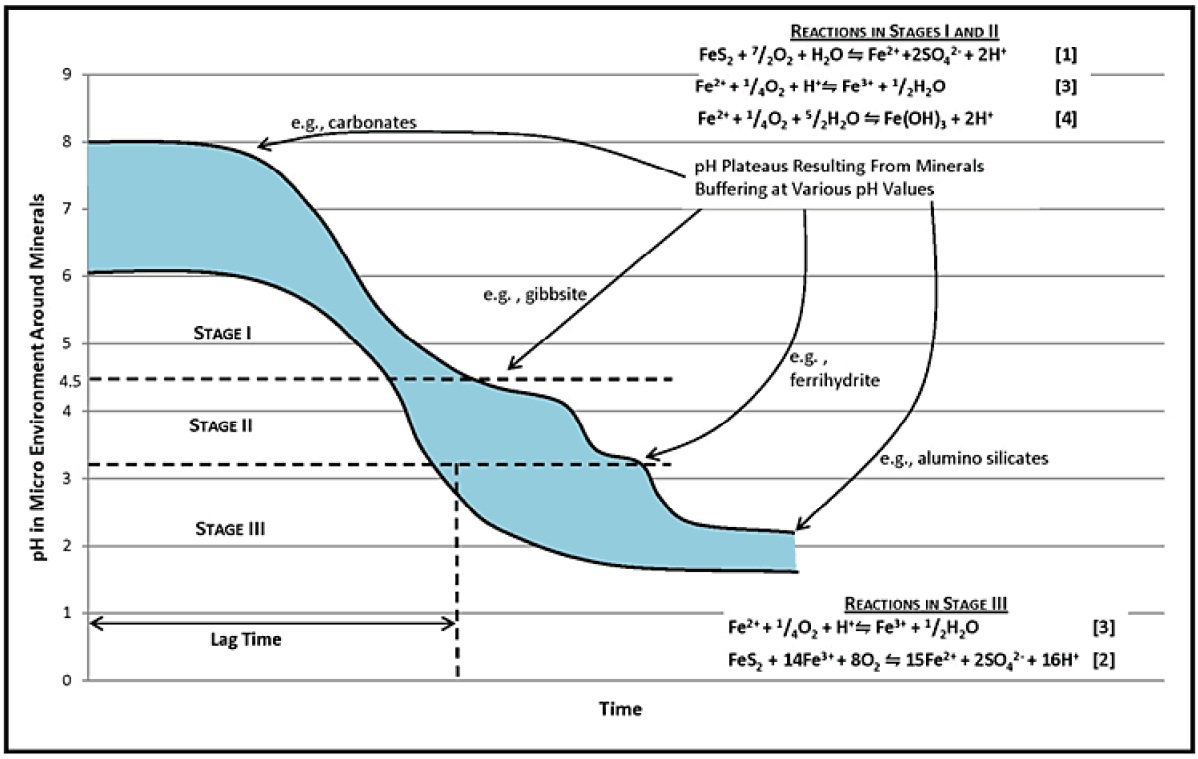

Figure 2 - Stages in the Formation of ARD (INAP (2009))

2.3 Waste Rock Characterization

To improve construction techniques, management methodology, and closure plans for waste rock dumps, it is important to gain a better understanding of the material characteristics that drive ARD reactions. These reactions are driven by the flow of oxygen and meteoric water and it is of paramount importance that we can characterize and control them (Wilson 2011). This is not an easy prospect, as these materials are highly heterogeneous with volumes of millions or billions of tonnes at most mine sites. Direct measurement of hydraulic conductivity and unsaturated material properties may be difficult to achieve due to the size of the piles. Analytical methods exist that use estimation techniques to determine values for unsaturated properties and hydraulic conductivity. These methods generally rely on PSD data that may be easier (though still difficult) to collect.

2.3.1 Particle Size Distribution

Hydraulic properties of waste rock piles are controlled by the particle size distribution, along with the structure that is created during placement (Andrina 2009). PSD testing is a well-known test in geotechnical engineering, and can provide data for classification and material property estimation. The test requires collection of field samples, and sieving of the material into a range of particle sizes. While the methodology is well known, it is a challenge to collect samples that represent the full size distribution of waste rock material. Logistically it can be difficult to collect in situ samples, and it can be extremely difficult to collect samples of the largest particle sizes.

2.3.1.1 Sample Collection

The particle size distribution of soils and aggregates is an important set of data for characterizing material, and predicting material properties. As such, it is important that this data be collected in a standardized way. The American Society for Testing and Materials (ASTM) International maintains thousands of standards for materials testing. Several ASTM standards exist that describe standard methodologies for collecting and testing samples to determine the PSD. ASTM C136 and ASTM D 6913 are two standards that are commonly used in civil and geotechnical engineering practice. These standards outline the testing method, the required apparatus', sampling techniques, calculations, and reporting requirements. As described by ASTM the "test method outlines the majority of conditions and procedures but does not cover every conceivable variation or contingency." (ASTM International 2009) The variability that exists in earth materials makes it very difficult to provide strict guidelines for every soil type in every scenario. The guidelines instead try to establish best practices that can be used to design testing procedures that are appropriate and representative for a given site or soil type.

Samples may be collected in a variety of sizes, and for a variety of purposes. For the determination of PSD, generally sample sizes are dependent on the nominal maximum particle size that is being collected.

Table 2.1 illustrates a design table that can be used to determine the required sample size. The standards usually assume that proper sampling practices are being used to ensure that representative samples are being collected, and preserved prior to testing. They often reference other ASTM standards that deal more specifically with individual steps and procedures. Depending on the sample size, considerations should be made for the appropriate tools required to collect samples, and the appropriate storage containers (jars, pail, sample bags, etc.).

Table 2.1 – Table for Determining Sample Size (after ASTM D6913)

Particle size (mm)	Mass of Specimen
0.425	50 g
2.00	50 g
4.75	75 g
9.5	165 g
19.0	1.3 kg
25.4	3 kg
38.1	10 kg
50.8	25 kg
76.2	70 kg

2.3.1.2 Laboratory Processing

Laboratory processing of PSD samples requires the use of sieves with varying sizes of mesh openings, and often a mechanical machine to provide a shaking motion. Several procedures exist that address a variety of sample conditions. The simplest case is a sample of moderate size that can be tested with a single sieve stack. Larger samples may require composite sieving, as the range of particle sizes is too great for a single set of sieves to handle. The moisture content is also an important consideration. Certain cases require that the samples be air-dried or oven-dried prior to sieving, while others must remain moist. The standards cannot explain every situation, and the specific method should reflect the goals of the project.

2.3.1.3 Challenges

Challenges can arise in choosing the proper procedure to match the study goals. Due to the inter-referencing of ASTM standards, there are situations where contradictory information exists. These contradictions usually arise where standards are written for well-known materials such as aggregate, sands, and clays. However, in the mining industry many of the materials are not well studied, and specific procedures do not exist.

Characterization of mine waste is also problematic in that it generally has a large range of particle sizes. Waste rock is produced as a by-product of the mining process. Open pit, and underground mines both utilize blasting techniques to break the rock apart for transport and milling. This creates angular particles that range from clay size particles, up to boulders that are many meters in size. Using traditional sieving methods can be impractical, if not impossible, to measure the entire range of particle sizes at many mine sites. As such, only a portion of the particle size distribution curve can be measured, while the larger fraction may need to be estimated.

2.3.1.4 Soil Classification

Many systems exist for classifying soils, and they include industrial standards and company specific standards. Each system has its own advantages and disadvantages. Perhaps the most well-known system in North America is the Unified Soil Classification System (USCS) described in ASTM D2487. It is a system for classifying mineral and organo-mineral soils for engineering purposes based on laboratory determination of particle-size characteristics, liquid limit, and plasticity index and shall be used when precise classification is required (ASTM International 1966). Using USCS to classify a soil will result in a classification that is presented by a group symbol and group name. These data can be used for

stratigraphic mapping of project sites that aid design efforts. The data can also be used to confirm material properties, which is useful in locating appropriate material sources, and QA/QC programs. Soils are classified in three main categories (coarse, fine, and organic soils) based on size and behaviour. There are also numerous sub-categories. Boulders and cobbles are the largest particles, followed by gravel, then sand. Silt is non-plastic or only very slightly plastic, and has little to no strength when it is dry. Clay is plastic over a range of moisture contents, and has considerable strength when dry. With enough organic material, both silts and clays can be considered organic soils, along with peat, which is almost entirely organic (ASTM International 1966). Table 2.2 lists the various particle sizes and names.

Table 2.2 - List of Particle Sizes

Classification	Minimum Size (mm)	Maximum Size (mm)
Boulder	300	--
Cobble	75	300
Coarse Gravel	19	75
Fine Gravel	4.75	19
Coarse Sand	2.0	4.75
Medium Sand	0.425	2.0
Fine Sand	0.075	0.425
Silt/Clay	--	0.075

There are several index properties that are commonly used to further aid in soil classification. Size fractions are often described by a d_x value. For example d_{10} describes the size for which 10 percent of the material is finer. A d_{10} of 1 mm would mean that 10 percent of the material is finer than 1 mm. These d_x values can describe any percentage. For geotechnical classification, d_{10}, d_{30}, and d_{60} are commonly used, as they describe the Coefficient of Uniformity (C_u), and Coefficient of Curvature (C_c). Together these coefficients can be used to classify the grading of the soil that can help describe other material properties such as strength, compressibility, and conductivity (Das 2008).

$$C_u = \frac{d_{60}}{d_{10}} \qquad \text{Equation 1}$$

$$C_c = \frac{(d_{30})^2}{(d_{10} * d_{60})} \qquad \text{Equation 2}$$

Waste rock can also be classified based on its overall PSD. Smith (2009) describes the classification of waste rock presented by Dawson and Morgenstern (1995). This classification uses the d_{20} to categorize

between soil-like and rock-like waste rock based on liquefaction potential. A soil-like pile will exhibit behaviour similar to a soil, and has a d_{20} greater than 2 mm. A rock-like pile will behave more like a rock mass and has a d_{20} less than 2 mm.

2.3.1.5 Curve Fitting PSD Data

Whether the PSD data is being used for classification, or for the estimation of material properties, it is often advantageous to fit a curve to the experimental data. Several techniques exist to do this, and provide researchers with an equation for the PSD curve. Once the curve is defined as an equation, values can be calculated precisely. This is important when determining index values such as % sand, silt, or clay, and d_{10}, d_{20}, d_{60}, etc. These calculations can also be made with computer software, which is advantageous when working with large data sets.

(Fredlund et al. 2000) described two methods of fitting an equation to experimental PSD data. The unimodal and bimodal equations use a series of fitting parameters that are solved using a quasi-newton least squares regression algorithm. Adjustment of these parameters creates a best fit equation for the experimental data. The unimodal equation describes data for well graded and/or uniform soils. The bimodal equation can be used to fit data that is gap graded. By differentiating these equations the user can produce a probability density function (PDF) of the particle size. This allows for the probability of any particle size to be calculated for the data. Equation 3 is the unimodal equation, while Equation 4 is the bimodal equation. The variables for the equations are presented in Table 2.3.

$$P_p(d) = \frac{1}{\left\{ln\left[exp(1)+\left(\frac{a_{gr}}{d}\right)^{n_{gr}}\right]\right\}^{m_{gr}}}\left\{1-\left[\frac{ln\left(1+\frac{d_{rgr}}{d}\right)}{ln\left(1+\frac{d_{rgr}}{d_m}\right)}\right]^7\right\} \quad \text{Equation 3}$$

$$P_p(d) = \left\{w\left[\frac{1}{\left\{ln\left[exp(1)+\left(\frac{a_{bi}}{d}\right)^{n_{bi}}\right]\right\}^{m_{bi}}}\right]+(1-w)\left[\frac{1}{\left\{ln\left[exp(1)+\left(\frac{j_{bi}}{d}\right)^{k_{bi}}\right]\right\}^{l_{bi}}}\right]\right\}\left\{1-\left[\frac{ln\left(1+\frac{d_{rbi}}{d}\right)}{ln\left(1+\frac{d_{rbi}}{d}\right)}\right]^7\right\} \quad \text{Equation 4}$$

(Chapuis et al. 2014) continued to build on the methods for fitting an equation to grain size data, developing the multimodal approach. The basis behind this method is the ability to determine the proportions of up to three materials that make up a mixed soil. In doing so, the stratigraphy can be partially understood using data collected from grab samples. The multimodal equation can be fit to data with up to three modes. It can be useful in situations where unimodal and bimodal equations have a poor fit to the data.

Table 2.3 - Variables for Unimodal and Bimodal Fitting Equations

$P_p(d)$	Percentage, by mass, of particles passing a particular size
a_{gr}	A parameter designating the inflection point on the curve; related to the initial break point on the curve
n_{gr}	A parameter related to the steepest slope on the curve; represents uniformity of PSD
m_{gr}	Related to the shape of the curve as it approaches the fines region
d_{rgr}	Related to the amount of fines in a soil
d	Diameter of any particle size under consideration
d_m	Diameter of the minimum allowable size particle
a_{bi}	Parameter related to the initial breakpoint of the curve
n_{bi}	Parameter related to the steepest slope along the curve
m_{bi}	Parameter related to the shape of the curve
j_{bi}	Parameter related to the second break point of the curve
k_{bi}	Parameter related to the second steep slope
l_{bi}	Parameter related to the second shape along the curve
d_{rbi}	Parameter related to the amount of fines in a soil

2.3.2 Saturated Hydraulic Conductivity

To predict ARD generation from waste rock, it is important to understand how water will move within the material. The saturated hydraulic conductivity (k_{sat}) (or coefficient of permeability as it is sometimes called when referring to unsaturated conditions) defines the rate at which water will move through the porous material. The hydraulic conductivity of soils depends on the fluid viscosity, pore size distribution, particle size distribution, void ratio, particle roughness, and degree of saturation (Das 2008). In order to determine the saturated hydraulic conductivity, it is required to gain some understanding of the porosity (n), void ratio (e), and particle size distribution. Craig (2004) defines porosity and void ratio as follows:

- Porosity – the ratio of the volume of voids to the total volume of the soil

$$n = \frac{V_v}{V} \qquad \text{Equation 5}$$

- Void Ratio – the ratio of the volume of voids to the volume of solids

$$e = \frac{V_V}{V_S} \qquad \text{Equation 6}$$

- These two properties are inter-related

$$n = \frac{e}{1+e} \qquad \text{Equation 7}$$

$$e = \frac{n}{1-n} \qquad \text{Equation 8}$$

Waste rock is a complex heterogeneous material. The spatial variability of mineralogy, particle size, and porosity creates fluctuations in hydrogeological and geochemical properties. This can make it difficult to measure, interpret, or predict water flow and storage within a waste rock pile (Fala et al. 2013). The material matrix and the voids create pathways for fluid flow. In dry climates, low flow rates will cause fluids to move primarily in the matrix material. In wet climates, high rate fluid flow will occur in preferential pathways created by voids (Neuner 2009). Using traditional testing methods to collect porosity and void ratio data for waste rock may not be practical. Recreating in situ conditions of such a heterogeneous material in a laboratory setting is difficult, as the void space is related to the degree of compaction, and the method of material placement. Researchers have developed empirical methods for estimating the hydraulic conductivity based on more easily measurable material properties like PSD. In a review of estimation methods for hydraulic conductivity the Hazen (1911) equation was among seven methods with good potential for non-plastic soils (Chapuis 2012). The Hazen (1911) equation also

required the least amount of information, making it a quick and basic method for estimating the saturated hydraulic conductivity. The Hazen (1911) equation works best when it satisfies four conditions:

- Non-plastic soil;
- "loose" soil, where e is close to e_{max};
- $C_u \leq 5$; and,
- $0.1\ mm \leq d_{10} \leq 3.0\ mm$.

The Hazen (1911) equation is often presented as:

$$\boldsymbol{k_{sat} = C(d_{10})^2} \qquad \textbf{Equation 9}$$

The coefficient can be expanded to show the original form of the equation from 1892 that allows for the inclusion of the water temperature in Celsius. Typical forms of the equation exist for the field (5.5°C), and the lab (20°C).

$$\boldsymbol{k_{sat} = 1.157\left(\frac{d_{10}}{1mm}\right)^2\left[0.07 + 0.03\left(\frac{T}{1°C}\right)\right]} \qquad \textbf{Equation 10}$$

Numerous other methods exist, with different levels of complexity. A well-known and commonly used method is the Kozeny-Carman equation. It yields the hydraulic conductivity as a function of porosity, the specific surface (S), and a shape factor (C) that accounts for tortuosity. Additional parameters include the gravitational constant (g), dynamic viscosity of water μ_w, specific weight (D_R), and material densities (Chapuis and Aubertin 2003).

$$\boldsymbol{k_{sat} = C \times \frac{g}{\mu_w \rho_w} \times \frac{e^3}{S^2 {D_R}^2 (1+e)}} \qquad \textbf{Equation 11}$$

This method can be difficult to use due to the number of parameters required. In order to determine the specific surface a complete PSD is required (sieving and sedimentation). Normally, when testing PSD of a non-plastic soil, the sedimentation process is not completed (Chapuis 2012). Chapuis (2004) continued to develop a better predictive equation based on the Kozeny-Carman, and Hazen (1892) equations. The equation he presented produced better predictions than previous methods, and required less terms. The equation is:

$$k(cm/s) = 2.4622[d_{10}^2 e^3/(1+e)]^{0.7825} \qquad \textbf{Equation 12}$$

None of the predictive methods explored were ideal for mine waste materials. The K_{sat} of mine waste soils are difficult to predict as they have angular particles, and unnatural void-space geometry, increasing the tortuosity (Chapuis and Aubertin 2003). Results presented in Chapuis (2004) showed that measured samples of crushed stone and sand did not match the prediction. However, the results appeared to be within one order of magnitude, with the prediction generally being the larger value. No additional methods were found that work well with mine waste material, and use sufficiently few parameters to make K_{sat} estimations using the deconstruction PSD data set.

2.3.3 Unsaturated Soil Properties

Waste rock material is very heterogeneous. The large range in particle sizes creates a large range in the size of void spaces. The void distribution causes the waste rock to be free draining. This behaviour coupled with the location of the pile above the groundwater table results in waste rock that is unsaturated (Cash 2014).

Soils that are unsaturated contain both air and water in the voids, and form the largest category of soils that do not behave according to classical soil mechanics. Physical applications of unsaturated soil mechanics include water flow, air flow, heat flow, shear strength, and volume-mass changes (Fredlund et al. 2012). These mechanisms are all important in understanding the behaviour of waste rock, and are influenced by the material properties.

The flow rate of water through unsaturated porous media is controlled by the coefficient of permeability. This value is generally constant in a saturated media but can vary greatly with changes in the saturation. As soil desaturates the coefficient of permeability will decrease, as there are fewer connected pathways for flow to occur. This relationship is hysteretic, as the coefficient of permeability will react differently when the soil is wetting vs. drying (Fredlund et al. 2012).

The Soil Water Characteristic Curve (SWCC) provides an understanding of the distribution of water in the void spaces. Soil texture, gradation, and void ratio also influence the SWCC. This relationship between properties has led to the development of methods that use PSD data to estimate the SWCC (Fredlund et al. 2012). A PSD curve can be broken up into many incremental particle size ranges. Each increment can be used to build a SWCC, and then all the incremental SWCC's can be combined to form an overall SWCC (Fredlund et al. 2000). The SWCC is predominantly controlled by the PSD, but is also influenced by the density, which reflects the initial porosity (Fredlund et al. 2012). There are also numerous equations to calculate a SWCC.

This research made use of the Fredlund and Xing (1994) equation, presented below. An example SWCC generated using Equation 13 is shown in figure 3. These techniques allow the coefficient of permeability to be estimated from PSD data, by using an estimated SWCC. Numerous methods exist to define this relationship, and are not described here but can be found in Fredlund et al (2012). This research made use of the Fredlund, Xing, and Huang (1994) estimation, with Figure 4 showing a typical relationship between SWCC and permeability functions.

$$w_w = w_s\left[1 - \frac{ln\left(1+\frac{\psi}{h_r}\right)}{ln\left(1+\frac{10^6}{h_r}\right)}\right]\left[\frac{1}{\left[ln\left[exp(1)+\left(\frac{\Psi}{a_f}\right)^{n_f}\right]\right]^{m_f}}\right] \qquad \text{Equation 13}$$

Table 2.4 - Variables in Fredlund and Xing (1994) Equation

w_w	Gravimetric water content at any soil suction
w_s	Saturated gravimetric water content
a_f	Parameter related to the air entry value (kPa)
n_f	Parameter related to the rate of water extraction from the soil after the air entry value
m_f	Parameter related to the residual water content
h_r	Suction at which residual water content occurs (kPa)
ψ	Soil Suction (kPa)

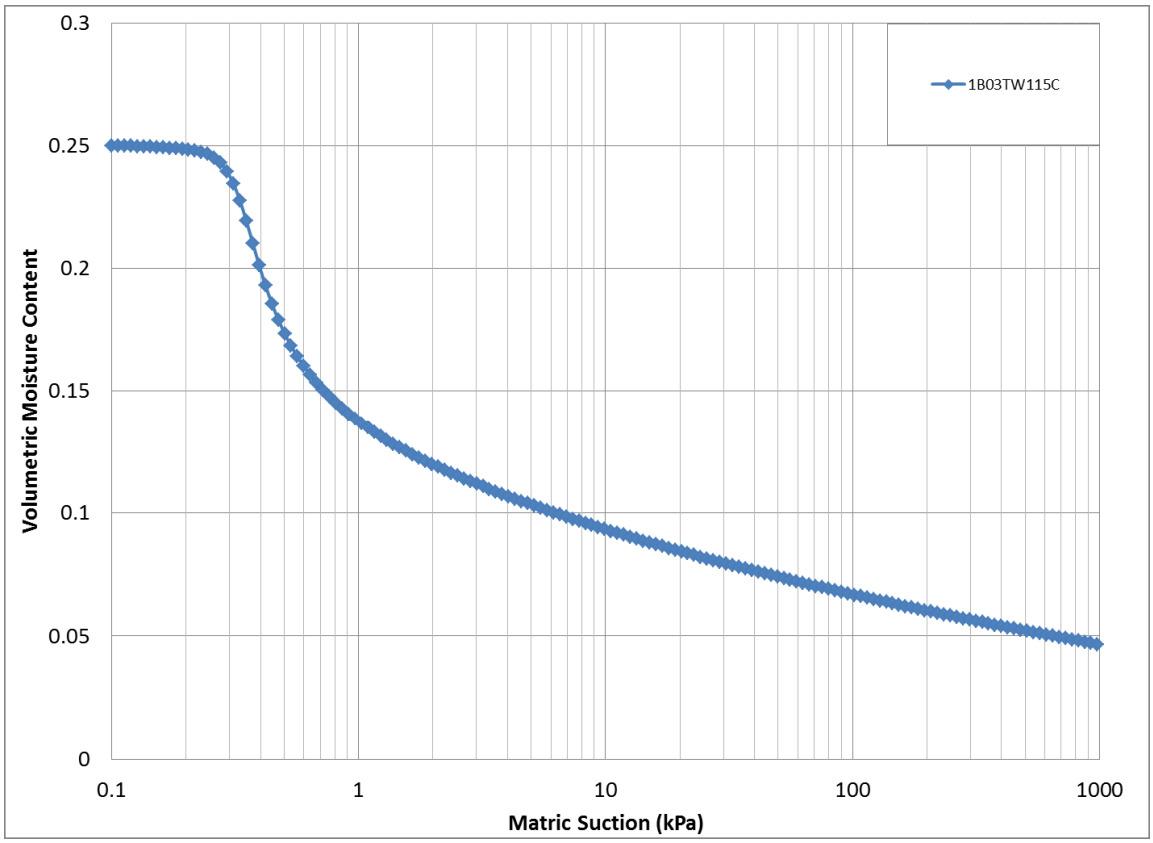

Figure 3 - SWCC estimated using Fredlund and Xing (1994) method

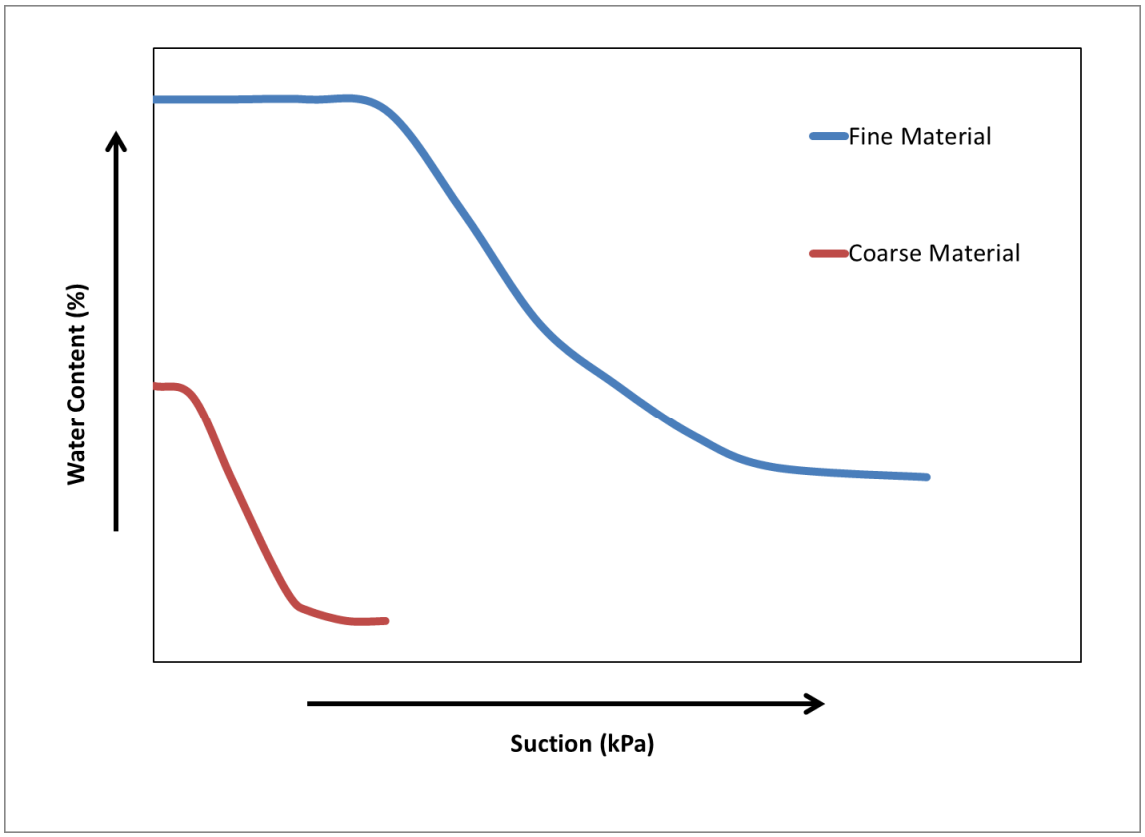
Fine Material
Coarse Material
Water Content (%)
Suction (kPa)

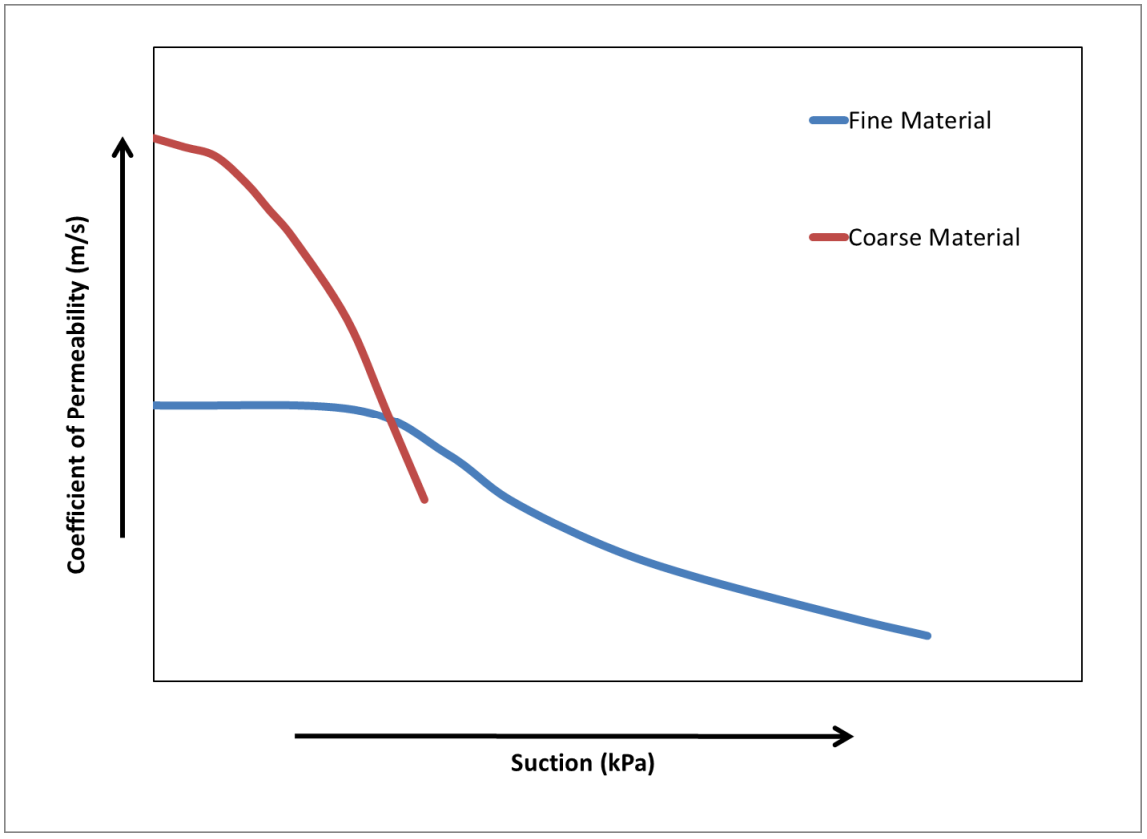
Fine Material
Coarse Material
Coefficient of Permeability (m/s)
Suction (kPa)

Figure 4 - Typical Relationship between SWCC and Estimated Permeability Function (after Fredlund et al. 2012)

2.4 Previous Studies

Numerous studies have taken place in the past to study how waste rock and waste rock dumps are characterized, and to gain a better understanding of the structure and hydraulic behaviour of the material. A number of these studies have included a review of several sites to determine the state of practice, as well as, site-specific studies to improve the knowledge base. The studies presented in this section were chosen as they provide summaries of characterization practices at many sites, over time, and they present some of the theories that continue to develop as research continues in this field.

Herasymuik (1996), Hydrogeology of a Sulphide Waste Rock Dump

Herasymuik (1996) was the first to update the model for traditional waste rock dumps to reflect the common structures that exist. Based on his study of waste rock at the Golden Sunlight Mine, he presented a model that included discontinuous, dipping coarse and fine layers of material, with a coarse rubble zone at the base. This conceptual model introduced new complexity into the understanding of waste rock piles, and the material characteristics. His research also demonstrated how the fine layers of material preferentially store and transport water in unsaturated conditions. The coarse rubble zone provides an important pathway for airflow into the pile, providing fresh oxygen for ARD reactions. Material properties are also subject to change over time as they weather. These complexities will affect the movement of water within waste rock. The new model demonstrates the importance of understanding additional processes such as the generation of heat, gas flow, and the movement of water as a vapour.

The research included studies of numerous mines and their waste rock characterization techniques. Herasymuik remarked that “current models are weak due to lack of understanding of the interaction between the hydrogeologic and geochemical processes active in waste rock piles. There is a lack of understanding how water moves in unsaturated waste rock piles”. The research suggests that it is essential to characterize heterogeneous waste rock in order to understand water flow and solute transport. This will also allow for further development and validation of numerical models that may be useful in predicting ARD generation. Several factors required for the generation of ARD are tied to PSD, making it an important property to characterize. At the time of the research only 2 of 17 mines surveyed were collecting PSD data.

Wilson (2011), Waste Dump Hydrology: An Overview of Full-Scale Excavations and Scale-Up Experiments Conducted During the Last Two Decades

A number of studies of waste rock characterization were conducted at mine sites all over the world, in the 20 years following the research of Herasymuik (1996). These mine sites included a large variety of geological settings, and climatic conditions, and are summarized by Wilson (2011). Many studies included observation and numerical modelling, and qualitatively confirmed the conceptual model put forward by Herasymuik (1996). Two North American sites were studied by researchers for INAP, and provided data about the hydrology at each site. Site 1 had soil-like waste rock, with low permeabilities, while site 2 had rock-like waste rock, with higher permeabilities. Soil-like and rock-like materials were distinguished by their ability to retain water under suction. This study demonstrated how different the hydrology could be between different sites, yet both sites still produced ARD, with some layers providing storage of oxidation products, and others providing transport. The study also demonstrated how effective waste rock can be at storing oxidation products, such as metal ions, sulfate, and protons. Methods current to the time assumed that all oxidation products would be fully leached, leading to an over prediction of field performance. This is detrimental to cover design, as even a successful cover may stop further oxidation, yet the stored oxidation products may continue to react for long periods.

Wilson (2011) continues the discussion by reviewing scale-up experiments at several mine sites around the world including Grasberg Mine in Indonesia, Antamina Mine in Peru, and Diavik Mine in Canada. These scale-up experiments are important as design of waste rock structures is traditionally based on bench scale testing. The experiment at Grasberg Mine revealed large variations in the measured net infiltration between different lysimeter locations, even though the average value was reasonable. This reinforces the complexity that exists in these materials.

As part of the Grasberg study, a meso-scale experiment was built by Andrina (2009) to investigate flow mechanisms in greater detail. The lab experiment included a 1.5 m high panel with alternating dipping beds of coarse and fine material. By varying infiltration rates it was shown that the flow is influenced by the structure, and that it will change with the infiltration rate. Moisture was retained in the finer material with low infiltration, and moved into coarser material as the infiltration rate increased.

Wilson (2011) concludes that the conceptual model proposed by Herasymuik (1996) is valid. Dipping layers of fine and coarse material, overlying a coarse rubble zone are an efficient reactor for the oxidation of waste rock. The reaction may be so rapid, that some waste rock piles may become fully

oxidized long before covers can be built. These materials are more complex than previously believed, and it may be impossible to develop a reliable model. Wilson argues that perhaps instead of attempting to build an impossible model, new efforts should be focused on building better structures, by eliminating the segregation of materials.

Fala et al. (2013), A Numerical Modelling Approach to Assess Long-Term Unsaturated Flow and Geochemical Transport in a Waste Rock Pile

Fala et al. (2013) summarized their studies of unsaturated flow in waste rock, using finite element modeling. In this study numerous 2D simulations were run using HYDRUS2D to estimate the hydrogeological and geochemical response of reactive waste rock. The simulations included sandy and gravelly materials. The properties of the model materials were based on field samples that were characterised with laboratory testing, including the saturated hydraulic conductivity and water retention curve.

Stochastic representation of these materials and an autocorrelation algorithm was used to create a heterogeneous fabric that represented the spatial variability in material properties. By varying the parameters, the correlations could align in certain directions (horizontal, vertical, or oblique). These correlations are similar to stratifications that are seen in waste rock structures. Simulations of moisture content were able to show the tendency for water to move along the stratification, and that this tendency was less obvious as the materials became coarser. The standard deviation of the material size could be increased to model greater ranges in particle size. It was found that with larger ranges of particle size the flow tended to be more preferential. Simulations of seepage velocity showed that flow became more tortuous with mixed hydrogeological properties. By increasing the standard deviation of the hydrogeological properties, there was more rapid moisture movement in the preferential areas. The model could also be used to simulate geochemical transport, showing how the rate of sulphide oxidation is affected by the particle size, and moisture content. The model results showed similar behaviour to real world observations of waste rock.

Fala et al. (2013), concluded that the numerical models were able to illustrate the general effects of heterogeneous properties on the behaviour of reactive waste rock. The models could provide indications of water distribution, seepage velocity, and reactive transport. The model was unable to simultaneously use multiple correlations, meaning that material properties were limited to one orientation per simulation. The approach in the study also could not address all the scales issues involved between laboratory and field scales. Even so, the simulations are a useful tool to assess the

unsaturated behaviour of waste rock, and may provide insight into construction and monitoring techniques.

Cash (2014), Structural and Hydrologic Characterization of Two Historic Waste Rock Piles

Cash (2014) continued the research of waste rock characterization, studying historic waste rock dumps at Detour Lake Mine in Ontario, Canada. The gold mine was owned and operated by Detour Gold Corporation on a 540 km^2 property, starting in 2006. The mine was originally operated by Placer Dome Inc. between 1983 and 1999. Two historic waste rock piles left by Placer Dome were relocated by Detour Gold in preparation for a new open pit. This transition period provided a good opportunity to study the evolution of mine waste after closure. The research included field and laboratory characterization of geotechnical properties and hydrologic behaviour. By excavating test pits and profiles in the waste rock, observations and measurements of oxidation, pore water parameters, and temperature were made. An inventory of 100 samples was also collected and tested in the lab to determine PSD, paste pH, moisture content, Munsell colour, hydraulic conductivity, and soil water characteristic curves.

Field observations confirmed a typical waste rock structure with a coarse base overlain with dipping beds at the angle of repose. Various lifts were separated by compacted traffic surfaces. The stockpiles were clast supported structures with fine material in the voids. Oxidation was evident throughout the piles, on the surfaces of larger particles and within the matric fines (< 4.75 mm particles). There were large ranges in the values for measured moisture, and in situ matric suction. There were no significant trends with depth, indicating that the structural profile was heterogeneous. The measured PSD data included clay size material up to 75 mm and was able to define the fine grained end point of particle sizes. Particles larger than 75 mm could not be physically measured. Less than 40% of the material passed the 4.75 mm sieve. Digital image processing was used to characterize the larger grain size fraction effectively. However, larger photographs may be required to fully capture the coarse grained endpoint. It was concluded that water will primarily flow in the <4.75 mm material, which makes up 17% of the total mass of the waste rock. The effective porosity of this material is low (0.5 to 0.12) due to the small volume fraction of fines.

Cash noted a few areas where further research would be beneficial. Additional study of the coarse grained endpoint, and the spatial area required using digital image processing is required. Larger particles (2 m and larger) were not represented using current methods, although they were observed

visually. Digital image processing techniques have the potential to reduce future sampling requirements, saving costs, and avoiding logistical challenges. Further work can be done to improve the concept of a rock-corrected SWCC, including larger size fractions that are not commonly associated with unsaturated soil properties, but represent materials as they exist in field conditions. Digital image processing can predict porosity that can be compared to porosity from SWCC with coarse material. Digital image processing was also used to quantify open voids. Where possible such studies should be compared with air permeability measurements to assess the validity.

Amos et. al (2015), Waste-rock hydrogeology and geochemistry

Amos et. al. (2015) present a study of several integrated field-scale investigations of waste rock characterization. These investigations included the study of the large-scale coupling of geochemical, hydrological, heat and gas transport processes. The study also reviews the attempts to model the cross coupling of various processes. Data in the individual studies was collected from mine sites around the world, including Australia, Canada, Germany, Kalimantan, Peru, and Sweden.

When considering the particle size of waste rock, there are generally two fractions. There is a fine fraction where capillary forces are important and a coarse fraction where capillary forces are irrelevant. Research from the Diavik Mine determined that the waste rock is rock-like, and clast supported. The low precipitation rates result in water flow being controlled primarily by the fine matrix. This leads to a higher tendency for reactivity in the finer fraction of material.

Permeability is a strong controlling factor of fluid flow, and will influence chemical and heat transfer processes. Permeability instrumentation was installed in waste rock pile test piles at the Diavik site. Different construction techniques were used between two of the piles, with one being end-dumped, and one being push-dumped. The permeability measurements saw no major difference between the two construction methods. Permeability measurements from the Rum Jungle mine, and Aitik mine saw a wide range of values throughout waste rock piles, but did not conclusively show that permeability increases with depth into the piles.

The hydrology and flow mechanisms associated with any given waste rock are heavily dependent on the material properties, and the climatic regime. Studies at Cluff Lake mine, Diavik mine, and Antamina mine illustrate three very different mixes of material properties and climates. This results in different flow mechanisms at each site.

Heat transfer is often coupled with gas transport and geochemical processes. Convective/advective heat transfer is associated with high permeability materials. Conductive heat transfer is better associated with low permeability materials. A study of two contrasting mines in Canada and Germany illustrated this relationship, with greater convection measured in the high permeability materials, and limited convection measured in low permeability materials.

After reviewing the numerous studies it was concluded that scale-up experiments are still often problematic. The review highlights the importance of site specific waste rock characterization. The variability of waste rock properties that exists between mine sites also leads to variability in the various mechanisms, and how they behave together.

Lahmira et. al (2016), Effect of Heterogeneity and Anisotropy Related to the Construction Method on Transfer Processes in Waste Rock Piles

Lahmira et. al (2016) present a study of the effects of heterogeneity and anisotropy caused by construction techniques, on the flow and transport mechanisms in waste rock. A thorough review of previous studies is summarized, outlining the knowledge base that exists for the structure, hydrogeology, and fluid flow mechanisms in waste rock piles. The previous studies outline the conceptual model that is used when describing and studying waste rock. Lahmira et al. (2016) summarize their study of numerical models used to simulate physical processes, and propose a new conceptual model for waste rock piles.

The research utilized the TOUGH2 numerical code to study the effects of heterogeneity. The simulations could represent the distribution of fluids, and provide insight into how they affect flow and transport processes. The models were given a random distribution of four material types in a 2D mesh, with regions that were 1.5 m X 1.5 m. Unfortunately, no reasons were given to explain the choice of mesh size. The material properties of waste rock from four mine sites were studied to generate representative values for the four model materials. The model used climate conditions and pile geometry from the Doyon Mine. The model did not represent the full range of permeabilities that may exist in a waste rock pile. By limiting the permeability range (and excluding the lowest values) the model would accept more oxygen. This served to emphasize the mechanisms related to oxygen supply. The random nature of the model was not representative of real world structures in waste rock. However, the anisotropy could be varied to approximate different structures created by bench construction and end-dumping construction.

The simulations revealed significant spatial variation in the distribution of water in the pile. The finer material had higher saturation, and caused preferential water flow. These observations were also pronounced in warmer areas. Gas flow was found to move through all material sizes, but was preferential in the coarser zones. The different structures (from construction technique) caused different convection patterns. Heat transfer was primarily by advection in warm areas, though there was significant conduction near the pile edges. The oxidation process releases heat, which helps circulate oxygen into the pile interior, and helps to sustain or accelerate oxidation reactions.

The model was able to show the effects of heterogeneity and anisotropy on the magnitude of fluid flow, oxygen supply, and heat transfer processes. This provided a better understanding of preferential flow and transport processes. This information was used to develop a new conceptual model of waste rock. The new model better represents the complexity of preferential pathways for water, and different patterns for gas movement. The random arrangement of materials in the study does not obey stratigraphic principles or reflect the actual structure. It was noted that a representative characterization would be difficult to achieve with predictive methods.

3 Case Study

3.1 Introduction

In order to study the available applications for PSD data, a field and laboratory research program was undertaken at Diavik Diamond Mines. The objectives of the study were to collect bulk samples of waste rock, determine the PSD, and use estimation methods for hydraulic properties. The PSD and estimated hydraulic properties could then be used to study the spatial variability that exists in waste rock piles. The research was conducted on test piles that are small scale waste rock dumps, one of which was deconstructed during this study. Samples collected on site were shipped to the University of Alberta, where they were tested to determine the PSD. These data were then used to estimate the hydraulic properties.

3.2 Diavik Diamond Mines Site Description and History

Diavik Diamond Mine is an operating diamond mine located approximately 300 km northeast of Yellowknife, in the Northwest Territories, Canada. It is situated on a 20 km^2 island in Lac de Gras. Diavik is operated as a joint venture between Dominion Diamond Diavik Limited Partnership (40% ownership) and Diavik Diamond Mines Inc. (60% ownership, 100% operations) a subsidiary of Rio Tinto plc. The mine includes four diamond-bearing kimberlite pipes. Three of the pipes are in production, with the fourth in development. Diavik has operated continuously since 2003, and is expected to operate beyond 2020 (Yip and Thompson 2015).

Diavik is located in the Canadian sub-arctic, with cold, winter conditions for approximately seven months each year. The mean annual air temperature (MAAT) is -12°C. Temperatures on average can range from above 25°C to below -35°C, with extreme cold reaching below -50°C. The climate is also windy, with average velocity of 20 km/h. Extreme winds have exceeded 90 km/h. The mean annual precipitation is approximately 375 mm, with 60% falling as snow. Available daylight ranges from a high of 22 hours in June, to a low of 4 hours in December (Yip and Thompson 2015).

The Lac de Gras region is north of the tree line in the barren lands. The area is characterized by shallow lakes, impeded drainage, and hummocky boulder strewn terrain of low relief. Flat topography ranges from 400 to 435 m above sea level in elevation. The ground material at site is primarily bedrock, with a thin layer of overlying glacial till referred to as overburden (Yip and Thompson 2015). Once the bedrock is mined it is referred to as waste rock or country rock, and is divided into three categories based on sulphur content (Diavik 2009) as seen in Table 3.1.

Table 3.1 - Waste Rock Type Classification at Diavik Diamond Mines Inc.

Type I	< 0.04 wt% S	Considered non acid-generating
Type II	< 0.04 wt% S – 0.08 wt% S	Considered to have low acid-generating potential
Type III	> 0.08 wt% S	Considered potentially acid-generating

Type I rock is reserved as a construction material and is stockpiled in accessible areas. Type II and III rock is stored in large waste rock dumps. Prior to gaining approval for the third open pit (A21), it was estimated that the waste rock dumps would contain 112 Mt of waste rock (from A154 and A418 open pits). This would include 15 Mt of Type I, 13 Mt of Type II, and 84 Mt of Type III (Diavik 2009).

3.2.1 Test Piles Research Program

DDMI has supported a multiyear, multidisciplinary research program that is collectively known as the "test piles". The program studies the thermal, hydrological, geochemical, and gas transport regimes of large-scale, low-sulphide waste rock piles. Researchers from the University of Waterloo (UW), University of British Columbia (UBC), University of Alberta (UA), and Carleton University (CU) participate in the research efforts. Funding and support are provided by numerous agencies, including DDMI, INAP, and NSERC. The project includes three 15 m high instrumented waste rock piles, along with an active zone research pad (Smith 2006).

The piles were built with a suite of instrumentation to allow for the collection of field measurements; a full list is available in Table 3.2. Collected field and lab data can be used to evaluate the environmental implications of building low-sulphide waste rock piles in a region with continuous permafrost. Completed and ongoing research can help improve the design of waste rock stockpiles, and reclamation plans for mines in sub-arctic and arctic environments (Smith 2006). The piles were constructed between 2004 and 2006, and monitoring of the instrumentation has continued until present day.

Table 3.2 - Diavik Test Pile Instrumentation

Instrumentation	Target Measurement/Purpose
Air permeability probes	Internal test pile permeability to air flow
Basal collection lysimeters (BCL)	Discrete collection of basal water flow and quality
Basal drain collection lines	Bulk basal flow and quality
Gas sampling lines	Internal test pile gas phase composition
Microbiology access ports	Internal test pile microbial populations
Soil-water suction samplers (SWSS)	Internal test pile water quality
TDR probes	Internal test pile moisture content
Tensiometers	Internal test pile matric water potential (unsaturated rock moisture tension)
Thermal conductivity probe access lines	Internal test pile thermal conductivity characteristics
Thermistors	Bedrock and internal test pile temperature
Upper collection lysimeters (UCL)	Active zone water flow and quality

3.3 Deconstruction Program

3.3.1 Introduction

In 2014 the Type I test pile was deconstructed to observe, record, and sample the in-situ material properties of the entire pile. The instrumentation installed on the pile had passed its original design life, and was subject to increasing wear and tear. The instrumentation had collected numerous data sets at discrete locations within the pile for close to a decade. The deconstruction allowed for the collection of additional data sets that supplement existing data, and offer new information. The new data would also be useful in determining how the material properties evolved over time, and confirming theories derived in research theses using the existing data.

3.3.2 Deconstruction Plan and Timeline

The Type I pile was chosen for deconstruction, in order to preserve the Type III and covered pile for ongoing monitoring. The author, along with researchers from the University of British Columbia, University of Waterloo, and Carleton University were on site to guide the deconstruction process, and collect samples. The deconstruction process began on July 1, 2014 and continued until August 3, 2014.

Additional excavation and sample collection took place between September 4 and 11, 2014. Figures 5 to 9 show the Type I pile at various stages of deconstruction.

The deconstruction included general observations, and sample collection for a number of parameters to study the thermal regime, hydrology, geochemistry, microbiology, and particle size distribution of the Type I pile. While this thesis discusses the PSD research, studies were also undertaken by researchers from the other universities using the remaining data sets. Ongoing and future research studies will be able to use the PSD data and estimated material properties as a comparison to the other data sets mentioned above.

The deconstruction proceeded with an excavator digging a series of trenches 2 to 3 m deep, on successive benches. The trenches were oriented along the north-south axis of the pile, with 2 trenches per bench. The trenches were constructed with a 3:1 slope in order to ensure safe working slopes for field personnel. On lower benches, where the pile is wide enough, additional test pits were added beside the trenches for additional information gathering. All excavated material was loaded into haul trucks and removed for mine construction projects. Excavation took place during the day shift, while sampling and observation occurred during the night shift. This schedule was developed to minimize interaction between field personnel, and heavy equipment.

A sampling network was laid out prior to sampling on each bench, in order to easily locate stations and record data. Sampling profiles were laid out in 5 m intervals along the north-south axis, with sampling stations located approximately every 3 m along the east-west axis. Sampling stations were labelled from A through F, with each letter referencing a particular depth in the trench. Figure 10 shows an excavated bench, with researchers surveying the locations for sampling grid markers. Due to the numerous factors involved in referencing a location point, a standard system was developed amongst the research team, to ensure that the same terminology was used by the entire team. The details of the referencing system can be found in Appendix A.

Due to the relatively small foot print of the Type I pile, early estimates for excavation time required were low. It was believed that the entire deconstruction could proceed in under one week. This timeline heavily influenced the planning process for sample collection and material observation, as well as the required number of personnel. It was estimated that one bench could be excavated during each day shift, and the entire bench could be surveyed, observed, and sampled during the following night shift. This required observation and sampling techniques that were fast and simple, as well as a large group of

researchers. A priority system was developed to guide the order for sampling type, along with sample location.

Figure 5 - Type I test Pile Before Deconstruction (June 29, 2014)

Figure 6 - Type I test Pile During Deconstruction (July 3, 2014)

Figure 7 - Type I test Pile During Deconstruction (July 7, 2014)

Figure 8 - Type I test Pile During Deconstruction (July 28, 2014)

Figure 9 - Type I test Pile During Deconstruction (August 2, 2014)

Figure 10 - Deconstruction of the Type I Test Pile

The deconstruction was planned to begin in July of 2014, with a smaller advance crew arriving earlier to make preparations. The schedule aimed to take advantage of the long daylight hours, allowing the researchers to work during the night shift with no need for additional lighting equipment. However, the excavation did not proceed as quickly as planned. Material could not be excavated as quickly as estimated, and there were several equipment breakdowns during the deconstruction program. The full deconstruction required seven weeks to complete. This necessitated schedule changes for project personnel, and some modifications to the sampling program. In some cases, it was possible to include additional samples, or additional locations, while other methods were unable to be improved upon.

3.3.3 Sample Collection and Observations

Due to the destructive nature of collecting samples, a priority system was developed to ensure the highest chances of acquiring reliable data for all of the research studies. These studies include (in order of sampling priority):

- DNA Isolation,
- Most Probable Number (MPN) enumeration,
- Mineralogy,
- Pore water extraction,
- Volumetric Moisture Content (VMC),
- Particle Size Distribution, and
- Matrix and/or void filling ice.

Non-intrusive observations included thorough digital photography of each trench face, as well as sample locations, colour mapping using the Munsell colour system, and a 'time lapse' photographic record of the deconstruction. The photographic records may later be used for three dimensional observations and analysis of the particle size distribution, using photogrammetry techniques.

Samples collected for PSD analysis were stored in 12 mil polypropylene sample bags that were double bagged, with barcode stickers, and handwritten labels. The barcodes were scanned into a computer database that tracked the sample name, the sample type, and the sample location. Each PSD sample consisted of two sample bags with a cumulative mass of approximately 70 kg. The entire sample (both bags) was used for PSD testing.

The subject of this thesis is the spatial variability in the particle size distribution of the Type I pile, and as such will focus on that portion of the deconstruction. Details of the other research studies that occurred during the deconstruction are not provided in this thesis. The specific procedure for the collection of samples for particle size distribution analysis is presented below.

3.3.4 Sample Storage and Shipment

Once collected, samples were stored outdoors, at the test piles site. Initially the samples were laid out on the ground, in groups representing different benches. Eventually all of the samples would be transferred into large "mega-bags" (1.5x1.5x1.5 m heavy duty shipping bags). Due to shipping logistics on site, there were not enough mega bags available to pack all of the samples in the summer of 2014. Ten mega bags were packed during the deconstruction program, representing about two thirds of the collected PSD samples. These remained at site, until January 2015, when they were shipped to Edmonton, arriving in early February. The remaining samples were packed during the winter of 2014/2015. These samples were buried in snow, and often frozen to the ground. A large number of these samples were damaged during packing. The remaining samples were packed into an additional five mega bags, and shipped to the U of A in June 2015.

Once the samples arrived at the U of A, they were stored in an outdoor storage yard at the University's South Campus. These samples were exposed to weather during storage in 2015 and 2016, as the laboratory testing was underway. Smaller batches of samples were collected on a regular basis, and driven to the U of A laboratory for PSD testing. Once testing was completed the samples were returned to the storage yard.

3.4 Laboratory Testing

Of the 244 PSD samples that were collected as part of the physical characterization study, 141 were processed in a laboratory setting. Many samples were damaged during shipping, or while in various storage areas. At site, many samples became frozen to the ground, and their bags were torn open as they were transferred into shipping bags. Many other sample bags were torn open by rough handling by equipment. Any samples that had large visible tears in both inner and outer bags were deemed unfit for testing, as they may have lost material. There were approximately 60 samples that could not be processed due to missing labels or lack of time at the end of the research program. All of the PSD samples were shipped to the University of Alberta for this phase of the study. The primary laboratory analysis was for particle size distribution of the physical samples which also included measurements of moisture content. Munsell colours were recorded for each processed sample to determine if there were any relevant trends between colour and physical properties of the material. The resulting data sets were used for physical property estimation of the material. It was also compared to data sets from similar studies during the construction of the pile, to observe any evolution of material properties over time, or differences in sampling methods.

3.4.1 Moisture Content

During the deconstruction measurements of the volumetric moisture content were collected from in-situ material. However, the planning and execution of this work was led by researchers from UBC. As such, this work is not included in this thesis.

Gravimetric moisture content measurements were recorded on all processed samples prior to particle size distribution testing. The samples were removed from their poly bags and placed into metal trays (4"x12"x20") for drying. Based on the volume of the samples, four trays were required to hold one entire sample. The filled trays were measured for mass (±1 g) before being placed into an oven. The samples were then dried for approximately 24 hours at 110 ± 5°C. Once the samples were dried, they were removed from the oven and weighed once again. The loss in mass represents the gravimetric water content. The oven dried method was chosen based on past studies at this site, and their testing methodology. Oven drying also allowed for simple determination of the moisture content, as well as preventing further geochemical or biological reactions from occurring. It was noted in several samples that a type of algae was growing, during their time in storage. The existence of algae in some samples may have slightly increased the moisture content of those samples; however, this was not investigated in detail in this thesis.

The gravimetric moisture content data that were determined in the lab are subject to error. Shipping the materials from site, and preparing the laboratory program was a slow process, with the first samples being tested almost one year after being collected. Prior to that, they were stored outside first at the mine site, and later at a storage yard in Edmonton. Most samples were double bagged to ensure samples were preserved and to limit moisture loss. However, they were not immune to damage, with numerous holes and tears being observed in some bags. This damage could have led to changes in the moisture content, and may not be representative of in-situ conditions.

3.4.2 Procedure for Determining Particle Size Distribution

The laboratory procedure for determining particle size distribution of the sampled material was developed from ASTM D6913 Method A, ASTM C136, and previous studies at the test piles site, and other waste rock studies.

This methodology included the moisture content determination, and composite sieving of the material. Due to the large particle sizes (up to 75 mm) it was required to use two different sieve sets for composite sieving, with one set for coarser material, and one set for finer material. Normally coarse and

fine material is differentiated by the 4.75 mm sieve. For logistical purposes of this research the coarse and fine sieved materials were divided by the 9.5 mm sieve. The initial sieve set was used to measure the material greater than 9.5 mm, and the second sieve set measured material less than 9.5 mm. Cobble sized particles (75 to 300 mm) could be measured manually, using appropriately sized squares. No particles in this size range were encountered in the samples that were processed.

The coarse sieve set included 75.0, 50.0, 37.5, 25.0, 19.0, and 9.5 mm sieves, and a pan to capture the remaining material. The masses of each sieve tray, as well as the pan were recorded before testing began. These sieves were installed in a TS-2 Gilson Testing Screen (shown in Figure 11). It was required to sieve the samples in batches in order to not overload any of the testing screens. Based on the screens that were used the maximum capacity ranged from approximately 6 to 18 kg (ASTM International 2009). As such it was convenient to use one drying tray of material per batch, as this kept the screens loaded below capacity. There were four drying trays for each sample that divided a sample into manageable volumes. Each batch was shaken for 10 minutes. All four dryer trays of material were tested for each sample, producing coarse distribution data for the entire sample. At the completion of each batch the sieve trays were removed, the mass was recorded, and the material was removed for further sieve testing of the finer portion.

The fine portion of this material accounts for roughly half of the mass of each sample. As such, it was impractical to process the entire fine portion of each sample. The fine portion of the sample was split into subsamples for further testing. Once material was removed from the coarse sieving circuit it was placed into a mechanical chute splitter (Figure 12). The chute splitter was equipped with an equal number of 12.5 mm gaps oriented in opposite directions, with identical catch containers on either side. Upon opening the chute, the sample is split into two equal portions. This method was used several times until an appropriate sub-sample size remained (5 kg or less).

The finer sieves can only handle a maximum capacity of 550 grams (ASTM International 2009), meaning a 5 kg sub-sample would still require ten batches in order to not overload them. Sub-samples were divided into batches that were approximately 300 to 500 grams by scooping material into a pan on a scale. Each batch was shaken for 10 minutes, using 4.75, 2.0, 0.85, 0.425, 0.25, 0.15, 0.106, and 0.075 mm sieves, along with a pan at the bottom (Figure 13). At the end of each batch, the sieves were separated and the mass of each was recorded. The data from all the batches was later summed together in order to represent the entire subsample.

Washed sieving was not used during this investigation for several reasons. Previous studies at this site have not employed washed sieving. Therefore, a similar methodology devoid of washed sieving was used in this study, in order to compare results to earlier studies. The U of A labs did not have the proper facilities to perform wash sieving on such large samples. It is recognized that the dry sieving technique contributed to an unquantifiable loss of fine material less than 0.075 mm, in the form of dust.

Figure 14 shows an example of a PSD data set plotted from the laboratory measurements. The full set of plots is available in Appendix C.

Figure 11 - Gilson TS-1 Mechanical Sieve Shaker

Figure 12 - Mechanical Chute Splitter

Figure 13 - Mechanical Sieve Shaker

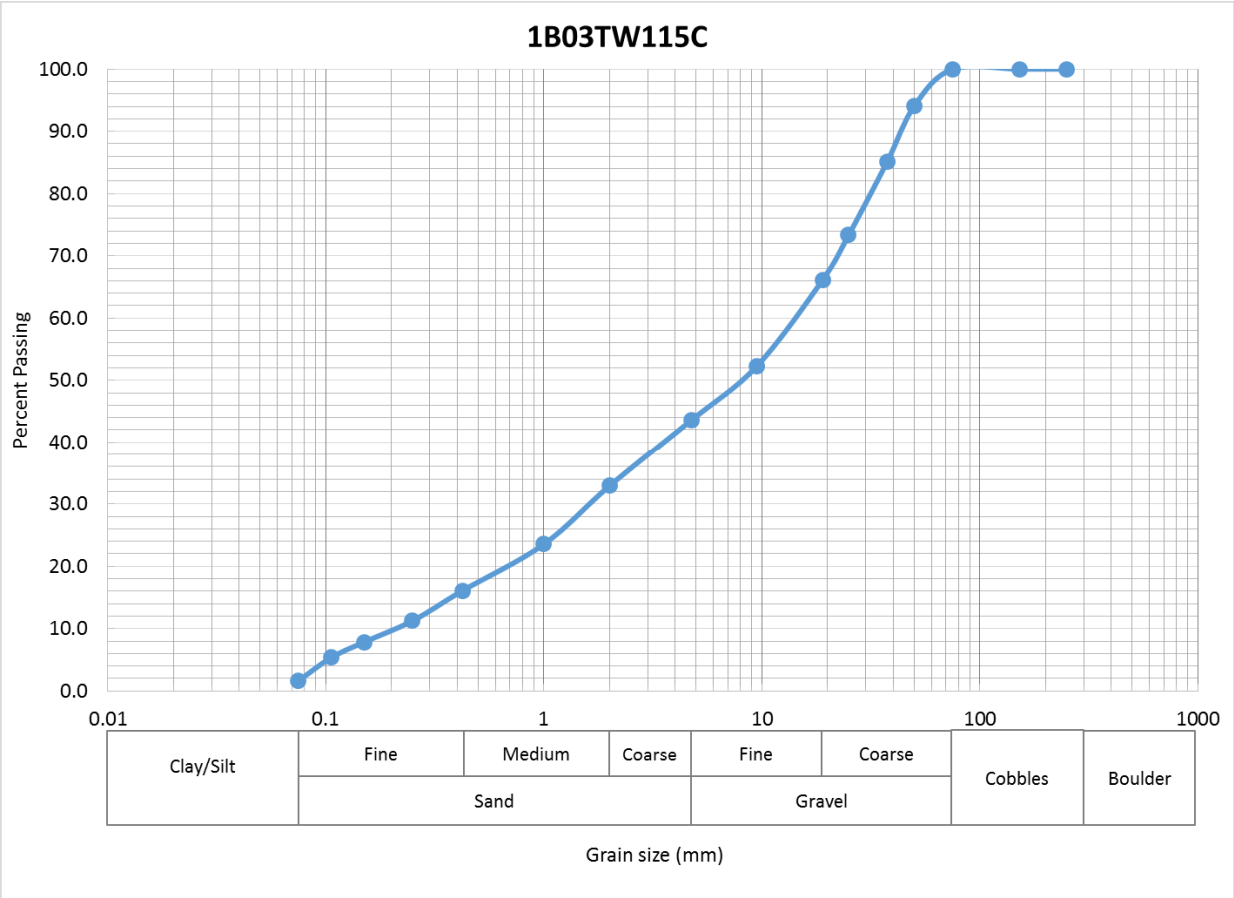

Figure 14 - Example PSD Curve from Laboratory Data

The unimodal curve fitting method from Chapuis (2014) was used to fit functions to the measured PSD data collected in the laboratory. The equations to calculate the PSD functions were entered into Microsoft Excel, and the Solver function was used to determine the best fit. This method was able to provide a tight fit to the laboratory data with R^2 values of greater than 0.999 throughout the data set. A series of macros were written that allowed the database of completed PSD data to be explored and solved efficiently. The macros completed the best fit curve function, and computed values for d_5, d_{10}, d_{15}, d_{20}, d_{25}, d_{30}, d_{35}, d_{40}, d_{45}, d_{50}, d_{55}, d_{60}, d_{65}, d_{70}, d_{75}, d_{80}, d_{85}, d_{90}, and d_{95} from the fitted data. This data was then exported to a new database, where it was analysed for spatial trends, and used for saturated hydraulic conductivity estimations. Figure 15 shows an example of Chapuis (2014) fitted data vs laboratory measured data. The entire series of function fitted PSD curves is available in Appendix C.

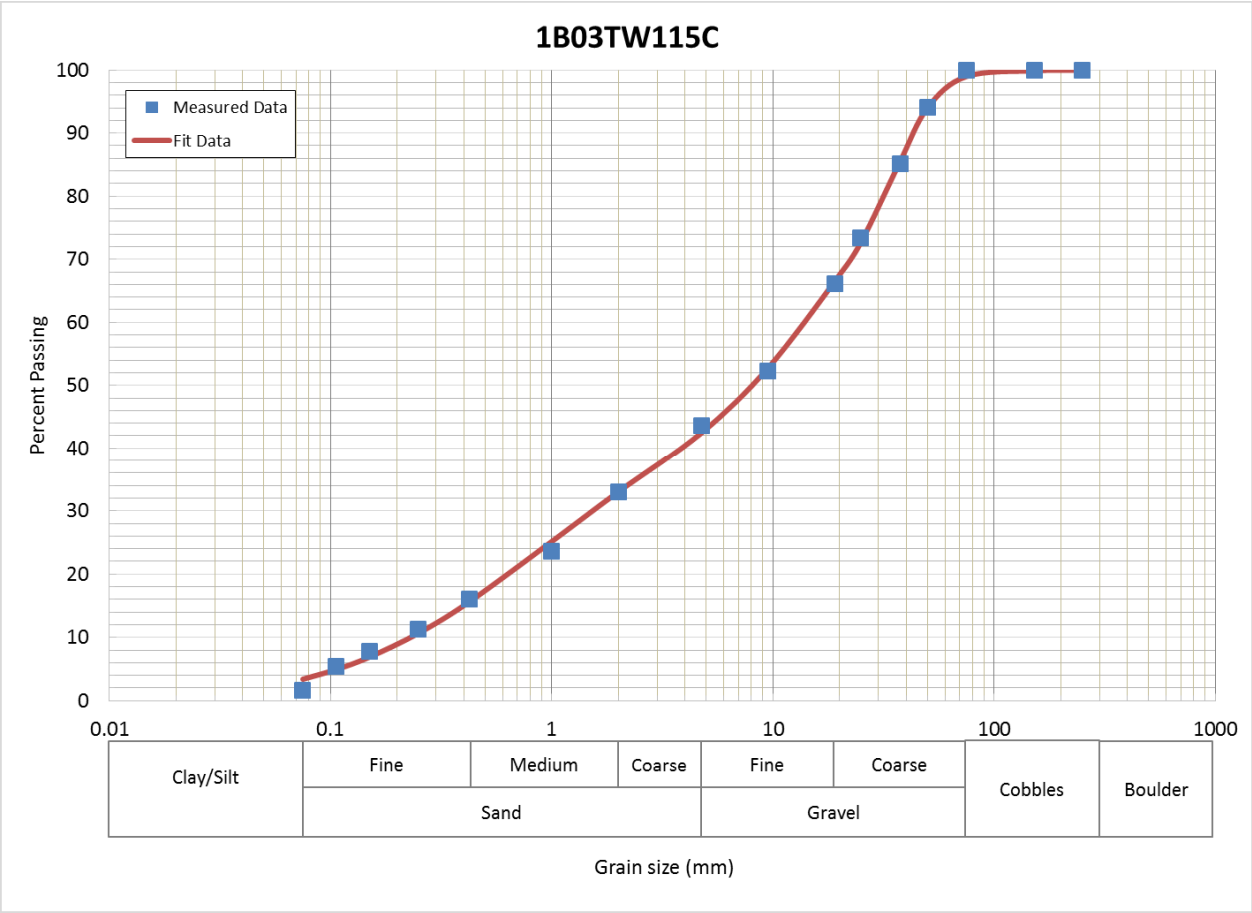

Figure 15 - PSD with best fit multimodal curve after Chapuis (2014)

Estimations of unsaturated material properties required the use of SVSoils, a computer program that can estimate the SWCC and the relationship between permeability and suction, from PSD data. In order to fit functions to the PSD data, SVSoils offers the unimodal and bimodal techniques presented by Fredlund et. al. (2000) (Section 2.3.3). For this data set both the bimodal and unimodal techniques were used. The data set for each sample was carried forward using the method that provided the highest R^2 value. Approximately half of the samples had a better bimodal fit (average R^2 of 0.9936), while the other half had a better unimodal fit (average R^2 of 0.9897). However, it was noted that neither the unimodal nor bimodal techniques had as close of a fit as the multimodal approach of Chapuis (2014) that had an average R^2 value of 0.9996. SVSoils allows the user to choose the fit method, and it produces a graph, generates data for d_n values, and provides statistics on the fitted curve. These generated data are then used to classify the soil (Fredlund et al. 2000). An example of fitted PSD data using SVSoils is provided in Figure 16.

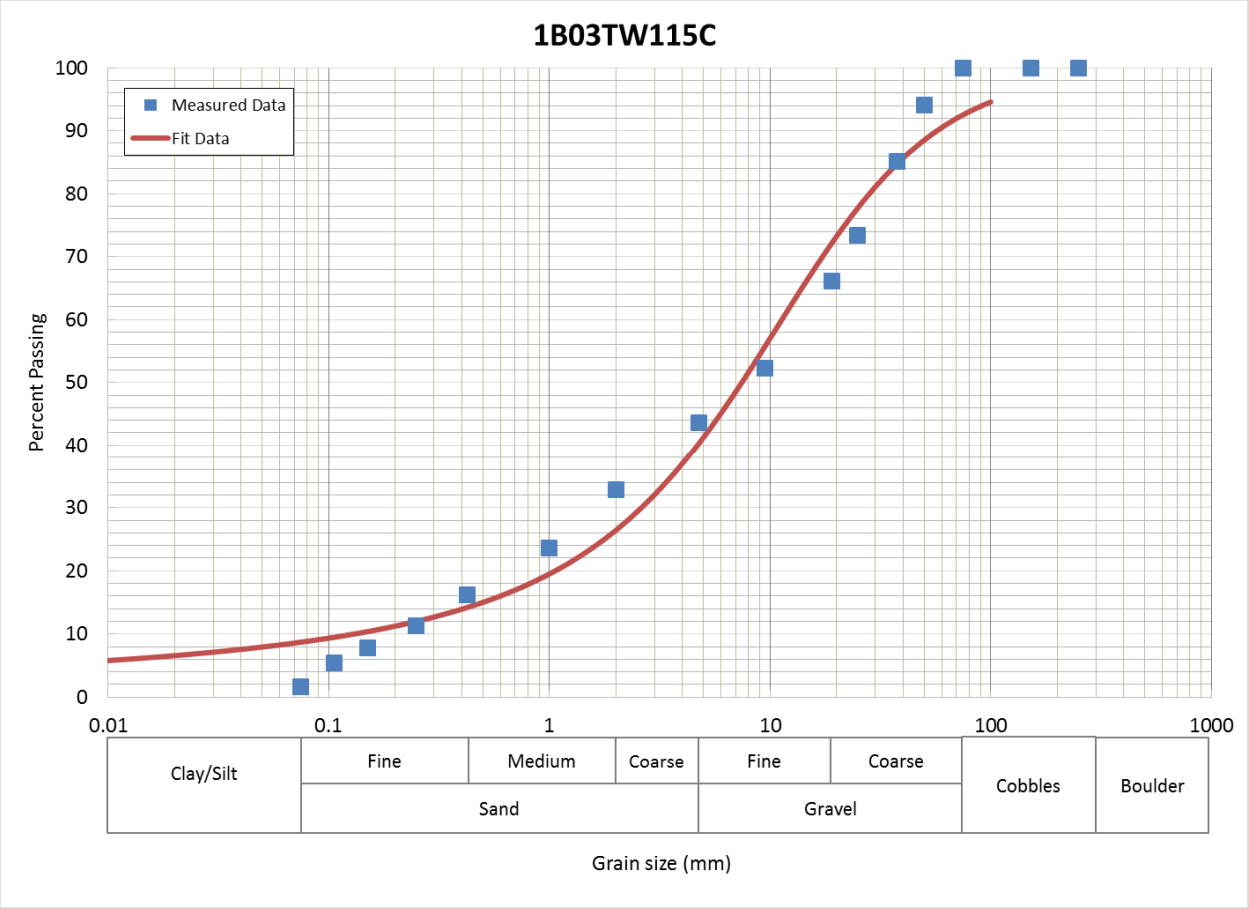

Figure 16 - Example Plot of PSD Data Fitted using SVSoils

3.4.3 Data Management

Samples that were collected during the deconstruction were labelled with permanent marker, as well as with a pair of durable barcode stickers. The barcode stickers were scanned into a digital database that linked them to the corresponding location, collection date, type of sample, and who it was collected by. This database was used to record relevant data for all the samples that were collected during the deconstruction.

The barcodes were again useful when moving samples in and out of storage, and completing lab testing. An initial inventory list was built by scanning in all the samples that were shipped to U of A into a new database. As samples were moved from the storage facility to the lab facility they were scanned again. This allowed for quick and accurate tracking of the samples. The barcodes were also the first piece of information that was written on each data sheet during the lab processing.

A data sheet template was developed at the beginning of the lab program in order to record the information in a systematic way. These sheets included the sample barcodes (two bags for one sample location), the sample location, the date, the person doing the testing, and the material properties. These properties included, Munsell colours (moist and dry), moist mass, dry mass, masses of drying tins, masses of sieve trays, and material masses after sieving. An example of the template is available in Appendix A.

The information that was recorded on the data sheets was later entered into a digital data sheet using Microsoft Excel software. Each sample location was given its own separate data sheet. A template was created that had space to input all of the recorded information, as well as having all the required calculations built in. This allowed for rapid generation of PSD data, along with accompanying plots. The template also allowed for a similar format to be carried through all of the data sheets.

3.4.4 PSD Data Validation

As described in earlier sections it was impractical to sieve the entire portion of finer material (less than 9.5 mm), as this portion was generally above 30 kg, and the small sieves should not be loaded with more than 500 g. A sub sample of 2 to 5 kg was collected from each sample and run in batches of less than 500 g. This method allowed for the fines portion to be tested in a time efficient manner.

During the processing of PSD data several duplicate sub samples were processed to ensure that the testing methodology was producing consistent results. Approximately 10% of the data set was tested with duplicate sub samples, chosen at random during the laboratory testing program. The duplicate sub samples represent the finer portion of the sample (less than 9.5 mm), as the entire coarse fraction was tested for every sample. The sub sample was collected using the same splitting procedure as the primary finer sub sample, and was processed using the same sieving procedure. The percent difference was calculated using Equation 14. Positive values represent more mass in the original sample, and negative values represent more mass in the duplicate. The most critical size fraction is 4.75 mm, as it is used to classify the material into six different groups as explained in later sections (see section 4.1 for details). The average percent difference between the original and duplicate sub samples for the 4.75 mm size was -4.2%, with maximum and minimum percent differences of 8.1% and -11.7% respectively. This equates to actual differences of up to ± 3.9% passing the 4.75 mm sieve, with an average of ± 1.4%. This means that some of the samples may be classified into two different groups depending on the fines portion that was measured. However, the sample would need to be on the borderline of the two

classification groups already, to have a chance to switch between them. It is also expected that changes could happen both ways, with some samples moving to a higher group, and some moving to a lower group.

$$\% \, difference = \left(\frac{original - duplicate}{\left(\frac{original + duplicate}{2} \right)} \right) * 100 \qquad \text{Equation 14}$$

3.5 Hydraulic Property Estimation

The collection of PSD data at over 100 locations in the Type I test pile has also provided the opportunity to estimate hydraulic properties for these same locations. Estimation of hydraulic properties of porous media can rely on many different techniques depending on the information and resources available. In this study the PSD data was used to develop two distinct databases for the estimation of hydraulic properties. The first database used the multimodal curve fitting approach proposed by Chapuis (2014). The second database utilized SVSoils from SoilVision, which includes curve fitting methods, and estimation techniques.

3.5.1 Manual Estimations of Saturated Hydraulic Conductivity

Equation 12, proposed by Chapuis (2004), for the estimation of saturated hydraulic conductivity was applied to the data set. It was chosen as it is simple, and relies on data that is derived from the PSD, and either the void ratio or porosity. The porosity was set at 0.25 to reflect field testing work by Nuener (2009) at the Diavik Test Piles. The d_{10} value was taken from the fitted PSD data generated using the Chapuis (2014) multimodal method. At each PSD data location, the saturated hydraulic conductivity was calculated. Results for these estimations are presented and discussed in chapters 4 and 5, respectively.

3.5.2 Estimation of SWCC and Unsaturated Permeability

Waste rock dumps can have both saturated and unsaturated zones, due to their construction, PSD, and location above the local groundwater table. As such, it is important to investigate the unsaturated hydraulic properties in addition to the saturated hydraulic properties. The added complexity in the unsaturated soil system means that estimation techniques often require greater computing power. Section 2.3.3 provides discussion on the complexity of unsaturated soils, along with methods for calculating relevant parameters. A commonly used computer code is available from Soil Vision Systems Ltd. This software includes techniques for fitting a function to PSD data, estimating the SWCC, and estimating the relationship between permeability and suction.

The SVSoils database from Soil Vision was used to estimate the unsaturated permeability for the Type I test pile data set. Estimation of these properties is an acceptable practice for preliminary engineering design. Detailed and final design would require the measurement of these properties (Fredlund et al. 2012). The research in this thesis is an investigation of the spatial variability in material properties. As such, estimations are sufficient to demonstrate the methodology, and illustrate a preliminary model of the spatial variability.

The workflow in SVSoils included entering laboratory PSD for each sample location, fitting a curve to the data, estimation of an SWCC, and finally estimating unsaturated permeability and saturated hydraulic conductivity. The estimation techniques also require other mass-volume properties that can be calculated with a built-in mass-volume calculator that requires three known quantities. The software is designed to estimate the SWCC, beginning from a point of complete saturation. As such, one of the known properties was a saturation of 100%. The other two known values that were used were a specific gravity of 2.65 (Yip and Thompson 2015), and a porosity of 0.25 (Neuner 2009).

SVSoils has several methods included for estimating the SWCC using soil classification data (Soil Vision Systems Ltd. 2016). For this analysis the Fredlund and Wilson (1997) estimation was used to predict the SWCC. Fredlund (2000) compared this and other methods and concluded that it provided the highest confidence among methods for estimating the air entry value (AEV), along with reasonable accuracy in predicting the maximum slope. The Fredlund and Xing (1994) equation was used to describe the SWCC at each individual particle size in the Fredlund and Wilson (1997) estimation (Soil Vision Systems Ltd. 2016). The Soil Vision Theory Manual (2016) makes a note about the applicability of this method to waste rock. Normally the packing porosity is determined by a neural net implemented in the software. However, the neural net was not trained using mine waste soils. Limited study by Soil Vision has shown that the packing porosity will need to be increased when estimating the SWCC for waste rock. Analysis of five waste rock samples from a single site required an average increase to the packing porosity of 27.9% in order to match measured data (Soil Vision Systems Ltd. 2016). For the purpose of this study it was decided not to alter the packing porosity as determined by the neural net. Too little information was available to determine what an appropriate adjustment would be. As a result, the data presented in further sections of this thesis may be underestimated. However, the trends will still be appropriate in the discussion of spatial variability.

4 Field and Laboratory Results

The research conducted during this study has provided information about the physical properties of the Type I waste rock material. Physical measurements of the PSD were collected along a 3D grid. This allowed for a quantitative assessment of the range of particle sizes in 3D space. In addition this data set was used along with estimation techniques to approximate the saturated and unsaturated material properties of the Type I waste rock. The data sets were also divided into subsets using a classification system proposed by Herasymuik (1996), allowing for similar materials to be grouped together based on the percent passing the 4.75 mm sieve. The classification system, and the divided data sets are presented in the following sections of this chapter.

4.1 Material Classification

Herasymuik (1996) proposed a classification scheme for waste rock material based on the amount of material passing the 4.75 mm (#4) sieve. The classification groups contained 0% to 10%, 10% to 19%, 20% to 29%, 30% to 39%, 40% to 49%, and greater than 50% material passing the 4.75 mm sieve. Samples with greater than 40% passing the 4.75 mm sieve are considered to be soil like, with larger clasts supported in a fine matrix. Conversely, samples with less than 40% passing the 4.75 mm sieve would be considered rock-like, with larger clasts having grain to grain contact (Herasymuik 1996). Cash (2014) followed this classification system, and it was adopted in this current study as well. There were no samples that fell into the 0% to 10% category. The number of samples in each category is shown in Table 4.1 (the nomenclature of the groupings has been adjusted for clarity). It should be noted that studies by Herasymuik and Cash used samples with a maximum particle size of 50 mm, while this study used a maximum particle size of 75 mm. The number of samples in each category was not greatly affected by the inclusion of the additional size fraction, with plotted averages being almost identical. However, if numerous larger size fractions were included it is expected that the classification system would need to be adjusted in order to compare results between studies. The results in the following sections are based off the 75 mm data set.

Table 4.1 - Size Fraction Classification

Group Name	Classification (passing 4.75 mm)	Deconstruction PSD (75 mm)	Deconstruction PSD (50 mm)
Group A	0% to 10%	0	0
Group B	10% to 20%	1	1
Group C	20% to 30%	16	11
Group D	30% to 40%	73	68
Group E	40% to 50%	50	60
Group F	> 50%	1	1

4.2 Particle Size Distribution

The PSD of the material was the only property that was physically measured in this portion of the Type I Deconstruction project. Samples collected during the deconstruction were processed in a laboratory following ASTM D6913, to determine the PSD. The data was then plotted using a multimodal curve fitting algorithm developed by Chapuis (2014). The PSD data was then grouped together using the previously described classification system. There were no samples in Group A. Group B had 1 sample, Group C had 16 samples, Group D had 73 samples, Group E had 50 samples, and Group F had 1 sample. Approximately one third of the samples had greater than 40% passing the 4.75 mm sieve, and would be considered soil like, with the remaining two thirds being considered rock like. Plots of the PSD groupings are shown in the following figures (18 to 22).

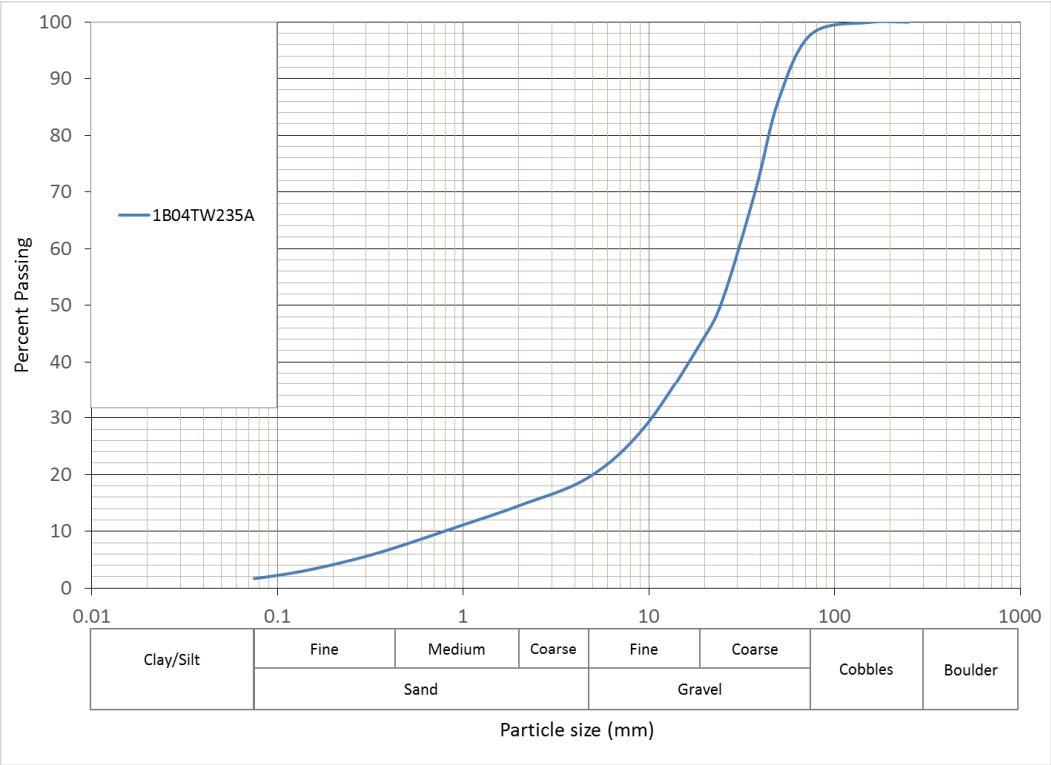

Figure 17 - PSD for Group B

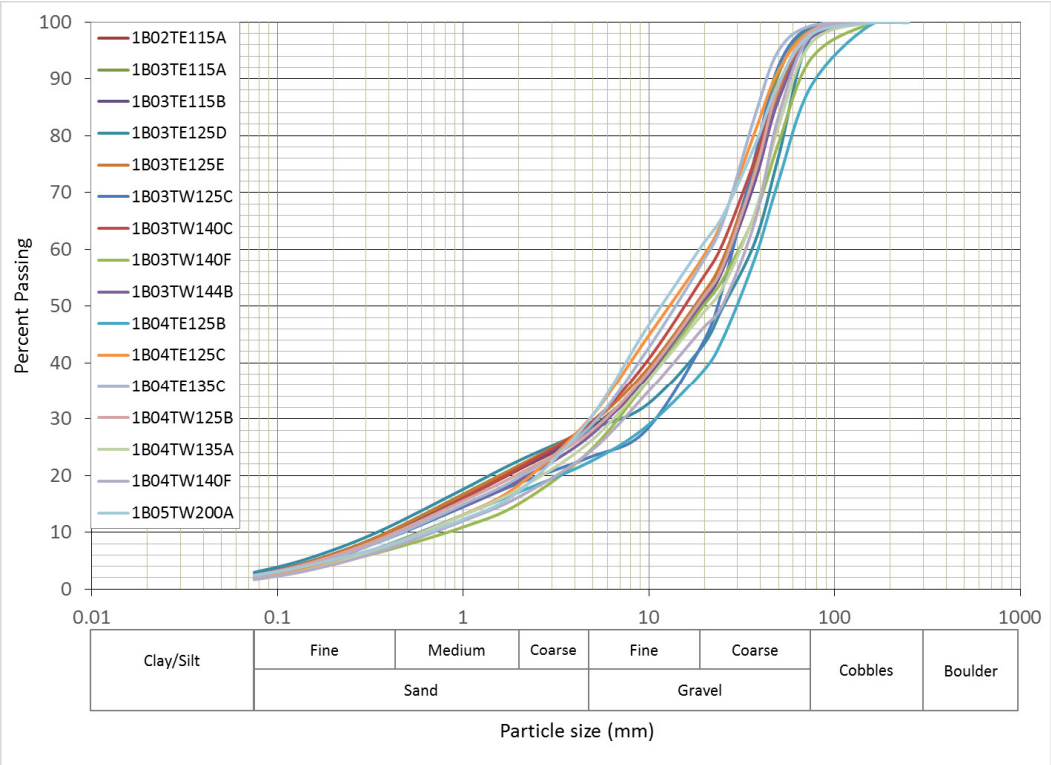

Figure 18 - PSD for Group C

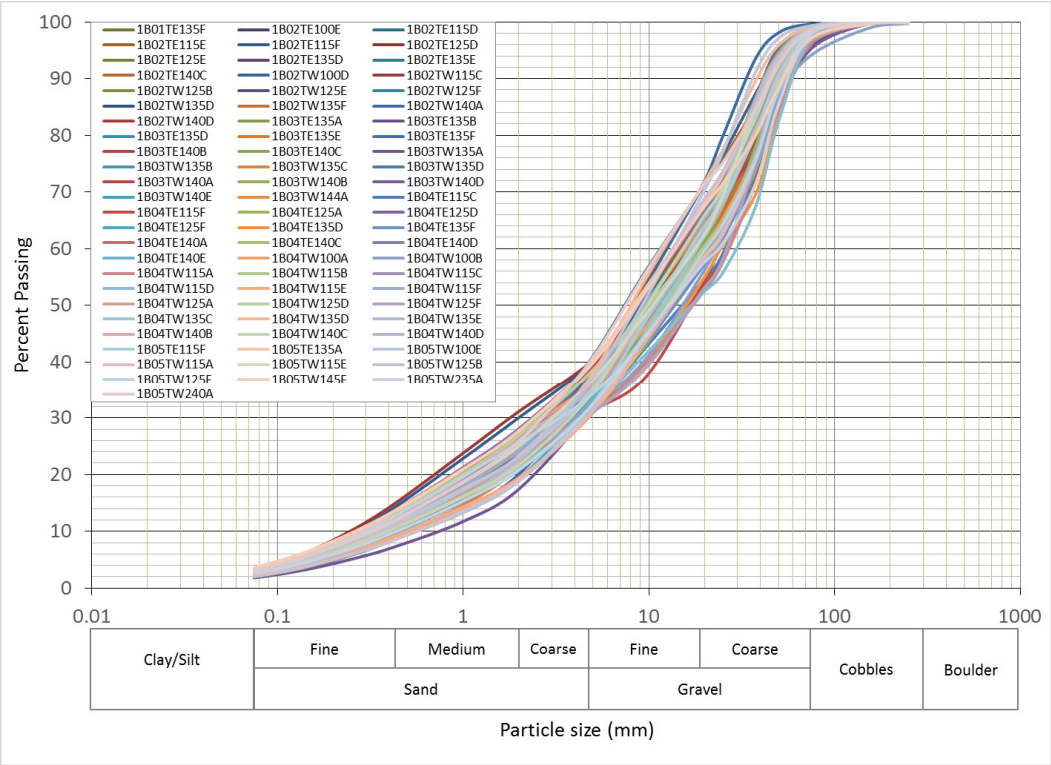

Figure 19 - PSD for Group D

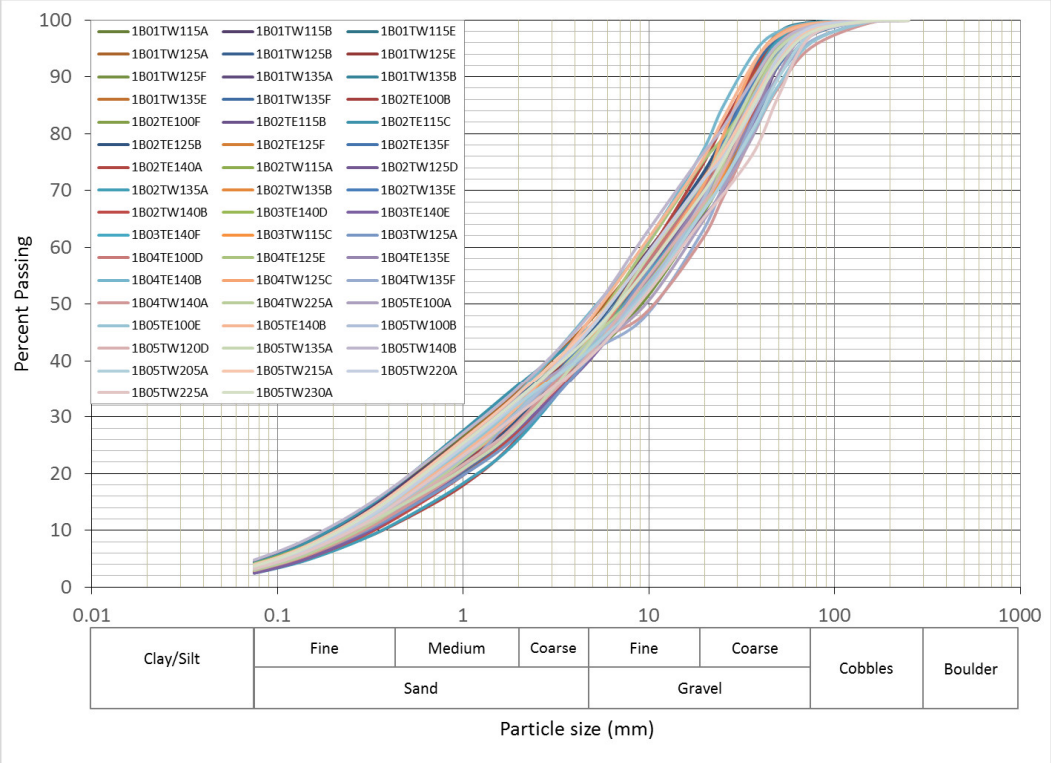

Figure 20 - PSD for Group E

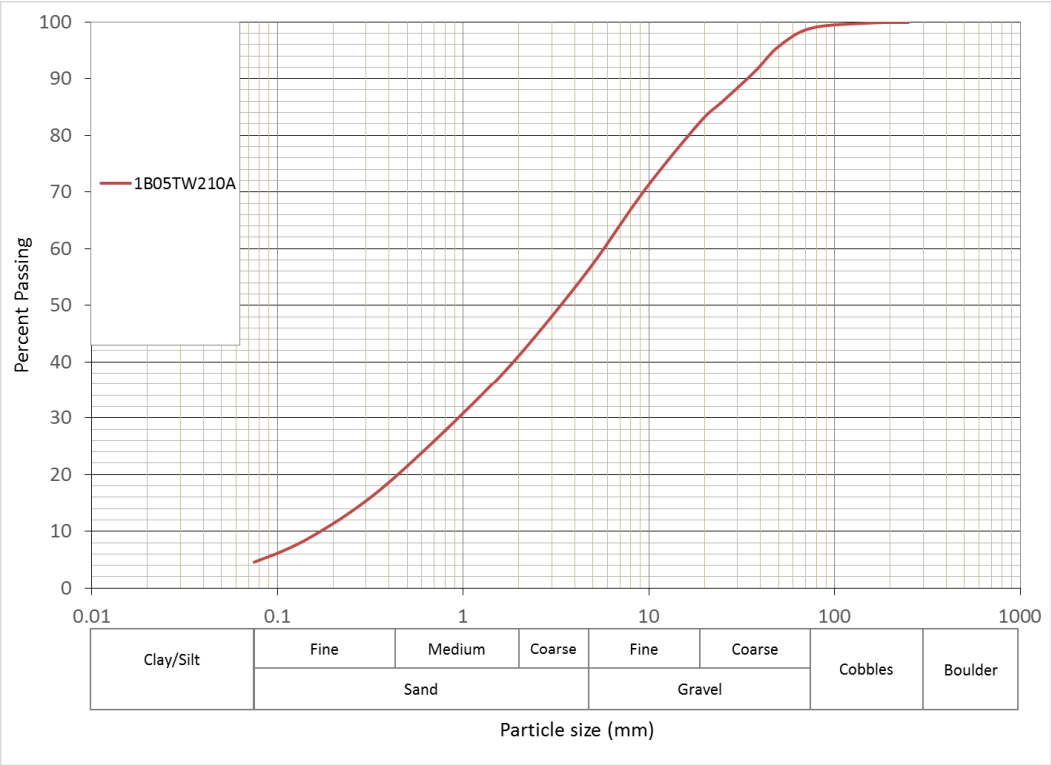

Figure 21 - PSD for Group F

4.3 Estimated Material Properties

The generation of ARD is tied to the availability of oxygen and water. As such, it is useful to know how these gas and fluids will move through the waste rock pile. The PSD data set that was collected for this research is sufficient to make use of estimation techniques for saturated hydraulic conductivity. With the aid of SVSoils, that data can also be used to estimate unsaturated hydraulic conductivity, soil water characteristic curves, and water storage. These data can then be examined for trends or grouped together in order to classify the material.

4.3.1 Soil Water Characteristic Curve Using SVSoils

SVSoils was used to estimate the SWCC for each of the processed samples in the PSD study. The software uses the PSD data as well as material properties to estimate the SWCC. To calculate the required material properties, the software requires three known quantities. In this study the known values were the specific gravity, porosity, and an initial saturation. The specific gravity of the waste rock material was 2.65 as outlined by Yip and Thompson (2015). The porosity was set at 0.25 based on work by Neuner (2009), and Zak (in progress). The initial saturation was set at 100% in order to estimate the drying SWCC.

Using these material properties, the software was able to calculate any remaining material properties that were required for the estimation technique. The Fredlund and Wilson method was used to estimate the SWCC, and the Fredlund and Xing method was used to fit the SWCC data. The SWCC data set was classified using the size fraction described in previous sections, and the data from each category were grouped together. Table 4.2 lists the average air entry value and residual saturation values for the classification groups. The plotted data for each classification group is shown in Figures 23 to 27. Further discussion of these data can be found in section 5.3.3.

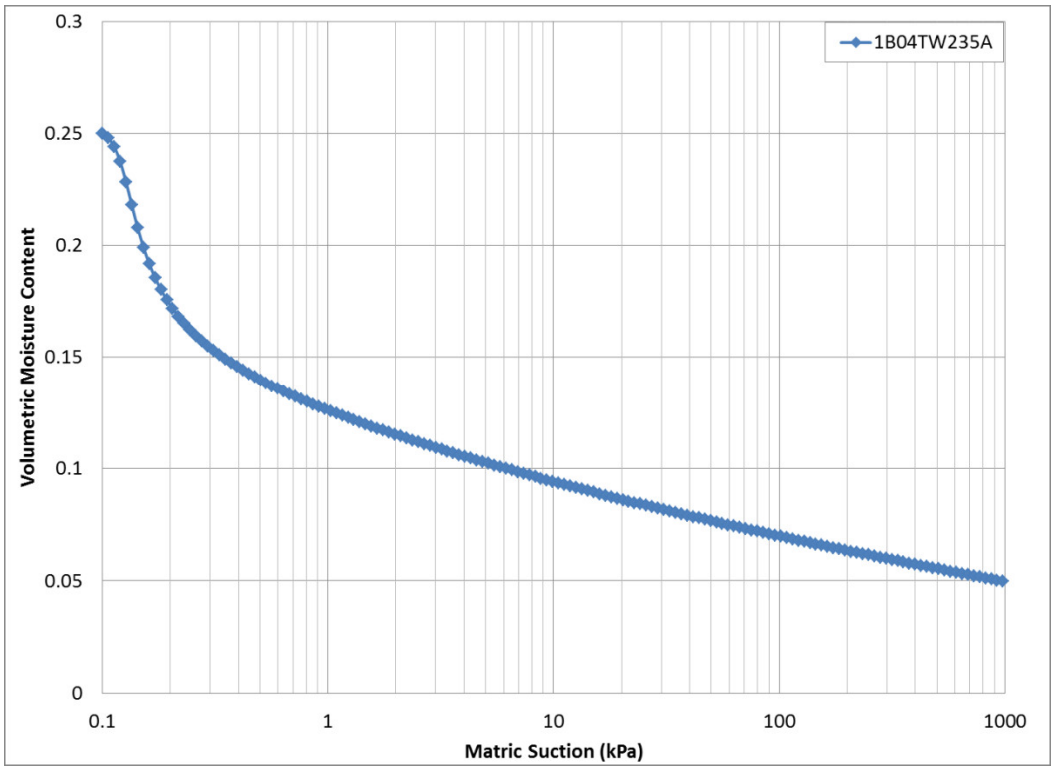

Figure 22 - Soil Water Characteristic Curves for Group B

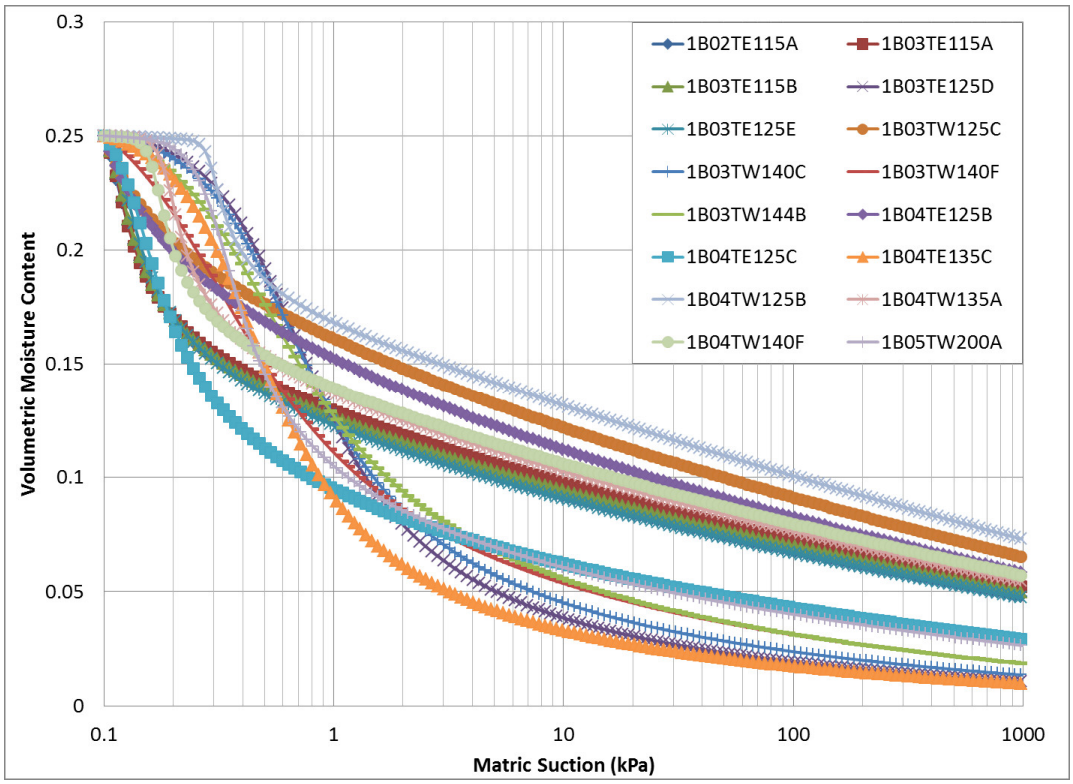

Figure 23 - Soil Water Characteristic Curves for Group C

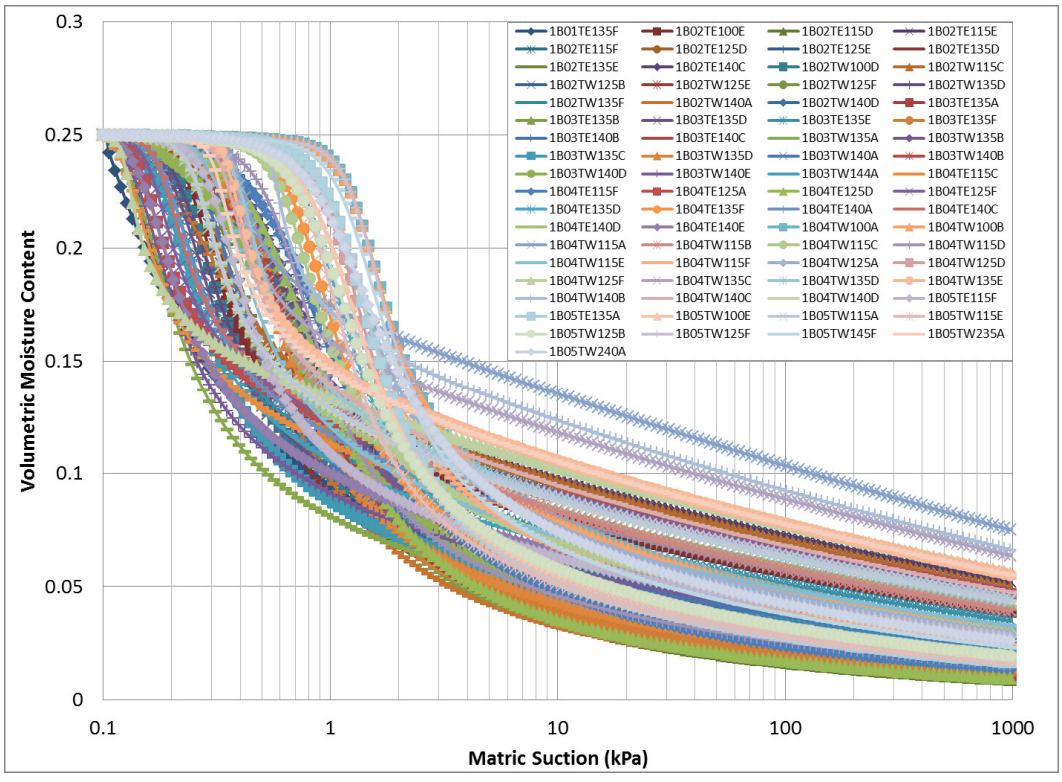

Figure 24 - Soil Water Characteristic Curves for Group D

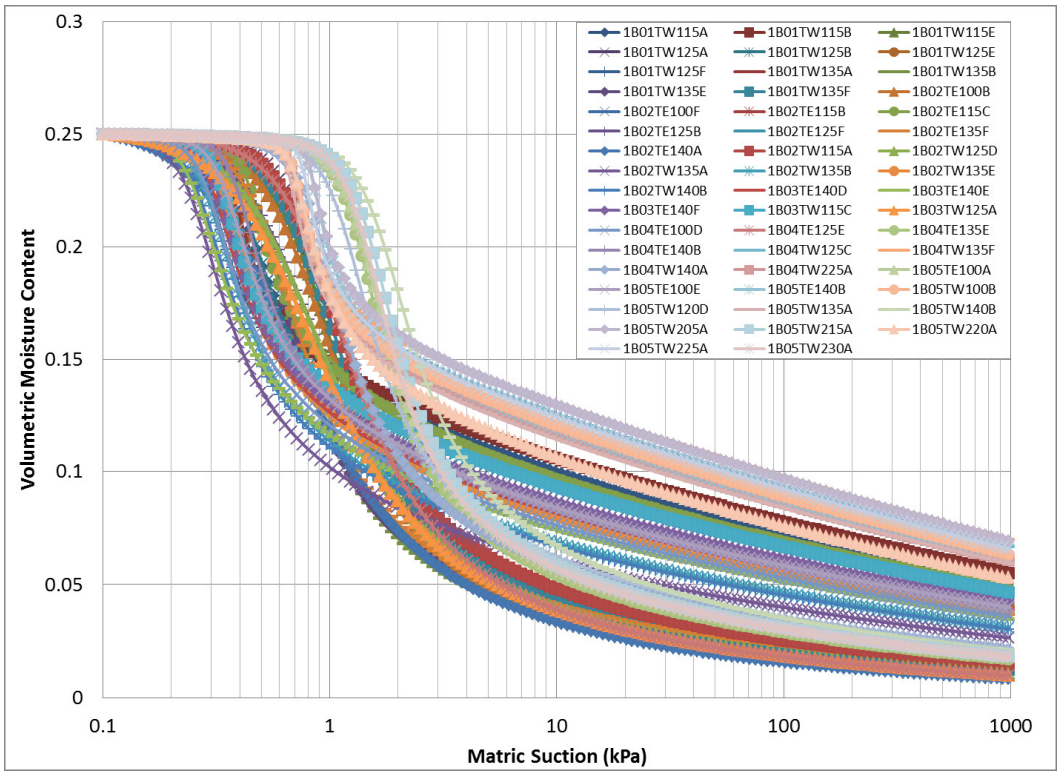

Figure 25 - Soil Water Characteristic Curves for Group E

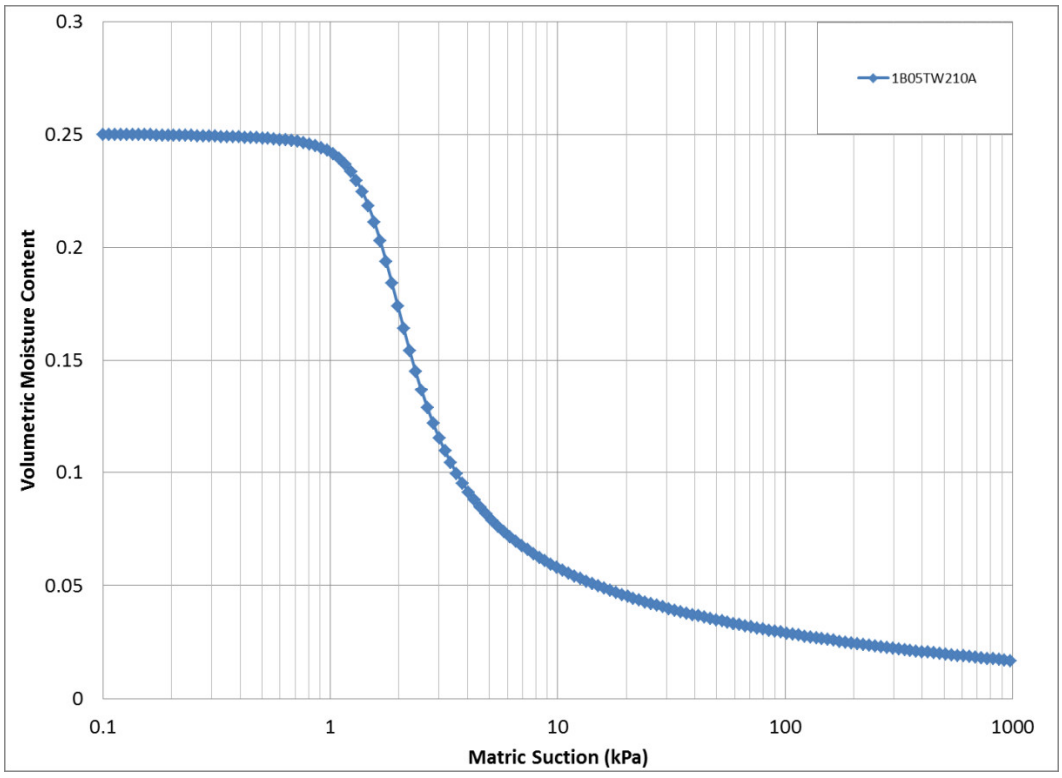

Figure 26 - Soil Water Characteristic Curves for Group F

Table 4.2 - Air Entry Value and Residual Saturation Values

Group Name	Classification (passing 4.75 mm)	Deconstruction PSD (75 mm)	AEV (kPa)	Residual Saturation (%)
Group A	0% to 10%	0	--	--
Group B	10% to 20%	1	0.1	10.74
Group C	20% to 30%	16	0.16	8.46
Group D	30% to 40%	73	0.36	6.64
Group E	40% to 50%	50	0.48	7.55
Group F	> 50%	1	1.23	4.18

4.3.2 Saturated Hydraulic Conductivity

A multimodal algorithm was used to fit an equation to the measured PSD data set. The resulting fitted equation was then used to determine the value of d_{10}, a parameter required for the estimation of saturated hydraulic conductivity, using the Chapuis (2004) method. This equation also requires the void ratio, which was calculated using a porosity of 0.25. The saturated hydraulic conductivity was then calculated for each sample in the data set. SVSoils has numerous estimation methods available for estimating the saturated hydraulic conductivity, and it was also used to calculate the Chapuis hydraulic conductivity. There were some differences between the two data sets, due to differences in d_{10}. SVSoils uses different techniques to curve fit PSD data, and will generate a different d_{10} value than the multimodal algorithm. Table 4.3 summarizes the K_{sat} values using the two different approaches.

Table 4.3 - Saturated Hydraulic Conductivity

Group Name	Classification (passing 4.75 mm)	Deconstruction PSD (75 mm)	Chapuis k_{sat} (m/s)	SVSoils Chapuis k_{sat} (m/s)
Total Data Set	--	141	3.0 E-04	2.5 E-04
Group A	0% to 10%	0	--	--
Group B	10% to 20%	1	1.4 E-04	1.6 E-03
Group C	20% to 30%	16	3.6 E-04	4.2 E-04
Group D	30% to 40%	73	3.0 E-04	2.8 E-04
Group E	40% to 50%	50	2.7 E-04	1.4 E-04
Group F	> 50%	1	1.5 E-04	9.0 E-05

4.3.3 Unsaturated Coefficient of Permeability using SVSoils

SVSoils also can estimate the unsaturated coefficient of permeability for soils. The software provides several empirical methods that can be used to estimate the relationship between the permeability and the change in saturation. For this study the Fredlund, Xing, and Huang (1994) estimation was used. The data was then grouped into the various size fractions and plotted (Figures 28 to 32).

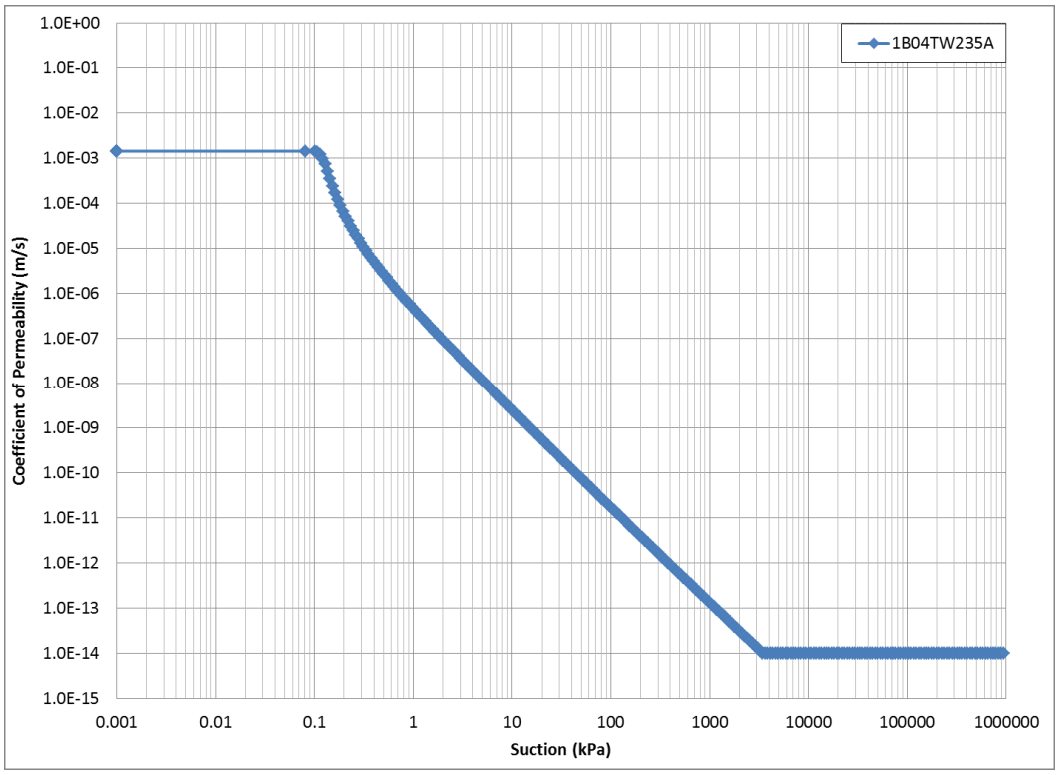

Figure 27 - Unsaturated Coefficient of Permeability for Group B

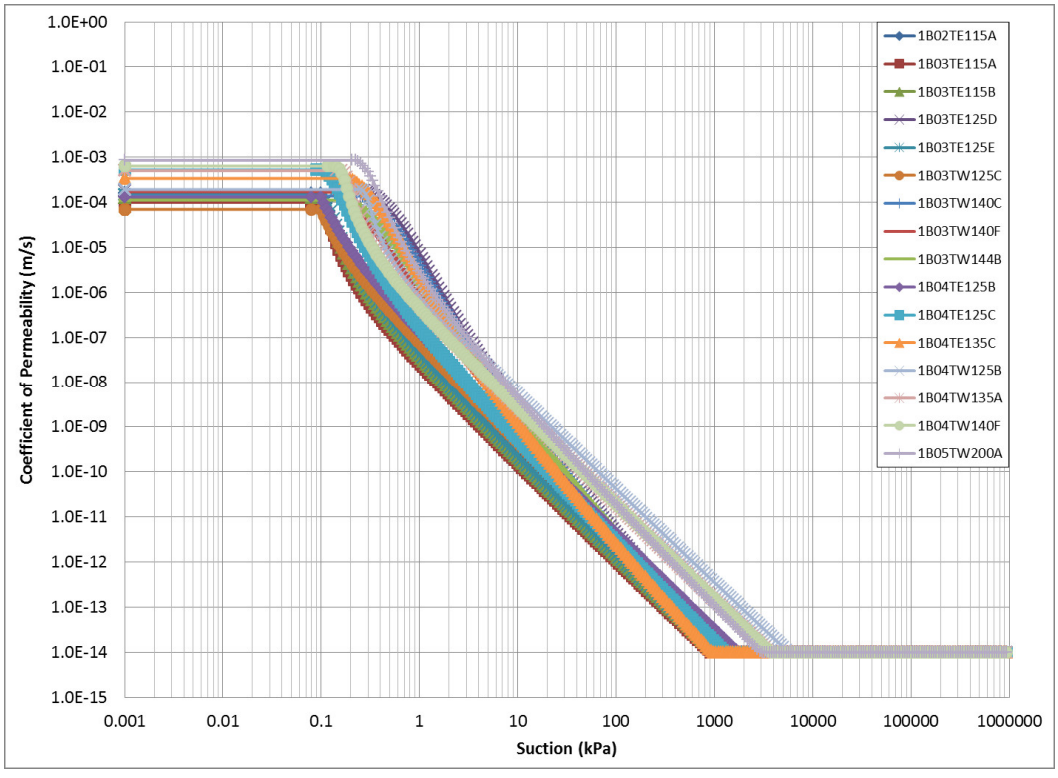

Figure 28 - Unsaturated Coefficient of Permeability for Group C

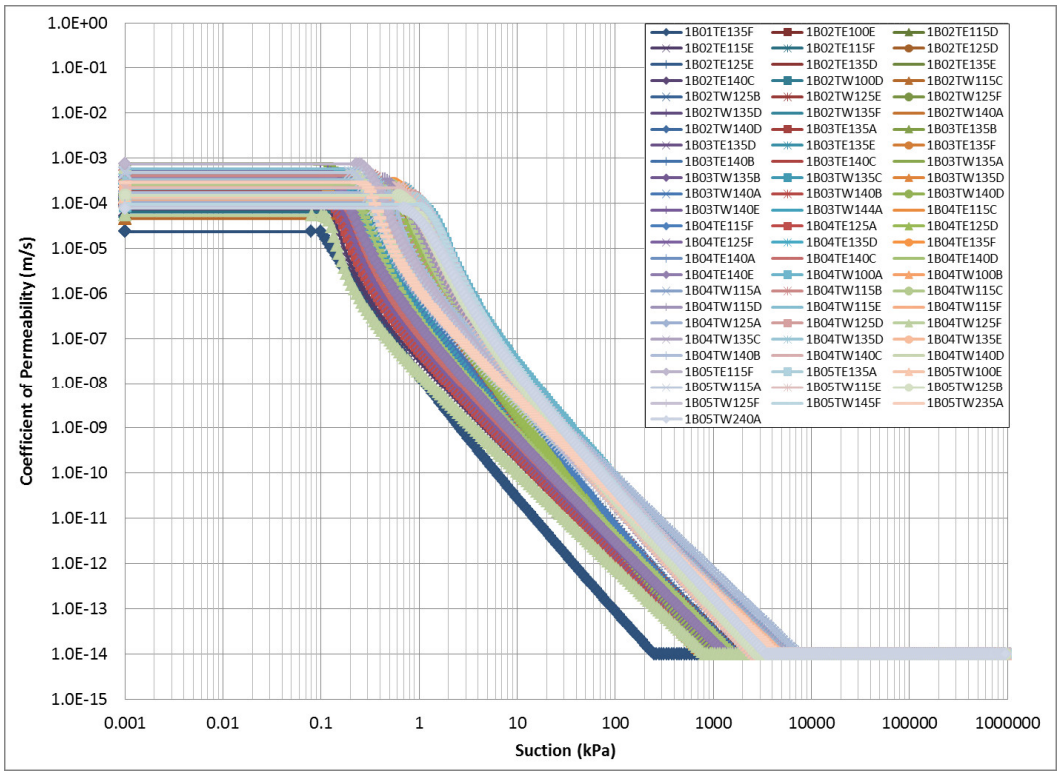

Figure 29 - Unsaturated Coefficient of Permeability for Group D

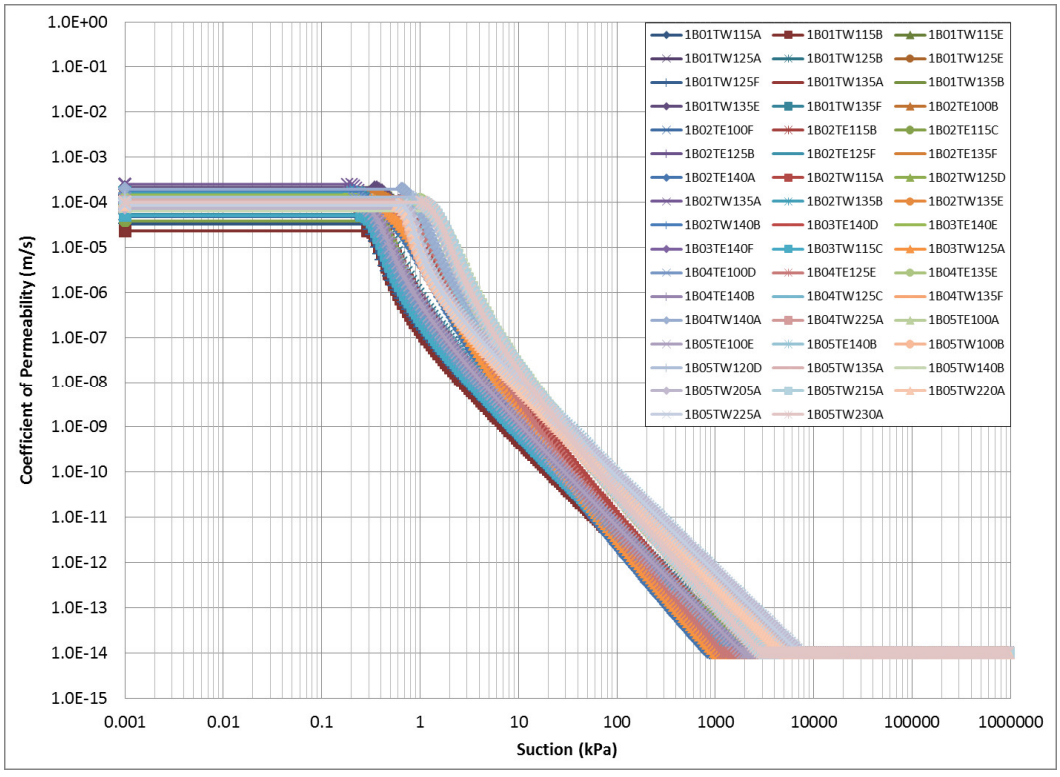

Figure 30 - Unsaturated Coefficient of Permeability for Group E

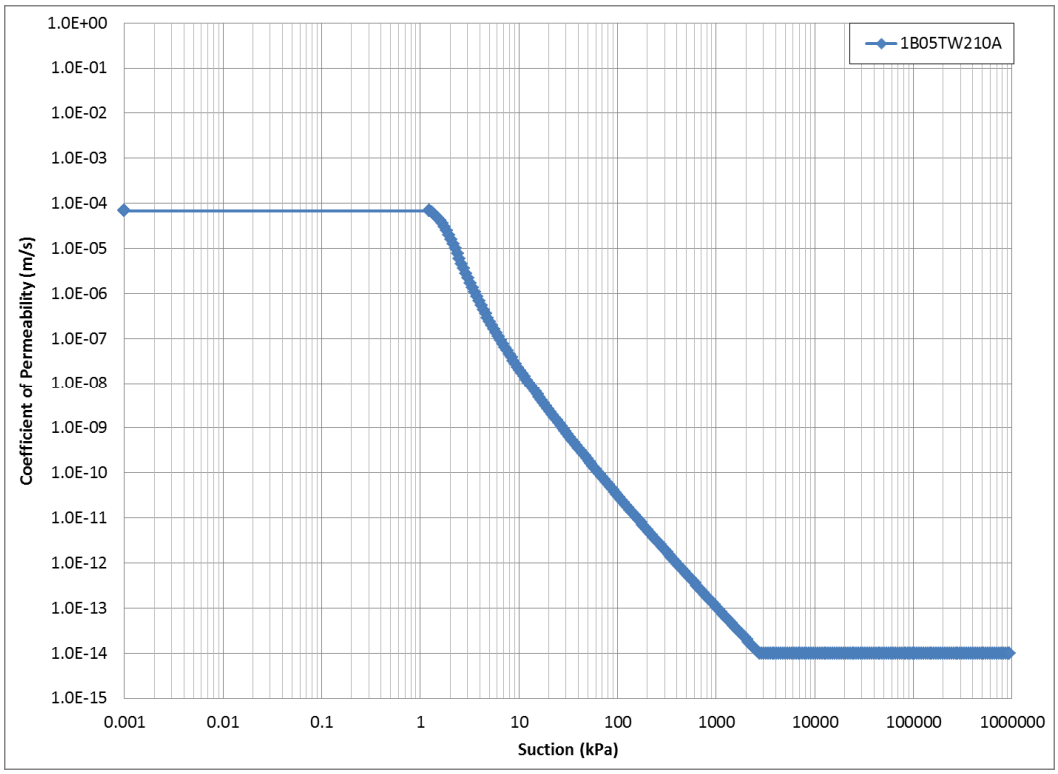

Figure 31 - Unsaturated Coefficient of Permeability for Group F

4.3.4 Water Storage Using SVSoils

SVSoils can also be used to estimate the volume of water that can be stored in the soil, over the range of suctions. This data may be useful in hydraulic studies of the pile, providing information for the determination of residence times, ice formation, and ARD reactions. The water storage data generated in SVSoils was divided into the various classification groups, and plotted (Figures 33 to 37).

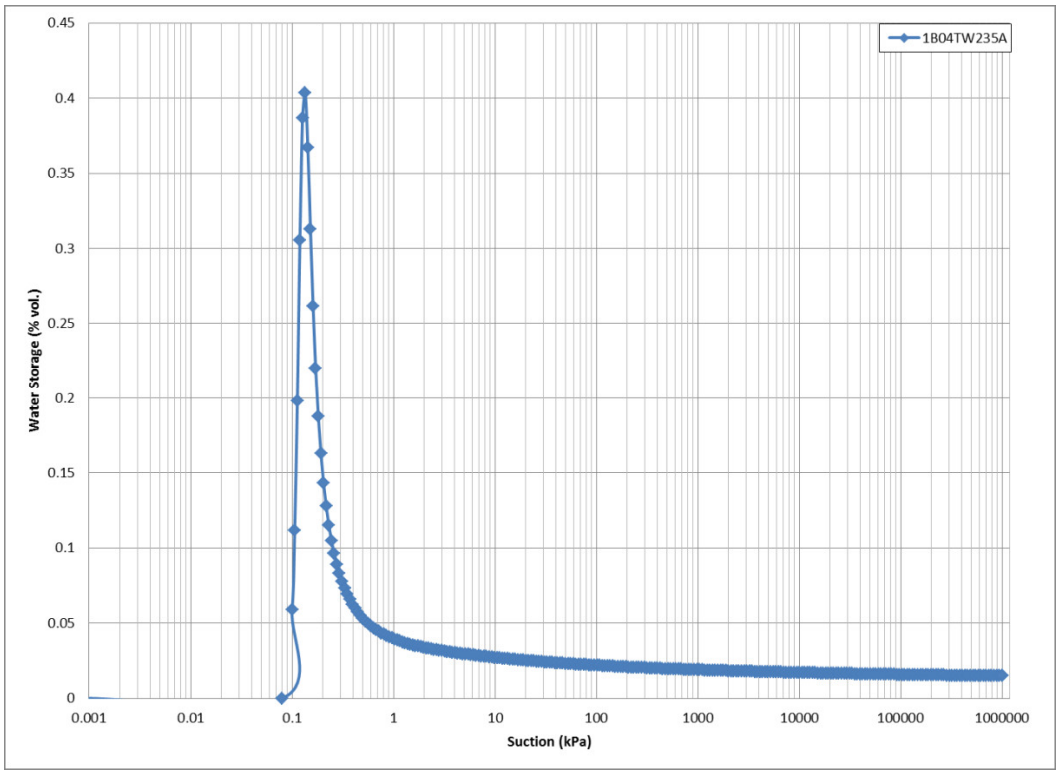

Figure 32 - Water Storage for Group B

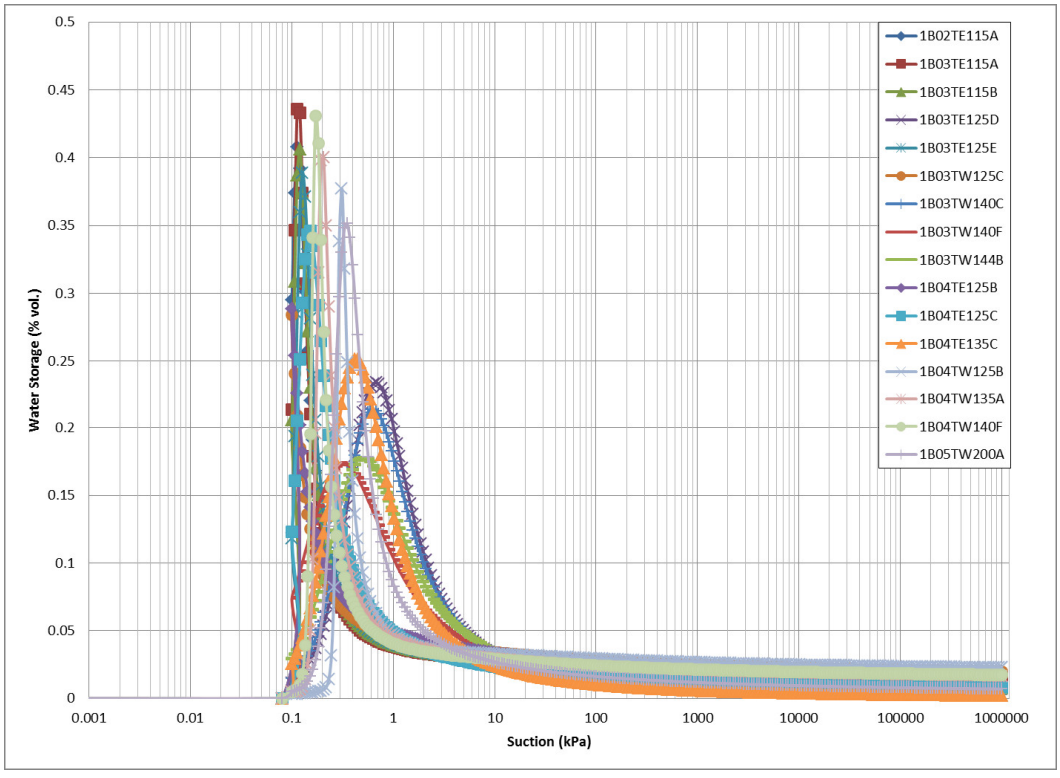

Figure 33 - Water Storage for Group C

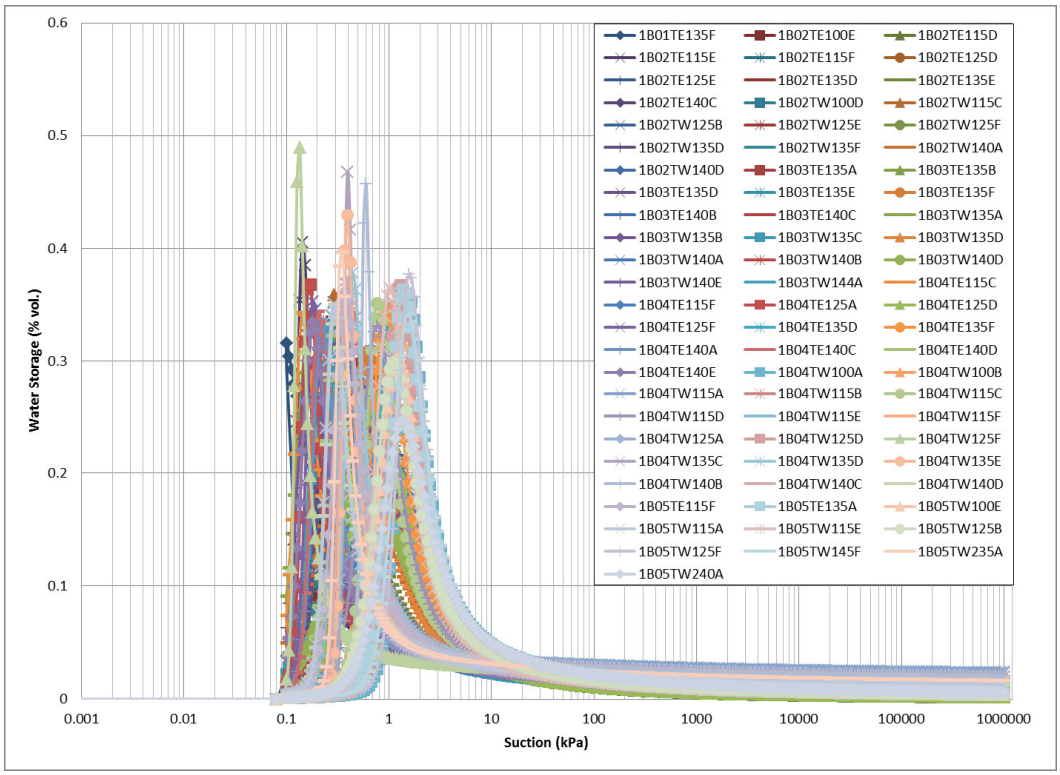

Figure 34 - Water Storage for Group D

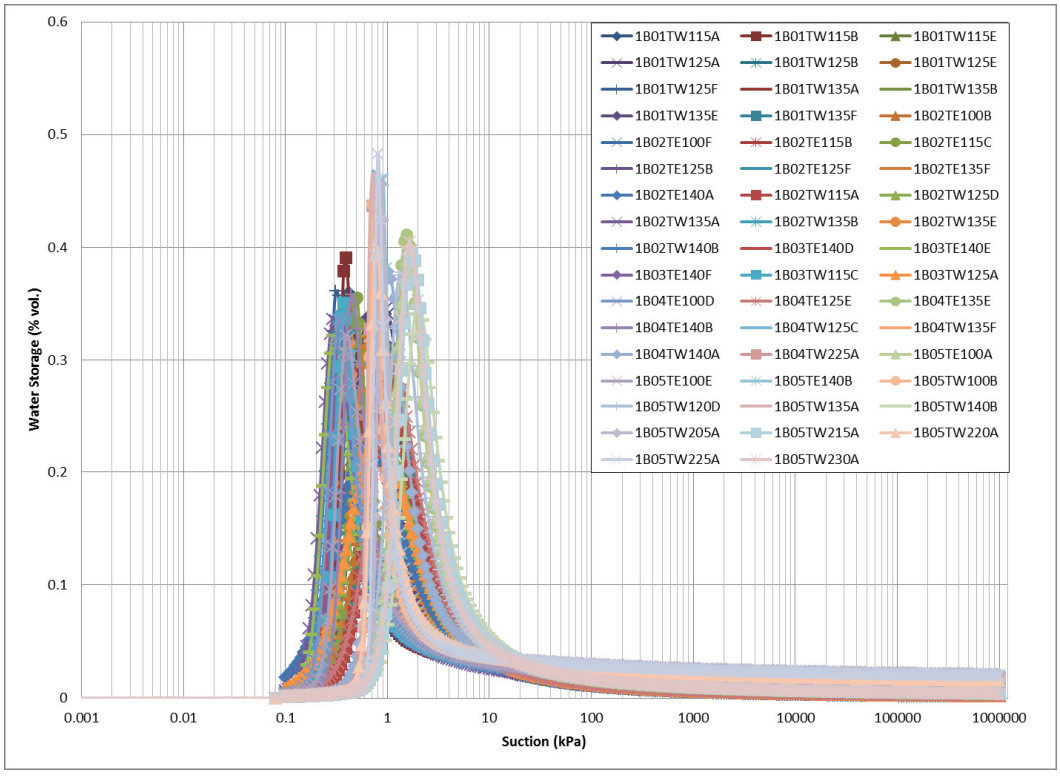

Figure 35 - Water Storage for Group E

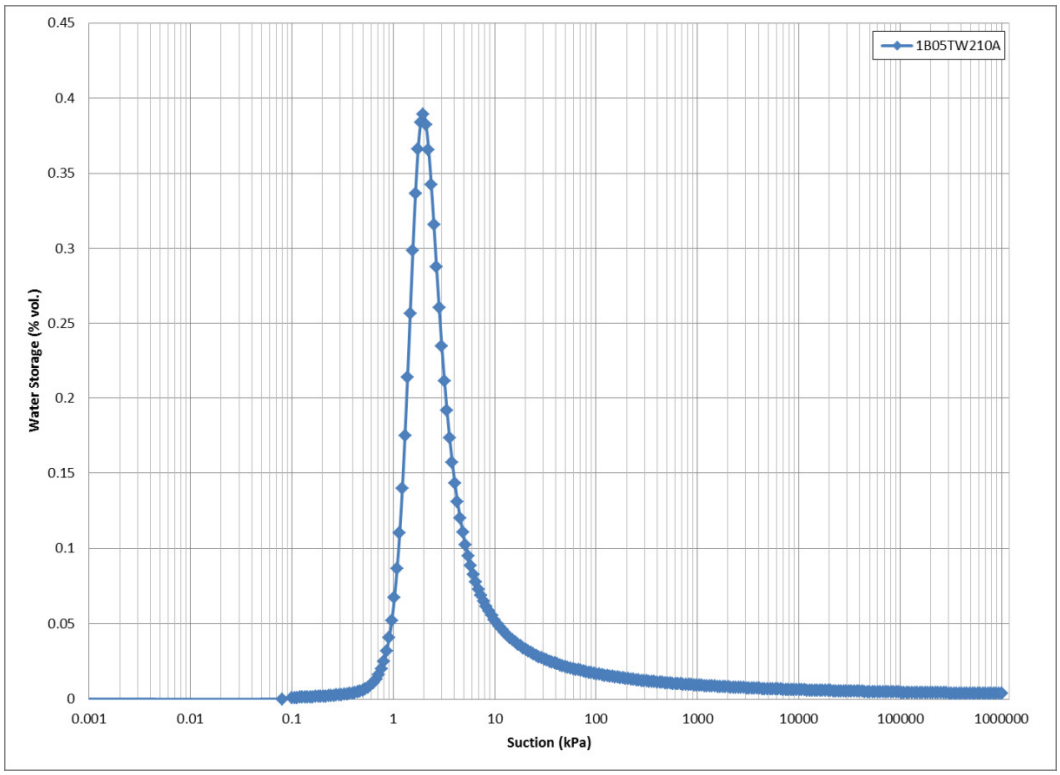

Figure 36 - Water Storage for Group F

5 Discussion of Results

The test piles research program has provided a unique opportunity to study a waste rock pile at several different stages of its life. During construction, and its early life, studies by Neuner (2009), Smith (2009), and Chi (2010) produced data sets that describe the material before and after placement. Instrumentation within the test piles collected data for several years, providing information on temperature, chemistry, moisture content, and gas concentrations. Finally, with the deconstruction, additional samples were collected to measure how the in situ properties have evolved. With respect to PSD, the various studies have all produced similar data sets, suggesting that the various methodologies have all been effective at collecting accurate data and that no particle breakdown has occurred. As such these data sets may be useful for further research into improved collection methods for PSD. The data collected during the deconstruction has also provided additional information on material segregation, and spatial variability within the Type I test pile. This chapter will include discussion of the results from the deconstruction PSD study, along with comparisons to previous studies at this site.

5.1 Previous PSD studies of the Type I Test Pile

Neuner (2009) and Smith (2009) were both involved with the construction of the Diavik test piles. Together they collected and shared PSD data from the Type I pile construction using similar methods (ASTM D422). They each produced their own sets of data based on the samples they chose to include in their respective studies. As described in earlier sections, a different testing standard was used during the deconstruction research program (ASTM D6913), following work by Cash (2014). The differences between the construction and deconstruction sampling methodologies are summarized in Table 5.1. The methodology used in the deconstruction program allowed for larger, more representative samples to be collected. Larger samples were chosen to enhance the future use of the PSD data, allowing it to be linked to imagery and remote sensing data, which are subject to a minimum resolution. Deconstruction samples were also collected systematically using a 3D grid. This allows the processed data to be linked to specific locations within the pile.

Table 5.1 - PSD Data Sets from the Type I Pile

Data Set	# of Samples	Sample Mass (kg)	Maximum Particle Size (mm)	ASTM
Deconstruction	141	70	75	D6913
Neuner (2009) Construction	197	10	100	D422
Smith (2009) Construction	66	5-10	50	D422

Chi (2010) followed the PSD work of Neuner and Smith at the Diavik Test Piles. His research used two dimensional image analysis to determine the PSD of the Type I and Type III test piles. He made use of a region growing algorithm with edge detection to map individual grains, allowing for the calculation of size, mass and surface area. The imagery was collected on the final as-built faces of the piles. Chi's data set allowed for the investigation of spatial variability in PSD on the pile outer faces. He concluded that particle size decreases non-linearly with depth, with fine grains being preferentially retained at the top. He was also able to calculate that the largest mass fraction was in the coarse material, while the greatest surface area was in the fines portion. By using empirical methods to estimate permeability he was able to compare his data set to permeability measurements collected with instrumentation in the pile. By comparing permeability as well as measured grain size data he was able to determine that they were similar, and that his methodology was valid.

5.1.1 Comparison Between Studies

The comparison of the data sets between construction and deconstruction has provided a unique opportunity to examine the material in a "pre-segregation" and "post-segregation" environment. During construction the Type I pile was push dumped. Material was brought by haul truck to the pile, and dumped near the crest. At this point, test pile researchers collected samples from the freshly dumped stockpile. Once the stockpile was sampled, heavy equipment would push it over the edge, and the material would segregate due to gravity. The pile was built out in a series of tip faces. Each of the major tip faces was lined with instrumentation strings, and covered over as the pile was built out further. The tip faces are really 3D zones, and not flat planes when considering PSD. Due to the push dump construction method the PSD samples were spread over a zone that is up to and including the face (Neuner 2009). Figure 38 illustrates the tip faces, and the zones they encompass, for the Type I pile. Some samples were also collected from the face using a man lift, but were deemed as

unrepresentative by Smith (2009). As such, the samples collected during the construction represent material that is not segregated, as they were collected from surface stockpiles.

The deconstruction samples were collected in place, and represent the material after segregation during pile construction. As samples were collected using a 3D grid they cannot be directly compared to the data from the construction, which was collected at the pile crest, then mixed into a tip face zone. In order to compare data from the deconstruction to the construction, small data sets from several profiles, and several benches must be included. Figure 39 illustrates the different sample location geometries used in the construction and deconstruction studies. Figure 40 illustrates how the data set is refined, in order to compare specific zones; in this case samples from Tip Face 4 are compared to samples from the deconstruction.

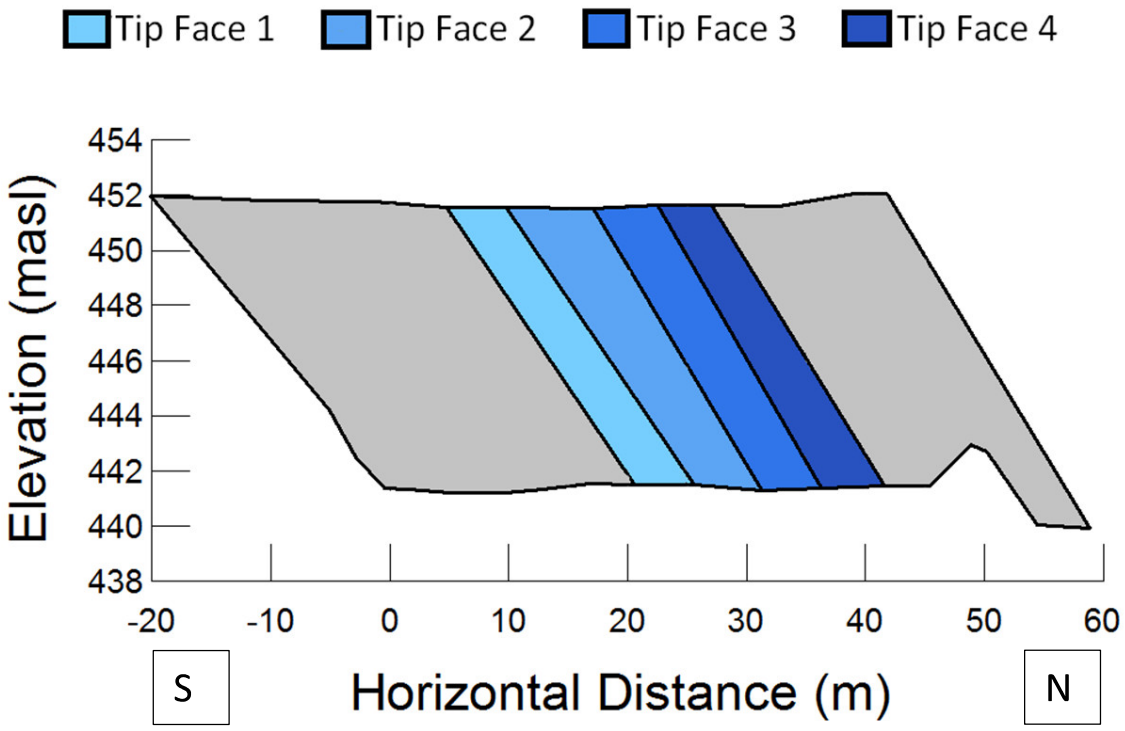

Figure 37 - Type I Pile Geometry with Tip Faces (blue shaded regions)

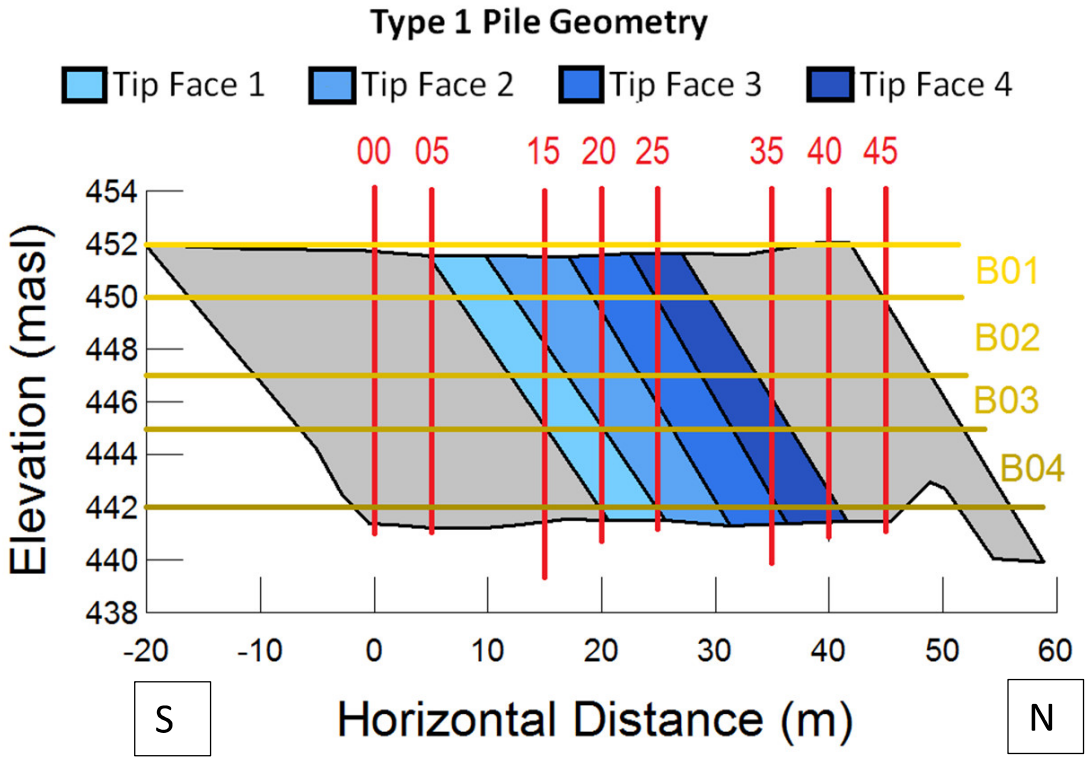

Figure 38 - Type 1 Pile Geometry with Deconstruction Profiles (red vertical lines) and Benches (gold horizontal lines)

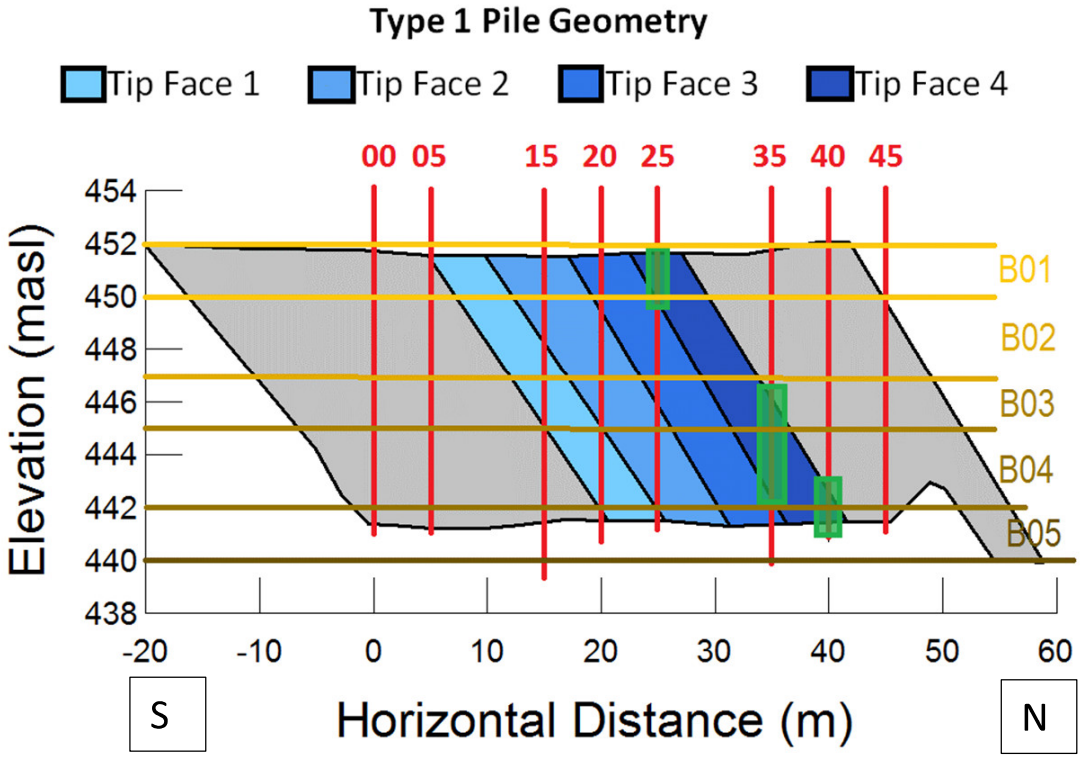

Figure 39 - Type I Pile with Paired Construction and Deconstruction Data (Green zones)

5.2 Material Segregation

One advantage of collecting samples using a 3D grid was that it allowed sample data to be associated with specific locations within the test pile. The PSD data set was divided in order to study the material segregation that occurred during placement. By dividing the data set into regions that represent the various benches that were excavated during deconstruction, trends could be examined with depth. In this portion of the analysis samples from Bench 5 were excluded. Many of the Bench 5 samples were collected at or below the base of the test pile, which was underlain by a layer of crush material placed to protect the geomembrane. As such, these samples were not representative of the waste rock, as they could have mixed with the crush layer.

The percent retained data from Benches 1, 2, 3, and 4 (top to bottom) were grouped into bins based on the particle sizes. The amount of each size fraction for each bench was then plotted, as presented in Figure 41. The histogram shows a general trend of material grading from finer to coarser with depth. The upper benches have higher proportions of finer material, while the lower benches have greater proportions of coarser material. This is the expected result; however this research provides a quantitative data set that shows where these differences occur, and by how much. The fine to coarse trend is clearly visible in most size fractions. It appears that medium sand, 50 mm gravel, and cobble size particles were affected the most by segregation with approximately 10% to 20% differences between upper and lower benches. The clay/silt size and the 25 mm gravel size saw very little change in their vertical distribution.

This analysis also reinforces how heterogeneous the waste rock pile is. The segregation does not simply divide the material into layers of differing material, as all size fractions are represented throughout the pile. The lower benches simply have more coarse material, which seems to get coarser with depth, and the upper benches have more fine material, which appears to get finer with elevation (see Figure 41). In addition to segregation, waste rock piles typically have some structure that includes dipping beds and traffic surfaces (see Figure 1) (Aubertin and Bussiere 2013). Based on the scale of the test pile being much smaller than a full scale pile, and the deconstruction methodology, the typical structure of a waste rock pile (i.e. Figure 1) was not observed in the test pile.

The PSD data collected by Neuner, and Smith during the construction of the test pile created a good base line description of the material. However, this data was collected prior to final placement, and does not represent the spatial variability of the placed material. Chi (2010) used image analysis

techniques on the final as-built faces of the pile. Chi's PSD data set had similar average values to the PSD data set produced by Neuner, but was able to capture a larger range of particle sizes within the test pile. Chi's data was also able to show that the material was segregated by gravity during placement. Using d_{50} values from multiple locations in each face, it was shown that there were greater proportions of coarser material with depth in the Type I pile. Chi's analysis could not always detect particles smaller than 200 mm due to the resolution of the images. He incorporated PSD data from Neuner (2009) to represent the fine fraction less than 200 mm.

Figure 40 - Vertical Segregation of PSD in Type I Pile

5.3 Spatial Variability

As detailed in earlier sections the deconstruction samples were collected along a 3D grid. Nodes were approximately 5 – 10 m apart on the north-south axis, 3 m apart on the east-west axis, and 2 – 3 m apart vertically. This grid sampling system allowed the data set to be broken down in to profiles (east-west plane), sections (north-south plane), and by bench (Figures 42 to 46). The material differences are not limited to vertically stacked layers. There is variability in material properties in all three dimensions. Numerous data sets were fit to the different 3D planes, to illustrate the spatial variability of material

properties, and also to look for trends that may identify preferential pathways for fluid flow. The data sets include saturated hydraulic conductivity, individual particle sizes, d_x values, and the Herasymuik classification.

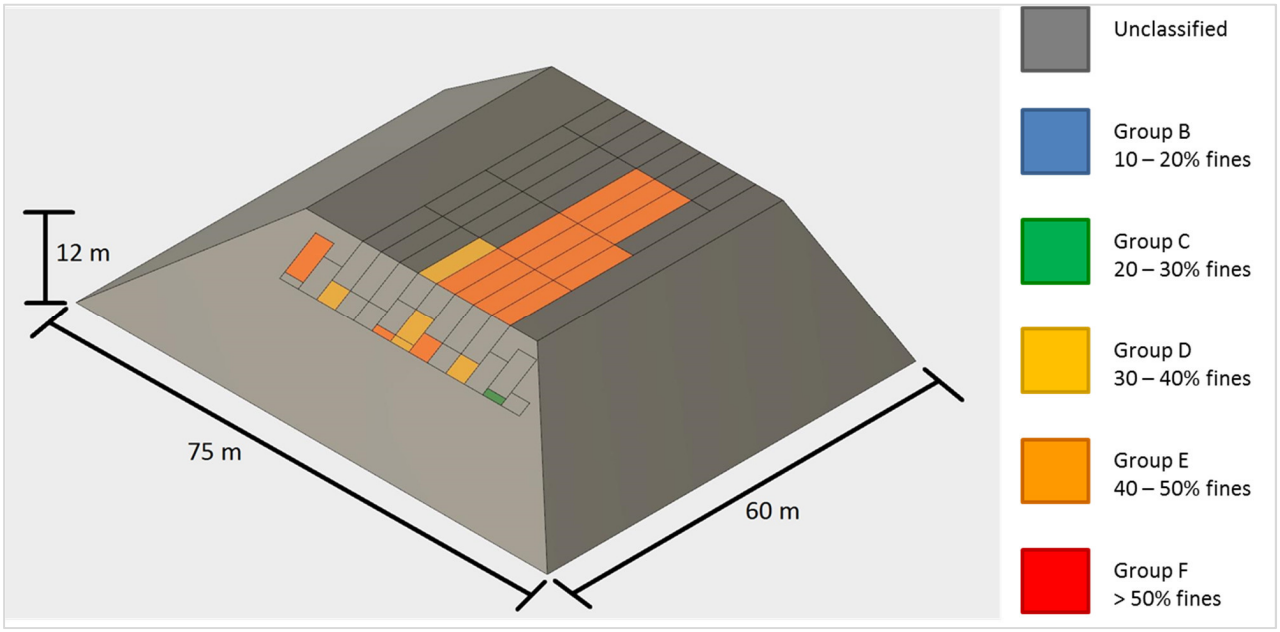

Figure 41 - Type I Test Pile with Herasymuik Classified Zones

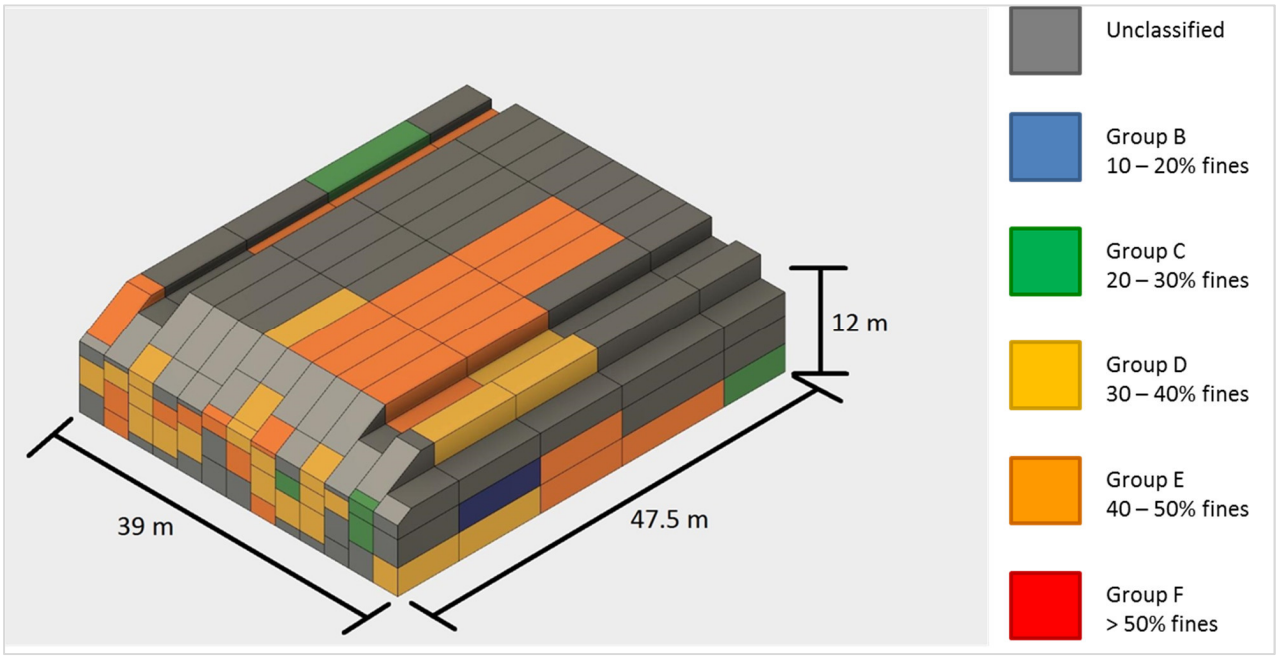

Figure 42 - Type I Test Pile Core with Herasymuik Classified Zones

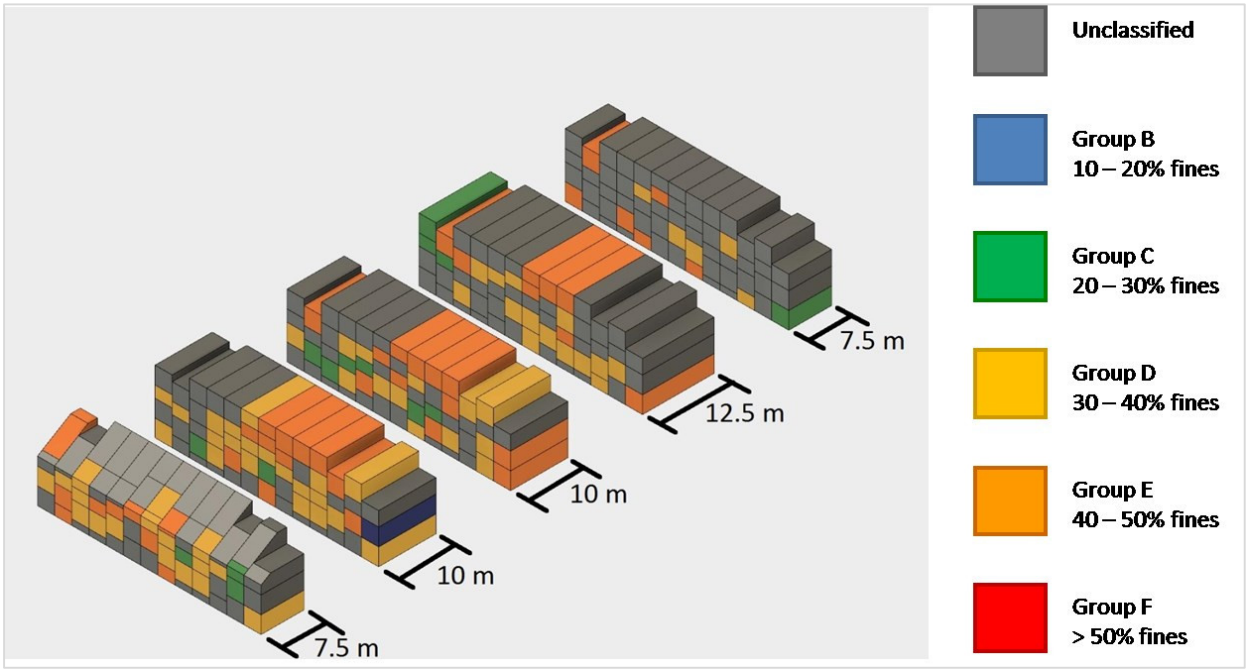

Figure 43 - Type I Test Pile Profiles with Herasymuik Classified Zones

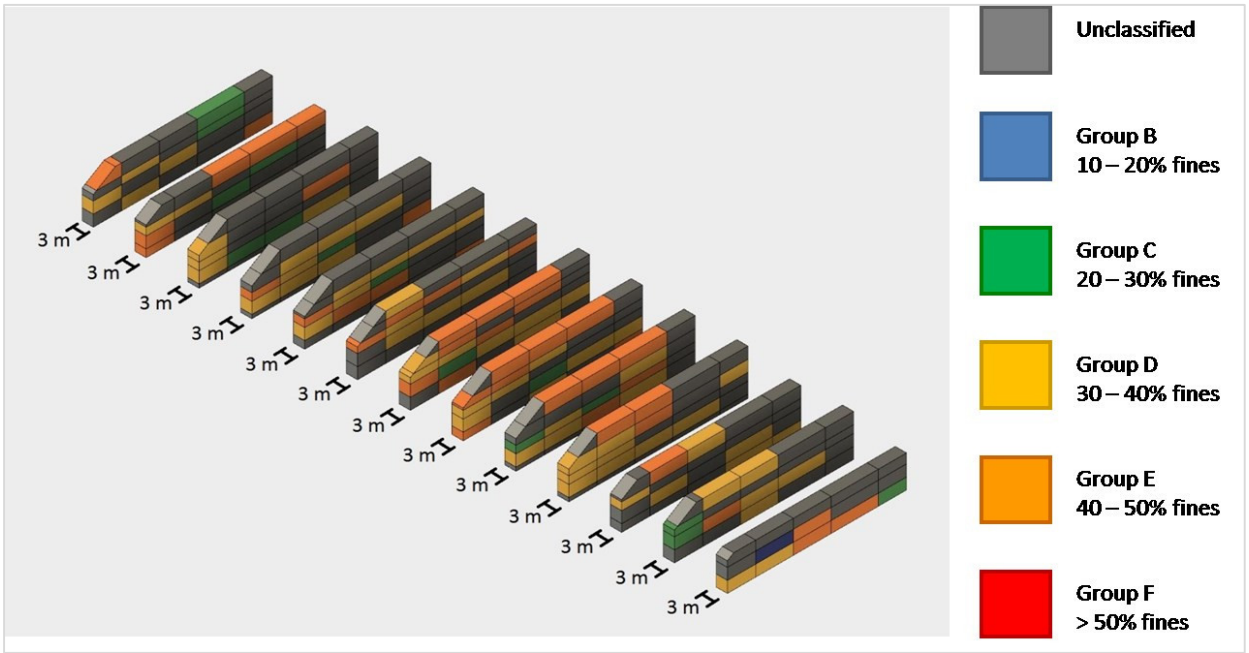

Figure 44 - Type I Test Pile Sections with Herasymuik Classified Zones

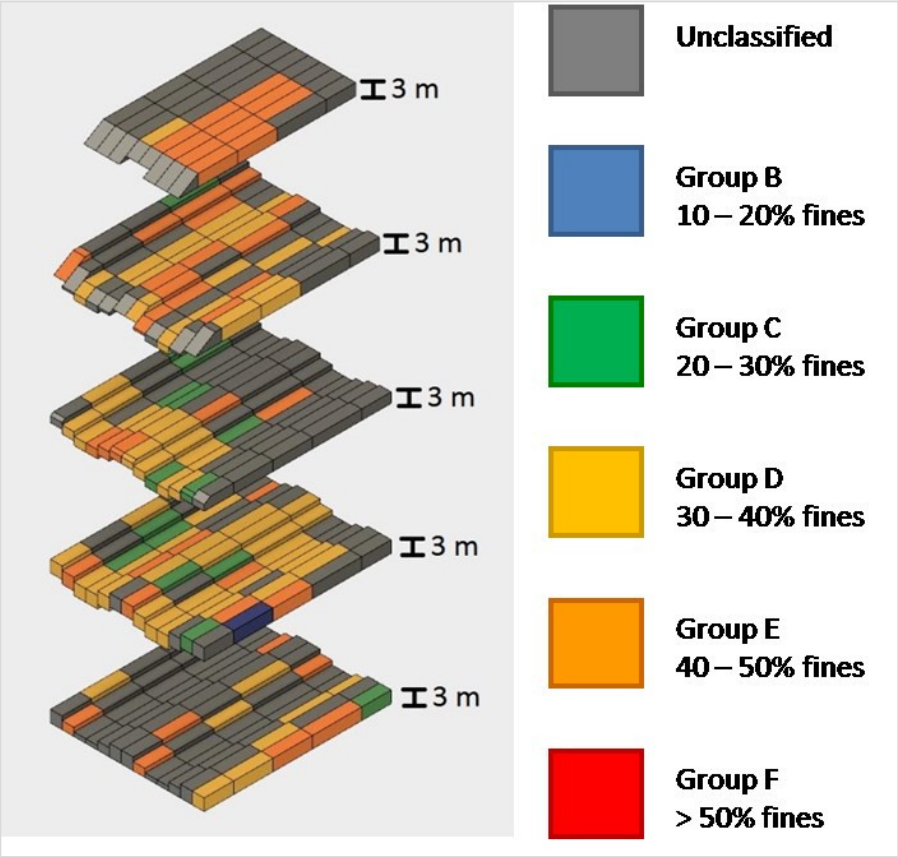

Figure 45 - Type I Test Pile Benches with Herasymuik Classified Zones

The regions shown in Figures 42 to 46 describe zones that are centered on the sampling location. The extents of each region are equivalent to half of the distance to the next sampling point. Sample spacing was very regular in the east to west, and vertical planes. The profiles were not as regularly spaced, causing some of the regions to be more elongate than others. Figure 47 illustrates the geometry of an example region where the sections and benches were 3 m apart, and the profiles were 10 m apart. The small, darker cube in the center represents the sampled volume for that region.

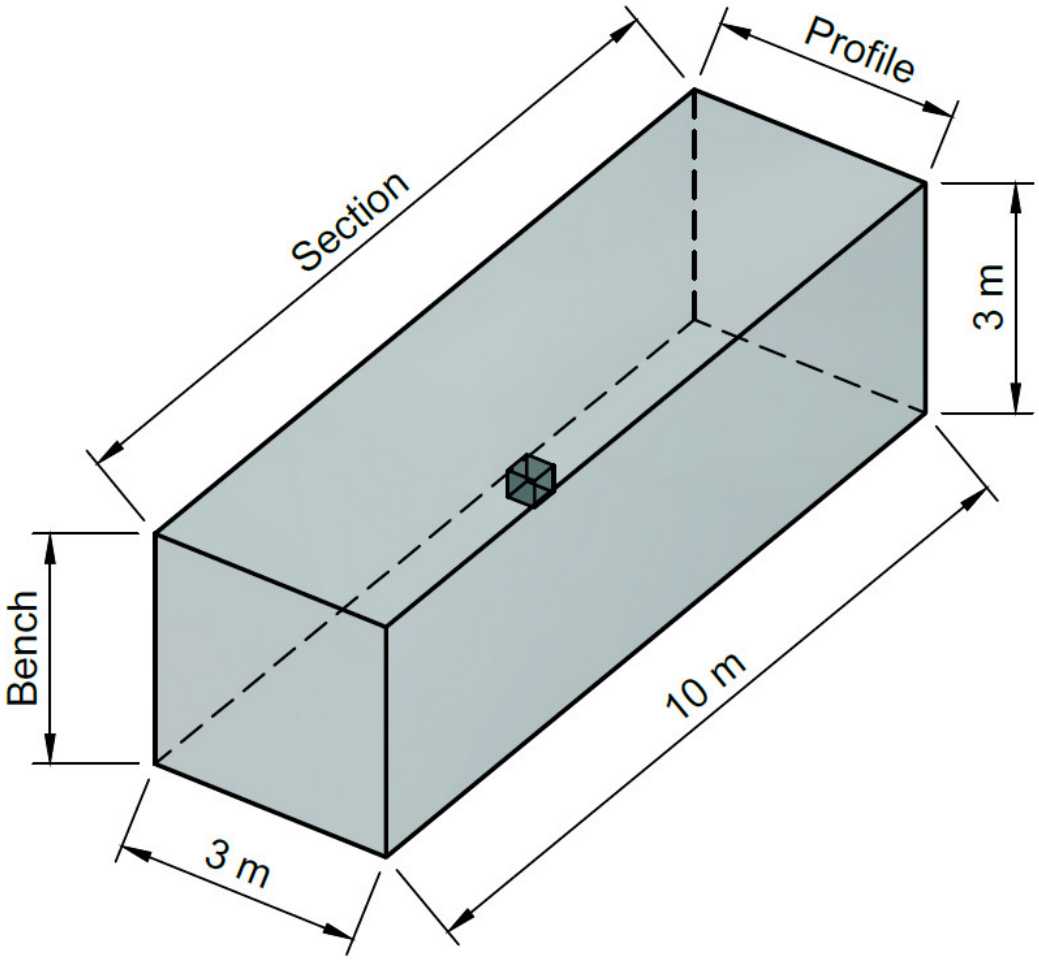

Figure 46 - Geomoetry of Sample Regions

5.3.1 Variability in Particle Size Distribution

The Herasymuik classification was used to group the PSD data into five groups (one of the six classifications had no samples). Figure 48 shows the average PSD curve for each of the five classifications. These average curves demonstrate how the PSD is expected to change between the various classification groups. Group B samples have the least amount of fines, and are dominated by coarser particle sizes. Group F samples show a much more even distribution of all particle sizes. When comparing the standard deviations between each group, there are cases with some overlap. However, the average values show that each classification has a distinct PSD. Table 5.2 shows the range in values for Groups C, D, and E. Groups B and F only have one sample each, and are not included in the table.

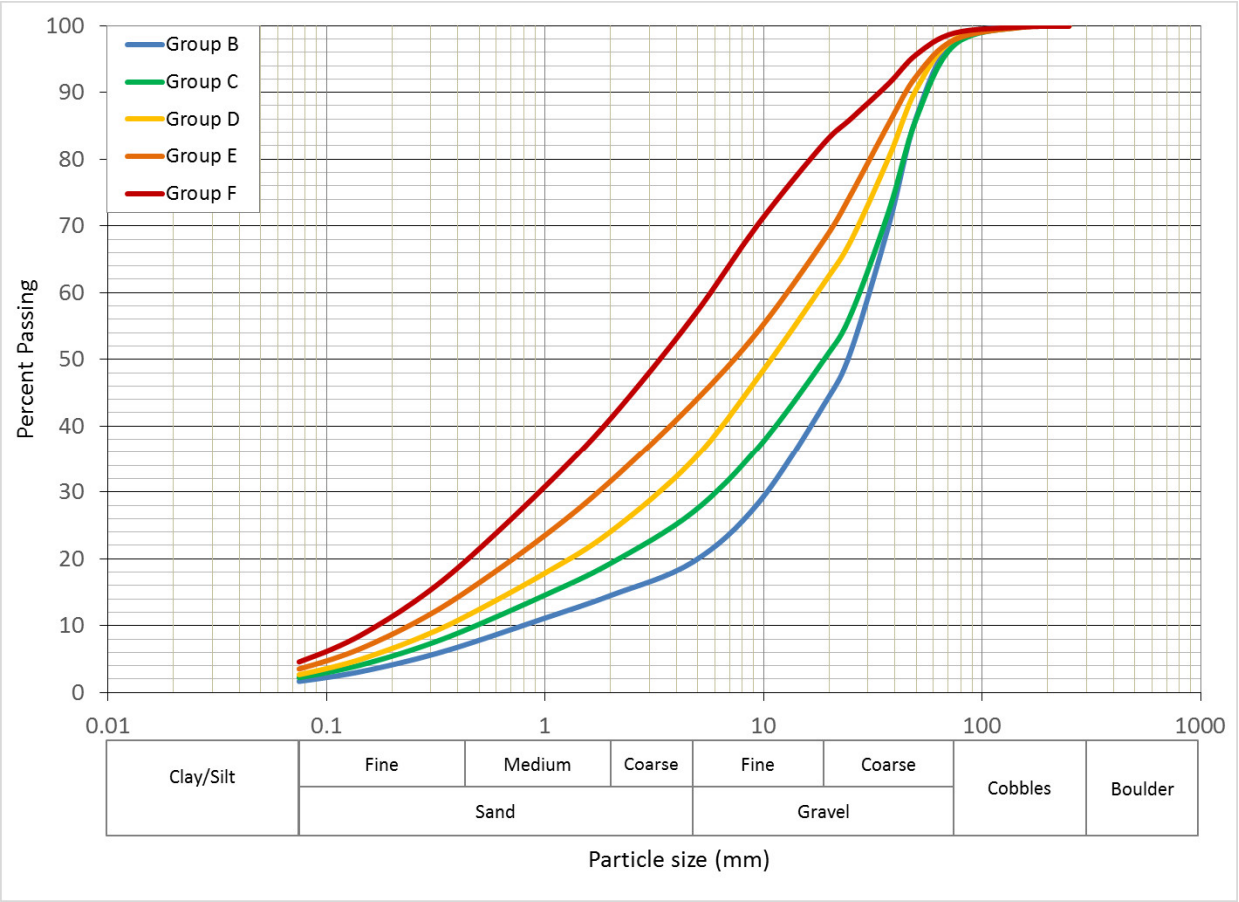

Figure 47 - Average PSD Curves for Herasymuik Classification Groups

Chi (2010) used image analysis on the external pile faces to determine PSD and observe trends in the data. Using d_{50} data he illustrated the segregation of the material, with finer material at the top surface, and coarser material towards the bottom. Plots of d_{50} were generated using deconstruction data points that lined up with Tip Faces 2 and 4. As seen in Figure 40 (earlier) only these two tips faces have good coverage of samples from the deconstruction. There are limited data points from the deconstruction data set that overlap with Tip Faces 1 and 3. Plots for these faces are not included in this comparison. The d_{50} for the 00m, 15m, 25m, 35m, and 40m profiles of the deconstruction data set were also plotted and compared with the plots by Chi (2010) (figure 49).

Table 5.2 - PSD Ranges for Groups C, D, and E

		Minimum	Maximum	Average	+1σ	-1σ
Group C	d10	0.34	0.82	0.51	0.64	0.38
	d30	4.80	11.26	6.52	8.39	4.65
	d50	11.48	30.15	19.22	23.94	14.51
	d60	18.70	38.66	28.05	33.27	22.83
	Cu	29.20	103.98	57.98	75.14	40.82
	Cc	1.83	9.25	3.20	4.96	1.44
Group D	d10	0.25	0.74	0.37	0.46	0.28
	d30	1.79	4.74	3.45	4.16	2.74
	d50	7.41	17.32	11.13	13.57	8.68
	d60	11.47	30.62	18.11	22.22	14.00
	Cu	22.97	81.83	50.72	64.26	37.17
	Cc	0.81	3.05	1.82	2.22	1.43
Group E	d10	0.18	0.29	0.24	0.27	0.21
	d30	1.28	2.25	1.76	2.03	1.49
	d50	5.31	11.07	7.74	9.42	6.06
	d60	8.63	18.29	13.16	15.93	10.40
	Cu	40.68	71.47	54.08	62.05	46.12
	Cc	0.60	1.88	1.02	1.34	0.70

The data sets could not be directly compared due to the location of the samples, as well as the available sizes. Chi's data set captured much larger particles by using image analysis, and presented a range in d_{50} from 10 to 400 mm. The deconstruction data set had a maximum particle size of 75 mm with a d_{50} range of 3.4 to 30.2 mm. Even though the size ranges are different, the same trends exist in both data sets. It appears that the upper pile has more fine material, and the size increases with depth, in both inclined and vertical profiles. Figures 49 to 56 give an example plot based on work by Chi (2010), and comparisons to the deconstruction data set.

Figure 48 - d_{50} Contours of the Type I North Face (after Chi (2010))

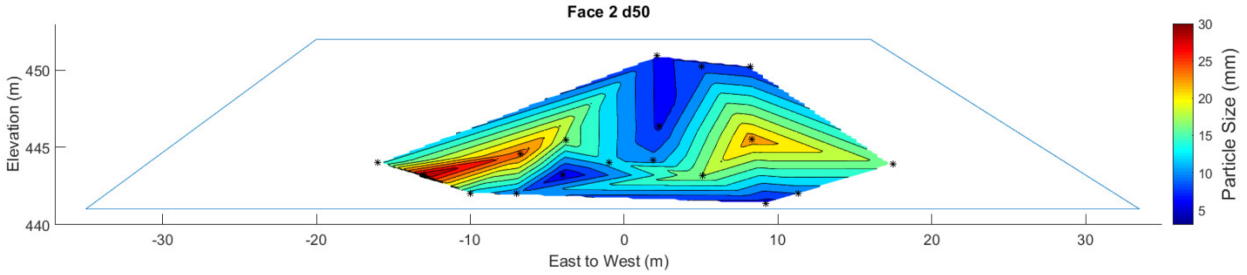

Figure 49 - d_{50} Contours of the Type I Tip Face 2

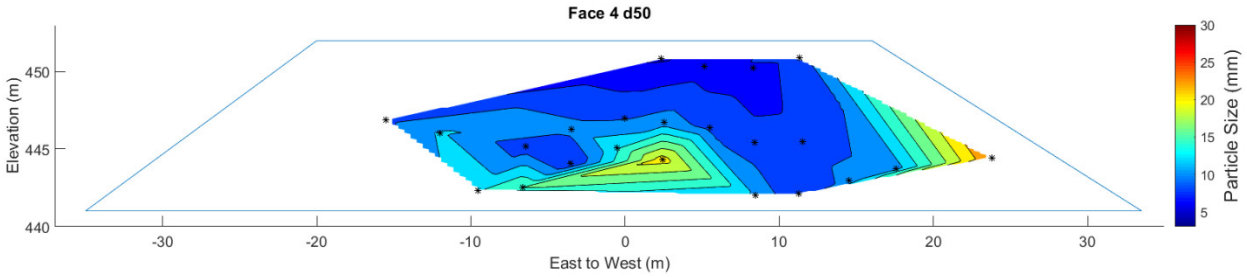

Figure 50 - d_{50} Contours of the Type I Tip Face 4

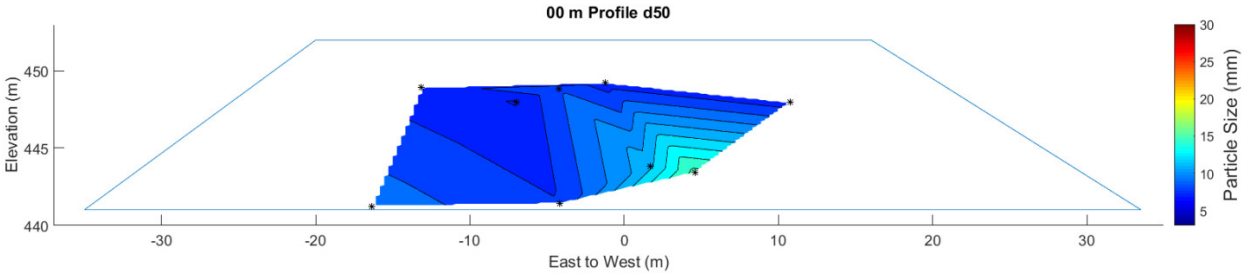

Figure 51 - d_{50} Contours for the 00m Profile

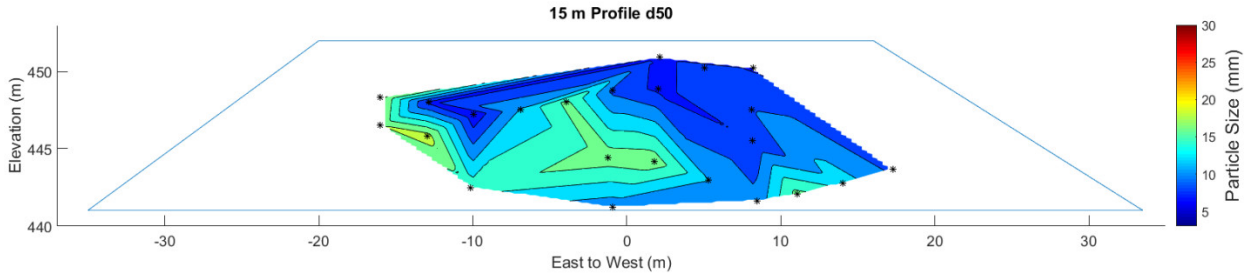

Figure 52 - d_{50} Contours for the 15m Profile

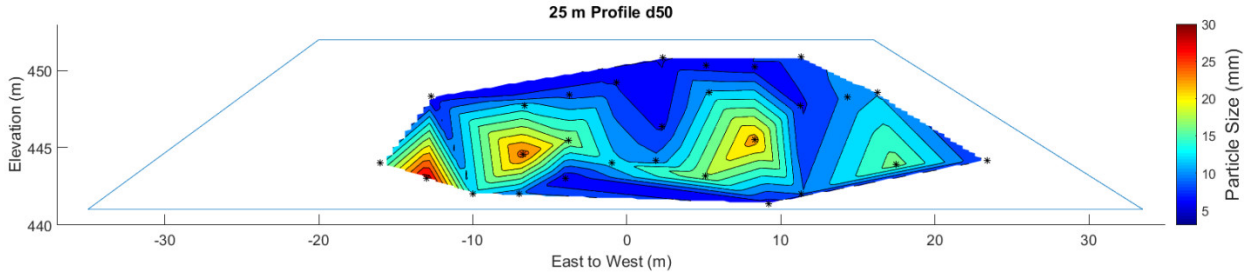

Figure 53 - d_{50} Contours for the 25m Profile

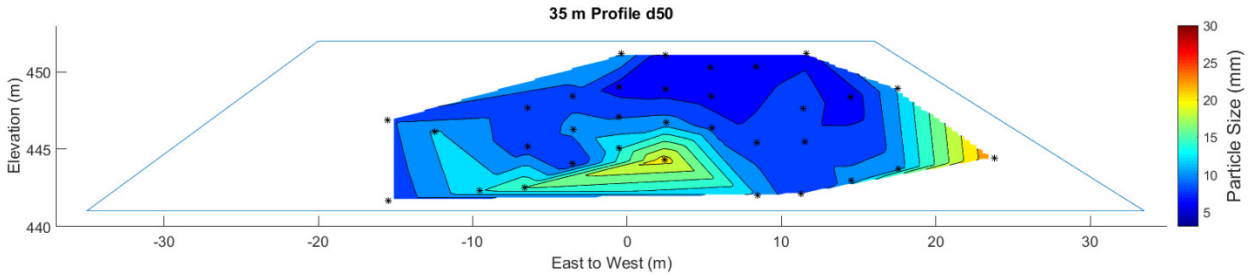

Figure 54 - d_{50} Contours for the 35m Profile

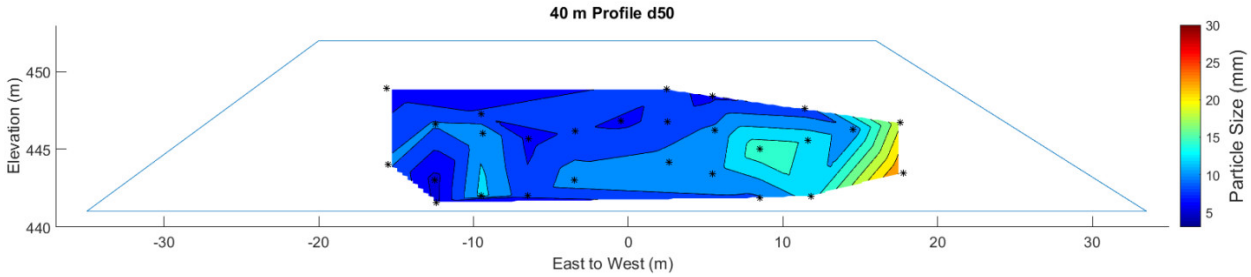

Figure 55 - d_{50} Contours for the 40m Profile

The classified zones can also be used to determine whether the material behaves in a soil like or rock like manner. Dawson and Morgenstern (1995) made the distinction between soil like and rock like materials based on the amount of material passing the 2 mm sieve. Materials with greater than 20% passing the 2 mm sieve behaved in a soil like manner, while materials with less than 20% passing the 2 mm sieve would show rock like behaviour. Herasymuik (1996) refined this definition on a basis of

capillarity, where material less than 4.75 mm is expected to retain water under suction. Materials with greater than 40% passing the 4.75 mm sieve (Groups E and F, colour orange and red) would behave in a soil like manner, Groups with less than 30% passing the 4.75 mm sieve (Groups B, and C, colours blue and green) would behave in a rock like manner, and materials with between 30 to 40% passing the 4.75 mm sieve (Group D, colour yellow) are in a transition zone between soil like and rock like (Figures 44, 45, 46).

The PSD data set from the deconstruction has materials that are soil like, rock like, and in the transition zone. Approximately 12% of the samples were rock like, while 36% were clearly soil like. Approximately 52% of the samples were in the rock like/soil like transition zone. These zones are likely clast supported, with much of the void space filled with fines. The fine zones would be more discontinuous than fine zones in a soil like material. This could increase water storage in these areas, as the fines would draw water in, but with a lack of material continuity, it may be difficult for the water to drain.

5.3.2 Material Variability Statistics

The PSD data demonstrates the heterogeneity that exists in the material of the Type I test pile. This is due to the large range of particle sizes and the tendency for material to segregate during placement. Statistical methods were used to analyze the PSD data set and determine some of the overall properties of the material. The data set was converted to the Udden-Wentworth scale, in order to compare results with those of Chi (2010). The Udden-Wentworth is a geological particle size scale, and can be seen in Table 5.3.

The converted data set was used to calculate the mean, standard deviation, skew, and kurtosis. The general equation for a moment is presented below; the specific equations for the calculation of these parameters are available in Appendix B. The mean presents the most common size fraction. The standard deviation gives a representation of the sorting of the material (< 0.7 = well sorted, 0.7 to 1 = moderately sorted, and >1 = poorly sorted). The skew and kurtosis provide information about the spread of data around the mean. Data can be skewed fine (positive skew) by being greater than the median or skewed coarse (negative skew) by being less than the overall median. The kurtosis is 1.0 when it represents a normal distribution, called mesokurtic. A kurtosis greater than 1.0 is called leptokurtic (excessively peaked), and a kurtosis less than 1.0 is called platykurtic (flat peak) (Lewis and McConchie 1994).

The median value of the measured sizes of the Udden-Wentworth scale is 0.5. From this data set it was found that the mean particle size was in the pebble range of the Udden-Wentworth scale that includes particles between 4 and 64 mm. The standard deviation indicates that the material is very poorly sorted. The material skews to the fine side of the distribution. It is leptokurtic, meaning that the data is more tightly clustered around the mean than a normal distribution. These data are plotted in Figure 58.

Chi (2010) presented similar statistics for PSD in the Type I test pile. He used image analysis techniques to determine the PSD for a range of larger particle sizes of two test piles at Diavik. An independent review of his reported data was used to determine statistical moments for just the Type I PSD data. Ultimately the statistics of his data set showed that mean particle size was in the cobble range (64 to 256 mm). By using image analysis techniques Chi was able to measure much larger particles than was possible with physical sampling during the deconstruction. This larger range in particle sizes explains the difference in mean particle sizes between Chi (2010) and the deconstruction PSD data sets. The standard deviation describes a very poorly sorted material. Chi's data is fine skewed, and leptokurtic. This could suggest that image analysis can better represent large or distinct particles similar to the cobble size range, while finer materials may blend together or be hidden by other particles, or shadows.

Due to the different sampling methods, these data sets cannot be directly compared. However, both data sets describe a material that is very poorly sorted, fine skewed, and leptokurtic, so we can determine that there is consistency at different scales.

$$n = \frac{\sum(f d^n)}{N}$$ Equation 15

Table 5.3 - Udden-Wentworth Geological Scale

Millimeters (mm)	Phi (ϕ)	Wentworth Size Class
4096	-12.0	
		Boulder
256	-8.0	----------
		Cobble
64	-6.0	----------
		Pebble
4	-2.0	----------
		Granule
2.00	-1.0	----------
		Very Coarse Sand
1.00	0.0	----------
		Coarse Sand
0.5	1.0	----------
		Medium Sand
0.25	2.0	----------
		Fine Sand
0.125	3.0	----------
		Very Fine Sand
0.0625	4.0	----------
		Coarse Silt
0.031	5.0	----------

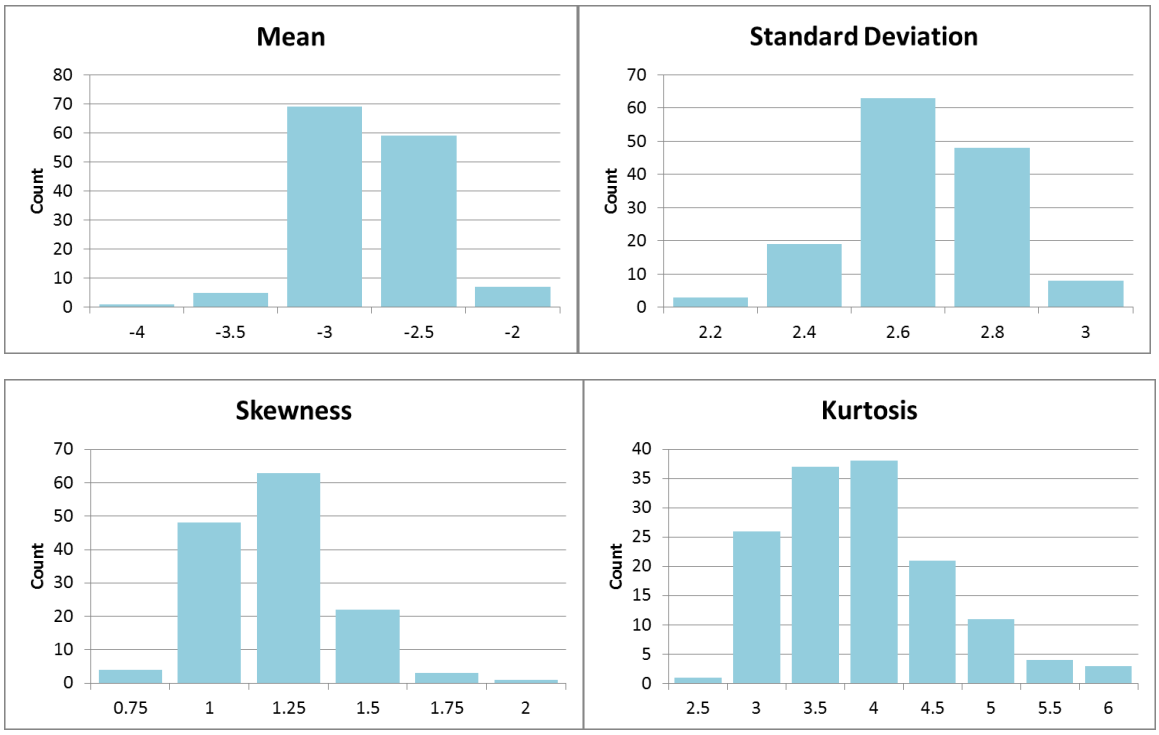

Figure 56 - Statistical Moments of PSD for Type I Pile Deconstruction

5.3.3 Variability in Soil Water Characteristic Curves

As described in earlier sections, the SWCC was estimated for each sample using SVSoils. The SWCC describes the moisture content versus the suction. The average values for each classification group are shown in Figure 59. The initial break in the curves moves steadily to the right with each classification group. This suggests that each group will see an increase in the AEV. This trend reflects the changing proportion of the largest particles in each group. Group B has the fewest fines, and it would be expected that it also has the largest voids. Group F has the largest amount of fines, and would have the fewest large voids. The large voids will drain first, and with more large voids in a sample it is expected that drainage will happen sooner, at lower suction values.

While the average values demonstrate this trend nicely, it should be noted that there is still overlap in the data between classification groups. In Groups C, D, and E – which are well populated – the minimum AEV value is similar. However, the maximum value increases in each group, reflecting the previously discussed trend. This is likely explained by the fact that the groups are classified based on one value, the percent passing the 4.75 mm sieve. The ratio of various sizes above and below that threshold can occur in any number of combinations that will affect the pore sizes and distribution. This in turn will affect how the drainage is estimated, and the corresponding SWCC that is generated.

The tail of the SWCC curves can be used to estimate the residual saturation of the material. The groups appear to decrease in saturation from B to F, with the exception of D and E. The decreasing trend would assume that group E has a lower residual saturation than group D. However, in this case group E has a higher residual saturation than group D. The estimated SWCC curves show a high degree of overlapping values at the tail end, when viewed as a whole. Table 5.4 lists the spread of residual saturation values for each group. Herasymuik (1996) also found that groups with 30 to 39%, 40 to 49%, and greater than 50% passing the 4.75 mm sieve all had similar values of residual saturation (at 100 kPa). It was suggested that this was due to the amount of fines in each group being high enough to restrict further drainage to the smaller pore spaces. Based on these two data sets, it is difficult to conclude that the classification groups can be used to determine appropriate ranges for residual saturation. The amount of overlap in the deconstruction data set suggests that the entire range of residual saturation values may be valid for any classification group. Measurement of the SWCC from field samples could help to better define the range of residual saturation values as compared to the estimated values.

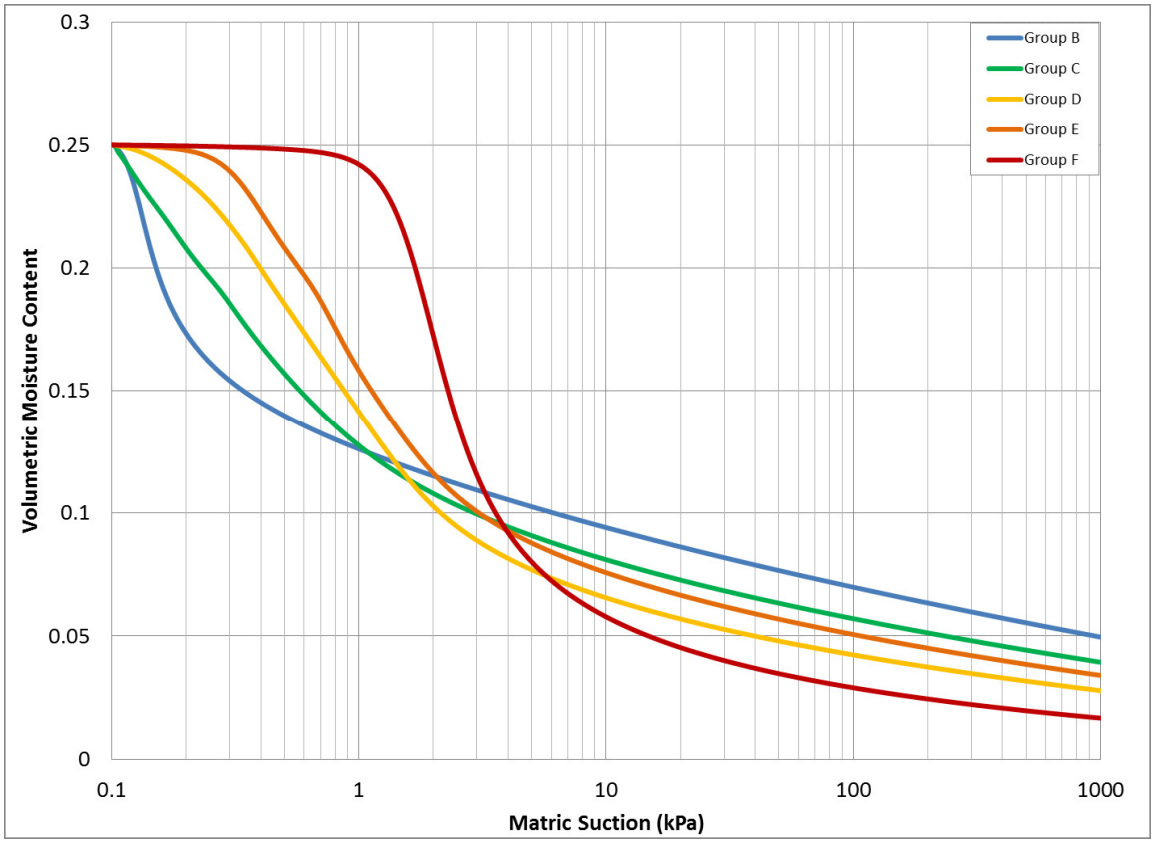

Figure 57 - Average SWCC's for Herasymuik Classification Groups of the Type I Test Pile

The estimation software is also working with a given porosity value of 0.25, as discussed in earlier sections. In reality each sample would have a unique porosity value based on its PSD, location, and deposition. The porosity value will change the initial saturation. This would shift the beginning of the curve upwards or downwards. Such a shift could affect the AEV, and the residual saturation values. Porosity measurements for each sample were not collected as part of this research, due to the difficulty in collecting this data quickly in the field.

Table 5.4 - Residual Saturation Data Spread by Group

Group Name	Average (%)	Minimum (%)	Maximum (%)
Group B	10.74	--	--
Group C	8.46	3.55	13.73
Group D	6.64	3.13	13.81
Group E	7.55	3.06	12.69
Group F	4.18	--	--

5.3.4 Variability in Hydraulic Conductivity

The saturated hydraulic conductivity was estimated using the Chapuis (2004) method. Manual estimations were done using data from the multimodal data set, and a second set of estimations were done using SVSoils. There were minor discrepancies in the results between the two data sets. The differences arise from differences in the d_{10} value between the two data sets. The deconstruction data set was processed using a multimodal curve fitting approach. SVSoils can use a unimodal or bimodal curve fitting approach. These different methods will fit the data differently, and produce different values for d_{10}. The data spread for each estimation method, for each classification group is summarized in Table 5.5. The table shows the average value for each group, as well as the minimum and maximum extents. It also shows the difference between the two estimation methods, where a negative value represents a larger result from SVSoils, and a positive number represents a larger result from manual estimations. The minimum and maximum difference values are for the group, and not a calculation between the maximum and minimum K_{sat} values listed in the table.

The manually estimated values show a decreasing trend among the average values from 10.4 $x10^{-4}$ m/s in Group B, down to 9.0 $x10^{-5}$ m/s in Group F. This result is expected, as greater amounts of fine material will decrease the K_{sat}. The K_{sat} from manual estimations varies by approximately one order of

magnitude between Group B and Group F. The K_{sat} estimations generated by SVSoils did not have as clear of a trend. The SVSoils data varied from a high of 3.3 $x10^{-4}$ m/s in Group C, to a low of 7.0 $x10^{-5}$ m/s in Group B. One possible reason for the spread in SVSoils data set may be from the curve fitting method used by the software. The program can use a unimodal or bimodal approach when fitting the PSD data. When applied to the entire data set, some samples had a tighter fit (R value closer to 1) with the unimodal method, while the others had a tighter fit from the bimodal method. Each method will fit portions of the PSD data differently, affecting the resulting d_{10} value. This may have caused the lack of a clear trend in the SVSoils K_{sat} data, by introducing greater variation. The differences between the manual and SVSoils K_{sat} data are generally within the same order of magnitude, with the manual estimations giving a larger value in four of the five classification groups.

Table 5.5 - Chapuis Ksat Values for Herasymuik Classification Groups

Classification Group	Chapuis Ksat	Average	Minimum	Maximum
Group B	SVSoils (m/s)	7.0 E-05	--	--
	Manual (m/s)	1.0 E-03	--	--
	Difference	9.7 E-04	--	--
Group C	SVSoils (m/s)	3.3 E-04	1.1 E-04	1.1 E-03
	Manual (m/s)	5.4 E-04	2.8 E-04	1.1 E-03
	Difference	2.1 E-04	-4.1 E-04	9.0 E-04
Group D	SVSoils (m/s)	2.4 E-04	4.0 E-05	7.5 E-04
	Manual (m/s)	3.2 E-04	1.7 E-04	9.4 E-04
	Difference	9.0 E-05	-4.5 E-04	5.0 E-04
Group E	SVSoils (m/s)	2.7 E-04	3.0 E-05	1.6 E-03
	Manual (m/s)	1.8 E-04	1.0 E-04	3.1 E-04
	Difference	-9.0 E-05	-1.5 E-03	1.5 E-04
Group F	SVSoils (m/s)	9.0 E-05	--	--
	Manual (m/s)	9.0 E-05	--	--
	Difference	9.0 E-05	--	--

The manual estimation data set was plotted to illustrate a visual approximation of saturated hydraulic conductivity throughout the Type I test pile. Plots are shown for Faces 2 and 4, along with Profiles 00m, 15m, 25m, 35m, and 40m in Figures 60 to 66. The zones of differing conductivity will be a controlling factor in how and where water moves in the pile. This will affect residence times, oxidation rates, and environmental loading. Faces 2 and 4 are presented as they can be directly compared to previous

studies and previous instrument data sets of the Type I test pile, as they follow the orientation of two of the instrumented tip faces. Neuner (2009) used Type I material in a 16 m^3 field permeameter test, and found that the material had an average K_{sat} of 0.01 m/s. He found that this measurement was similar to air permeability measurements in the Type I pile, and other waste rock materials at other sites. He reported the mean K_{sat} for 18 samples of finer than 5 mm was 2.0 $x10^{-5}$ m/s. There were no meaningful differences in K_{sat} between the samples, with the exception of near surface samples. Samples collected near the surface of the Type I test pile after construction was complete had K_{sat} values that were smaller by approximately one order of magnitude (Neuner 2009).

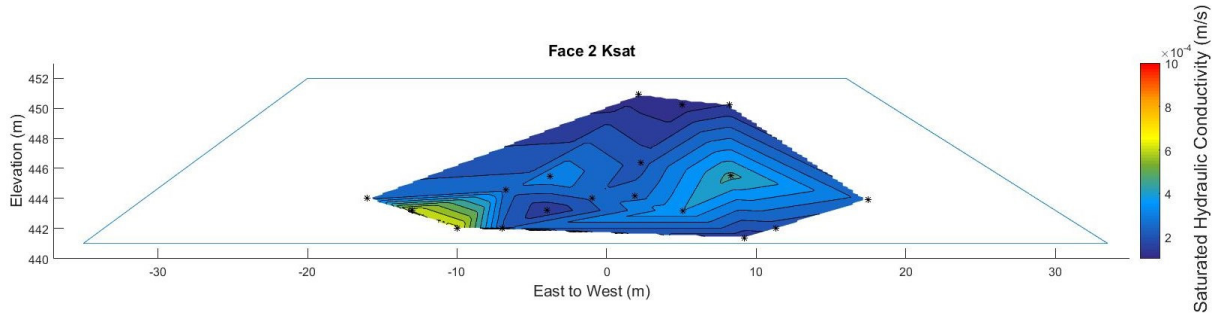

Figure 58 - Saturated Hydraulic Conductivity Contours for Face 2 of the Type I Test Pile

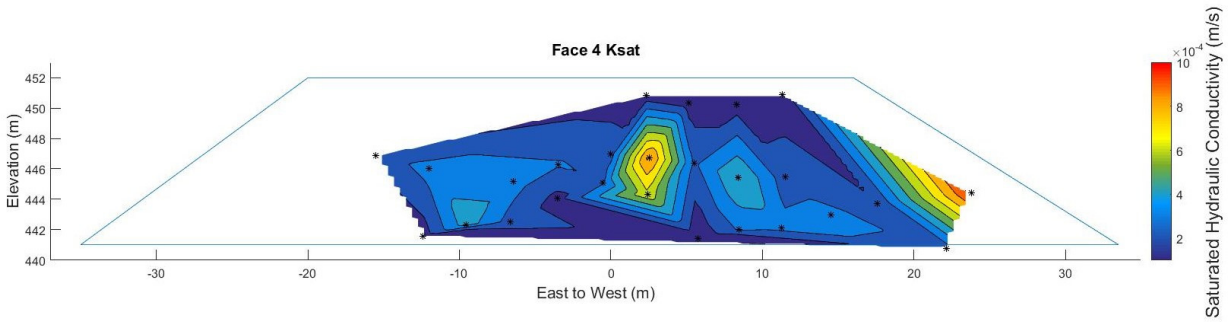

Figure 59 - Saturated Hydraulic Conductivity Contours for Face 4 of the Type I Test Pile

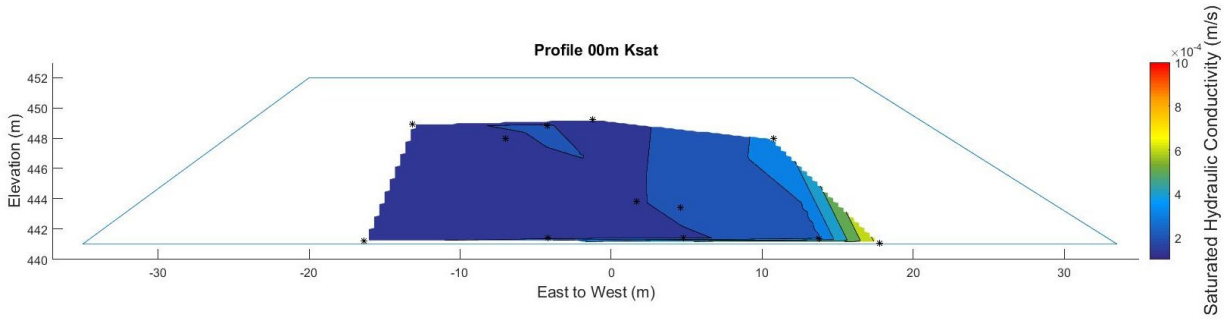

Figure 60 - Saturated Hydraulic Conductivity Contours for Profile 00m of the Type I Test Pile

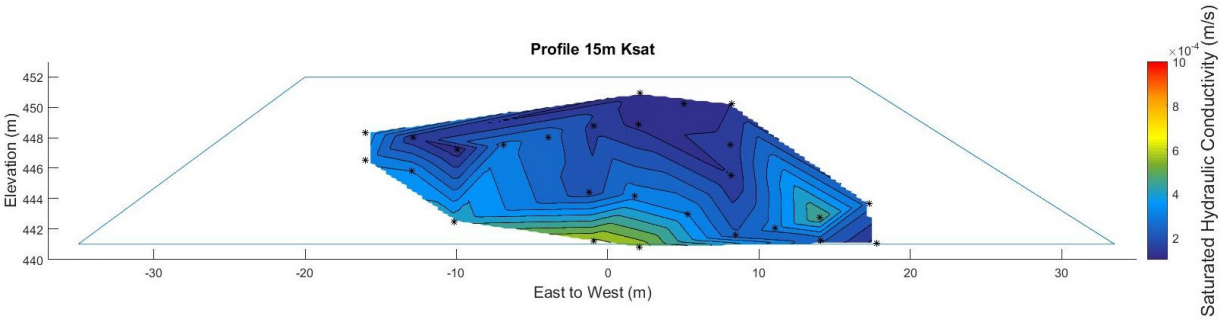

Figure 61 - Saturated Hydraulic Conductivity Contours for Profile 15m of the Type I Test Pile

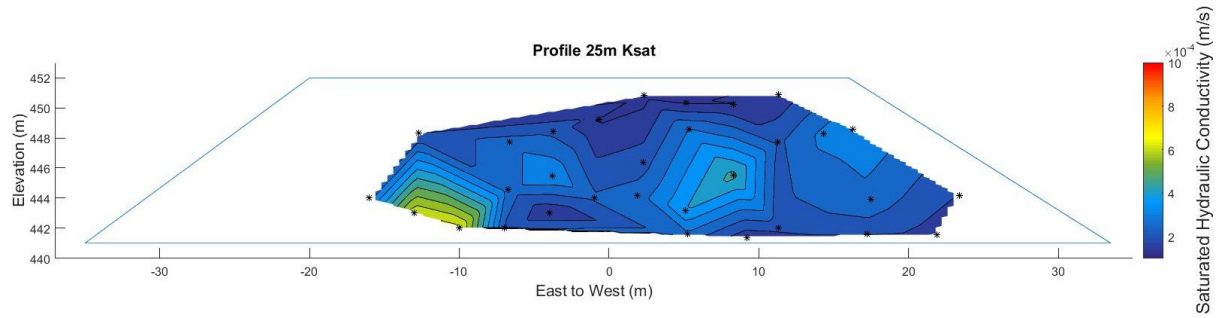

Figure 62 - Saturated Hydraulic Conductivity Contours for Profile 25m of the Type I Test Pile

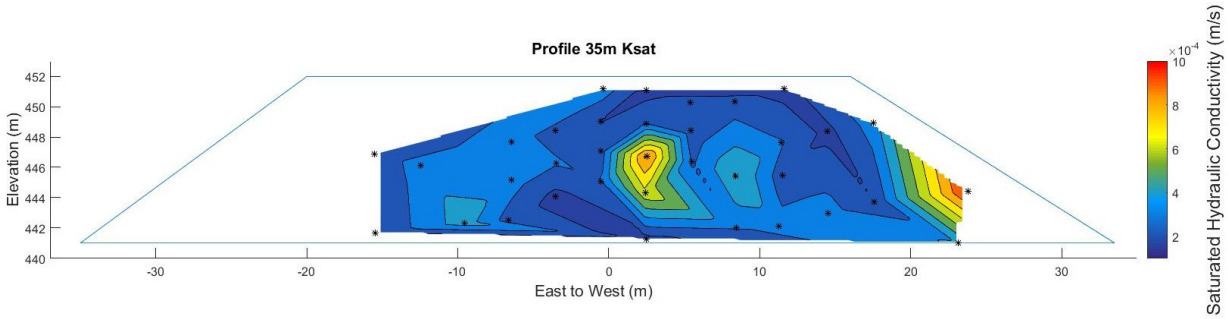

Figure 63 - Saturated Hydraulic Conductivity Contours for Profile 35 of the Type I Test Pile

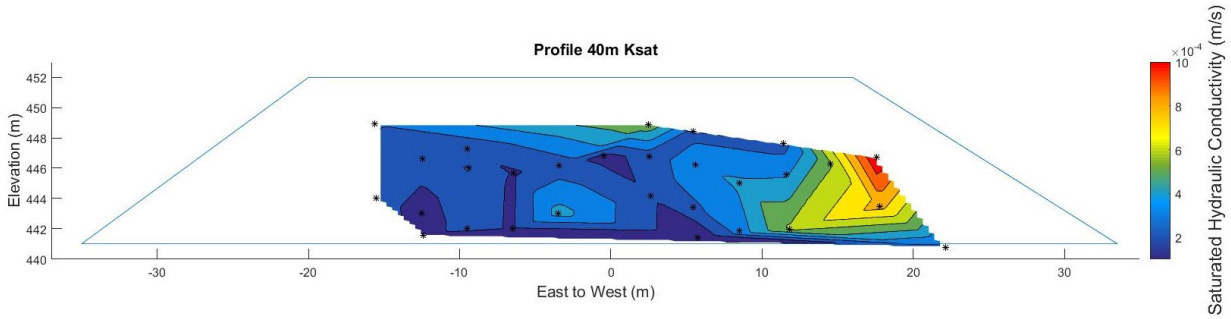

Figure 64 - Saturated Hydraulic Conductivity Contours for Profile 40m of the Type I Test Pile

The estimated K_{sat} values and plots illustrate that there is some spatial variation throughout the pile. However, these data are all approximately within one order of magnitude of each other. Neuner (2009) observed a similarly tight spread in the K_{sat} for Type I materials. This suggests that under fully saturated conditions there would be little variation in the movement of water throughout the pile. However, the Type I pile was generally unsaturated, and unsaturated mechanisms must also be considered. The following sections will discuss these mechanisms.

5.3.5 Variability in Unsaturated Coefficient of Permeability

The material in the Type I test pile was observed to be generally unsaturated during the deconstruction program. As such, it is important to consider the unsaturated properties of the material, in order to better understand how fluids will move through the material. SVSoils is capable of estimating the relationship between the coefficient of permeability and the suction. Figure 67 shows the average plots of unsaturated permeability for the classification groups. The curves all begin with a plateau in the low suction range. These plateaus represent the saturated hydraulic conductivity values of the classification group. The first break in the curve represents the average AEV, and the following slope illustrates how the coefficient of permeability changes with suction.

As in the previous discussion of group properties, we can see a transition between the various groups. The average K_{sat} values, represented by the plateaus, decrease in order from Group B to Group F. The average AEV value increases in order from Group B to Group F. These results are expected, as finer material will have a lower K_{sat}, and a higher AEV than coarser material. The early portion of the curve shows that the coefficient of permeability is approximately two orders of magnitude different between Group B and Group F at the same suction value. This suggests that Group F materials (> 50% passing the 4.75 mm sieve) would see more flow of water at 1 kPa than the other materials, with Group B having the lowest flow. The middle portion of the curve (10 kPa) still shows a range of one order of magnitude

between the classification groups. The groups all appear to converge at high suction values. This convergence likely occurs as a result of low moisture content, causing water to be discontinuous in the pores, and becoming increasingly difficult to mobilize. Table 5.6 summarizes the range of coefficient of permeability values between the classification groups, at different suctions.

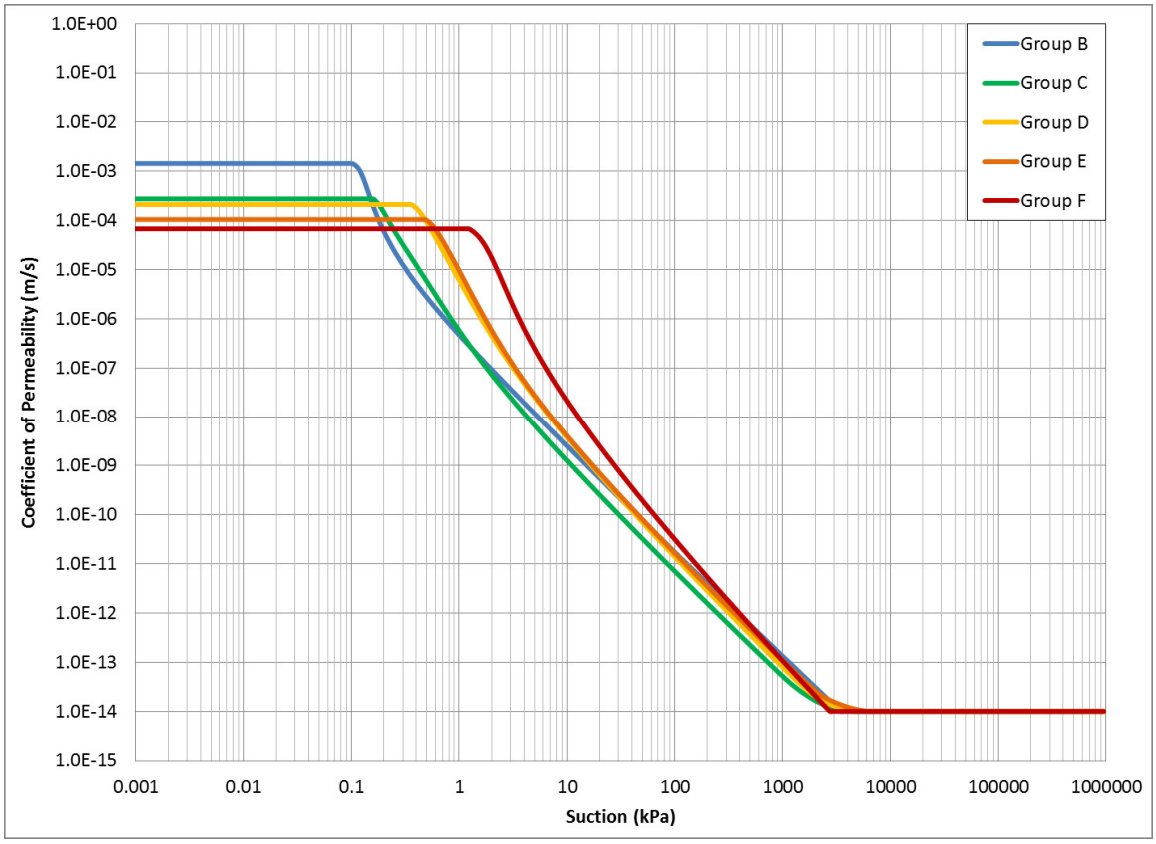

Figure 65 - Average Unsaturated Coefficient of Permeability for Herasymuik Classification Groups

Table 5.6 - Unsaturated Coefficient of Permeability Values for Herasymuik Classification Groups

Group Name	Suction (kPa)	Coefficient of Permeability (m/s)
Group B	0.1	1.43E-03
Group C		2.74E-04
Group D		2.10E-04
Group E		1.05E-04
Group F		6.76E-05
Group B	1	4.64E-07
Group C		5.61E-07
Group D		6.43E-06
Group E		9.64E-06
Group F		6.76E-05
Group B	10	2.50E-09
Group C		1.31E-09
Group D		3.57E-09
Group E		4.13E-09
Group F		2.12E-08
Group B	100	1.76E-11
Group C		7.09E-12
Group D		1.33E-11
Group E		1.66E-11
Group F		3.04E-11
Group B	1000	1.28E-13
Group C		5.02E-14
Group D		7.56E-14
Group E		1.06E-13
Group F		1.12E-13

5.3.6 Variability in Water Storage

A further way to investigate the unsaturated material properties is to look at the estimations of water storage. Again, SVSoils was used to generate water storage data that was then divided into the Herasymuik classification groups. The average values are plotted in Figure 68. At very low suctions there would be no water storage in any of the materials. The materials would be subject to saturated flow, at these low suctions, and would be governed by the K_{sat}. The material will begin to store water as the suction builds. As the suction increases, it can be seen that water will begin to reside in the pore spaces for longer times as the coefficient of permeability decreases. Eventually, each curve flattens out, with a small percentage of water remaining in storage, disconnected from other water droplets and unable to mobilize. Table 5.7 summarizes the spread in the data for each classification group. Groups B and F have limited data, and therefore display a distinct peak. Groups C, D, and E have much larger data sets, showing more of a plateau. The range of suctions in which water is stored increases in order from Group B to Group F. On average, a similar percentage of water will be stored in the material, although the suction ranges will be different.

Group B and C material appear to only store water with very low suctions. This is due to the low amount of fines, and the rock like behaviour of Group B and C materials. These materials would quickly move from a saturated to residual water content state. Materials from Groups D, E, and F appear to hold water over a larger range of suctions. These materials are part of the soil like, and rock like/soil like transition zone. The soil like material will have enough fines to retain water under suction. Group D material in the rock like/soil like transition zone will also have a large amount of fines, though they may be discontinuous in voids between larger clasts. This may increase the storage ability, as the fines are sufficient to draw water in, but lack connectivity so that water will be difficult to drain. This suggests that Group D, E, and F material would be the most likely to store reaction products, and to contribute to multiyear ice growth. Group B and C materials are more likely to transmit flow, and would contribute to more flushing of the pile in saturated conditions.

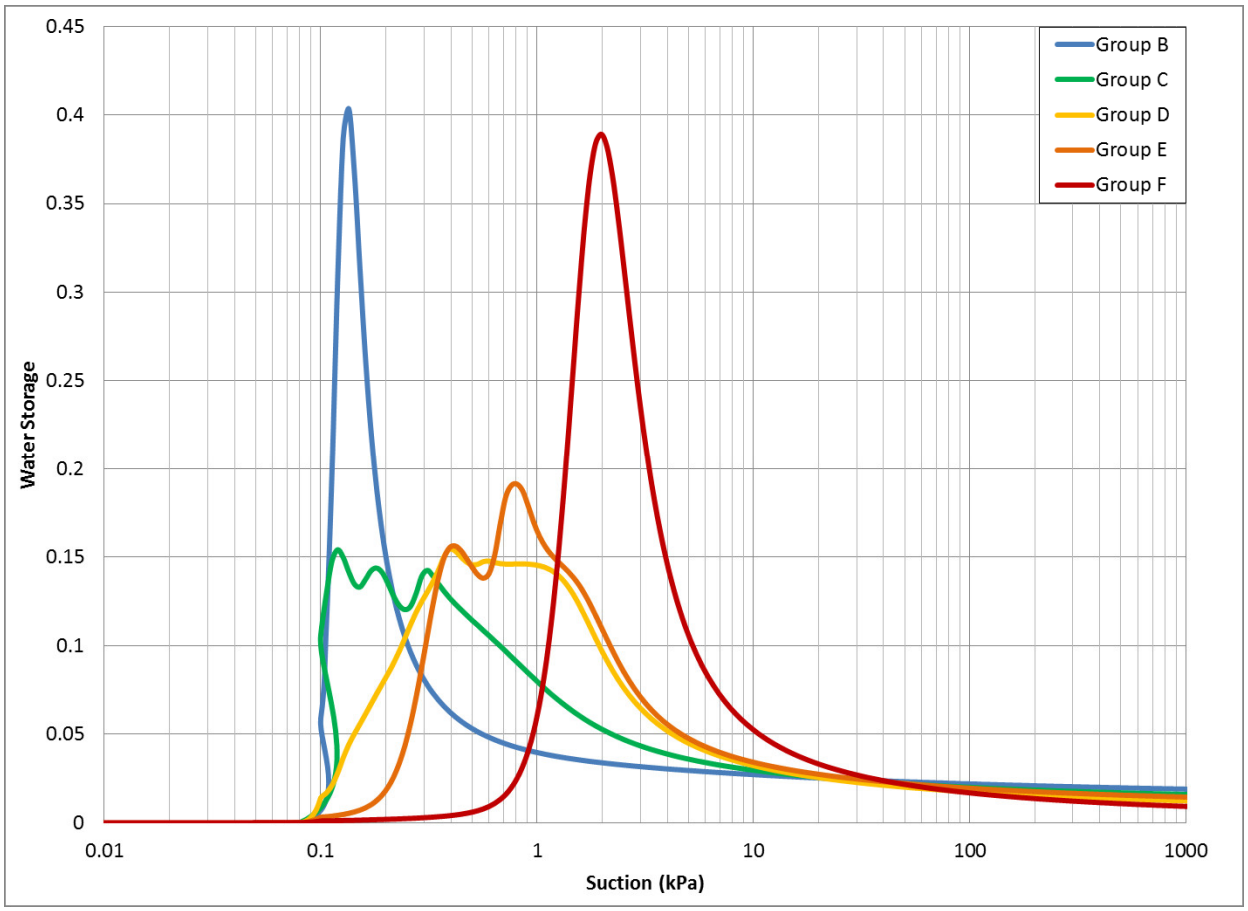

Figure 66 - Average Water Storage in Herasymuik Classification Groups

Table 5.7 - Summary of Water Storage Values

	Suction (kPa)		Water Storage	
Group Name	Minimum	Maximum	Plateau	Maximum
Group B	0.1	1	--	0.403
Group C	0.1	10	0.14	0.436
Group D	0.1	20	0.15	0.489
Group E	0.15	20	0.17	0.483
Group F	0.6	30	--	0.389

5.4 Material Classification

For the analyses in this thesis the classification system proposed by Herasymuik (1996) was used to group the materials together. The system uses the PSD data to determine the amount of material passing the 4.75 mm sieve. Unsaturated water flow will happen primarily in the <4.75 mm fraction of material. Herasymuik originally proposed six groups related to percent passing the 4.75 mm sieve. These groups were: less than 10%, 10 to 19%, 20 to 29%, 30 to 39%, 40 to 49% and greater than 50% passing the 4.75 mm sieve. For this study the groups were re-labelled as: less than 10%, 10 to 20%, 20 to 30%, 30 to 40%, 40 to 50%, and greater than 50% passing the 4.75 mm sieve. The modified distinctions were for clarity. They were further re-labelled as Group A, Group B, Group C, Group D, Group E, and Group F for ease of recognition.

This classification scheme has worked well to categorize and examine the material collected for this study. The classified groups were used to investigate the SWCC, hydraulic conductivity, coefficient of permeability, and water storage properties of the Type I material. The divisions that were chosen showed clear trends throughout each data set, describing the change in material properties with an increasing amount of fine material. In some cases the different groups were very distinct from each other, while in other cases the amount of overlap between groups was much larger. Even in cases where the group data overlapped, a range of data could still be defined for each group. The definition of data ranges will help to eliminate some uncertainty in model interpretation, by restricting the properties to measured ranges. The groups can also describe several properties at once, unlike traditional contour plots that only directly describe one property per plot. The generalized characteristics of each group are described below. No samples from Group A were measured in this study, and as such this group is not discussed.

It is also important to remember that the data that populates these groups is often a product of estimation. The SWCC, coefficient of permeability relationship, and water storage properties were all estimated using SVSoils. The saturated hydraulic conductivity values were estimated using manual methods, as well as SVSoils. Where possible, physical measurements of these values would provide additional information that could improve the understanding of the average group values.

Group B Materials - Blue

Group B Materials have 10 to 20% of their particles finer than 4.75 mm. They behave in a rock like manner with a clast supported structure. The small amount of fines that exist would be trapped in the voids between larger clasts. This group has the lowest AEV, and will not retain water under suction. It shows the highest average K_{sat} of the different groups. Unsaturated flow may occur with low suction for this group. This material would also have some of the lowest water storage capability due to the low amount of fine material.

Group C Materials - Green

Group C Materials have 20 to 30% of their particles finer than 4.75 mm. They would behave in a rock like manner with a largely clast supported structure. The fine material would be trapped in voids between larger clasts. The material has a low average AEV, ranging from 0.1 to 0.28 kPa. The saturated hydraulic conductivity has a lower average than Group B material, ranging from 2.8 $x10^{-4}$ to 1.1 $x10^{-3}$ m/s. The unsaturated permeability is similar to Group B, and the material can store water over a larger range of suctions (from 0.1 to 10 kPa).

Group D Materials - Yellow

Group D Materials have 30 to 40% of their particles finer than 4.75 mm, and were the most common in the Type I test pile, making up approximately 52% of the samples. These materials are in a transition zone between rock like and soil like behaviour. The structure is likely clast supported with the void almost entirely filled with fine material. Some large clasts may be separated by pockets of fine material as well. The AEV for the group ranges from 0.1 to 1.06 kPa, giving these materials some capacity to retain water under suction. The K_{sat} is lower than Groups B, and C, with a range between 1.7 $x10^{-4}$ to 9.4 $x10^{-4}$ m/s. This material requires higher suctions than previous groups in order to promote unsaturated flow. This group will store water over a large range of suctions, from 0.1 to 20 kPa.

Group E Materials - Orange

Group E Materials have 40 to 50% of their particles finer than 4.75 mm, and made up approximately 36% of measured samples. This group behaves in a soil like manner, exhibiting capillarity. The structure is likely matrix supported, with most large clasts suspended in the finer matrix. The AEV ranges from 0.2 to 1.23 kPa, allowing water to be retained under suction. The K_{sat} is at the low end of the groups, ranging from 1.0 $x10^{-4}$ to 3.1 $x10^{-4}$ m/s. Unsaturated flow will begin around 0.5 kPa, and the

permeability will continue to decrease with an increase in suction. Water storage will take place between 0.15 and 20 kPa.

Group F Materials - Red

Group F Materials have greater than 50% of their particles finer than 4.75 mm, and were rarely measured in the Type I test pile. These materials would be matrix supported. The average AEV was 1.23 kPa, allowing these materials to retain water under suction. The average K_{sat} is 9.4 $x10^{-5}$ m/s, which is approximately one order of magnitude smaller than Group B materials. This group requires the highest suction to initiate unsaturated flow, but it will also have the highest permeability under suction. This material will also store water up to 30 kPa.

Figure 69 shows examples of various sampling methodologies for collecting PSD data for waste rock. Herasymuik (1996) surveyed many mine sites, and found that at most sites little to no data was collected about the waste rock prior to placement. In such cases, assumed values over a large range would have to be considered, when making predictions of fluid movement in the material. Such a model would not provide reliable data, as it would have little relation to the real world properties and conditions. During the construction of the Diavik test piles, PSD samples were collected prior to final placement. These samples provided data about the PSD, but could not be used to demonstrate the spatial variability, as the material was segregated during placement. Data collected in this way would improve predictive methods by providing measured material properties. However, this data would still be applied over large zones, reducing the model detail. During the deconstruction project described in this thesis, PSD samples were collected using a 3D grid, as the pile was deconstructed. This allowed for the determination of material properties at distinct locations throughout the pile. By classifying this data set using the Herasymuik classification, zones with distinct properties can be incorporated into predictive models. However this method is not practical as it requires the deconstruction of the pile, along with an intense sampling regime. By implementing remote sensing and image analysis techniques, as studied by Chi (2011), and Cash (2014), it should be possible to collect PSD data remotely. This practice would have the advantage of capturing a larger range of particle sizes, and the collection of data without the need for physical sampling. If remote PSD data was collected on each face of a waste rock pile as it was built out, a 3D data set could be generated, similar to the deconstruction study. Provided that the remote sensing technique has the resolution to define materials down to the 4.75 mm size, then the material could be classified into the Herasymuik classification groups. Chi (2011) was able

to define the fine material as less than 10 mm in some cases, while Cash (2014) was able to define the fines as less than 4.75 mm using image analysis techniques.

By using the Herasymuik classification, discrete zones can be delineated, which have a given range of properties. These zones could be incorporated into models, and help identify zones of high flow, increased water storage, preferential pathways, etc. Remote sensing could be a good tool to collect this data as demonstrated by Chi (2011), and Cash (2014).

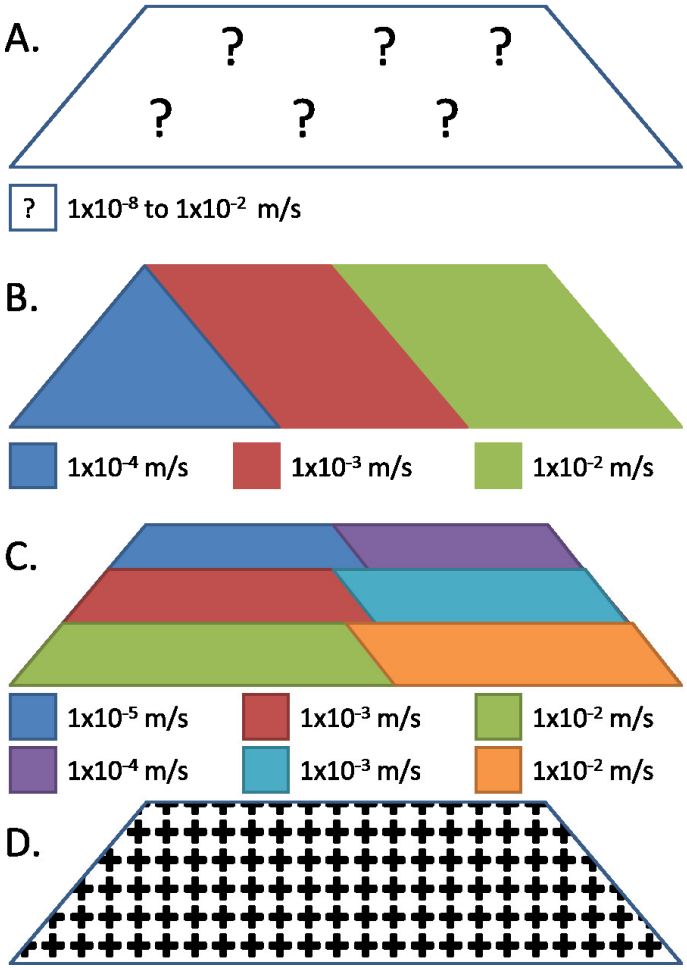

Figure 67 - PSD Sampling Methodologies (values are for demonstration only)

A – shows a waste rock pile with little to no data collected. No sampling effort.
B – shows PSD data collected during placement. Discrete zones become available. Moderate sampling effort required.
C – shows PSD data collected in place. More discrete zones are available. High sampling effort required.
D – shows PSD collected with remote sensing. Discrete information available at each node. Low sampling effort required.

5.5 Representative Elemental Volume

Classifying the material into groups shows that different portions of the material have some distinct characteristics. Delineating these zones is useful when interpreting and predicting fluid flow, and the potential to generate ARD. However, in order to get quality results for such predictions, it must be ensured that the material properties are representative over the defined zone. Bear (1972) introduced the concept of a Representative Elementary Volume (REV) for porous media. This concept replaces the particle-scale properties of a given volume of porous media with an equivalent fictitious continuum to which material properties can be assigned. In the REV the properties are the same no matter the location within the continuum. The REV describes the scale at which material properties can be parameterized (Neuner 2009). Bear (1972) calculated an REV for porosity, by varying the particle sizes and volume of material. Further work by Al-Raoush and Papadopoulos (2010) suggests that the REV will change for different material properties. In order to study hydraulic behaviour in waste rock Neuner (2009) determined REV's based on porosity, similar to Bear (1972), and Cash (2014) determined REV's that represented the PSD of material samples.

A similar approach to Neuner (2009) and Bear (1972) was used in this research to determine the REV based on porosity. The calculation was carried out by adding particles of a given volume to a volume of material, and then calculating a revised porosity. The original equation to calculate porosity (n) is:

$$n = \frac{V_v}{V_T} \qquad \text{Equation 16}$$

Where V_v is the volume of the voids, and V_T is the total volume. By adding a clast of maximum size (V_c), the original volume of voids will decrease, and an adjusted volume of voids will replace it.

$$V_v' = V_v - V_c \qquad \text{Equation 17}$$

This adjusted value can be used to calculate the adjusted porosity (n'):

$$n' = \frac{V_v'}{V_t} \qquad \text{Equation 18}$$

By comparing the difference between n and n', it can be observed how much effect the addition of the maximum clast size (V_c) has on the porosity of the material. For this study the initial porosity was set at 0.25, and the above equations were solved to reflect a change in porosity of 1%. At this point the addition or removal of a clast of the maximum size will have a negligible effect on the porosity of the total volume. This total volume is the REV, for the given maximum clast size. The total volume was

considered to be a cube, while the volume of the clast was set as either a sphere or an ellipsoid. Table 5.8 below, summarizes the REV's for various different maximum clast sizes.

This analysis shows the REV's for several different particle sizes. During the deconstruction, the maximum particles size that was collected was 75 mm, (0.075 m). With an expected porosity of 0.25, the REV would be approximately 0.09 m^3, which is equivalent to a cube with sides approximately 0.45 m long. The PSD samples that were collected had a volume of approximately 0.04 m^3 which is equivalent to a cube with sides 0.34 m. During the deconstruction boulders that were over 3.5 m^3 were measured, as seen in Figure 70. Including clasts of this size would increase the REV to approximately 1421 m^3. This volume would form a cube with sides over 11 m long.

Table 5.8 - Representative Elemental Volumes for Different Maximum Clast Sizes

Shape of Clast	Clast Dimension (m)	Volume of Clast (m^3)	REV (m^3)
Sphere	0.075	0.0002	0.09
Sphere	0.1	0.0005	0.21
Sphere	0.5	0.065	26.3
Sphere	1	0.52	211
Sphere	1.5	1.77	710
Sphere	2	4.19	1684
Ellipsoid	2x1x1	1.05	421
Ellipsoid	3x1.5x1.5	3.53	1421

Figure 68 - Large Boulder Observed during Deconstruction (Scale Square is 0.5 by 0.5 m)

5.6 PSD Collection

Each of the PSD studies at the Diavik Test Piles has provided a unique sampling situation. Studies during the construction of the piles allowed for the collection of a large data set. Samples were collected from truckloads as they were brought to the location. In practice, most waste rock piles are not sampled so regularly. The construction data set provided a baseline of the PSD for the pile, and represented the whole pile. The deconstruction PSD study provided a chance to collect samples after placement. This allowed for observations of how PSD differed with location in the pile. The deconstruction PSD data set was similar to the construction PSD data set, when looking at the overall average PSD. However, the deconstruction process provided additional information on spatial variability and material segregation, by providing data at specific locations. Image analysis of PSD by Chi (2010) produced similar conclusions to the deconstruction, with similar statistical moments, demonstrating material segregation, and spatial variability.

Figure 71 illustrates the PSD data from different studies during the construction and deconstruction of the Type I test pile. The overall distribution of the data follows a similar curve in each study. The standard deviation values for the construction studies show a wider spread in the data, especially on the high side of the mean. The standard deviation data from the construction studies ranges from a d_{10} of 0.15 to 0.42 mm. The d_{10} values for the deconstruction study ranged from 0.21 mm to 0.41 mm. The higher representation of fines from the construction data set, is likely due to the smaller maximum particle size that was collected during the construction. The lack of particles above 50 mm would cause the representation of smaller particles to increase relative to samples that were collected with particles greater than 50 mm. Chi (2010) measured a much larger range of particle sizes, which makes the PSD, and d_{10} values from that data set incomparable. The similarity in the PSD data sets that were compared suggest that there has been little physical breakdown of the material since its placement.

PSD data from the construction created a strong baseline data set that represented the pile as a whole, and not just one small sampled area. Deconstruction PSD data confirmed the results from the construction studies, and provided information on material segregation, and spatial variability. Image analysis techniques were also able to illustrate spatial variability and material segregation. Each method has advantages and disadvantages in the effort required to sample, and the information obtained.

The method used during the construction of the pile required a medium amount of sampling effort. Collecting samples prior to placement allows for a data set that describes the PSD over large zones that

are aligned with the tip faces of the pile. This data cannot reliably be used to illustrate the spatial variability of the material, as it is not linked to specific locations in the pile. The deconstruction method may provide the most amounts of data, but it is also the most impractical. It requires a high sampling effort, as well as the destruction of the pile that is being studied. However, this allows for the collection of in-situ samples that can be used to estimate material properties at specific locations within the pile. Such a data set would also need a high sample density, or additional geostatistics in order to create a representative model of the pile.

Image analysis methods are advantageous as the data can be collected remotely, and does not require physical samples to be collected. This allows for the collection of PSD data sets that can capture the maximum particle size. The minimum particle size that can be represented depends on the resolution of the imaging equipment. High quality equipment, and drone technology can allow this data to be collected safely at high resolutions. Chi (2010) and Cash (2014) both concluded that digital image processing techniques were effective methods, as they could characterize a larger range of grain sizes, and compared well to measured PSD values. This supports the idea of using image analysis techniques to map PSD of waste rock. The method is non-intrusive, and appears to provide similar results to field sampling methods.

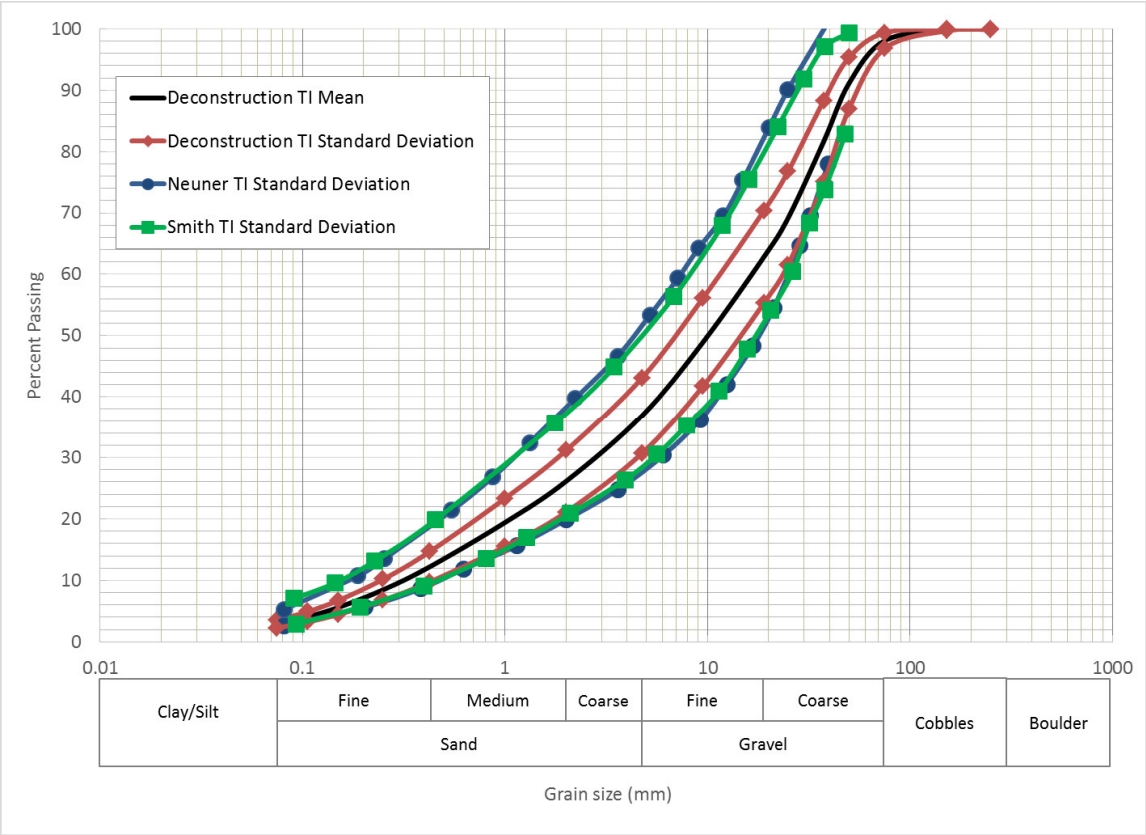

Figure 69 - PSD Data from Construction and Deconstruction Studies

6 Summary and Conclusions

6.1 Summary

The storage of mine waste is a challenge faced by all mining operations. Current methods of constructing waste dumps create ideal conditions for the generation of ARD. This potential to cause environmental damage is a liability for mining companies, governments, the public, and the environment. In order to address these issues, and design better waste management systems, it is important to understand the material properties of waste rock, and how they are influenced by their method of placement. Detailed study of waste rock materials and dumps is an emerging field, with much of the work occurring in the past twenty years. Relevant literature from this period was studied, to learn what is known about these materials, and how such information is collected. This thesis aimed to expand the knowledge base by studying the spatial variability of the material properties of waste rock. The research objectives were to, first, deconstruct a waste rock pile and collect samples using a 3D sampling grid. Secondly, to measure the PSD of the waste rock material using the sample inventory. Thirdly, to use the measured PSD data to estimate the saturated and unsaturated hydraulic properties of the material. And finally, to examine the spatial variability of these materials.

In the summer of 2014 the Type I test pile at Diavik Diamond Mines Inc. was deconstructed, to facilitate this and other research projects. An inventory of over 250 bulk samples was collected for the measurement of PSD. Following the field work these samples were tested in a laboratory to determine the PSD. These data were then used in various estimation methods to estimate the SWCC, the saturated hydraulic conductivity, the unsaturated coefficient of permeability, and water storage properties. The PSD data was used to study material segregation and spatial variability that existed in the test pile. The PSD data was also used to classify the samples into groups with similar amounts of fine material. The measured and estimated properties of these groups were compared to reveal trends and variability in the material properties. The conclusions from this research are presented in the following sections.

6.2 Conclusions

The objectives of this research were completed with a field sampling program, and laboratory and data analyses. The field program included the collection of in situ samples along a three dimensional grid. Laboratory analyses were conducted on the samples to measure the particle size distribution. The measured data was then used to classify the material, and to estimate material properties. The various

data sets were studied to identify and highlight the spatial variability of the material as it existed in the waste rock pile. The specific conclusions of this research are outlined below:

1. The PSD data that was measured during this research is a valid representation of the materials that existed in the Type I test pile. The deconstruction PSD data set has a similar mean, and range of data compared to PSD studies undertaken during the construction of the piles. The similarity in the overall data sets provides assurance that the measurement techniques were adequate.
2. The PSD data curves were fitted using a multimodal curve fitting technique described by Chapuis (2004). This method fit the data extremely well, with average R^2 values over 0.999. These tightly fit curves were then used to accurately predict different size fractions and d_n values. These parameters were used in further estimation techniques throughout this research.
3. The PSD data set collected during the deconstruction can provide quantitative data on the segregation and material variability of material from the Type I test pile. Analysing the data with respect to elevation showed that the pile becomes finer with an increase in elevation. The fine material becomes finer with elevation, while the coarse material becomes coarser with depth. The spatial variability was demonstrated using various plotting techniques. Representative zones, as well as contour plots of different size fractions along profiles and tip faces illustrated the existence of coarser and finer zones within the pile. Not all of these variations were related to changes in elevation, there were lateral differences as well.
4. The material collected for the study of PSD had material as fine as the silt size fraction, and as large as 75 mm. Field observations located boulders that were approximately 3 m in diameter, representing the maximum particle size. The majority of the measured material (52%) was classified as being in the transition zone between soil and rock like behaviour. Such material would likely be clast supported with voids mostly filled with finer material, capable of retaining water under suction. 12% of the measured material was strictly rock-like, with few fines capable of retaining water. These fines would be located in the voids between larger clasts. Approximately 36% of the measured material was soil-like. These materials would be matrix supported, with any larger clasts suspended in a finer matrix.
5. The classification system proposed by Herasymuik (1996) is a good system for classifying waste rock material. The classifications were given group names for clarity, and describe the material based on the amount of material passing the 4.75 mm sieve. The groupings can be used to describe average trends in material properties, and show results visually.

6. Estimations of the SWCC for the waste rock material saw a range of AEV's from 0.1 to 1.23 kPa. On average the AEV increased from Group B to Group F, corresponding to an increase in material finer than 4.75 mm. The low AEV values suggest that the material drains fairly easily. This corresponds to field observations of low moisture content throughout most of the Type I test pile.
7. Estimated saturated hydraulic conductivity values ranged over one order of magnitude from approximately 1.0 $x10^{-3}$ to 1.0 $x10^{-4}$ m/s. Group B materials had the highest K_{sat} decreasing by group to the lowest value in Group F.
8. The unsaturated permeability was estimated, and the highest permeability was in Group F and the lowest permeability was in Group B at the same suction value. Group B materials could have unsaturated flow at suctions as low as 0.1 kPa, while Group F soils required more than 1 kPa to initiate unsaturated flow.
9. The water storage properties were estimated. The average water storage was similar between all of the classification groups. However, the storage occurred over different ranges of suction. Group B materials stored water at the lowest suctions. The suction range for storing water increased through the groups from Group B to Group F.
10. Different PSD collection methods were compared using data sets collected from the Type I test pile. Studies during the construction of the pile required moderate to high sampling effort, and provided PSD information. This data was collected prior to final placement and could not be linked to specific locations within the pile. Image analysis studies on the completed faces of the pile were able to determine the PSD, including a large range of particle sizes. This data set was able to identify material segregation and spatial variability trends in the deposited material. The data collected during the deconstruction allowed for the measurement of PSD, and estimation of material properties. This data was collected in situ and can be linked to specific locations in the pile. This type of data set can be used to map segregation, and spatial variability, and classify different material types in different areas.
11. A study of Representative Elemental Volumes was conducted in order to understand the material volumes required to parameterize the Type I material. Based on the sample volume collected during the deconstruction it was found that a tighter sampling grid would be required to create a fully representative model. Alternatively geostatistical methods could be employed to bridge the data gaps between sampled zones. The REV incorporating the largest observed boulders in the Type I pile is approximately 1500 m^3. In order to work with such a large REV the

sampling method would need to measure particles with dimensions up to 3.5 m (maximum axis).

6.3 Recommendations for Further Research

The objectives of this research were to deconstruct a waste rock pile, collect samples for the measurement of PSD, estimate material properties using measured data, and to explore the spatial variability in material properties. These objectives were completed satisfactorily. However, during the course of this research, additional questions arose. Investigating these issues, and answering new questions may lead to better interpretation of these types of data sets, or lead to improvements in measurement techniques. A list of recommendations for further research into the measurement and interpretation of PSD data, for the estimation of material properties, and understanding of spatial variability follows:

1. Further study of the deconstruction data set should include some hydraulic testing of the physical samples. This could include permeabilty testing to determine the saturated hydraulic conductivity, or pressure plate or tempe cell tests to measure the SWCC. The measured results could be compared to the estimated data set for saturated and unsaturated properties, validating the data. If the resulting data set does not match the estimations, the measured data could be used to refine the results of this thesis. In particular, measured SWCC data could be used to determine appropriate packing porosity values for the estimation of SWCC from Type I waste rock. This could help determine if the packing porosity of waste rock is a general property, or more site specific.
2. The trends and ranges of data that were presented for the Hearsymuik classification groups could be compared to other waste rock data sets, from other sites. This could help to determine how easily the classifications can be applied to other sites. It is possible that the data ranges described in this thesis are dependent on the Type I material, and would not represent waste rock materials from other sites. A study of additional materials could help to better define the expected values and trends for the classification groups. This could lead to the development of guidelines for material testing and classification waste rock.
3. The Herasymuik classification groups describe material with differing amounts finer than the 4.75 mm sieve. The few studies to have used these classifications have used samples collected with a maximum particle size of 50 mm to 75 mm. If larger particle sizes are included in the PSD measurement, then the percentages of smaller materials will be less. This will affect how the

material is classified with this system. Further research would be required to determine how significant the inclusion of larger particles is, or to develop limits on maximum particle size when using this classification system.

4. This data set could be incorporated with existing and future research of the Type I test pile at Diavik. The Test Piles Research Program has explored many features and behaviours of the Type I test pile, including studies of chemical and microbiological evolution over time, hydraulic behaviour, and ice formation. The deconstruction data set can provide more detailed information about the spatial variability of material properties, and may help provide a deeper understanding of some of the processes that occurred in the Type I test pile.
5. A promising method of collecting PSD data is that of remote sensing. Image analysis of photographs of waste rock can be used to determine the PSD. Imagery was collected during the deconstruction, and includes panoramic images of the trenches that were created, as well as image sets at sampling locations. This imagery could be analysed using available 2D image analysis software, and compared to the existing data set. This could allow for the collection of larger particle sizes in the PSD.
6. The imagery was also collected in pairs and sets, allowing for the use of photogrammetry techniques. Photogrammetry can be used to generate 3D imagery of a subject. The 3D imagery could be used to develop techniques to determine the PSD from 3D imagery. This could provide a better PSD data set as it can eliminate some of the challenges of analysing PSD from 2D data, such as shadows and perspective errors. The 3D imagery may also be able to be used to map voids and other features. 3D imagery is recreated from many individual images, meaning a large face could be captured with many close up images. The individual images could be collected at higher resolution by focusing on a smaller area. The higher resolution will allow for smaller particles to be measured.
7. Additional research is required to better understand the REV that will be appropriate in future waste rock studies. The REV will be different for different material properties. A sensitivity analysis of different parameters could help determine if one REV can be prioritized over many. Further study could also help to develop better methodology for collecting data in the field. Perhaps image analysis will be appropriate, as capturing larger particles allows for the REV to be larger. Or perhaps geostatistical methods can be used fill in the gaps between smaller REV's based on small field samples.

References

Al-Raoush, R., and Papadopoulos, A. (2010). "Representative elementary volume analysis of porous media using X-ray computed tomography." *Powder Technol,* 200(1–2), 69-77.

Amos, R. T., Blowes, D. W., Bailey, B. L., Sego, D. C., Smith, L., and Ritchie, A. I. M. (2015). "Waste-rock hydrogeology and geochemistry." *Appl.Geochem.,* 57 140-156.

Andrina, J. (2009). "Physical and Geochemical Behavior of Mine Rock Stockpiles in High Rainfall Environments". University of British Columbia.

ASTM International. (2009). "Standard Test Methods for Particle-Size Distribution (Gradation) of Soils Using Sieve Analysis.".

ASTM International. (1966). "Standard Practice for Classification of Soils for Engineering Purposes (Unified Soil Classification System).".

ASTM International. (1938). "Standard Test Method for Sieve Analysis of Fine and Coarse Aggregates.".

Aubertin, M., and Bussiere, B. (2013). "Mine Wastes Management @RIME." Tailings and Mine Waste Conference 2013, Banff, Canada.

Bear, J. (1988; 1972). *Dynamics of fluids in porous media.* Dover, New York.

Bussiere, B. (2007). "Colloquium 2004: Hydrogeotechnical properties of hard rock tailings from metal mines and emerging geoenvironmental disposal approaches." *Can.Geotech.J.,* 44(9), 1019-1052.

Cash, A. E. (2014). "Structural and Hydrologic Characterization of Two Historic Waste Rock Piles". Masters. University of Alberta.

Chapuis, R. P., and Aubertin, M. (2003). "On the Use of the Kozeny-Carman Equation to Predict the Hydraulic Conductivity of Soils." *Canadian Geotechnical Journal,* 40 616.

Chapuis, R. P., Dallaire, V., and Saucier, A. (2014). "Getting Information from Modal Decomposition of Grain Size Distribution Curves." *Geotech Test J,* 37(2).

Chapuis, R. (2012). "Predicting the saturated hydraulic conductivity of soils: a review." *Bulletin of Engineering Geology & the Environment,* 71(3), 401-434.

Chapuis, R. P. (2004). "Predicting the saturated hydraulic conductivity of sand and gravel using effective diameter and void ratio." *Canadian Geotechnical Journal,* 41(5), 787-795.

Chi, X. (2011). "Characterizing low-sulfide instrumented waste-rock piles: image grain-size analysis and wind-induced gas transport.".

Chi, X., Amos, R. T., Stastna, M., Blowes, D. W., Sego, D. C., and Smith, L. (2013). "The Diavik Waste Rock Project: Implications of wind-induced gas transport." *Appl.Geochem.,* 36 246-255.

Craig, R. F. (2004). *Craig's Soil Mechanics.* Spon Press, New York.

Darling, P. (2011). "8.11.2 Types of Waste Piles, Dumps, and Heaps." *SME Mining Engineering Handbook (3rd Edition),* Society for Mining, Metallurgy, and Exploration (SME).

Das, B. M. (2008). *Fundamentals of geotechnical engineering.* Thomson, Toronto, Ont.

Diavik. (2009). "Interim Closure and Reclamation Plan - Version 3.0." Diavik Diamond Mine Inc.

Fala, O., Molson, J., Aubertin, M., Dawood, I., Bussière, B., and Chapuis, R. P. (2013). "A numerical modelling approach to assess long-term unsaturated flow and geochemical transport in a waste rock pile." *International Journal of Mining, Reclamation and Environment,* 27(1), 38-55.

Fredlund, D. G., Fredlund, M. D., and Rahardjo, H. (2012). *Unsaturated soil mechanics in engineering practice.* John Wiley & Sons, Inc., Hoboken, N.J.

Fredlund, M. D., Wilson, W. G., and Fredlund, D. G. (2000). "Use of grain-size functions in unsaturated soil mechanics." *Geotech Spec Publ,* 99 69-83.

Hazen, A. (1911). "Discussion of “Dams on sand formations,” by A.C. Koenig." *Transactions of the American Society of Civil Engineers,* 73 199.

Hazen, A. (1892). "Some physical properties of sand and gravel, with special reference to their use in filtration." *Rep. No. 24th Annual Report,* Massachusetts State Board of Health, Boston, Massachusetts.

Herasymuik, G. M. (1996). "Hydrogeology of a sulphide waste rock dump". Masters. University of Saskatchewan.

Lahmira, B., Lefebvre, R., Aubertin, M., and Bussière, B. (2016). "Effect of heterogeneity and anisotropy related to the construction method on transfer processes in waste rock piles." *J.Contam.Hydrol.,* 184 35-49.

Lewis, D. W., and McConchie, D. (1994). *Analytical sedimentology.* Chapman & Hall, New York.

Maqsoud, A., Bussiere, B., Aubertin, M., and Mbonimpa, M. (2012). "Predicting hysteresis of the water retention curve from basic properties of granular soils." *Geotech.Geol.Eng.,* 30(5; 5), 1147-1159.

Marshall, B. (2015). "Facts and Figures of the Canadian Mining Industry 2015." The Mining Association of Canada.

Munsell Color. (2012). *Munsell Soil Color Book.* Munsell Color, Grand Rapids, MI.

Neuner, M. (2009). "Water Flow Through Unsaturated Mine Waste Rock in a Region of Permafrost". Master of Science. University of British Columbia.

Neuner, M., Smith, L., Blowes, D. W., Sego, D. C., Smith, L. J. D., Fretz, N., and Gupton, M. (2013). "The Diavik waste rock project: Water flow through mine waste rock in a permafrost terrain." *Appl.Geochem.,* 36 222-233.

Price, W. A. (2009). "Prediction Manual for Drainage Chemistry From Sulphidic Geological Materials." *Rep. No. MEND 1.20.1,* Natural Resources Canada.

Smith, L. (2006). "Test Piles Project 2006 Construction Summary." FDA Engineering Ltd.

Smith, L., and Beckie, R. (2003). "Hydrologic and geochemical transport processes in mine waste rock." *Environmental Aspects of Mine Wastes,* E. J. J. Jambor, D. W. Blowes, and A. I. M. Ritchie, eds., Mineralogical Association of Canada.

Smith, L. J. D. (2009). "Building and characterizing low sulfide instrumented waste rock piles: Pile design and construction, particle size and sulfur characterization, and initial geochemical response.".

Smith, L. J. D., Blowes, D. W., Jambor, J. L., Smith, L., Sego, D. C., and Neuner, M. (2013). "The Diavik Waste Rock Project: Particle size distribution and sulfur characteristics of low-sulfide waste rock." *Appl.Geochem.,* 36 200-209.

Smith, L. J. D., Moncur, M. C., Neuner, M., Gupton, M., Blowes, D. W., Smith, L., and Sego, D. C. (2013). "The Diavik Waste Rock Project: Design, construction, and instrumentation of field-scale experimental waste-rock piles." *Appl.Geochem.,* 36 187-199.

Soil Vision Systems Ltd. (2016). "SVOFFIVE 5 Help Manual - 6/2/2016.".

The International Network for Acid Prevention (INAP), 2009. Global Acid Rock Drainage Guide (GARD Guide). http://www.gardguide.com/

Wilson, W. G. (2011). "Rock Dump Hydrology: An Overview of Full-Scale Excavations and Scale-Up Experiments Conducted During the Last Two Decades." *7th Australian Workshop on Acid and Metalliferous Drainage*.

Yip, C. G., and Thompson, K. S. (2015). "Diavik Diamond Mine NI 43-101 Technical Report." *Rep. No. NI 43-101*.

Appendix A

SAMPLE COLLECTION

Samples were collected for many different studies during the deconstruction. In order to maintain consistency between the different studies, a sample referencing system was developed. The referencing system was broken down into several components, and includes:

- Pile – 1, 2, or 3;
- Bench – B01, B02, B03, etc...;
- Trench Name – TW (west of centerline), or TE (east of centerline);
- Trench Number – 1 for the regular trenches, 2 or higher for test pits outside of the trenches;
- Profile – 00 through 45, moving from south to north horizontally; and,
- Depth – A, B, C, D, E, or F. A, B, and C are on the east face of each trench, while D, E, and F are on the west face of each trench. A and F are upper, B and E are middle, and C and D are lower.

Using this naming scheme the location 1B03TW115C would describe a spot on the Type 1 pile, on the third bench, in a trench on the west side of the pile, on a profile 15 m along the pile, near the base of the trench on the east face. The naming scheme provides a lot of very specific data, in a concise form. This system was set up as a database that was accessible via tablet computer in the field. The sample data could be quickly entered, and linked to a barcode that was scanned into the database, and applied to samples.

SAMPLE LABELS

Samples were given barcode stickers and hand written labels on the sample bags. The barcodes were very effective in maintaining good sample records, as they were very durable. In many cases the hand written labels were lost over time as the samples were left in outdoor storage. The barcodes were much more resistant to weathering, and were readable in almost every case. There were cases where the adhesive failed and the barcode fell off. However, barcodes were applied in pairs, so in these cases usually only one sticker was affected. Generally, the longer the bags remained in storage the more likely the labels were to be lost or damaged. There were also some situations where the bags themselves were damaged, with the labelled sections being torn off or otherwise removed from the bags. These

examples of damage led to a set of samples that were disqualified from testing due to their lack of location data.

SIEVE ANALYSIS DATA SHEET TEMPLATE

Date:
Technician:

Sieve Analysis Data Sheets

	Portion 1	Portion 2	Portion 3	Portion 4
Name:				
Bag:				
Barcode:				
Dry Time				
Tare:				
Wet Mass				
Dry Mass				
Munsell wet				
Munsell Dry				

New Barcodes	
Coarse	
Fine	

Date:	
Technician:	
Sample:	
Barcodes:	

Comments:

Coarse Subsample:					
Size (mm)	Mass (kg)				
250					
153					
75					
50					
37.5					
25					
19					
9.5					
pan					

Date:	
Technician:	
Sample:	
Barcode:	

Comments:

Fines Subsample:											
Sieve #	Mass (g)										
4											
10											
20											
40											
60											
100											
140											
200											
pan											

Appendix B

CALCULATIONS FOR STATISTICAL MOMENTS

The n^{th} moment:

$$n = \frac{\sum(f d^n)}{N}$$

Where *f* = frequency (weight %), *d* = diameter, and *N* = number of measurements (100 when dealing with percent).

The first moment, or mean:

$$mean, X = \frac{\sum f d}{N}$$

The standard deviation:

$$\sigma = \sqrt{\frac{\sum f(d-X)^2}{N}}$$

The third moment, or skewness:

$$Skewness = \frac{\sum f(d-X)^3}{N\sigma^3}$$

The fourth moment, or kurtosis:

$$Kurtosis = \frac{\sum f(d-X)^4}{N\sigma^4}$$

Formula from (Lewis and McConchie 1994).

Appendix C

ADDITIONAL DATA AND PLOTS

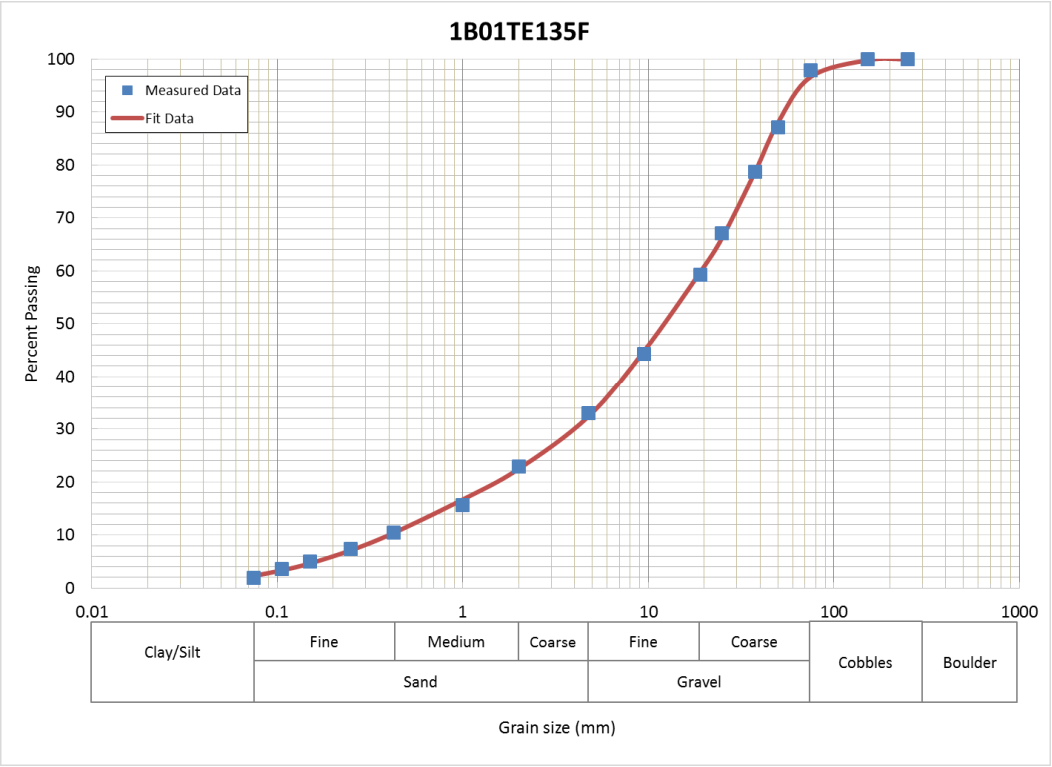
1B01TE135F
Measured Data
Fit Data
Percent Passing
100
90
80
70
60
50
40
30
20
10
0
0.01
0.1
1
10
100
1000
Clay/Silt
Fine
Medium
Coarse
Fine
Coarse
Sand
Gravel
Cobbles
Boulder
Grain size (mm)

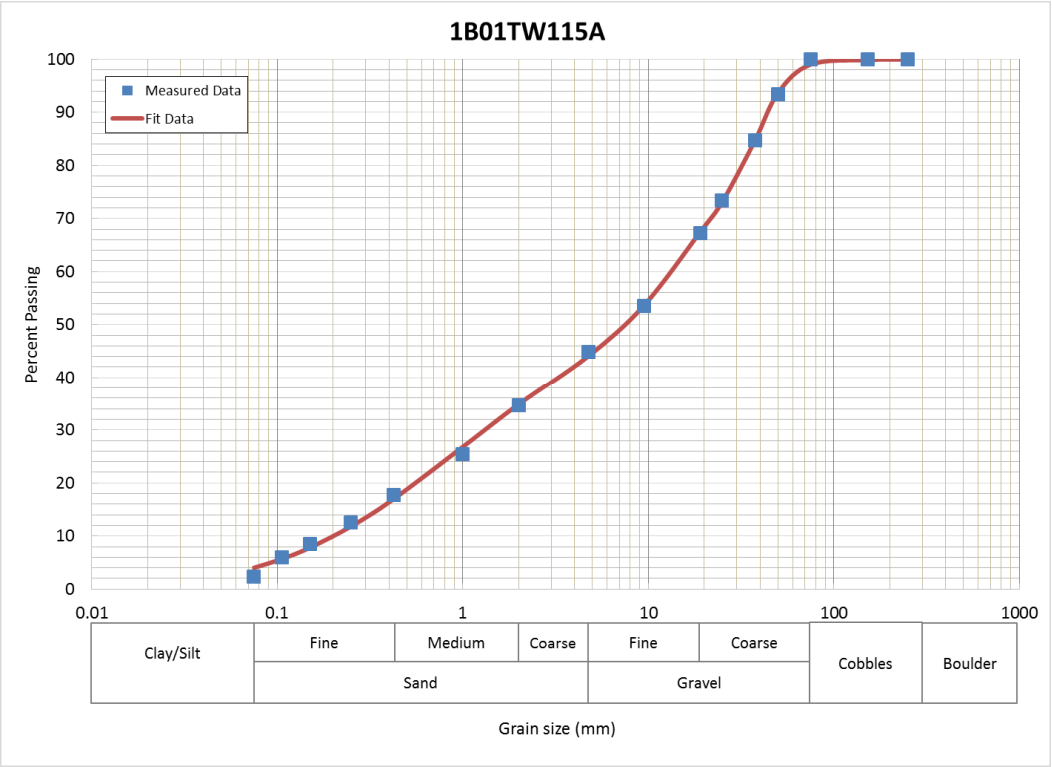
1B01TW115A
Measured Data
Fit Data
Percent Passing
100
90
80
70
60
50
40
30
20
10
0
0.01
0.1
1
10
100
1000
Clay/Silt
Fine
Medium
Coarse
Fine
Coarse
Sand
Gravel
Cobbles
Boulder
Grain size (mm)

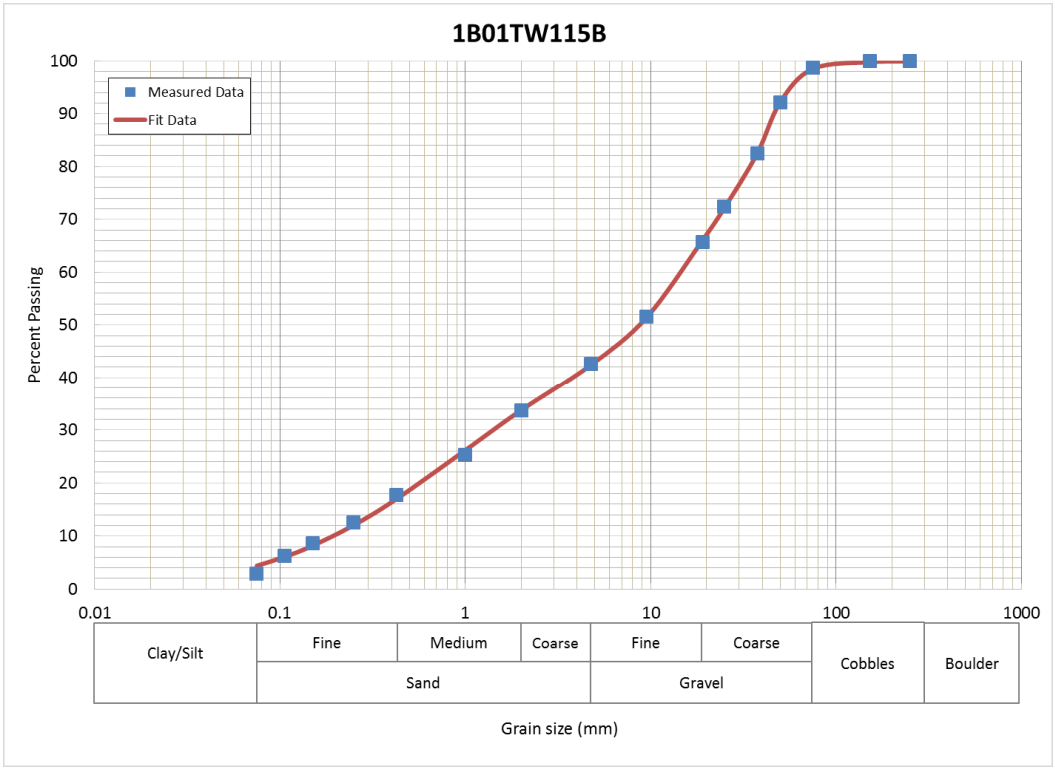
1B01TW115B
Measured Data
Fit Data
Percent Passing
100
90
80
70
60
50
40
30
20
10
0
0.01
0.1
1
10
100
1000
Clay/Silt
Fine
Medium
Coarse
Fine
Coarse
Cobbles
Boulder
Sand
Gravel
Grain size (mm)


1B01TW115E
Measured Data
Fit Data
Percent Passing
100
90
80
70
60
50
40
30
20
10
0
0.01
0.1
1
10
100
1000
Clay/Silt
Fine
Medium
Coarse
Fine
Coarse
Cobbles
Boulder
Sand
Gravel
Grain size (mm)

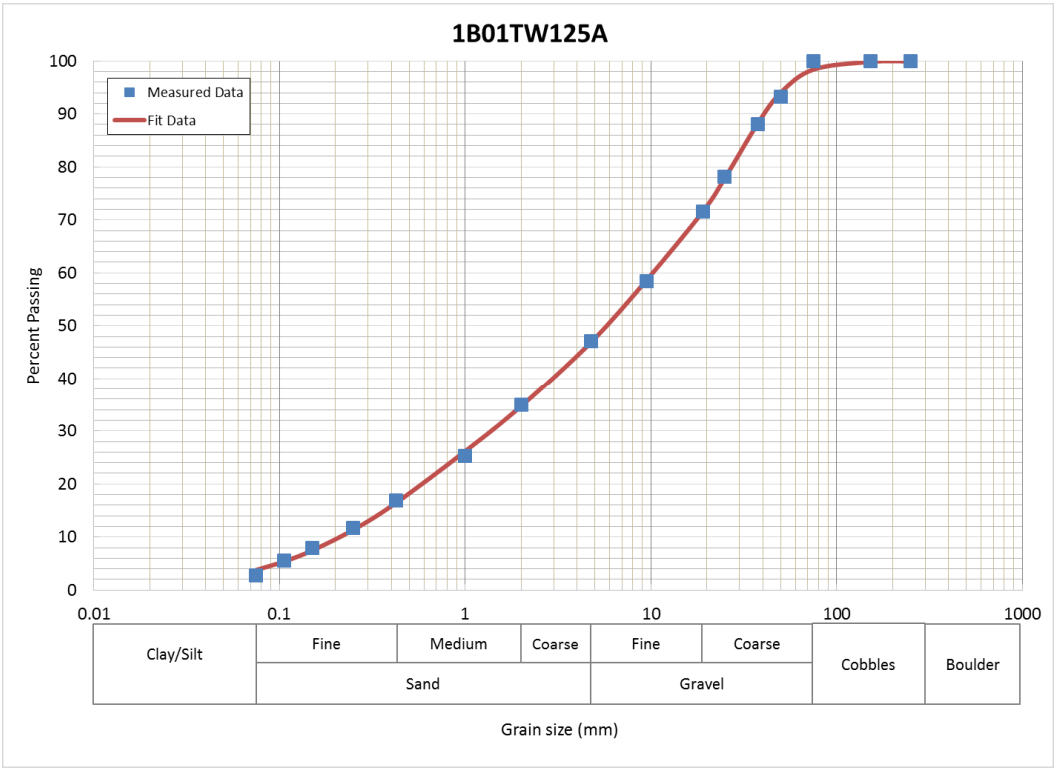
1B01TW125A
Measured Data
Fit Data
Percent Passing
100
90
80
70
60
50
40
30
20
10
0
0.01
0.1
1
10
100
1000
Clay/Silt
Fine
Medium
Coarse
Fine
Coarse
Cobbles
Boulder
Sand
Gravel
Grain size (mm)

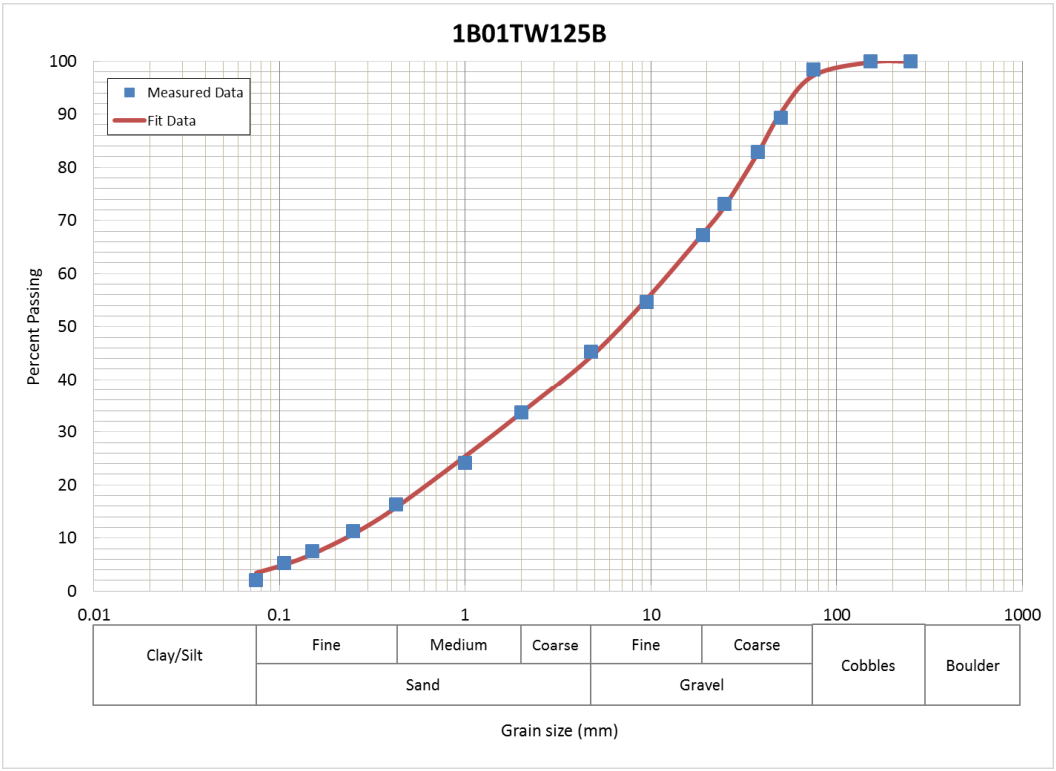
1B01TW125B
Measured Data
Fit Data
Percent Passing
100
90
80
70
60
50
40
30
20
10
0
0.01
0.1
1
10
100
1000
Clay/Silt
Fine
Medium
Coarse
Fine
Coarse
Cobbles
Boulder
Sand
Gravel
Grain size (mm)

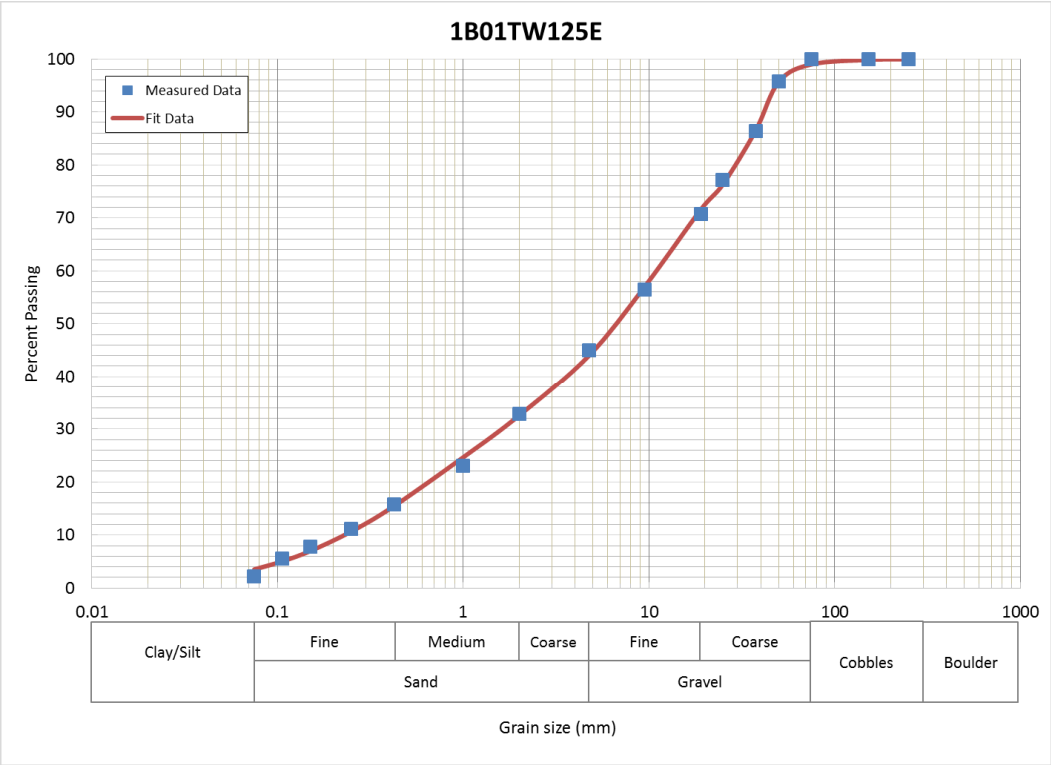
1B01TW125E
Measured Data
Fit Data
Percent Passing
100
90
80
70
60
50
40
30
20
10
0
0.01
0.1
1
10
100
1000
Clay/Silt
Fine
Medium
Coarse
Fine
Coarse
Sand
Gravel
Cobbles
Boulder
Grain size (mm)

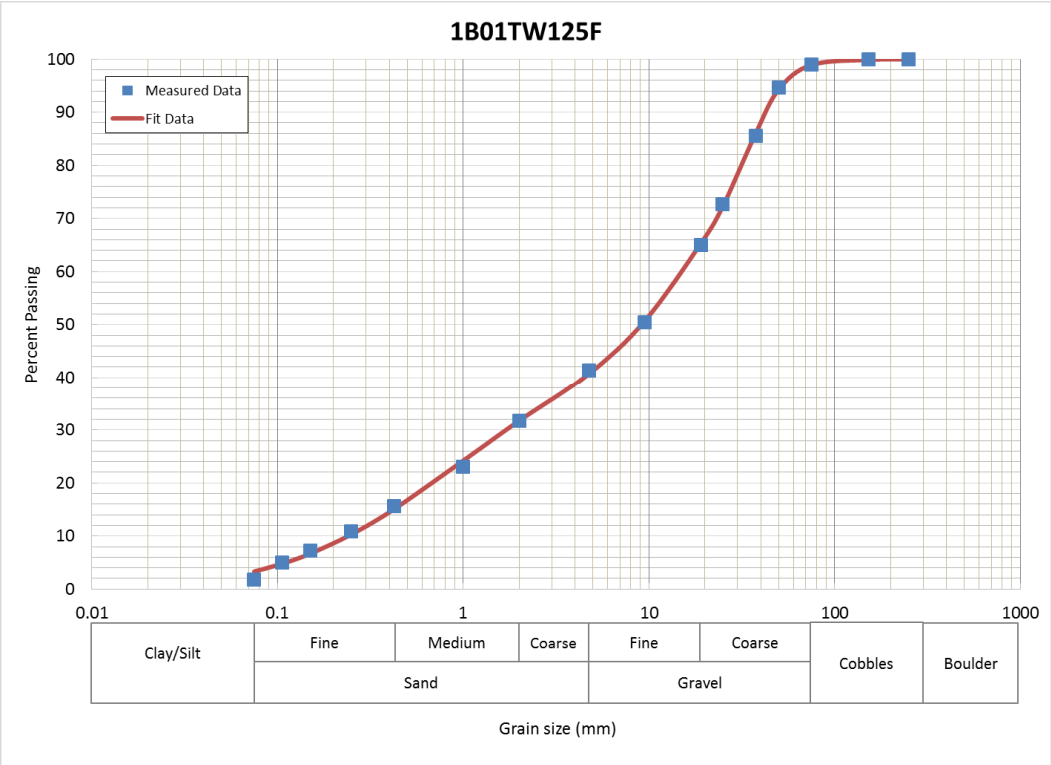
1B01TW125F
Measured Data
Fit Data
Percent Passing
100
90
80
70
60
50
40
30
20
10
0
0.01
0.1
1
10
100
1000
Clay/Silt
Fine
Medium
Coarse
Fine
Coarse
Sand
Gravel
Cobbles
Boulder
Grain size (mm)

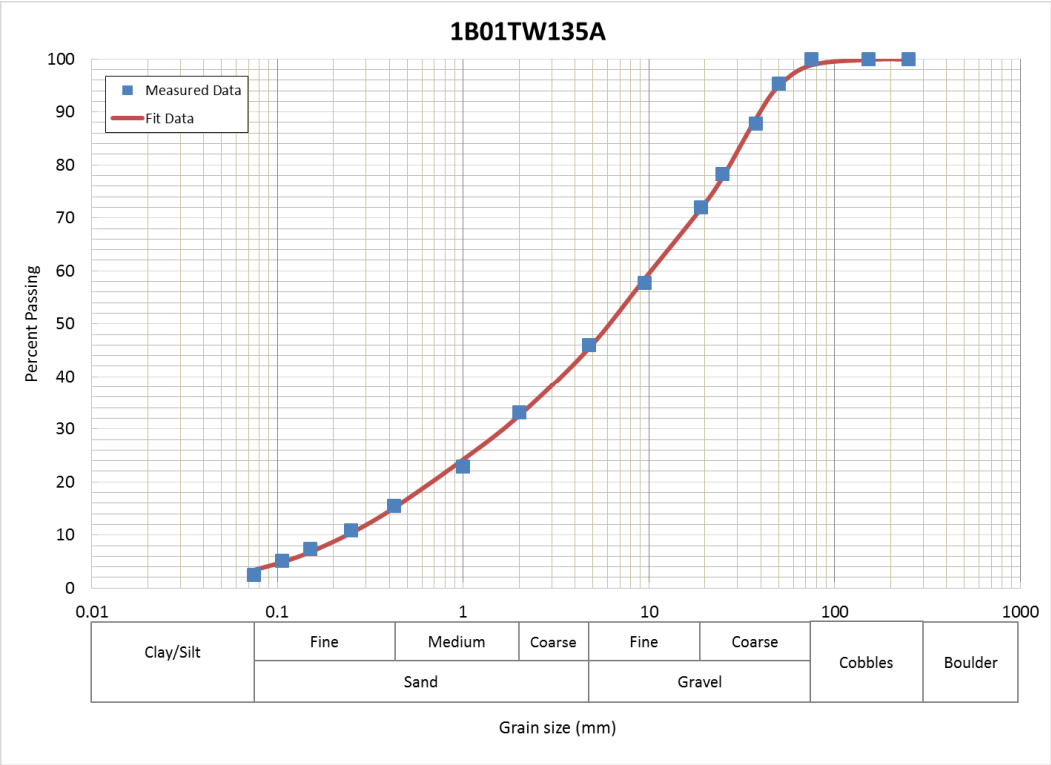
1B01TW135A
Measured Data
Fit Data
Percent Passing
100
90
80
70
60
50
40
30
20
10
0
0.01
0.1
1
10
100
1000
Clay/Silt
Fine
Medium
Coarse
Fine
Coarse
Cobbles
Boulder
Sand
Gravel
Grain size (mm)

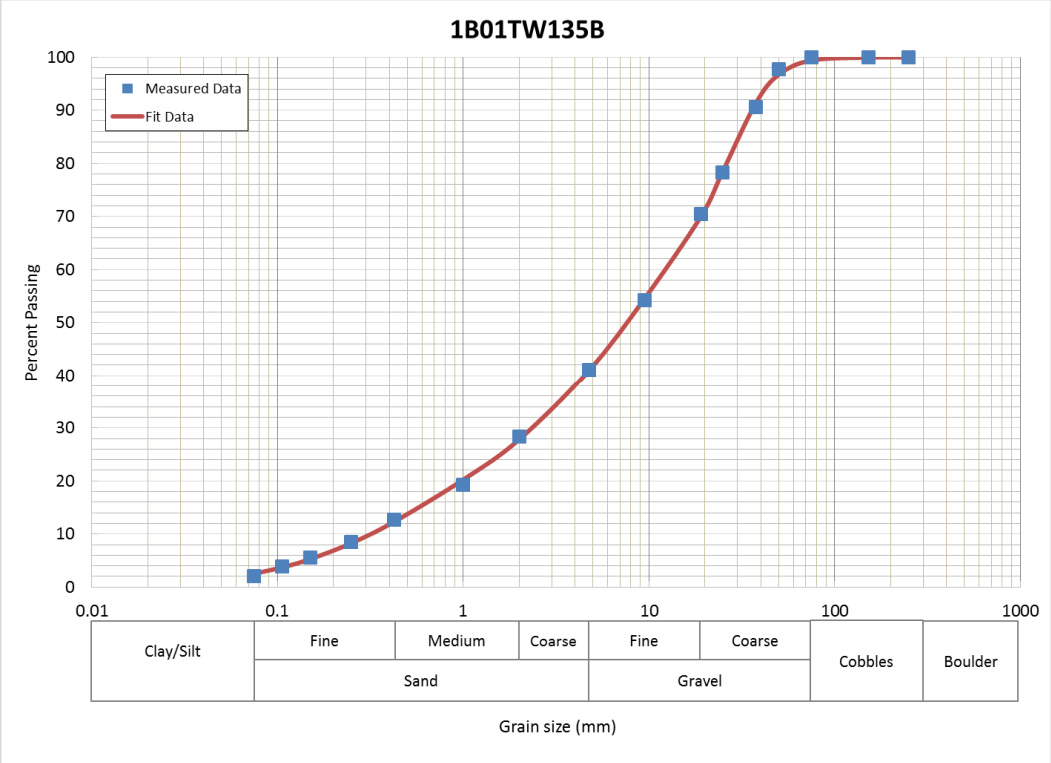
1B01TW135B
Measured Data
Fit Data
Percent Passing
100
90
80
70
60
50
40
30
20
10
0
0.01
0.1
1
10
100
1000
Clay/Silt
Fine
Medium
Coarse
Fine
Coarse
Cobbles
Boulder
Sand
Gravel
Grain size (mm)

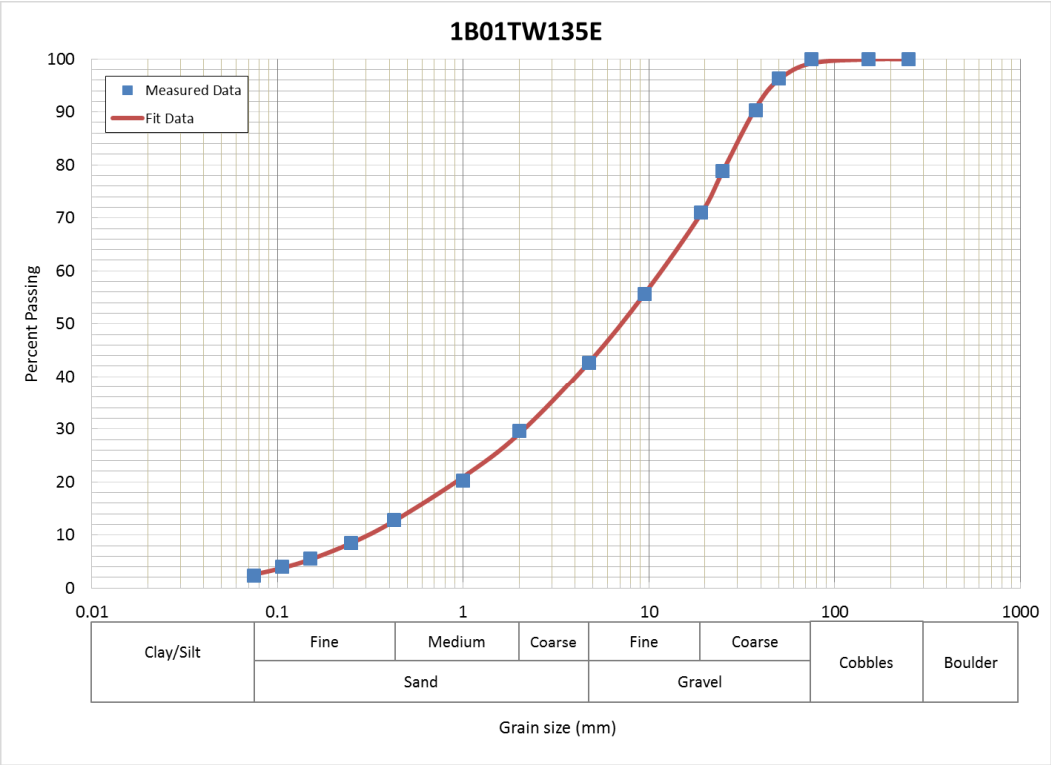
1B01TW135E
Measured Data
Fit Data
Percent Passing
100
90
80
70
60
50
40
30
20
10
0
0.01
0.1
1
10
100
1000
Clay/Silt
Fine
Medium
Coarse
Fine
Coarse
Cobbles
Boulder
Sand
Gravel
Grain size (mm)

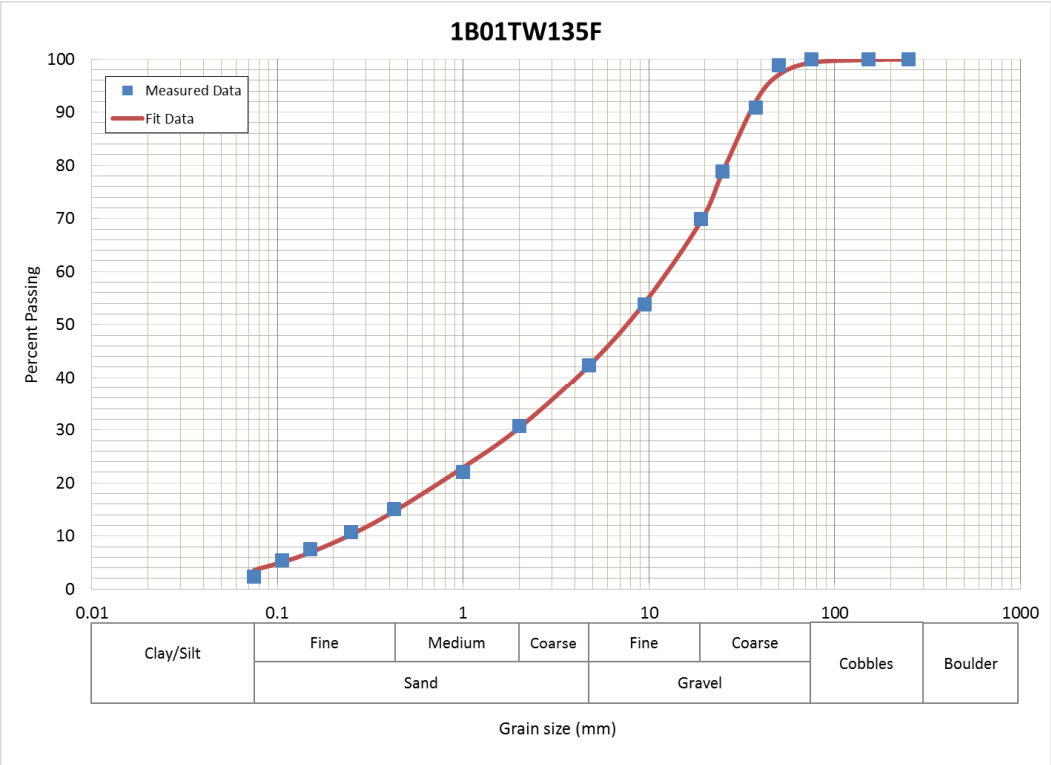
1B01TW135F
Measured Data
Fit Data
Percent Passing
100
90
80
70
60
50
40
30
20
10
0
0.01
0.1
1
10
100
1000
Clay/Silt
Fine
Medium
Coarse
Fine
Coarse
Cobbles
Boulder
Sand
Gravel
Grain size (mm)

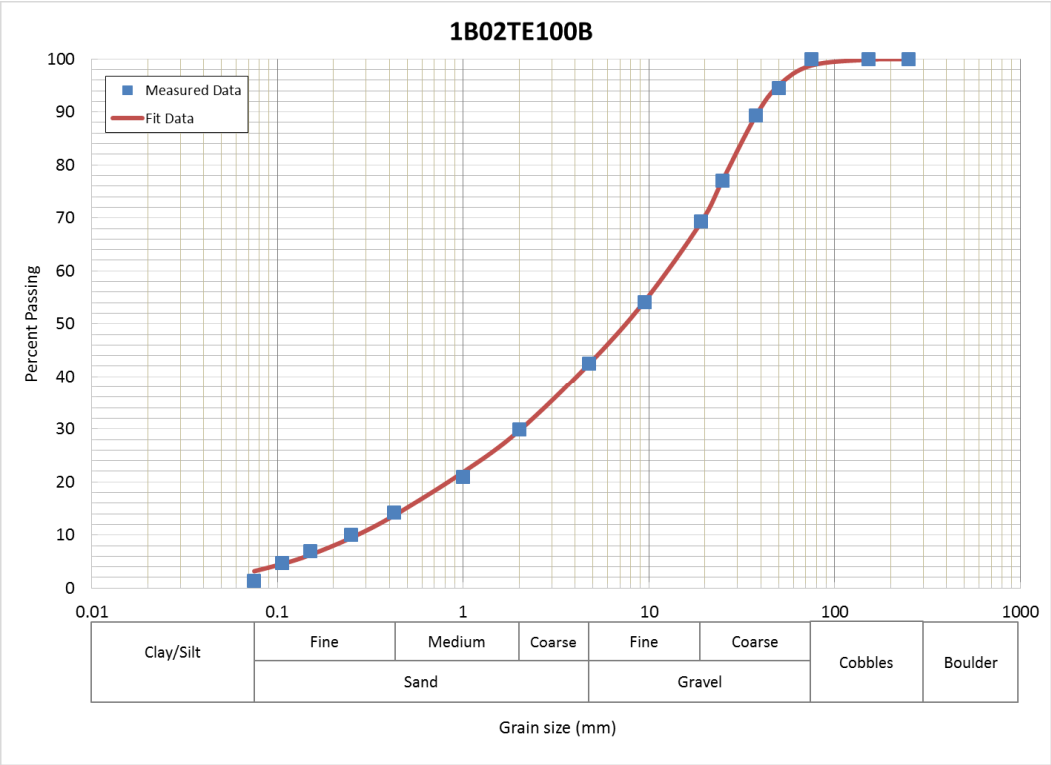
1B02TE100B
Measured Data
Fit Data
Percent Passing
100
90
80
70
60
50
40
30
20
10
0
0.01
0.1
1
10
100
1000
Clay/Silt
Fine
Medium
Coarse
Fine
Coarse
Cobbles
Boulder
Sand
Gravel
Grain size (mm)

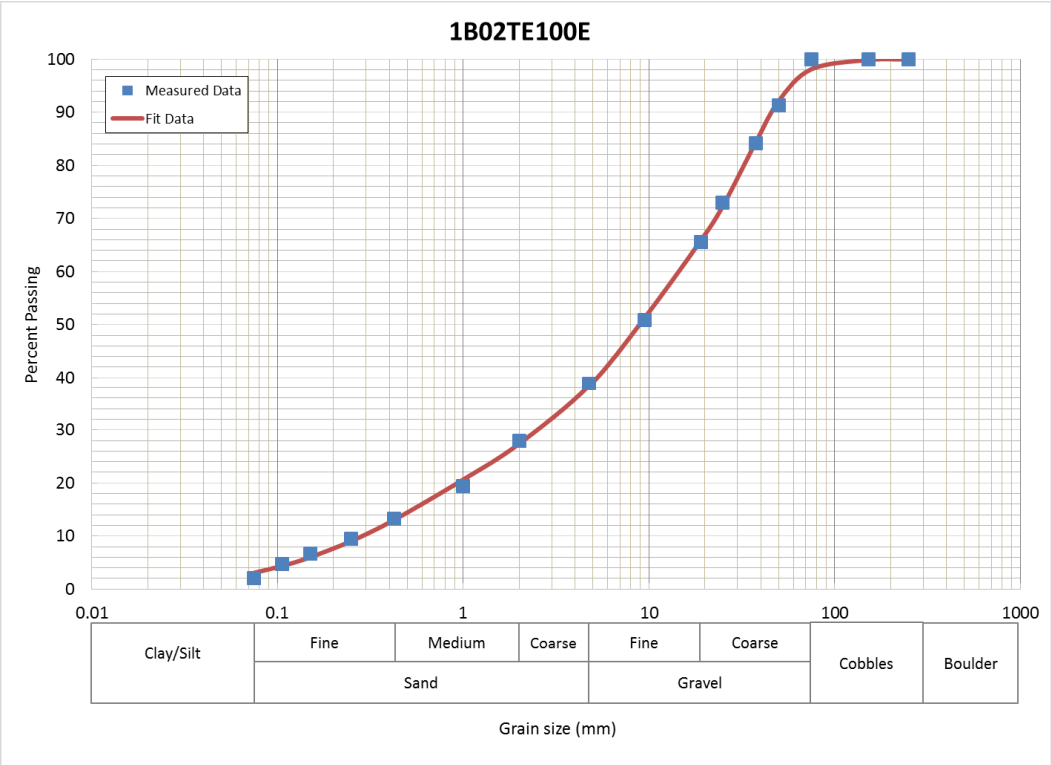
1B02TE100E
Measured Data
Fit Data
Percent Passing
100
90
80
70
60
50
40
30
20
10
0
0.01
0.1
1
10
100
1000
Clay/Silt
Fine
Medium
Coarse
Fine
Coarse
Cobbles
Boulder
Sand
Gravel
Grain size (mm)

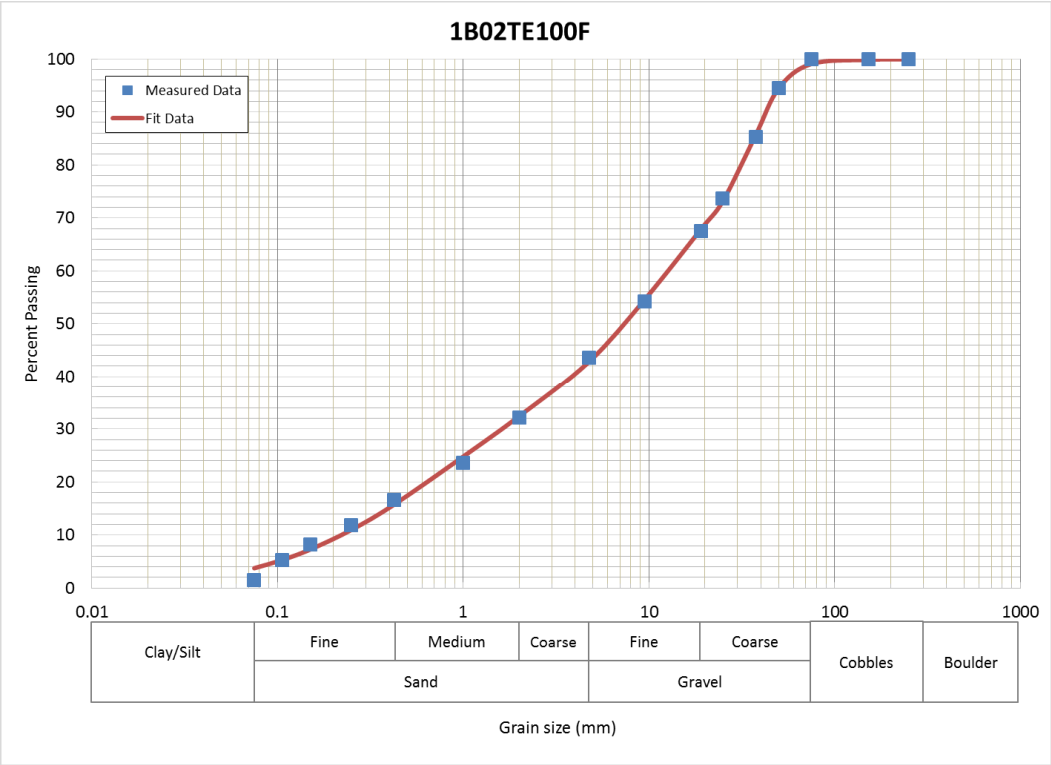
1B02TE100F
Measured Data
Fit Data
Percent Passing
100
90
80
70
60
50
40
30
20
10
0
0.01
0.1
1
10
100
1000
Clay/Silt
Fine
Medium
Coarse
Fine
Coarse
Cobbles
Boulder
Sand
Gravel
Grain size (mm)

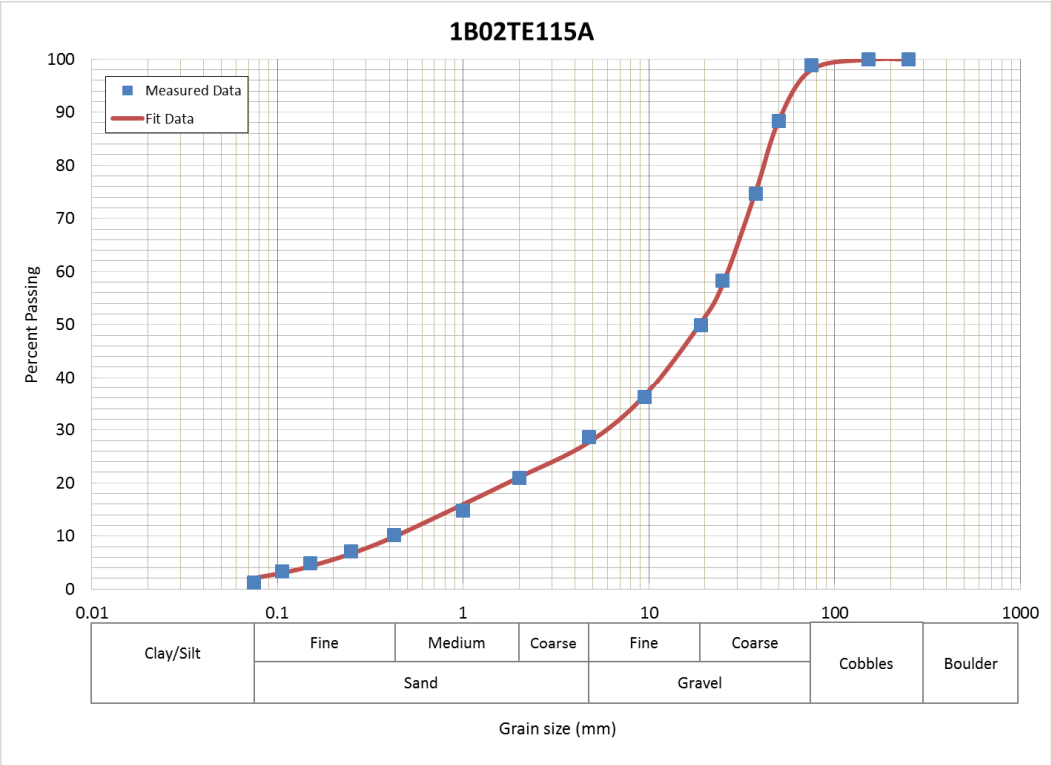
1B02TE115A
Measured Data
Fit Data
Percent Passing
100
90
80
70
60
50
40
30
20
10
0
0.01
0.1
1
10
100
1000
Clay/Silt
Fine
Medium
Coarse
Fine
Coarse
Cobbles
Boulder
Sand
Gravel
Grain size (mm)

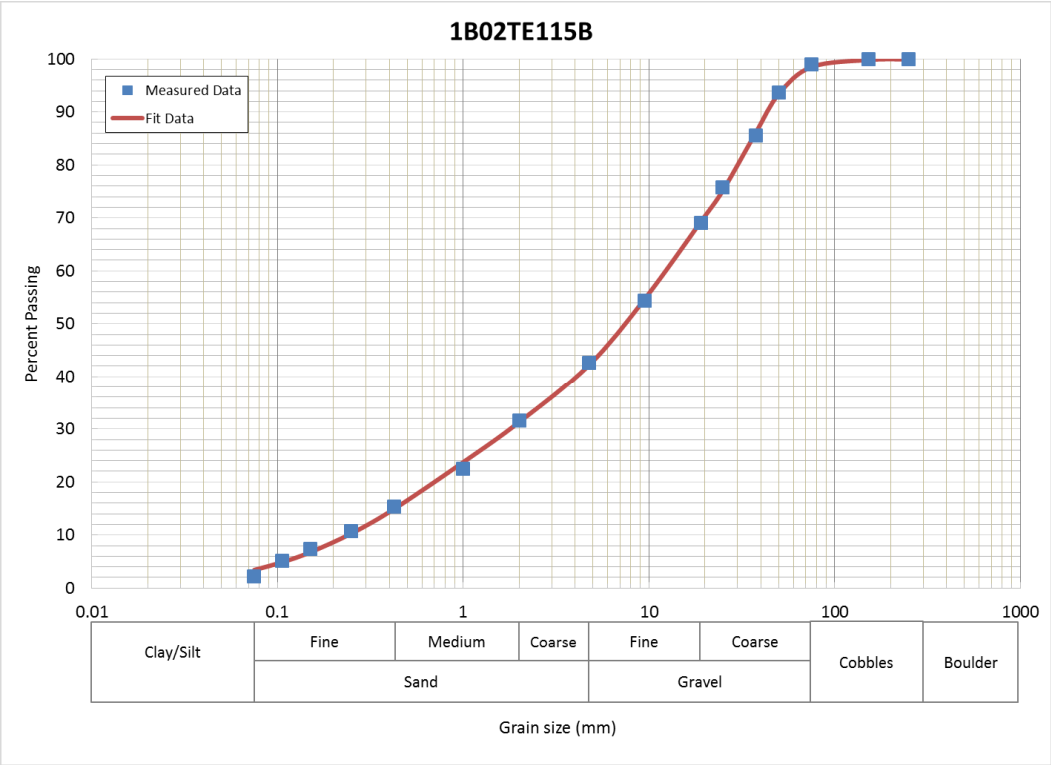
1B02TE115B
Measured Data
Fit Data
Percent Passing
100
90
80
70
60
50
40
30
20
10
0
0.01
0.1
1
10
100
1000
Clay/Silt
Fine
Medium
Coarse
Fine
Coarse
Cobbles
Boulder
Sand
Gravel
Grain size (mm)

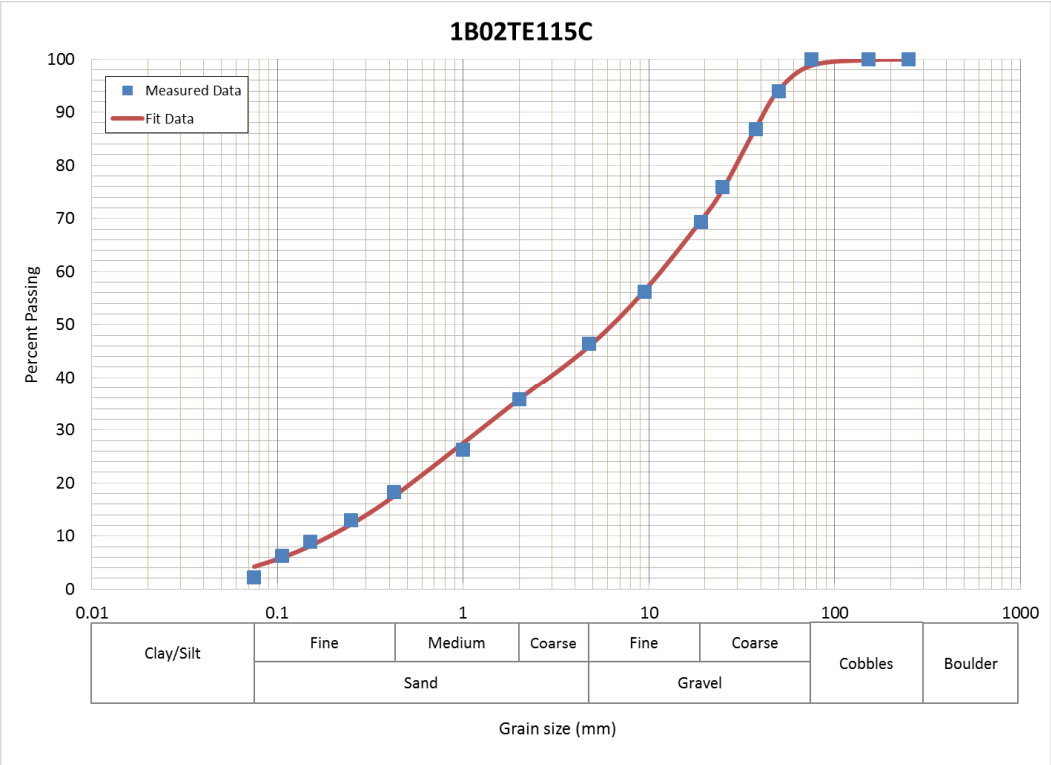
1B02TE115C
Measured Data
Fit Data
Percent Passing
100
90
80
70
60
50
40
30
20
10
0
0.01
0.1
1
10
100
1000
Clay/Silt
Fine
Medium
Coarse
Fine
Coarse
Cobbles
Boulder
Sand
Gravel
Grain size (mm)

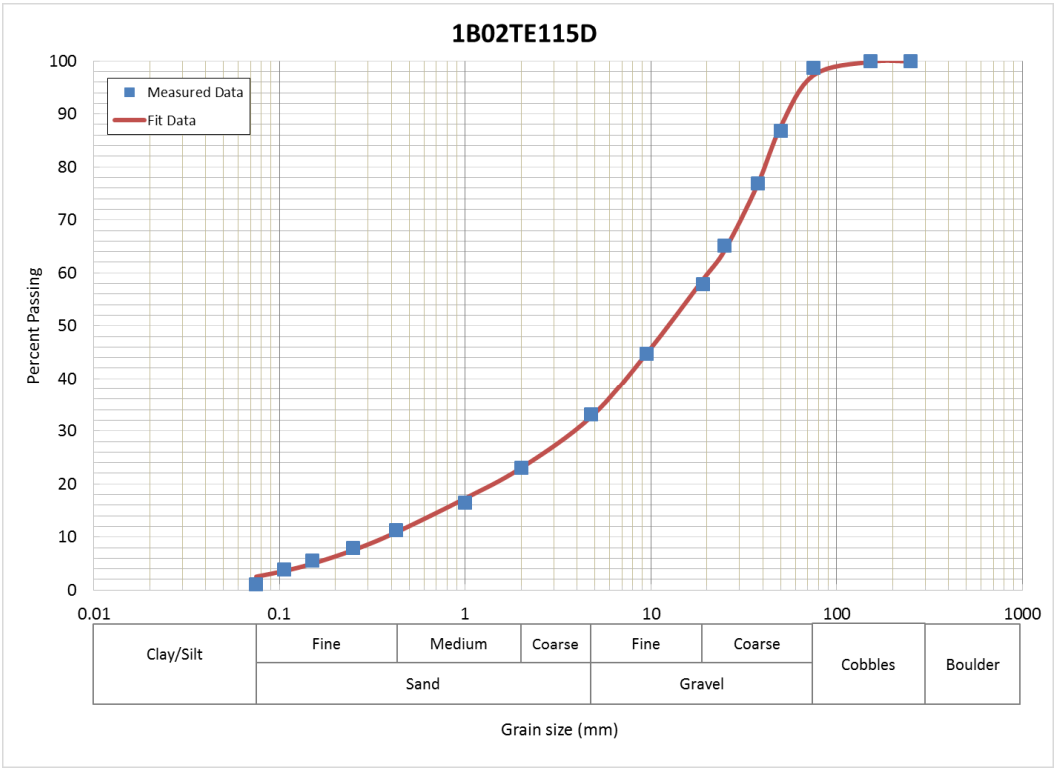
1B02TE115D
Measured Data
Fit Data
Percent Passing
100
90
80
70
60
50
40
30
20
10
0
0.01
0.1
1
10
100
1000
Clay/Silt
Fine
Medium
Coarse
Fine
Coarse
Cobbles
Boulder
Sand
Gravel
Grain size (mm)

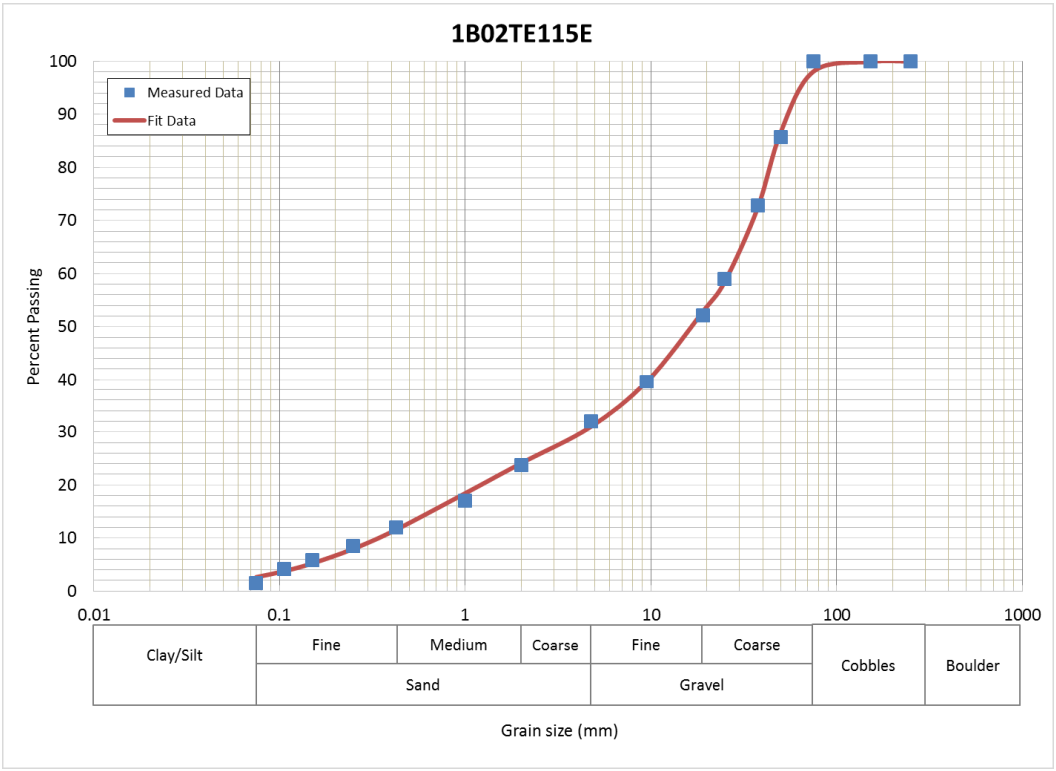
1B02TE115E
Measured Data
Fit Data
Percent Passing
100
90
80
70
60
50
40
30
20
10
0
0.01
0.1
1
10
100
1000
Clay/Silt
Fine
Medium
Coarse
Fine
Coarse
Cobbles
Boulder
Sand
Gravel
Grain size (mm)

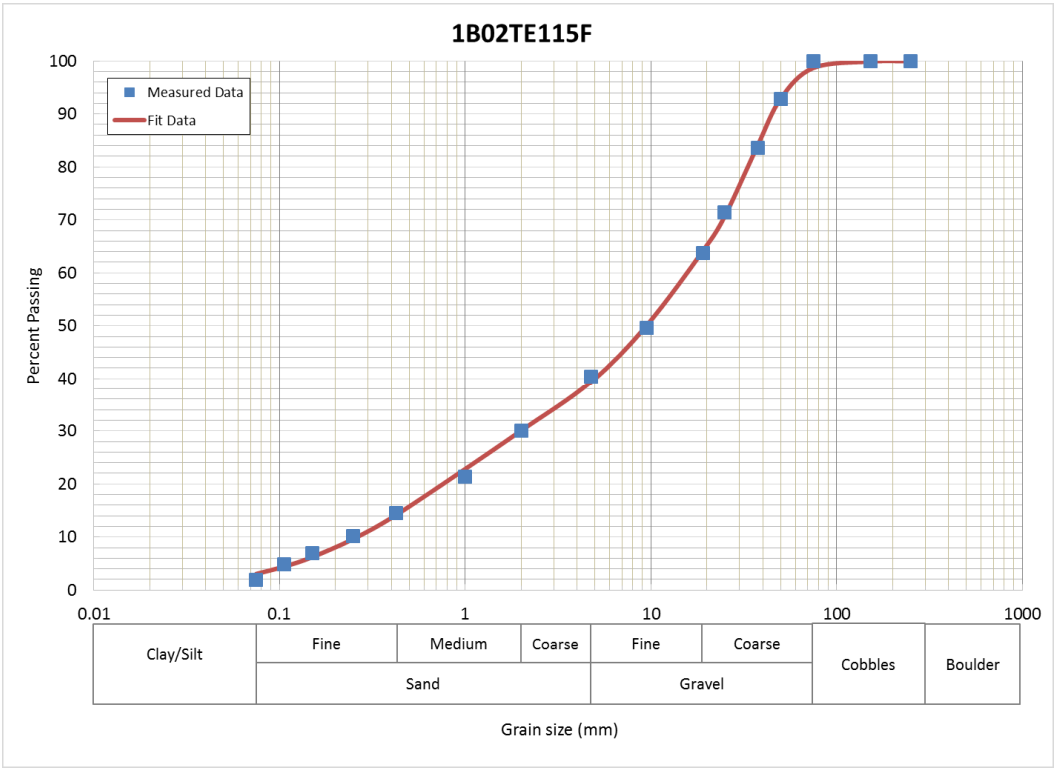
1B02TE115F
Measured Data
Fit Data
Percent Passing
100
90
80
70
60
50
40
30
20
10
0
0.01
0.1
1
10
100
1000
Clay/Silt
Fine
Medium
Coarse
Fine
Coarse
Cobbles
Boulder
Sand
Gravel
Grain size (mm)

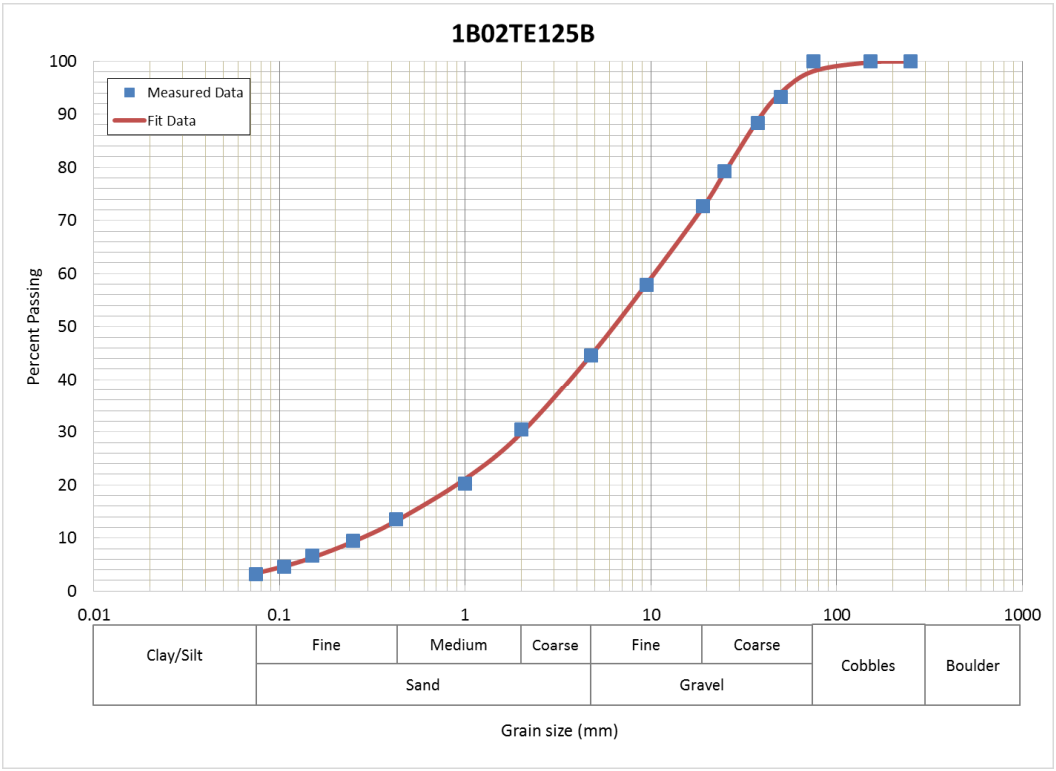
1B02TE125B
Measured Data
Fit Data
Percent Passing
100
90
80
70
60
50
40
30
20
10
0
0.01
0.1
1
10
100
1000
Clay/Silt
Fine
Medium
Coarse
Fine
Coarse
Cobbles
Boulder
Sand
Gravel
Grain size (mm)

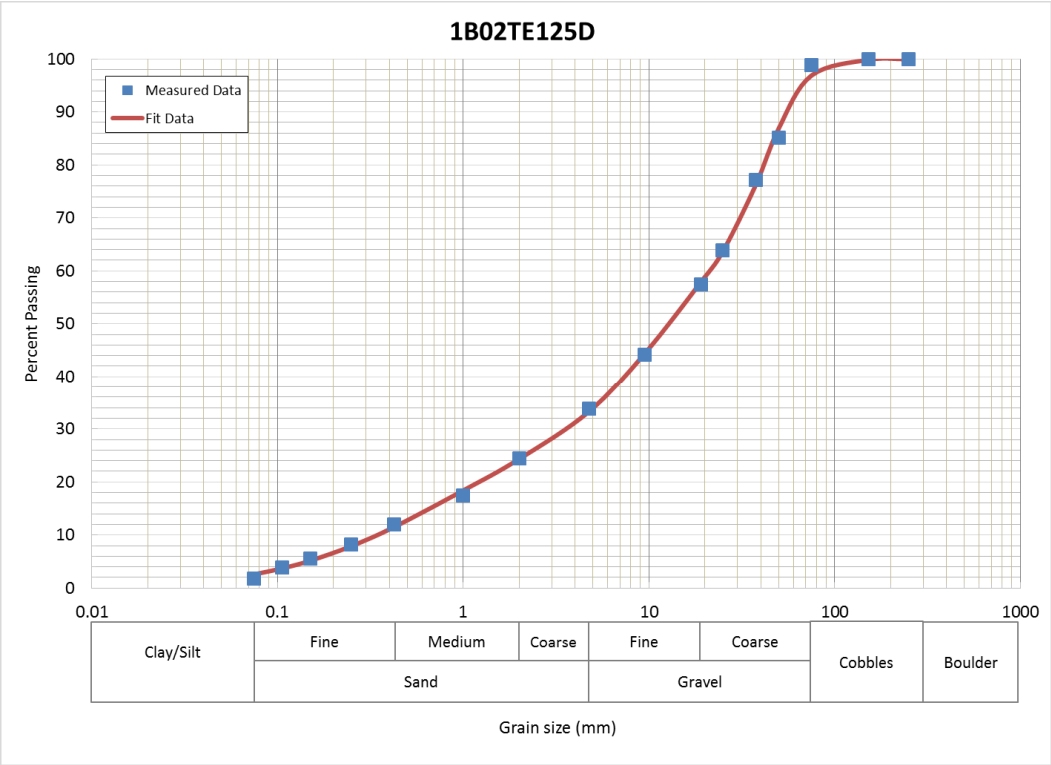
1B02TE125D
Measured Data
Fit Data
Percent Passing
100
90
80
70
60
50
40
30
20
10
0
0.01
0.1
1
10
100
1000
Clay/Silt
Fine
Medium
Coarse
Fine
Coarse
Cobbles
Boulder
Sand
Gravel
Grain size (mm)

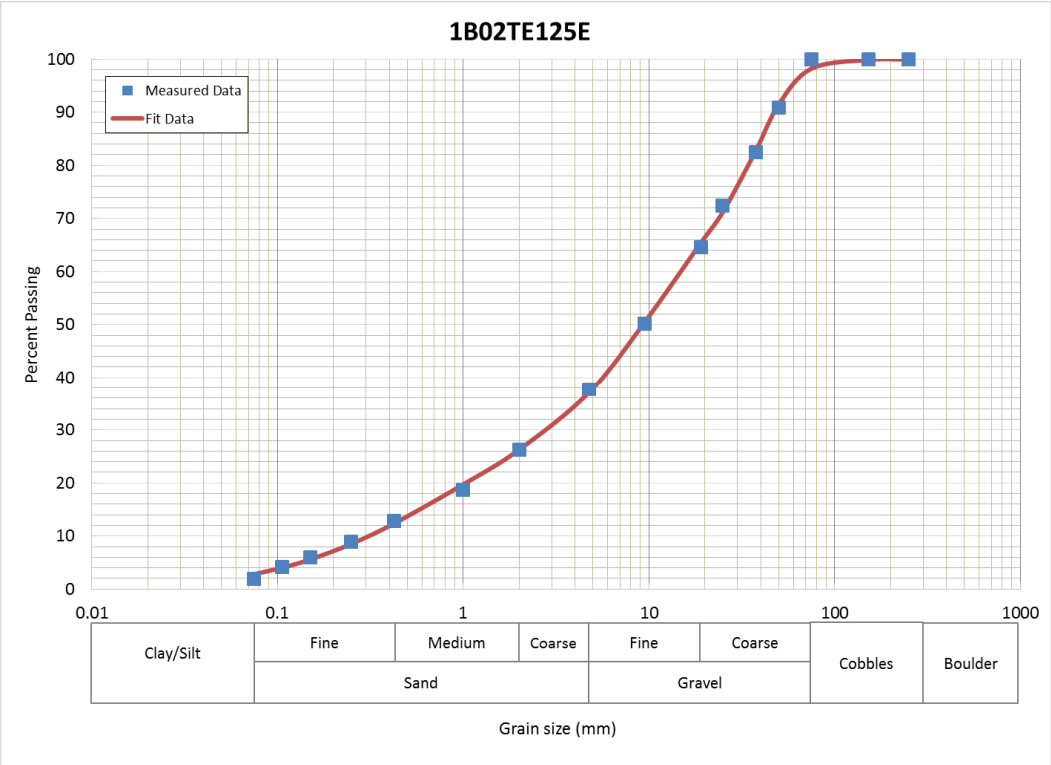
1B02TE125E
Measured Data
Fit Data
Percent Passing
100
90
80
70
60
50
40
30
20
10
0
0.01
0.1
1
10
100
1000
Clay/Silt
Fine
Medium
Coarse
Fine
Coarse
Cobbles
Boulder
Sand
Gravel
Grain size (mm)

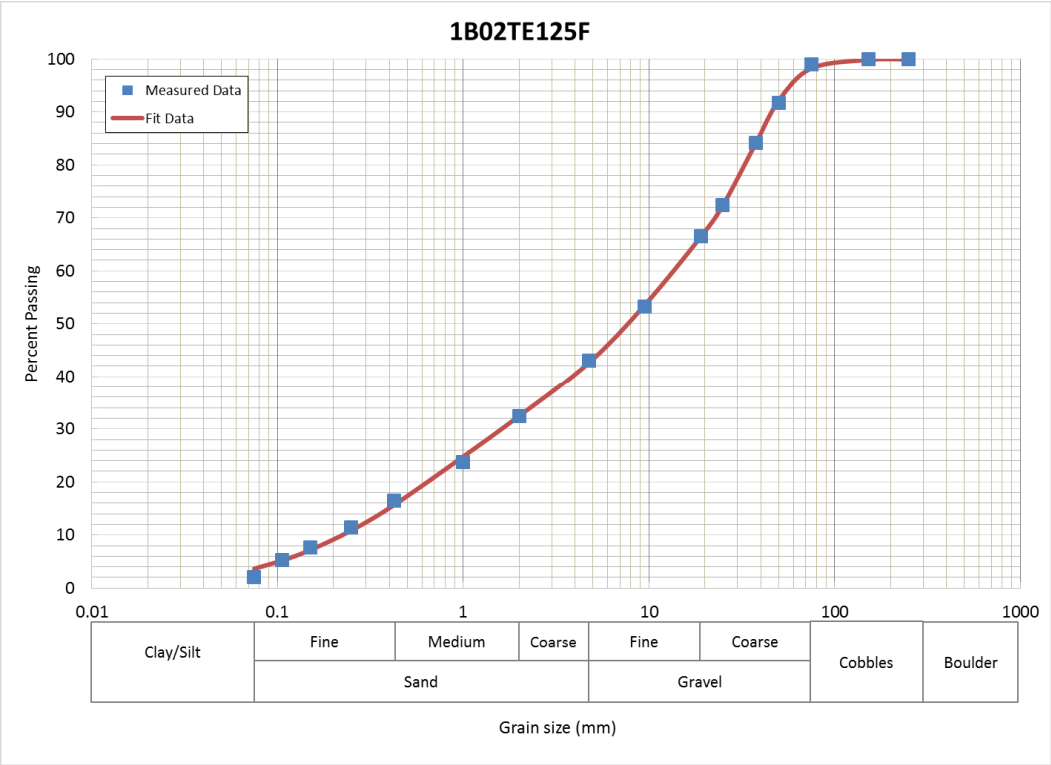
1B02TE125F
Measured Data
Fit Data
Percent Passing
100
90
80
70
60
50
40
30
20
10
0
0.01
0.1
1
10
100
1000
Clay/Silt
Fine
Medium
Coarse
Fine
Coarse
Cobbles
Boulder
Sand
Gravel
Grain size (mm)

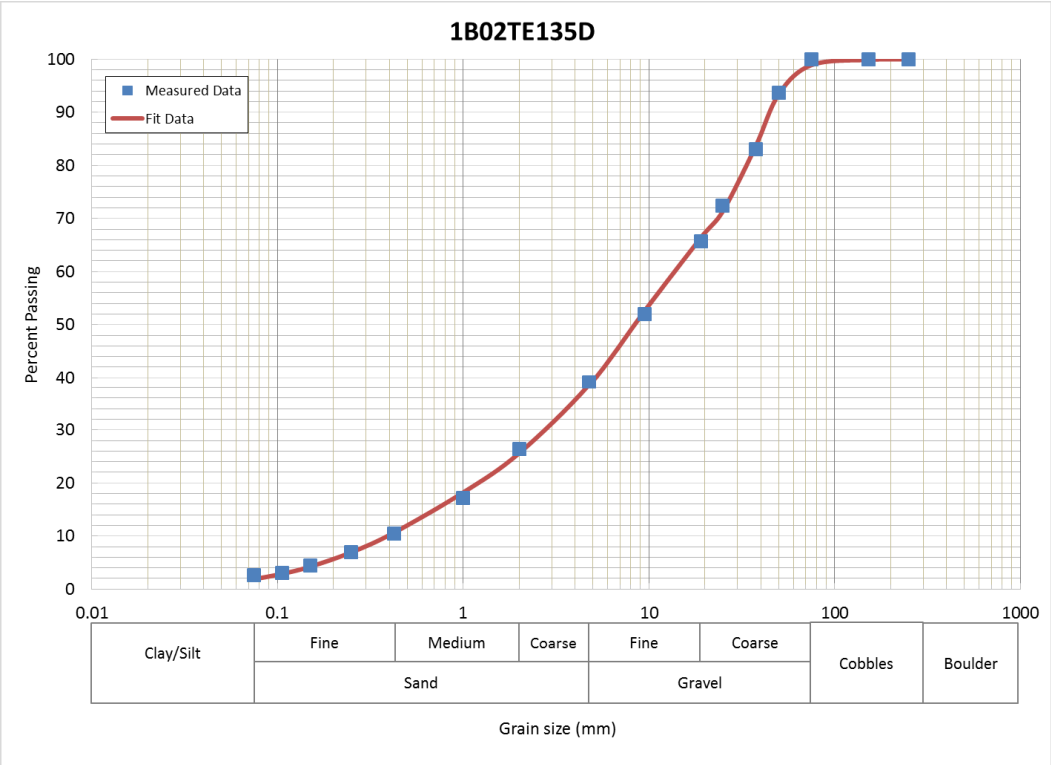
1B02TE135D
Measured Data
Fit Data
Percent Passing
100
90
80
70
60
50
40
30
20
10
0
0.01
0.1
1
10
100
1000
Clay/Silt
Fine
Medium
Coarse
Fine
Coarse
Cobbles
Boulder
Sand
Gravel
Grain size (mm)

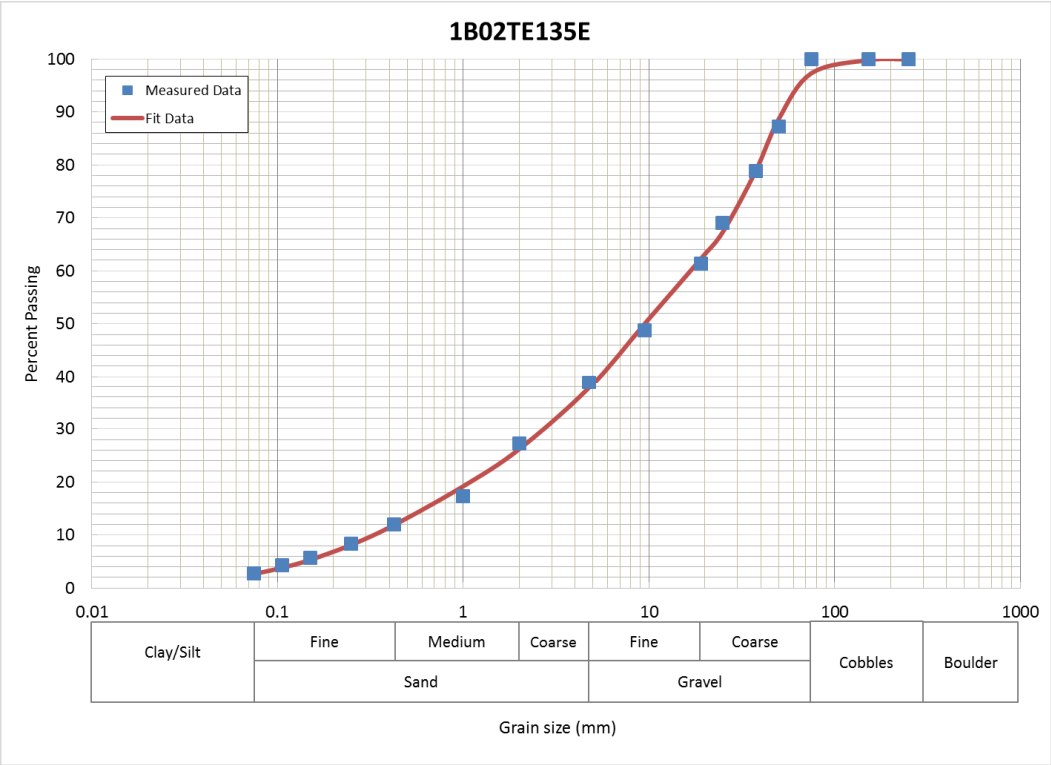
1B02TE135E
Measured Data
Fit Data
Percent Passing
100
90
80
70
60
50
40
30
20
10
0
0.01
0.1
1
10
100
1000
Clay/Silt
Fine
Medium
Coarse
Fine
Coarse
Cobbles
Boulder
Sand
Gravel
Grain size (mm)

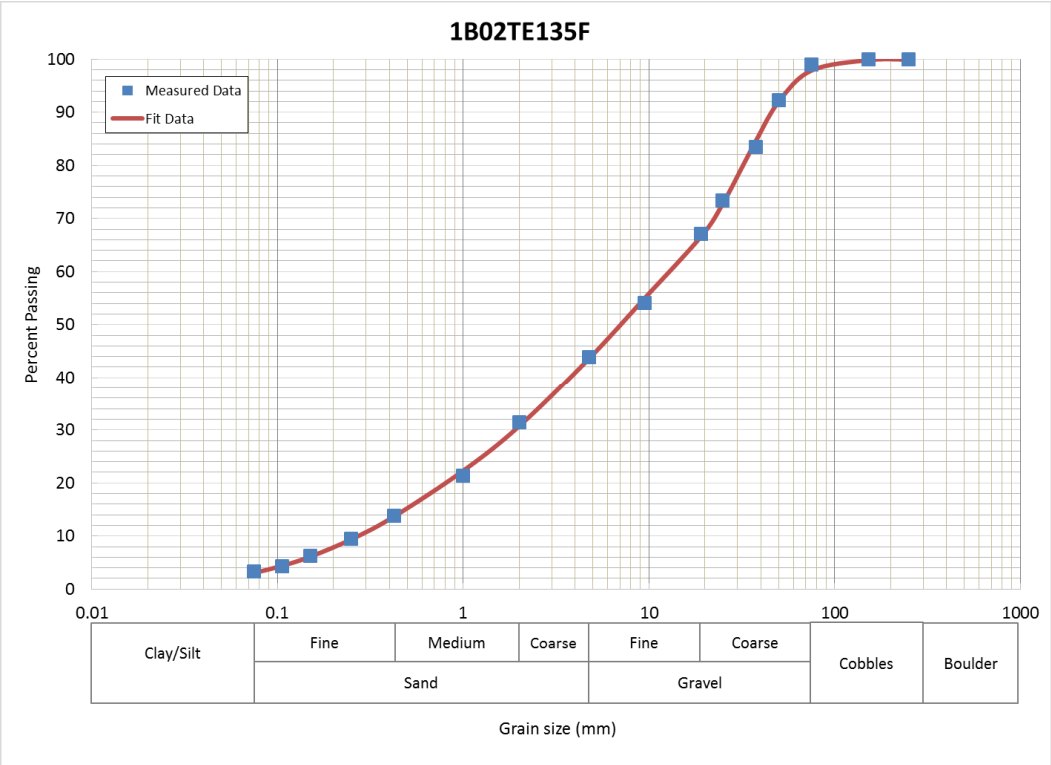
1B02TE135F
Measured Data
Fit Data
Percent Passing
100
90
80
70
60
50
40
30
20
10
0
0.01
0.1
1
10
100
1000
Clay/Silt
Fine
Medium
Coarse
Fine
Coarse
Cobbles
Boulder
Sand
Gravel
Grain size (mm)

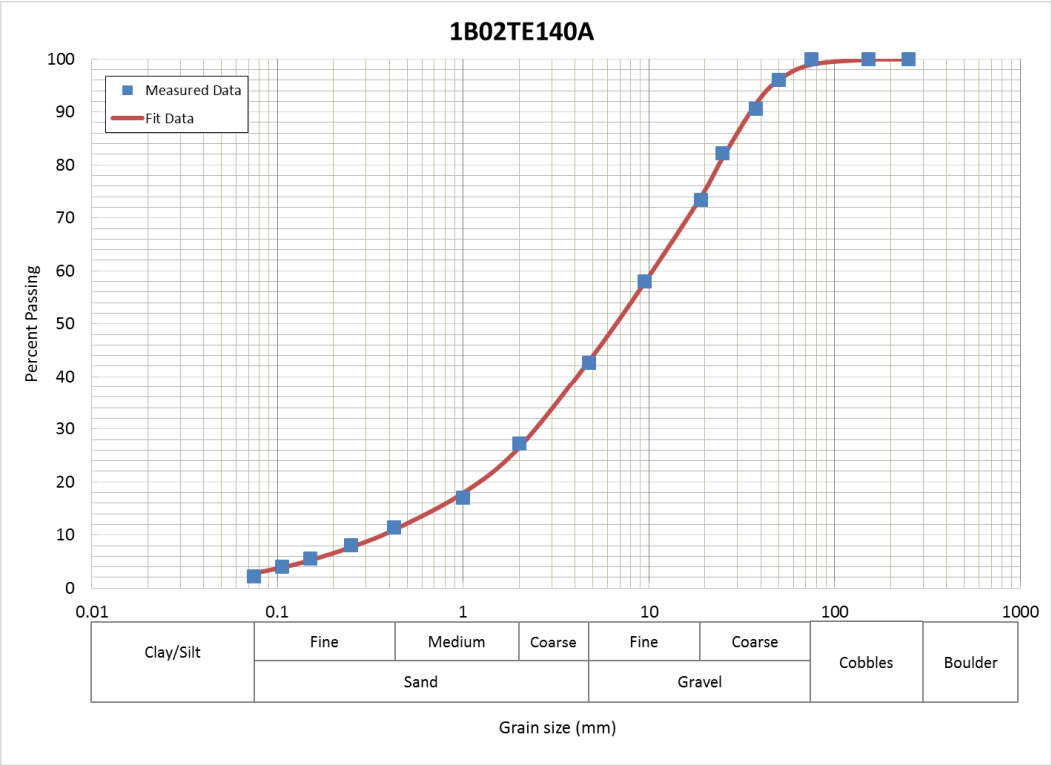
1B02TE140A
Measured Data
Fit Data
Percent Passing
100
90
80
70
60
50
40
30
20
10
0
0.01
0.1
1
10
100
1000
Clay/Silt
Fine
Medium
Coarse
Fine
Coarse
Cobbles
Boulder
Sand
Gravel
Grain size (mm)

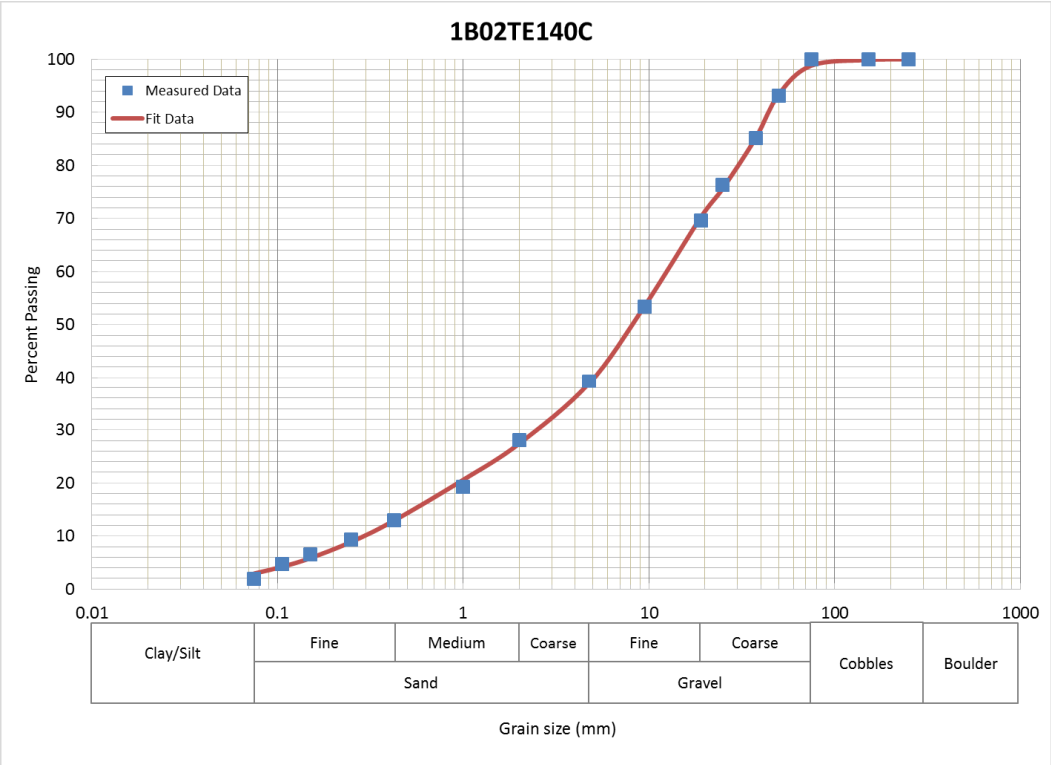
1B02TE140C
Measured Data
Fit Data
Percent Passing
100
90
80
70
60
50
40
30
20
10
0
0.01
0.1
1
10
100
1000
Clay/Silt
Fine
Medium
Coarse
Fine
Coarse
Cobbles
Boulder
Sand
Gravel
Grain size (mm)

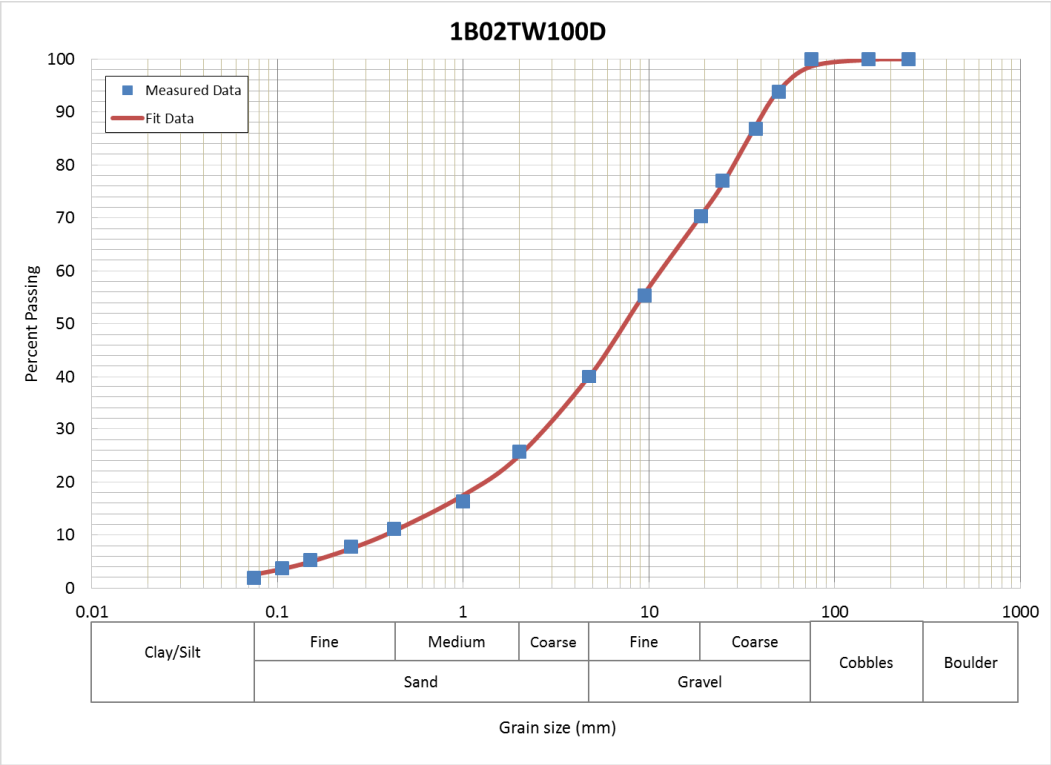
1B02TW100D
Measured Data
Fit Data
Percent Passing
100
90
80
70
60
50
40
30
20
10
0
0.01
0.1
1
10
100
1000
Clay/Silt
Fine
Medium
Coarse
Fine
Coarse
Cobbles
Boulder
Sand
Gravel
Grain size (mm)

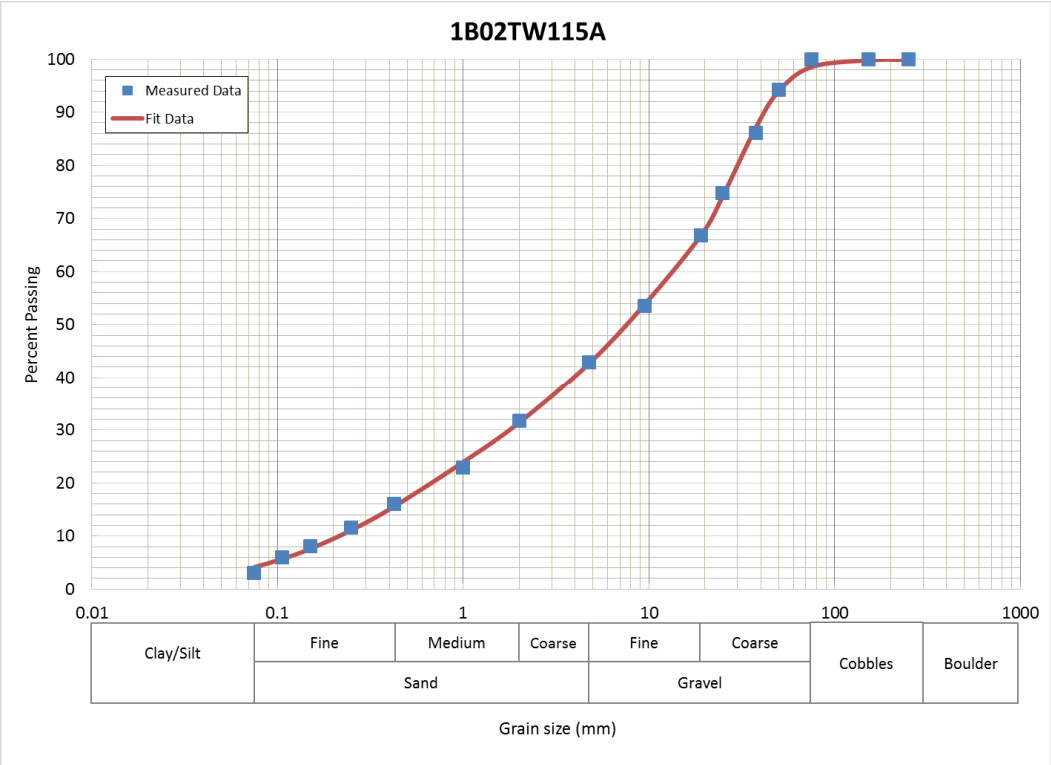
1B02TW115A
Measured Data
Fit Data
Percent Passing
100
90
80
70
60
50
40
30
20
10
0
0.01
0.1
1
10
100
1000
Clay/Silt
Fine
Medium
Coarse
Fine
Coarse
Cobbles
Boulder
Sand
Gravel
Grain size (mm)

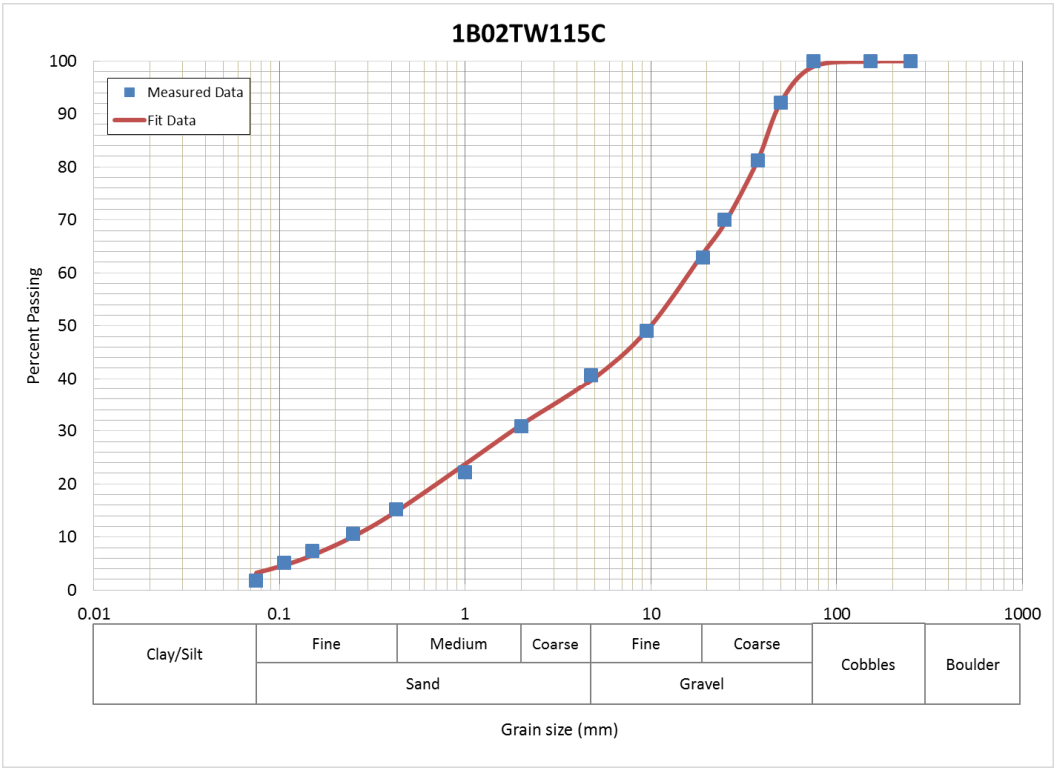
1B02TW115C
Measured Data
Fit Data
Percent Passing
100
90
80
70
60
50
40
30
20
10
0
0.01
0.1
1
10
100
1000
Clay/Silt
Fine
Medium
Coarse
Fine
Coarse
Cobbles
Boulder
Sand
Gravel
Grain size (mm)

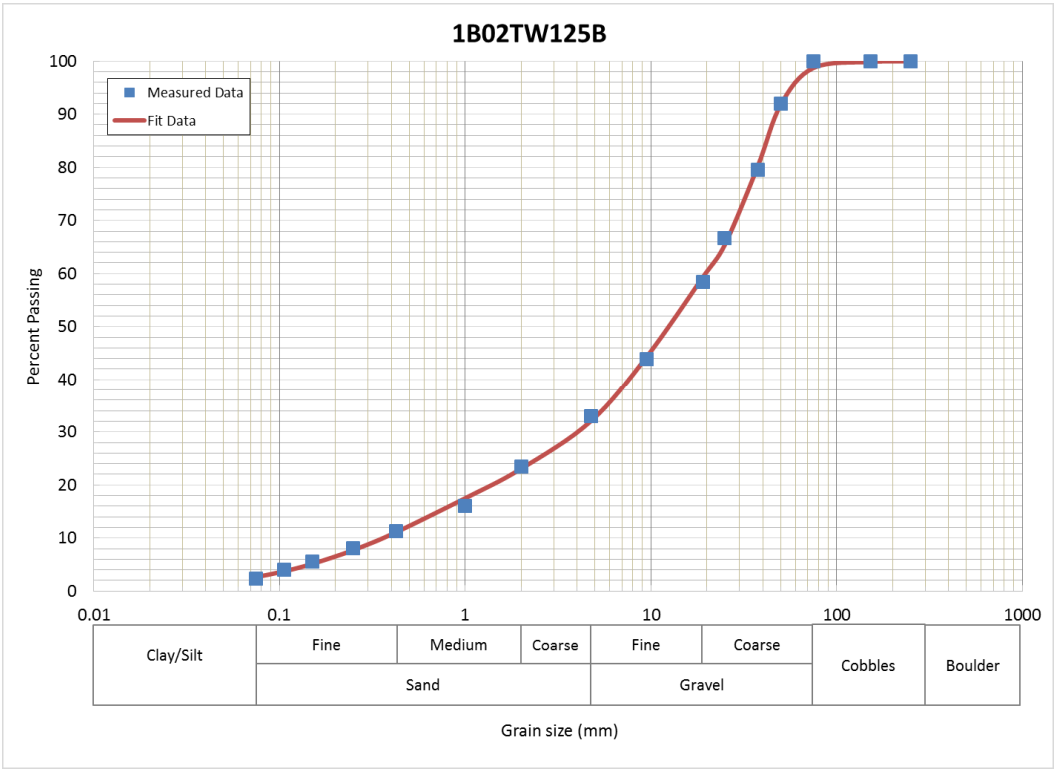
1B02TW125B
Measured Data
Fit Data
Percent Passing
100
90
80
70
60
50
40
30
20
10
0
0.01
0.1
1
10
100
1000
Clay/Silt
Fine
Medium
Coarse
Fine
Coarse
Cobbles
Boulder
Sand
Gravel
Grain size (mm)

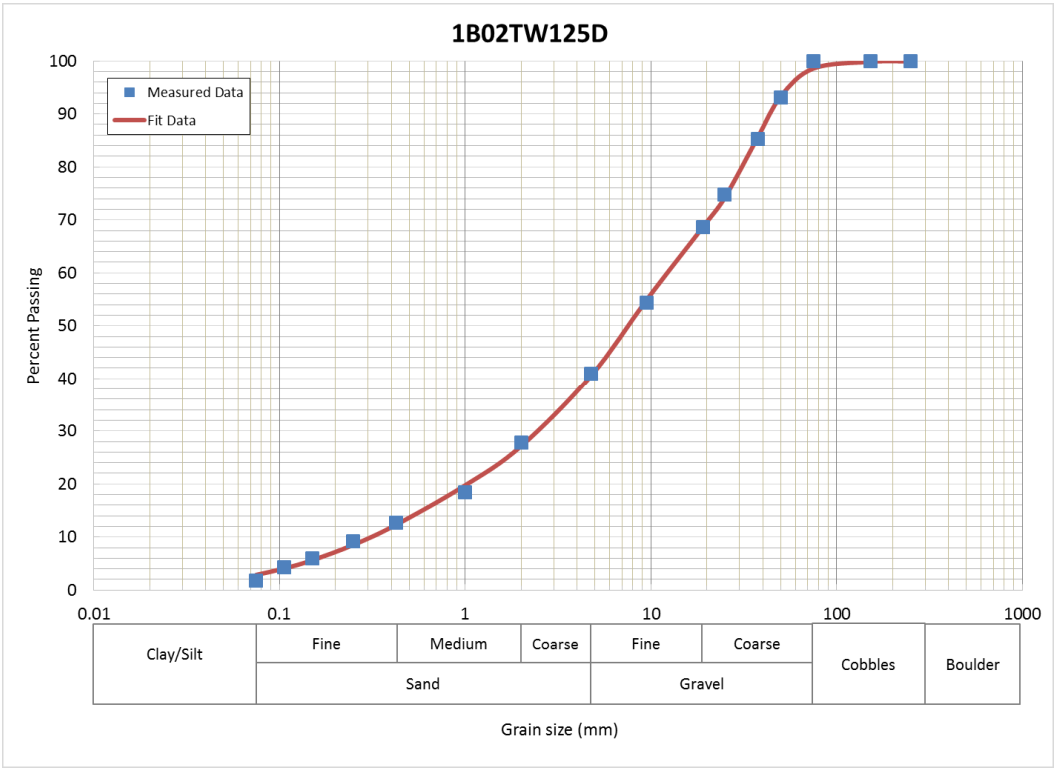
1B02TW125D
Measured Data
Fit Data
Percent Passing
100
90
80
70
60
50
40
30
20
10
0
0.01
0.1
1
10
100
1000
Clay/Silt
Fine
Medium
Coarse
Fine
Coarse
Cobbles
Boulder
Sand
Gravel
Grain size (mm)

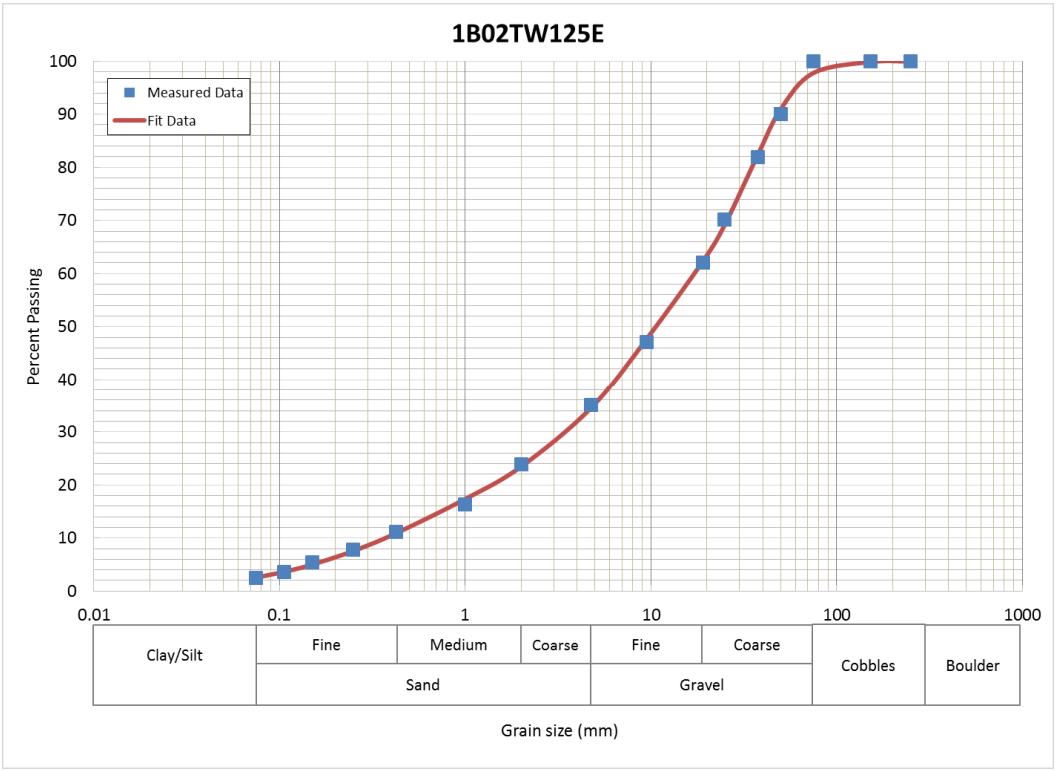
1B02TW125E
Measured Data
Fit Data
Percent Passing
100
90
80
70
60
50
40
30
20
10
0
0.01
0.1
1
10
100
1000
Clay/Silt
Fine
Medium
Coarse
Fine
Coarse
Cobbles
Boulder
Sand
Gravel
Grain size (mm)

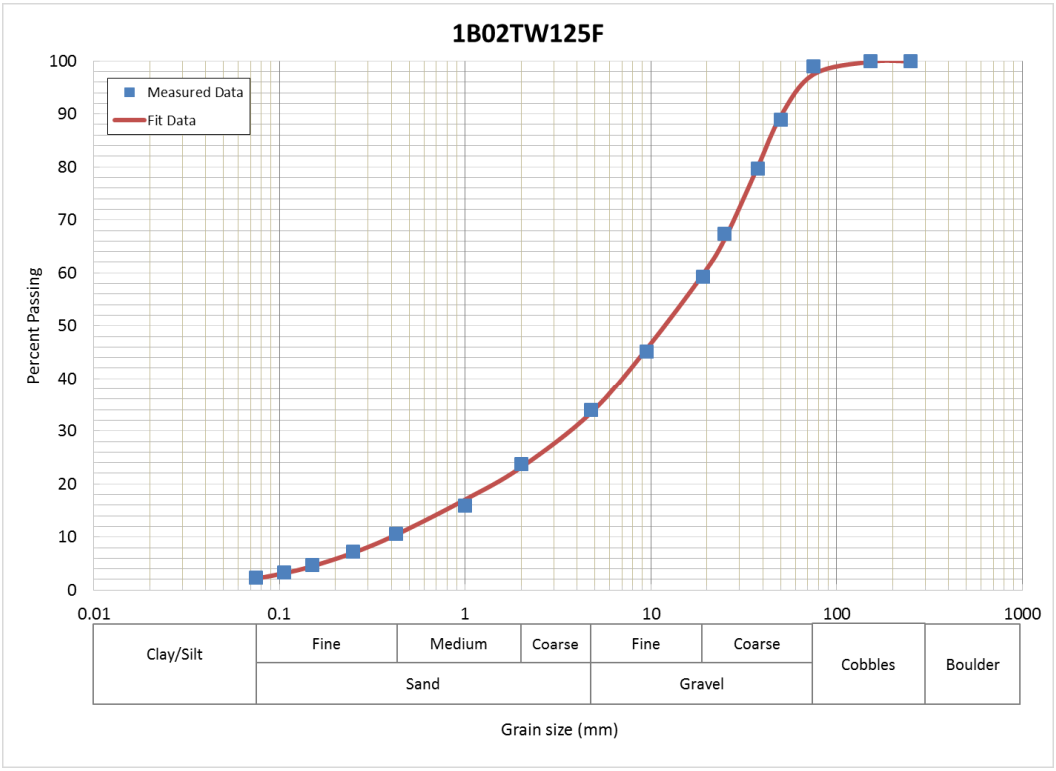
1B02TW125F
Measured Data
Fit Data
Percent Passing
100
90
80
70
60
50
40
30
20
10
0
0.01
0.1
1
10
100
1000
Clay/Silt
Fine
Medium
Coarse
Fine
Coarse
Cobbles
Boulder
Sand
Gravel
Grain size (mm)

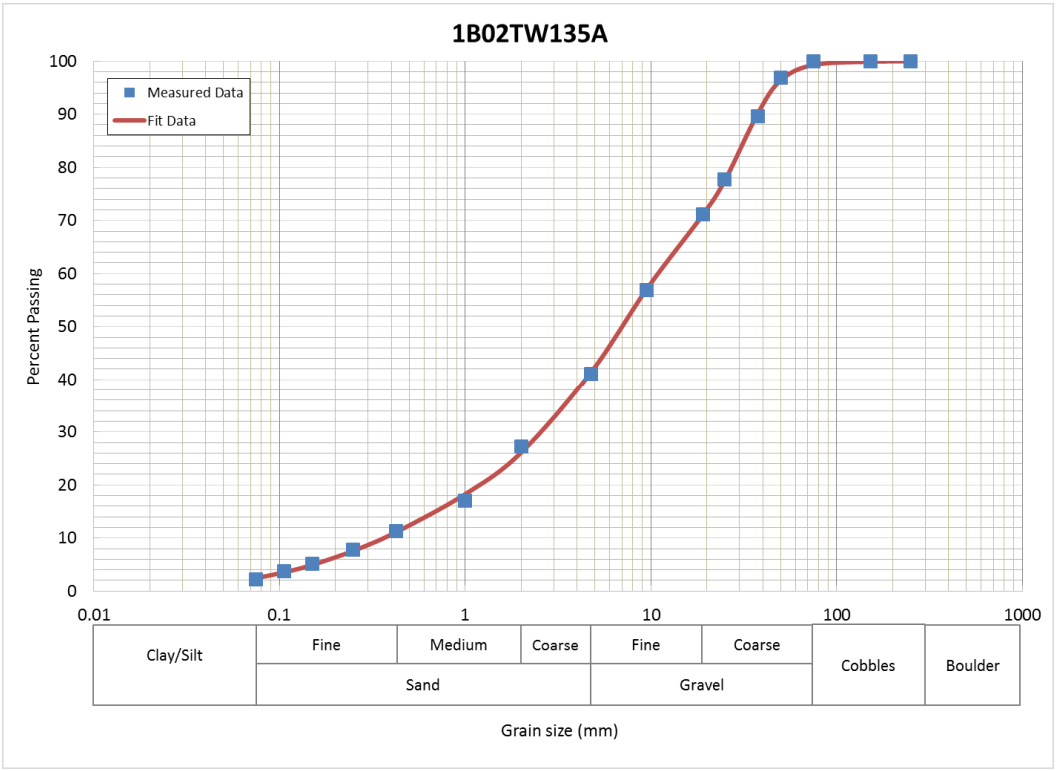
1B02TW135A
Measured Data
Fit Data
Percent Passing
100
90
80
70
60
50
40
30
20
10
0
0.01
0.1
1
10
100
1000
Clay/Silt
Fine
Medium
Coarse
Fine
Coarse
Cobbles
Boulder
Sand
Gravel
Grain size (mm)

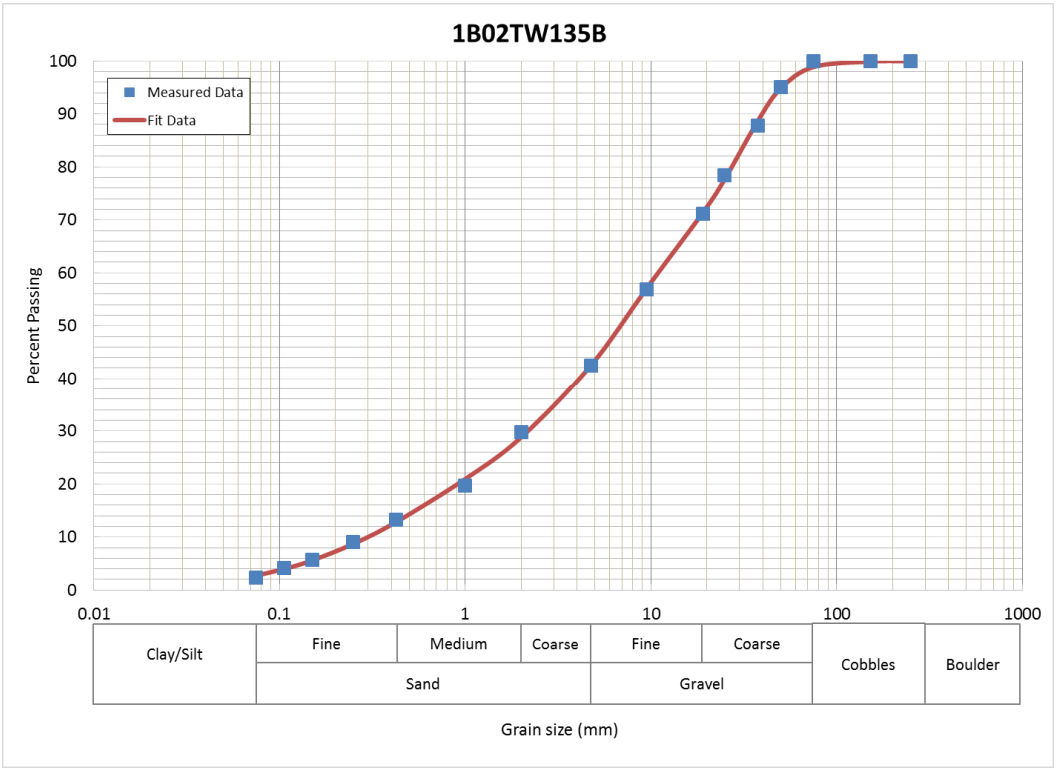
1B02TW135B
Measured Data
Fit Data
Percent Passing
100
90
80
70
60
50
40
30
20
10
0
0.01
0.1
1
10
100
1000
Clay/Silt
Fine
Medium
Coarse
Fine
Coarse
Cobbles
Boulder
Sand
Gravel
Grain size (mm)

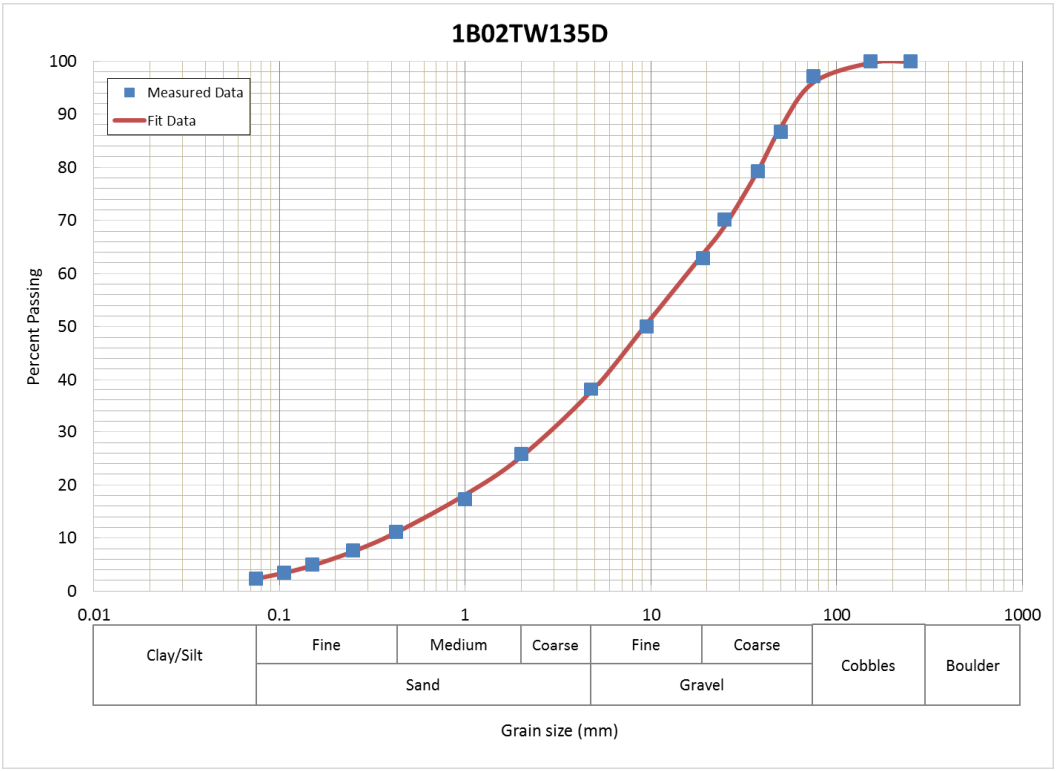
1B02TW135D
Measured Data
Fit Data
Percent Passing
100
90
80
70
60
50
40
30
20
10
0
0.01
0.1
1
10
100
1000
Clay/Silt
Fine
Medium
Coarse
Fine
Coarse
Cobbles
Boulder
Sand
Gravel
Grain size (mm)

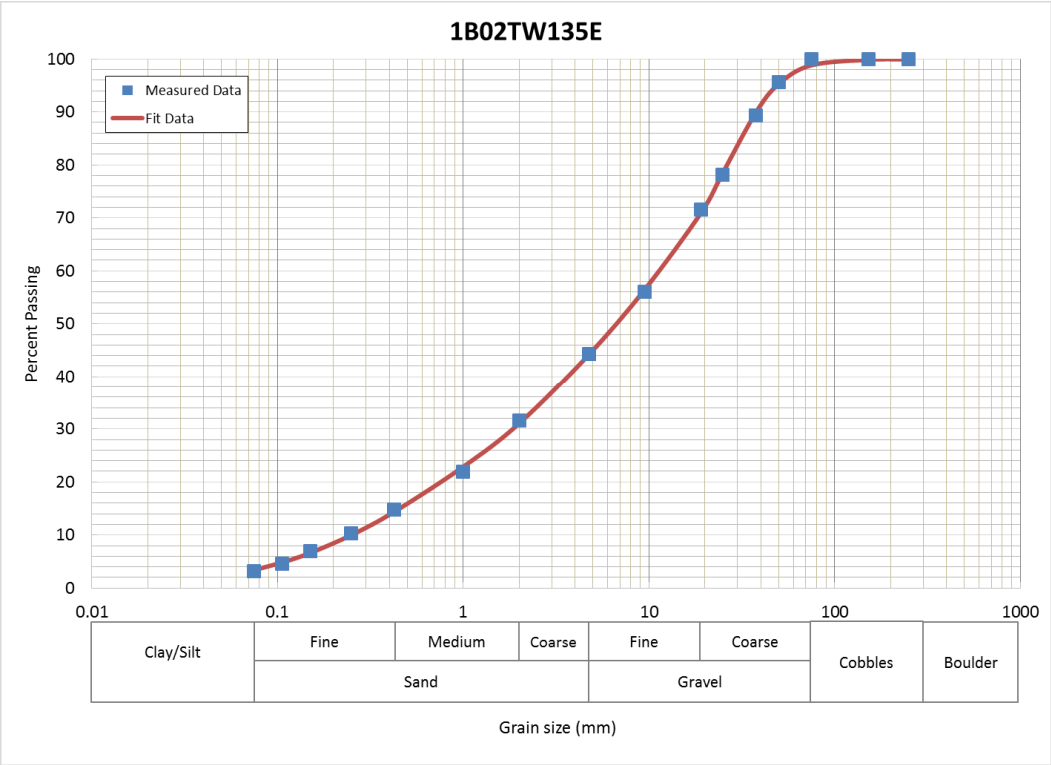
1B02TW135E
Measured Data
Fit Data
Percent Passing
100
90
80
70
60
50
40
30
20
10
0
0.01
0.1
1
10
100
1000
Clay/Silt
Fine
Medium
Coarse
Fine
Coarse
Cobbles
Boulder
Sand
Gravel
Grain size (mm)

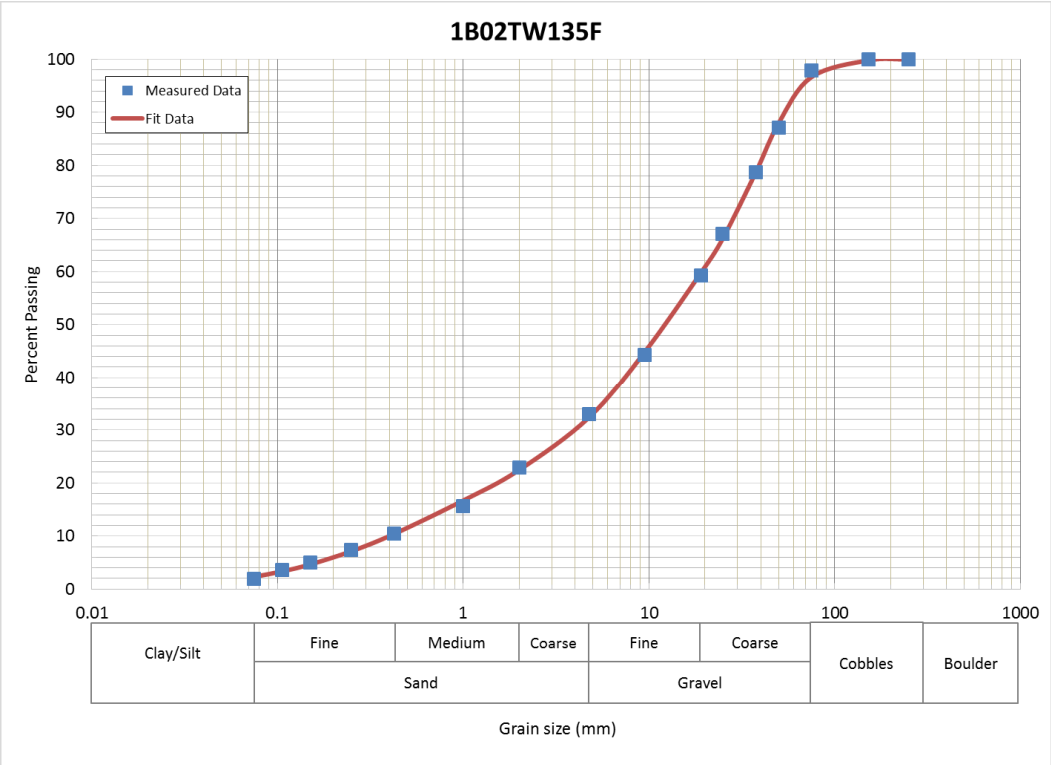
1B02TW135F
Measured Data
Fit Data
Percent Passing
100
90
80
70
60
50
40
30
20
10
0
0.01
0.1
1
10
100
1000
Clay/Silt
Fine
Medium
Coarse
Fine
Coarse
Cobbles
Boulder
Sand
Gravel
Grain size (mm)

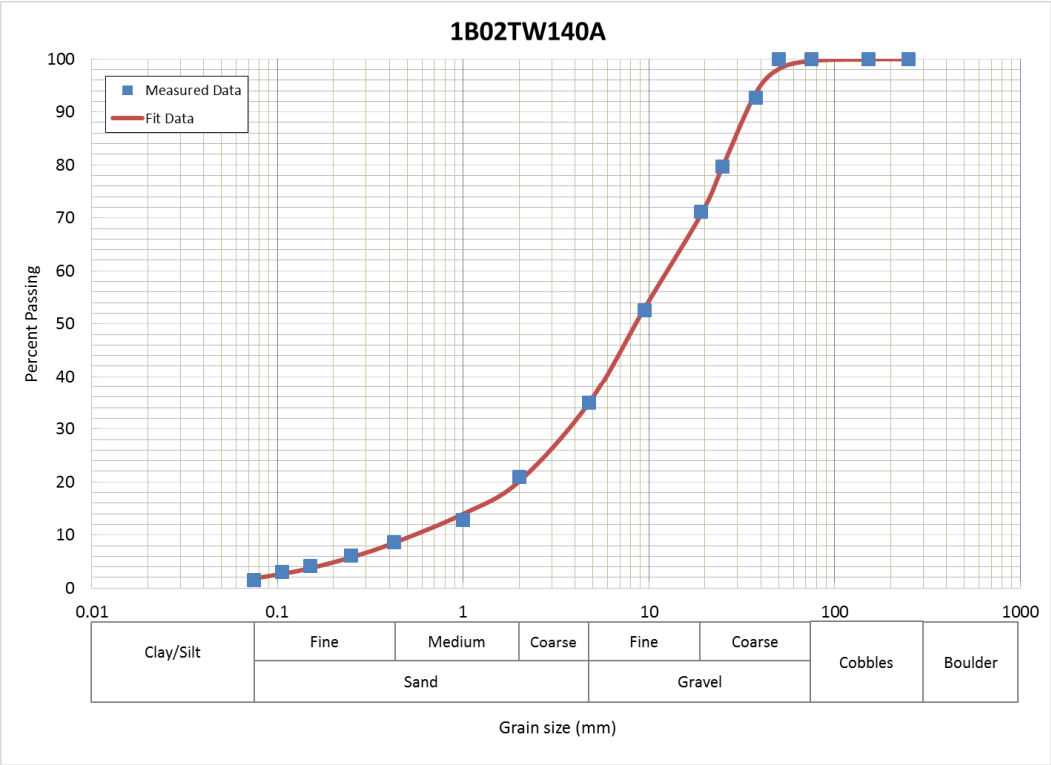
1B02TW140A
Measured Data
Fit Data
Percent Passing
100
90
80
70
60
50
40
30
20
10
0
0.01
0.1
1
10
100
1000
Clay/Silt
Fine
Medium
Coarse
Fine
Coarse
Cobbles
Boulder
Sand
Gravel
Grain size (mm)

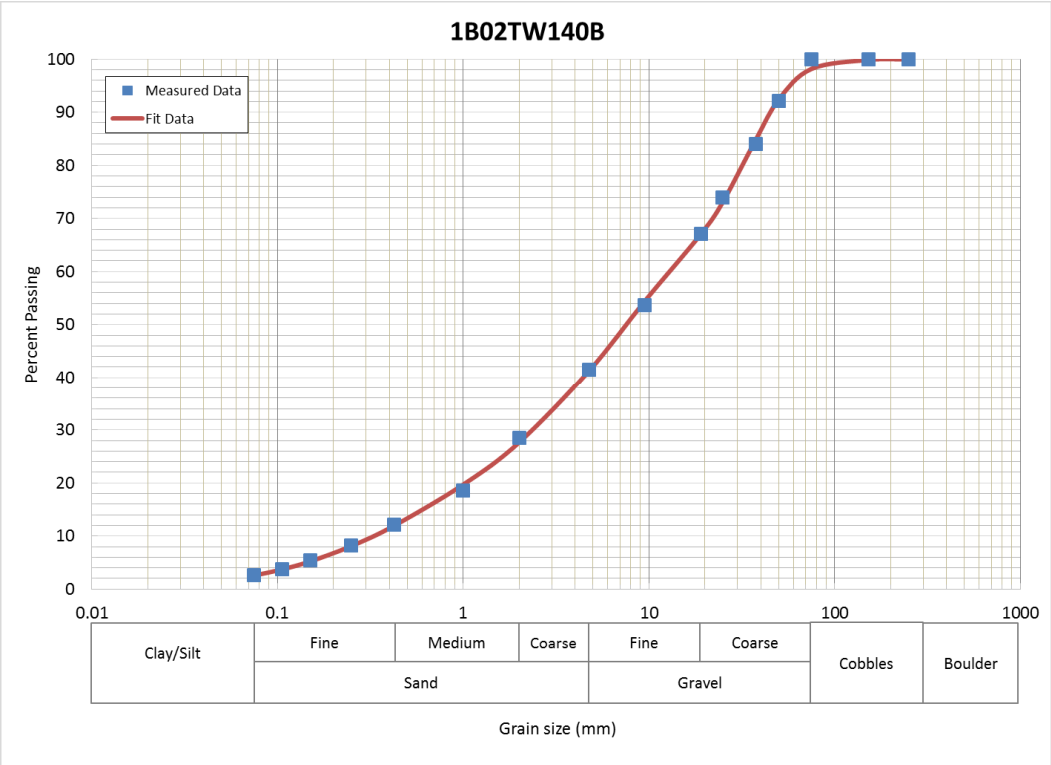
1B02TW140B
Measured Data
Fit Data
Percent Passing
100
90
80
70
60
50
40
30
20
10
0
0.01
0.1
1
10
100
1000
Clay/Silt
Fine
Medium
Coarse
Fine
Coarse
Cobbles
Boulder
Sand
Gravel
Grain size (mm)

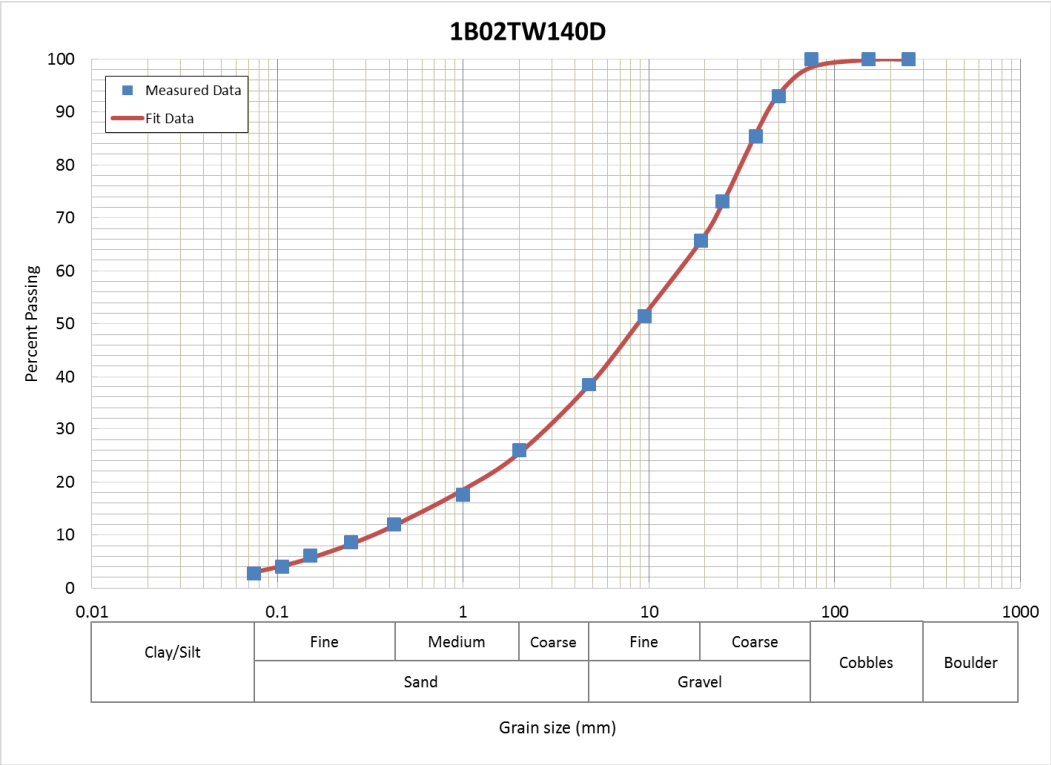
1B02TW140D
Measured Data
Fit Data
Percent Passing
100
90
80
70
60
50
40
30
20
10
0
0.01
0.1
1
10
100
1000
Clay/Silt
Fine
Medium
Coarse
Fine
Coarse
Cobbles
Boulder
Sand
Gravel
Grain size (mm)

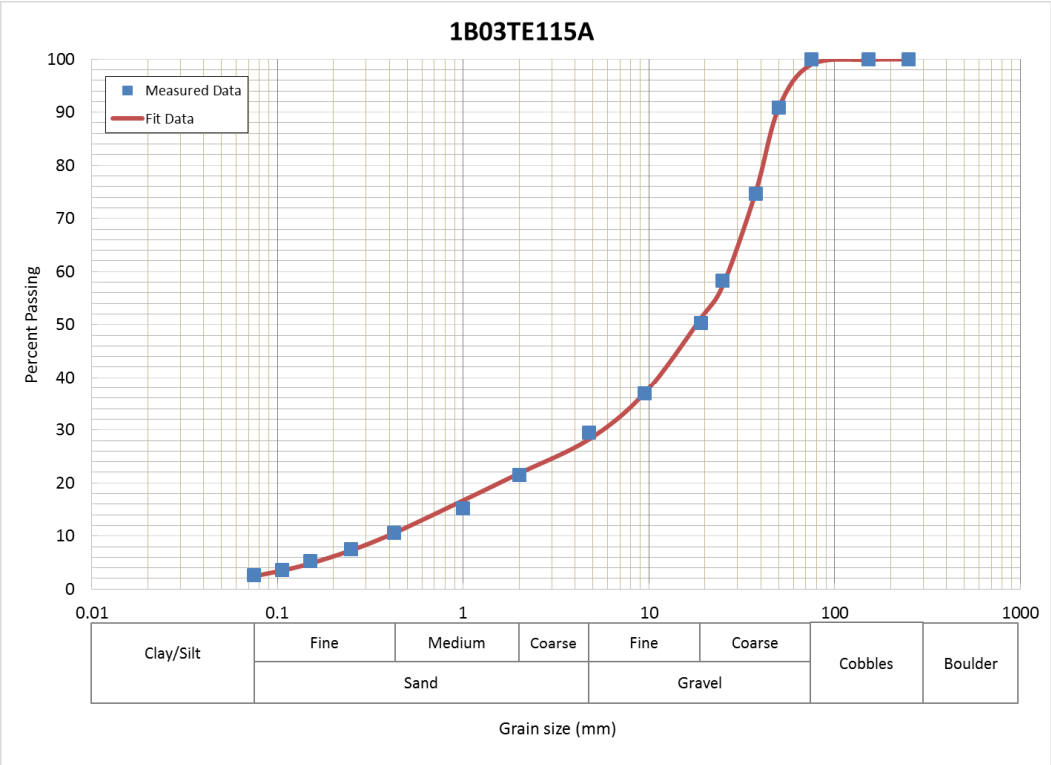
1B03TE115A
Measured Data
Fit Data
Percent Passing
100
90
80
70
60
50
40
30
20
10
0
0.01
0.1
1
10
100
1000
Clay/Silt
Fine
Medium
Coarse
Fine
Coarse
Cobbles
Boulder
Sand
Gravel
Grain size (mm)

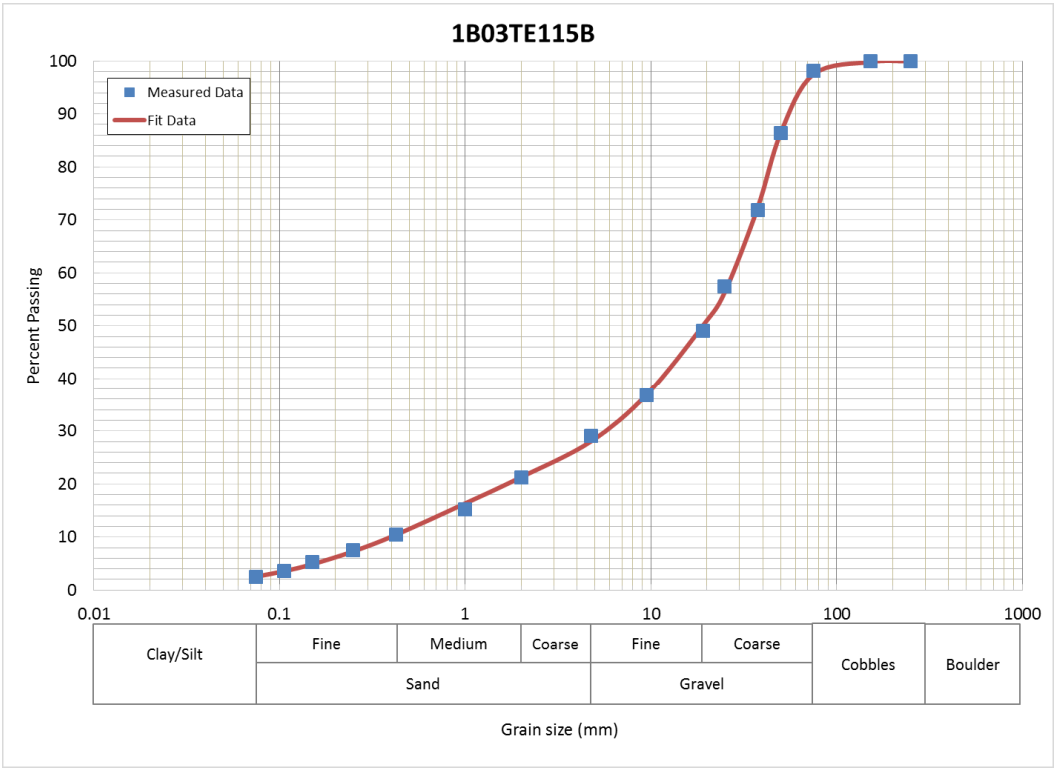
1B03TE115B
Measured Data
Fit Data
Percent Passing
100
90
80
70
60
50
40
30
20
10
0
0.01
0.1
1
10
100
1000
Clay/Silt
Fine
Medium
Coarse
Fine
Coarse
Cobbles
Boulder
Sand
Gravel
Grain size (mm)

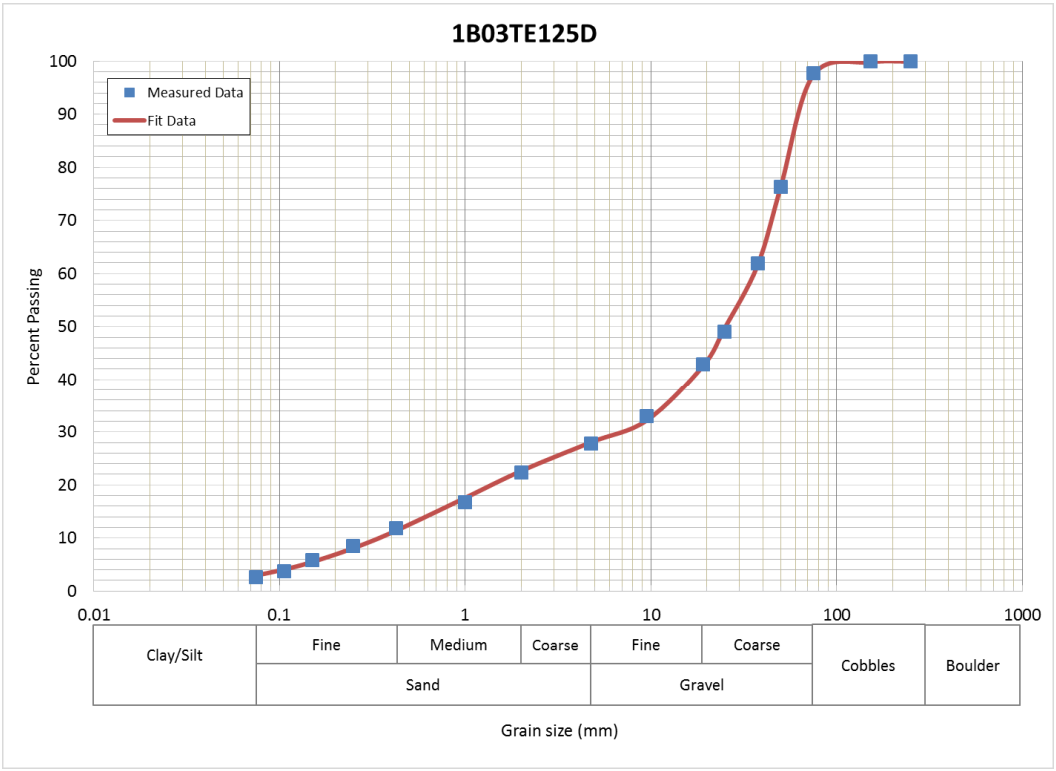
1B03TE125D
Measured Data
Fit Data
Percent Passing
100
90
80
70
60
50
40
30
20
10
0
0.01
0.1
1
10
100
1000
Clay/Silt
Fine
Medium
Coarse
Fine
Coarse
Cobbles
Boulder
Sand
Gravel
Grain size (mm)

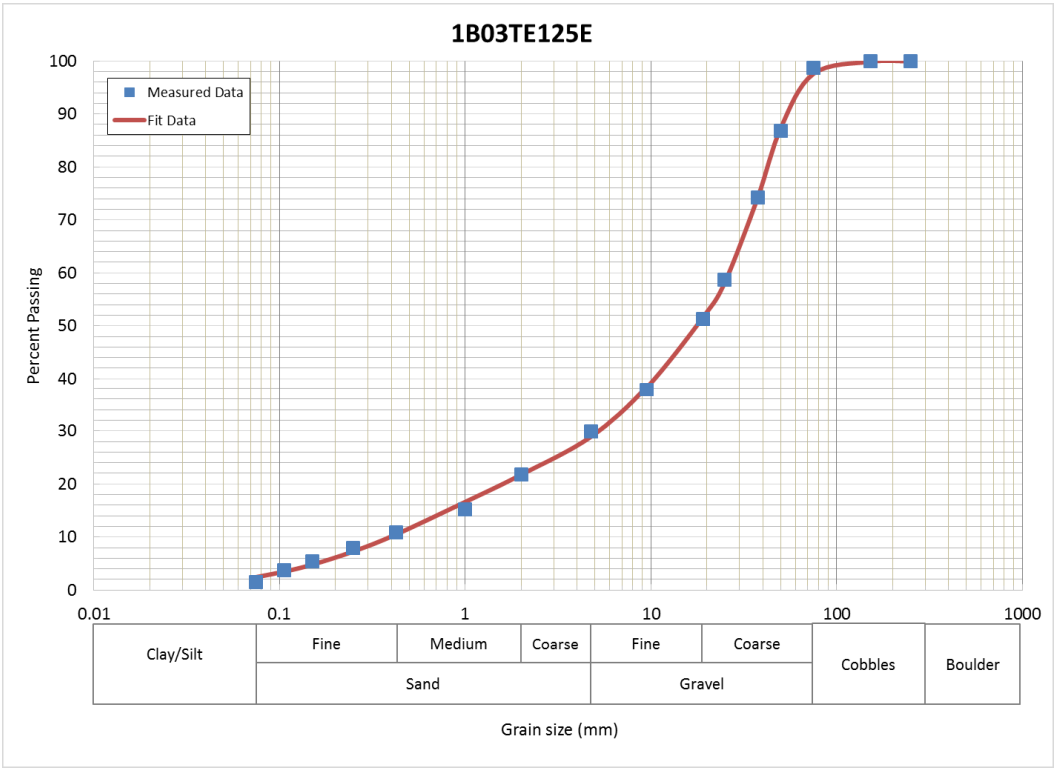
1B03TE125E
Measured Data
Fit Data
Percent Passing
100
90
80
70
60
50
40
30
20
10
0
0.01
0.1
1
10
100
1000
Clay/Silt
Fine
Medium
Coarse
Fine
Coarse
Cobbles
Boulder
Sand
Gravel
Grain size (mm)

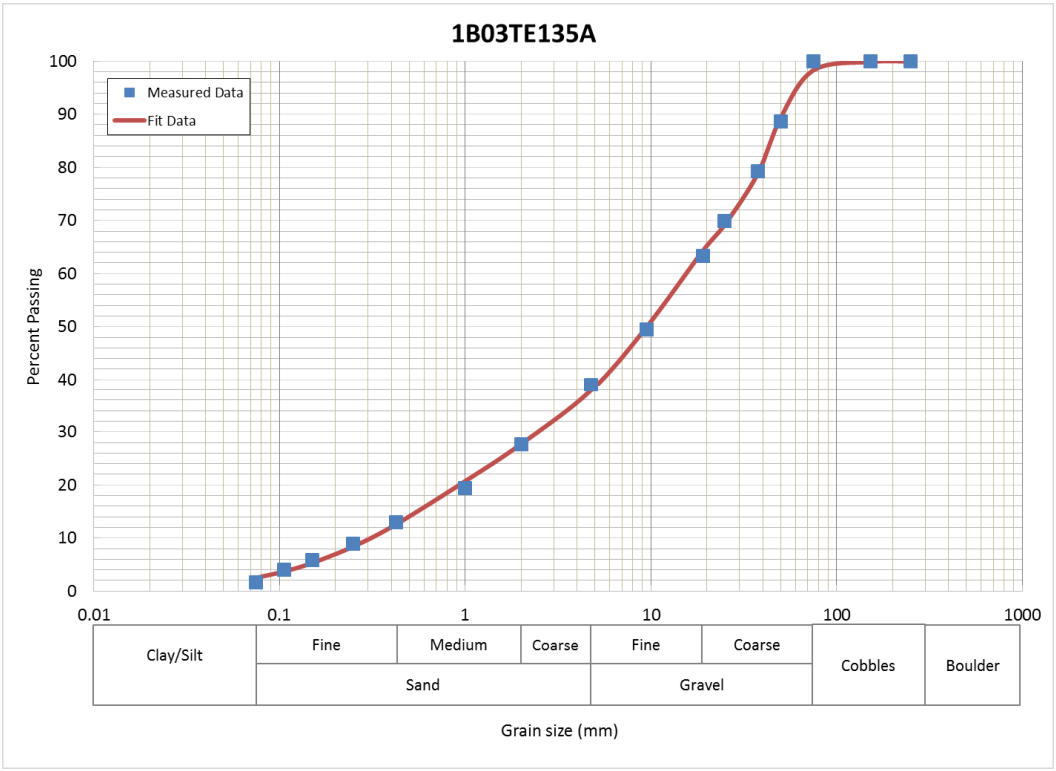
1B03TE135A
Measured Data
Fit Data
Percent Passing
100
90
80
70
60
50
40
30
20
10
0
0.01
0.1
1
10
100
1000
Clay/Silt
Fine
Medium
Coarse
Fine
Coarse
Cobbles
Boulder
Sand
Gravel
Grain size (mm)

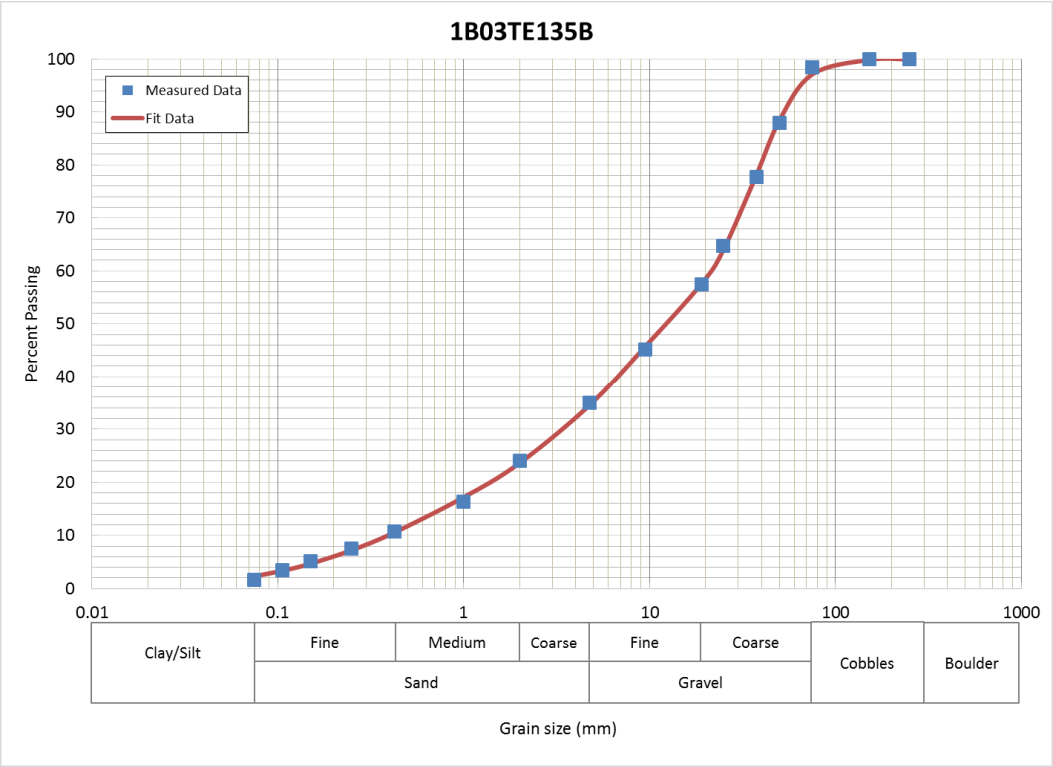
1B03TE135B
Measured Data
Fit Data
Percent Passing
100
90
80
70
60
50
40
30
20
10
0
0.01
0.1
1
10
100
1000
Clay/Silt
Fine
Medium
Coarse
Fine
Coarse
Cobbles
Boulder
Sand
Gravel
Grain size (mm)

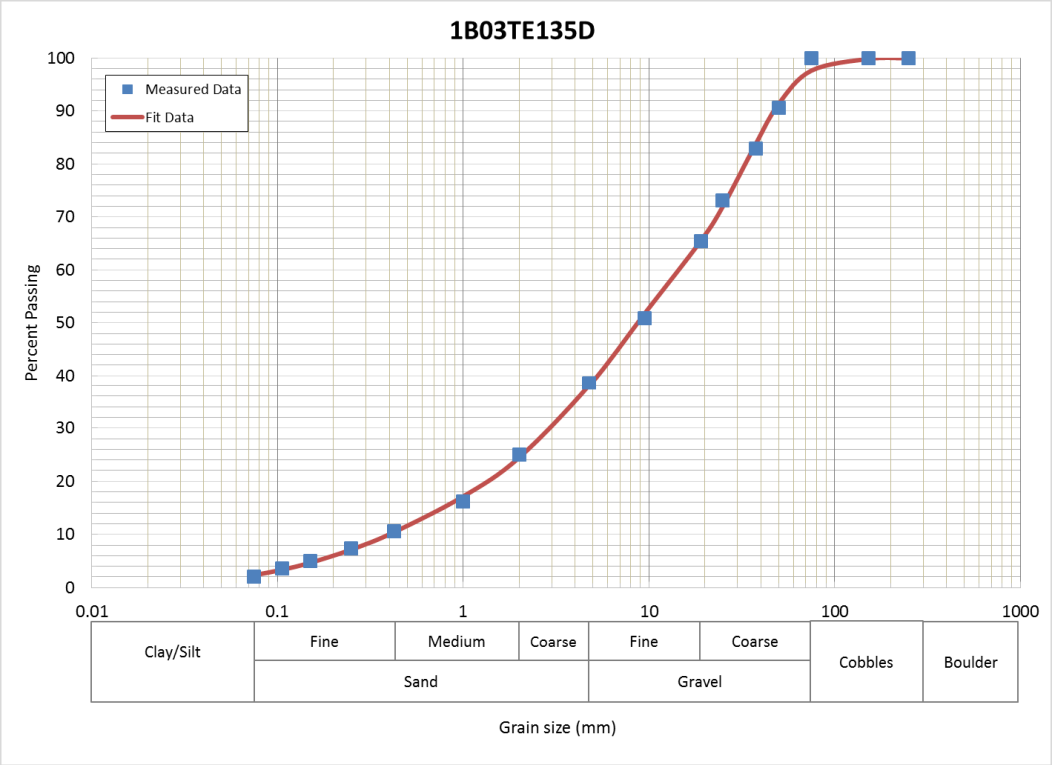
1B03TE135D
Measured Data
Fit Data
Percent Passing
100
90
80
70
60
50
40
30
20
10
0
0.01
0.1
1
10
100
1000
Clay/Silt
Fine
Medium
Coarse
Fine
Coarse
Cobbles
Boulder
Sand
Gravel
Grain size (mm)

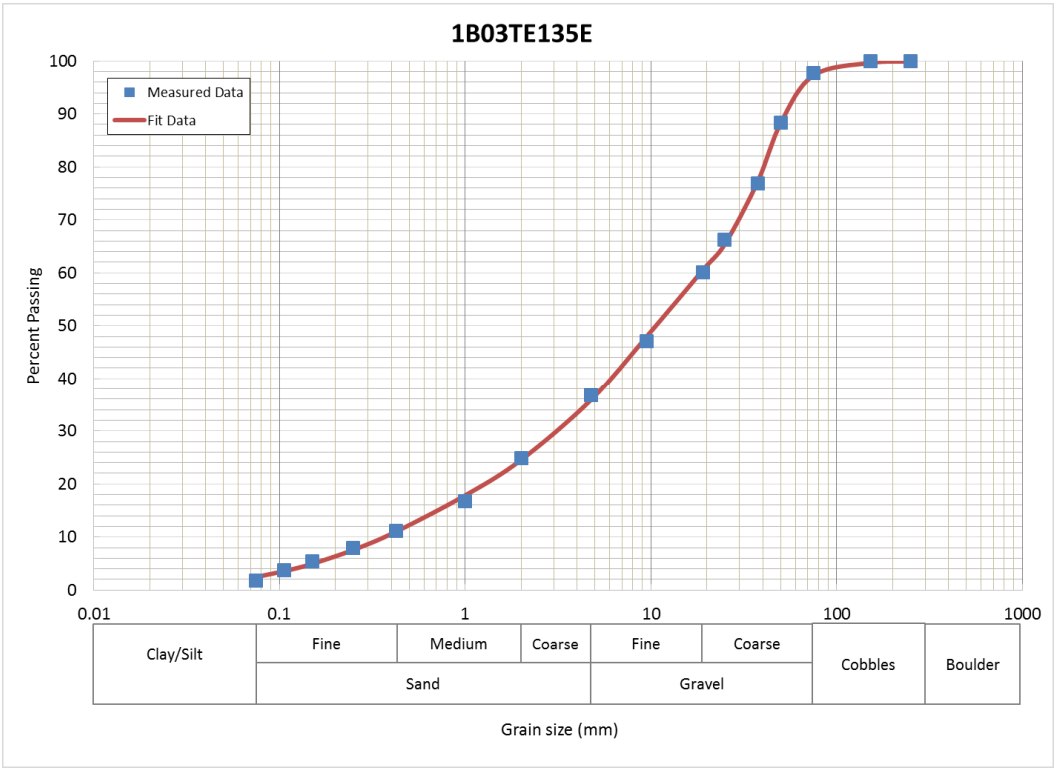
1B03TE135E
Measured Data
Fit Data
Percent Passing
100
90
80
70
60
50
40
30
20
10
0
0.01
0.1
1
10
100
1000
Clay/Silt
Fine
Medium
Coarse
Fine
Coarse
Cobbles
Boulder
Sand
Gravel
Grain size (mm)

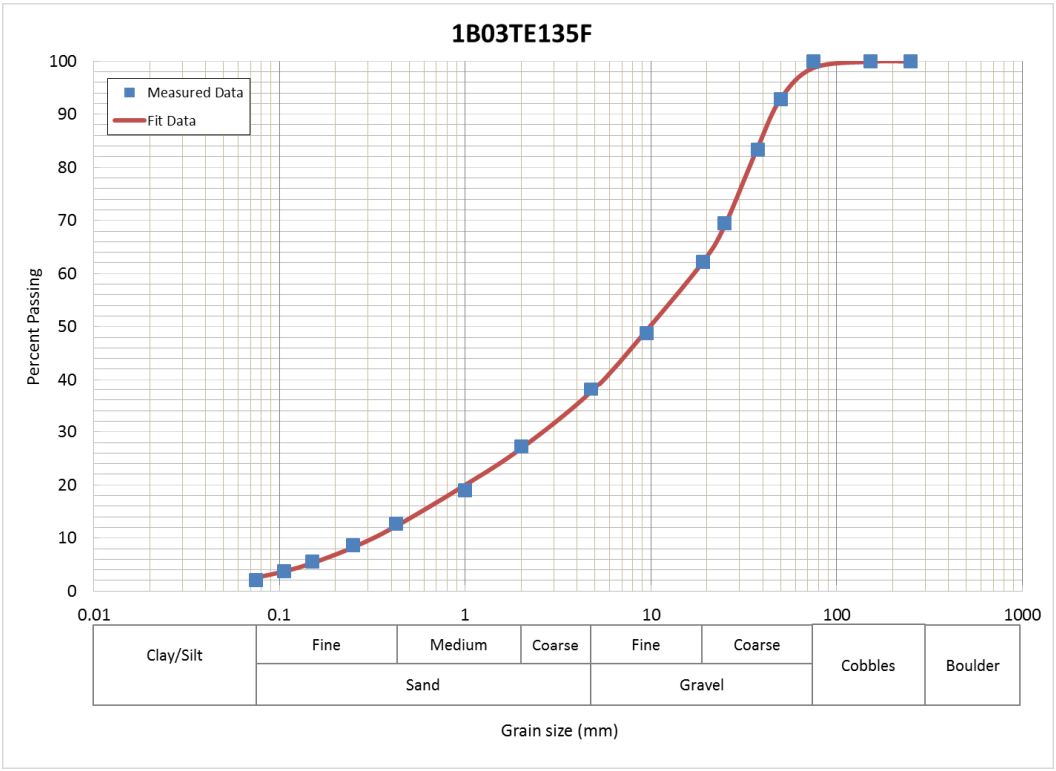
1B03TE135F
Measured Data
Fit Data
Percent Passing
100
90
80
70
60
50
40
30
20
10
0
0.01
0.1
1
10
100
1000
Clay/Silt
Fine
Medium
Coarse
Fine
Coarse
Cobbles
Boulder
Sand
Gravel
Grain size (mm)

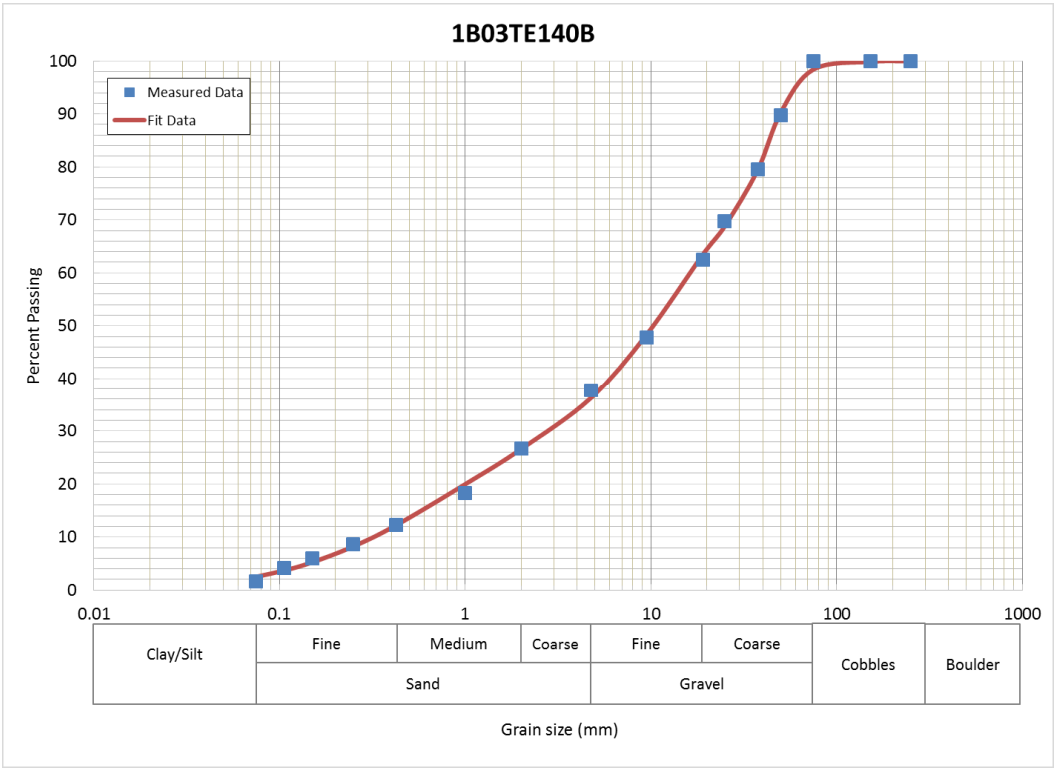
1B03TE140B
Measured Data
Fit Data
Percent Passing
100
90
80
70
60
50
40
30
20
10
0
0.01
0.1
1
10
100
1000
Clay/Silt
Fine
Medium
Coarse
Fine
Coarse
Cobbles
Boulder
Sand
Gravel
Grain size (mm)

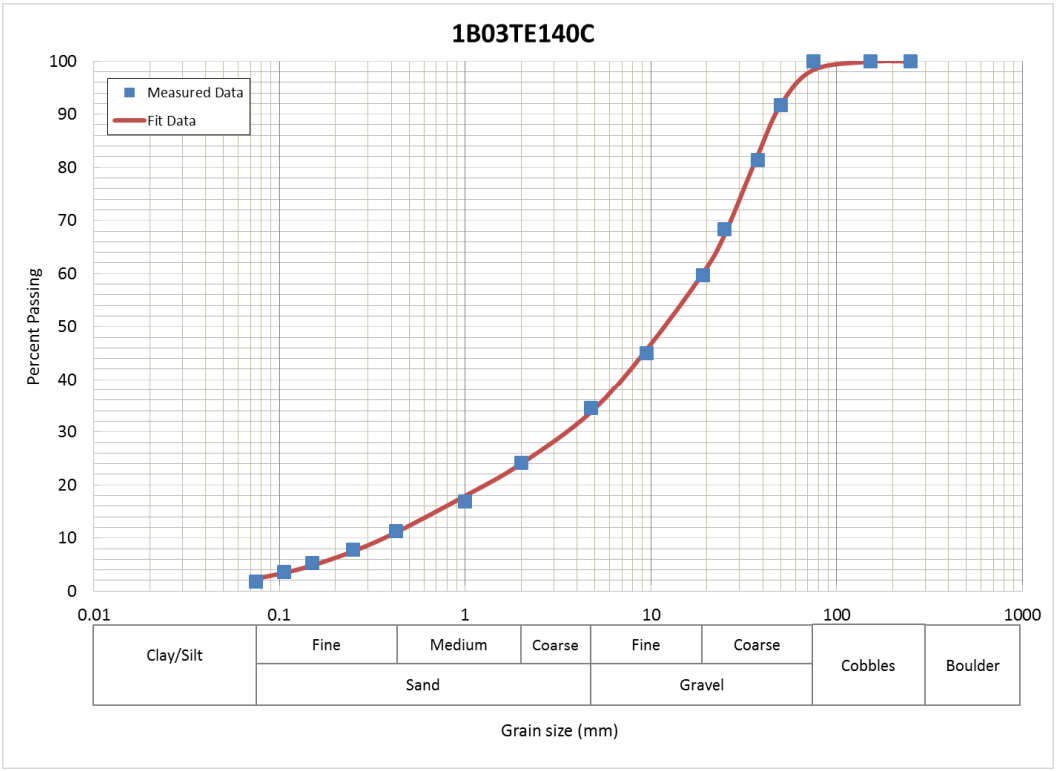
1B03TE140C
Measured Data
Fit Data
Percent Passing
100
90
80
70
60
50
40
30
20
10
0
0.01
0.1
1
10
100
1000
Clay/Silt
Fine
Medium
Coarse
Fine
Coarse
Cobbles
Boulder
Sand
Gravel
Grain size (mm)

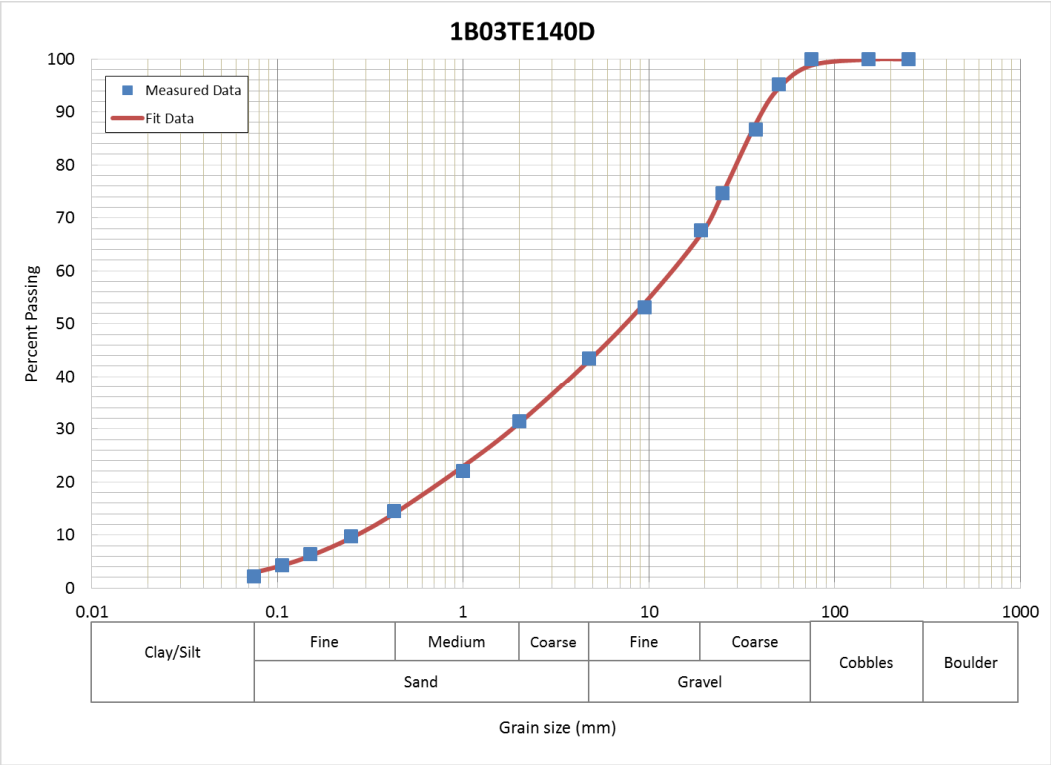
1B03TE140D
Measured Data
Fit Data
Percent Passing
100
90
80
70
60
50
40
30
20
10
0
0.01
0.1
1
10
100
1000
Clay/Silt
Fine
Medium
Coarse
Fine
Coarse
Cobbles
Boulder
Sand
Gravel
Grain size (mm)

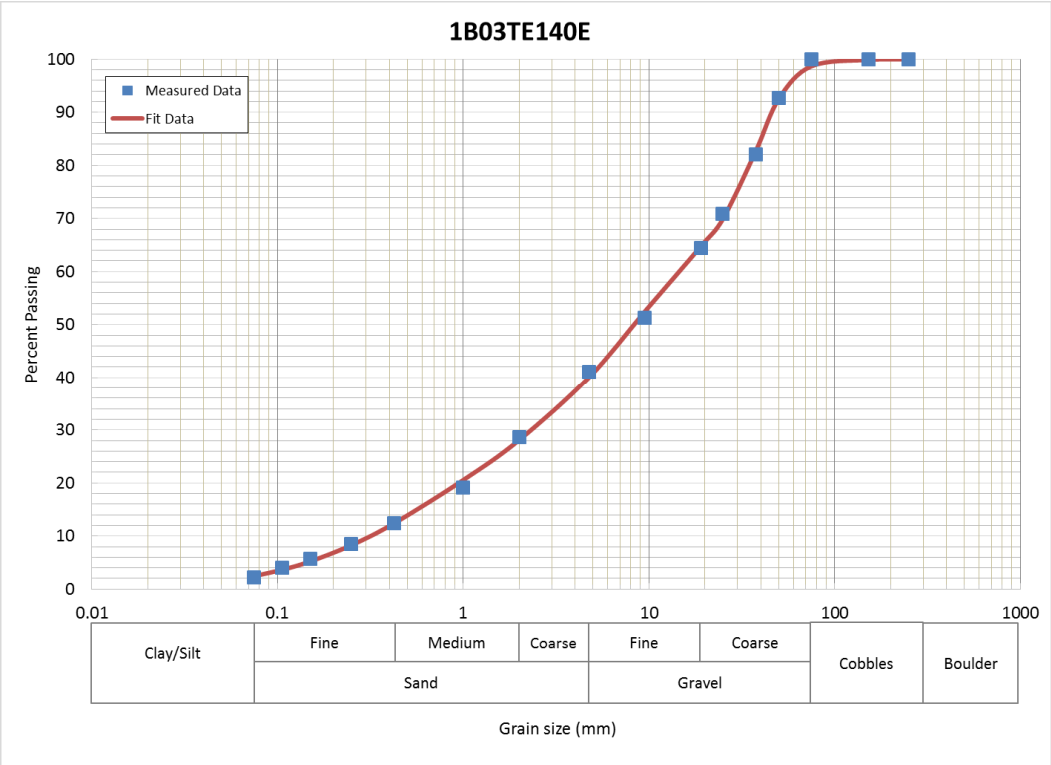
1B03TE140E
Measured Data
Fit Data
Percent Passing
100
90
80
70
60
50
40
30
20
10
0
0.01
0.1
1
10
100
1000
Clay/Silt
Fine
Medium
Coarse
Fine
Coarse
Cobbles
Boulder
Sand
Gravel
Grain size (mm)

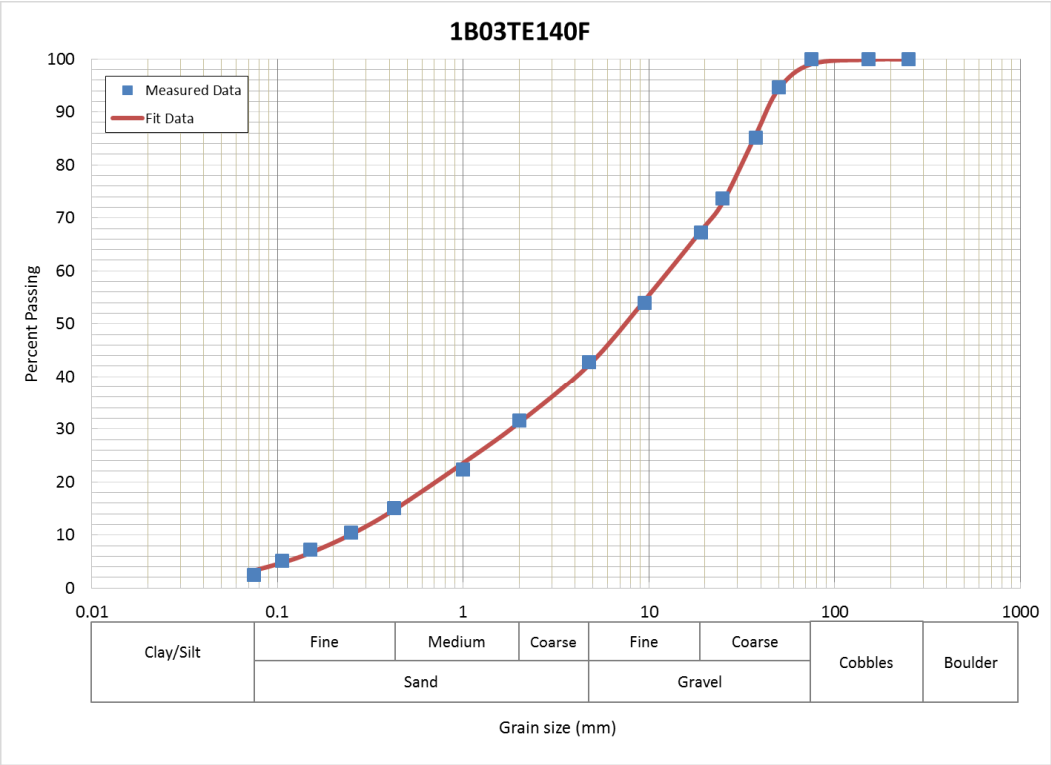
1B03TE140F
Measured Data
Fit Data
Percent Passing
100
90
80
70
60
50
40
30
20
10
0
0.01
0.1
1
10
100
1000
Clay/Silt
Fine
Medium
Coarse
Fine
Coarse
Cobbles
Boulder
Sand
Gravel
Grain size (mm)

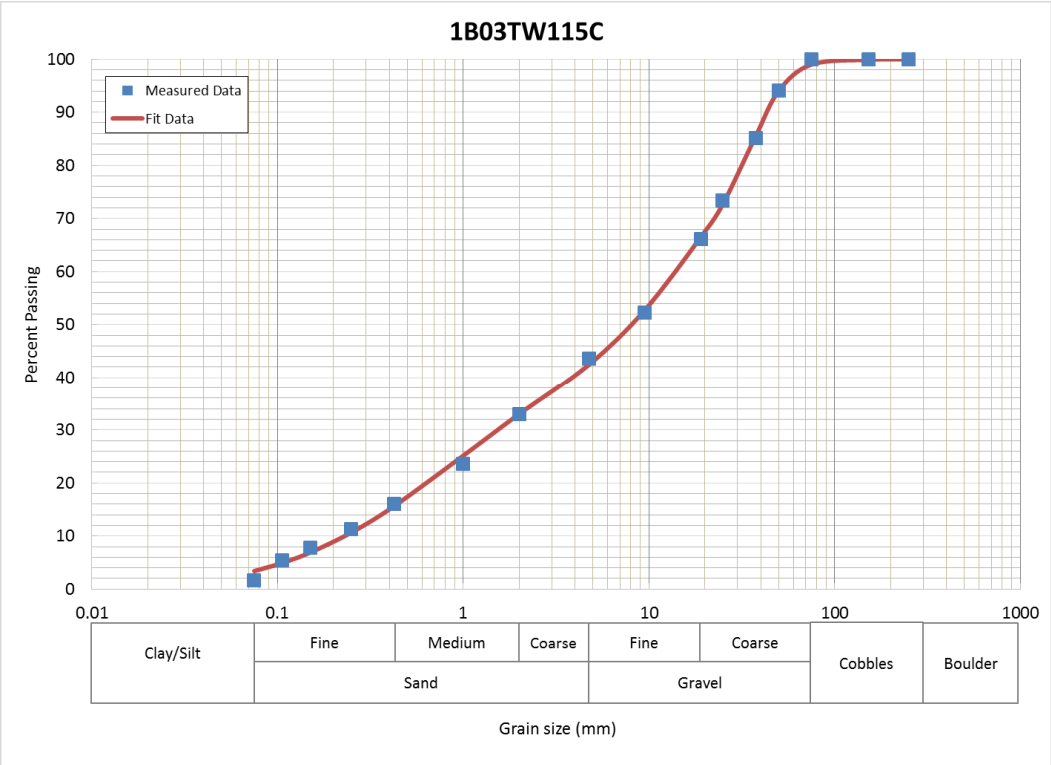
1B03TW115C
Measured Data
Fit Data
Percent Passing
100
90
80
70
60
50
40
30
20
10
0
0.01
0.1
1
10
100
1000
Clay/Silt
Fine
Medium
Coarse
Fine
Coarse
Cobbles
Boulder
Sand
Gravel
Grain size (mm)

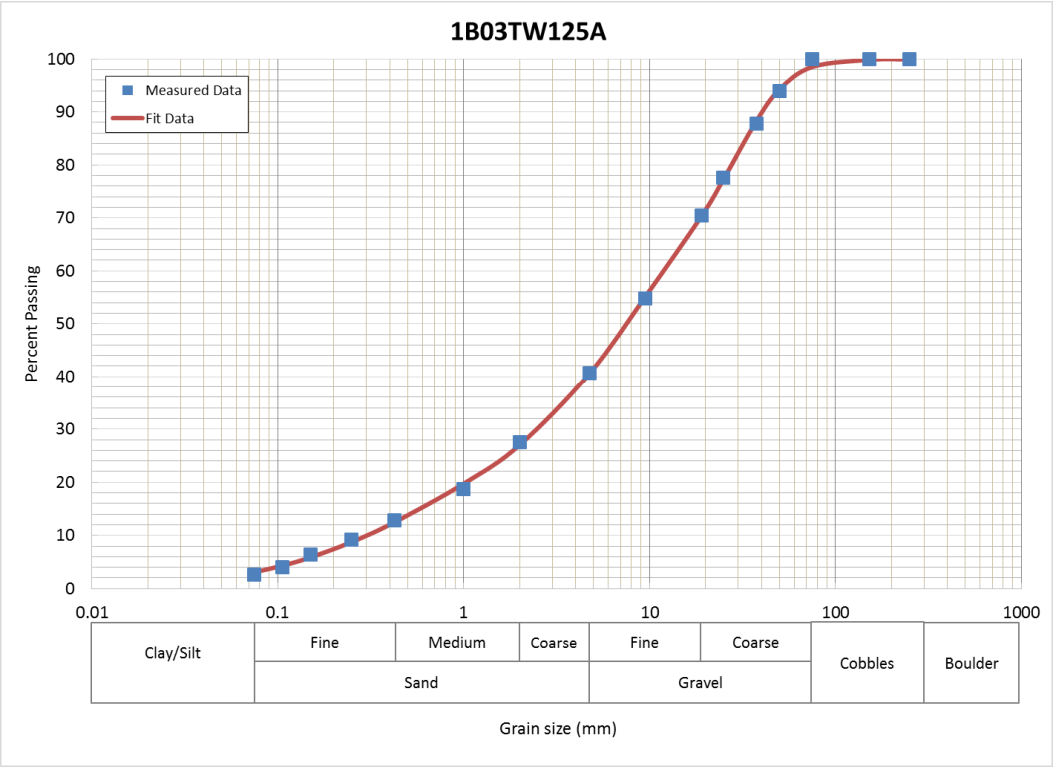
1B03TW125A
Measured Data
Fit Data
Percent Passing
100
90
80
70
60
50
40
30
20
10
0
0.01
0.1
1
10
100
1000
Clay/Silt
Fine
Medium
Coarse
Fine
Coarse
Cobbles
Boulder
Sand
Gravel
Grain size (mm)

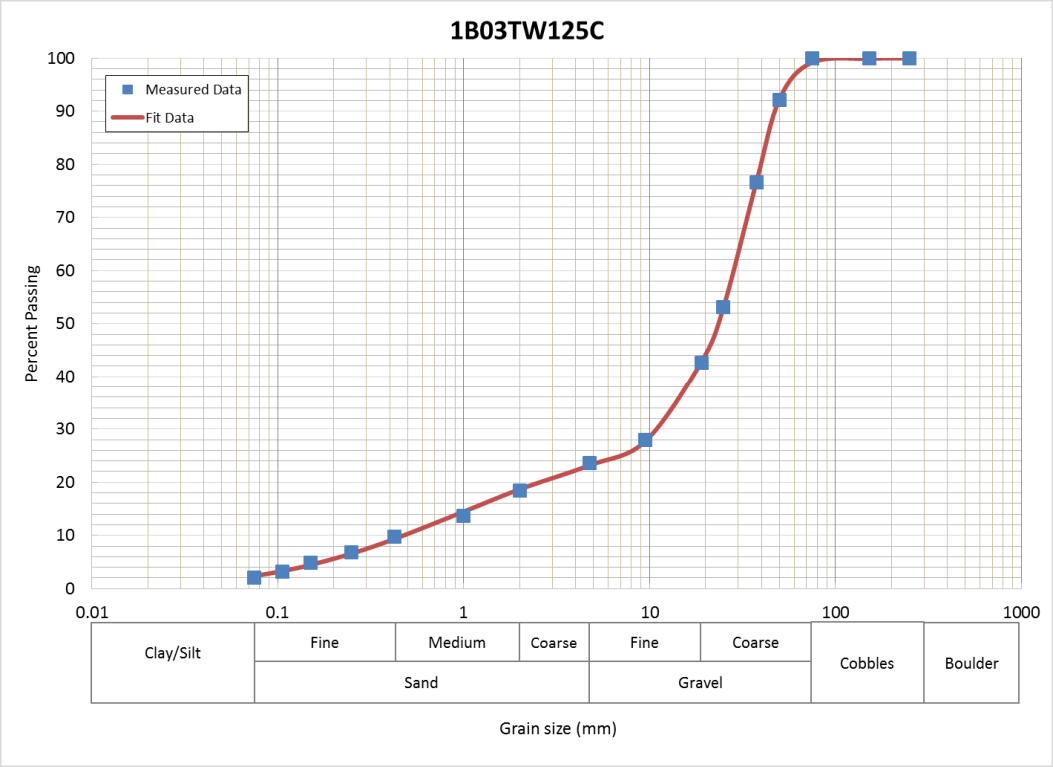
1B03TW125C
Measured Data
Fit Data
Percent Passing
100
90
80
70
60
50
40
30
20
10
0
0.01
0.1
1
10
100
1000
Clay/Silt
Fine
Medium
Coarse
Fine
Coarse
Cobbles
Boulder
Sand
Gravel
Grain size (mm)

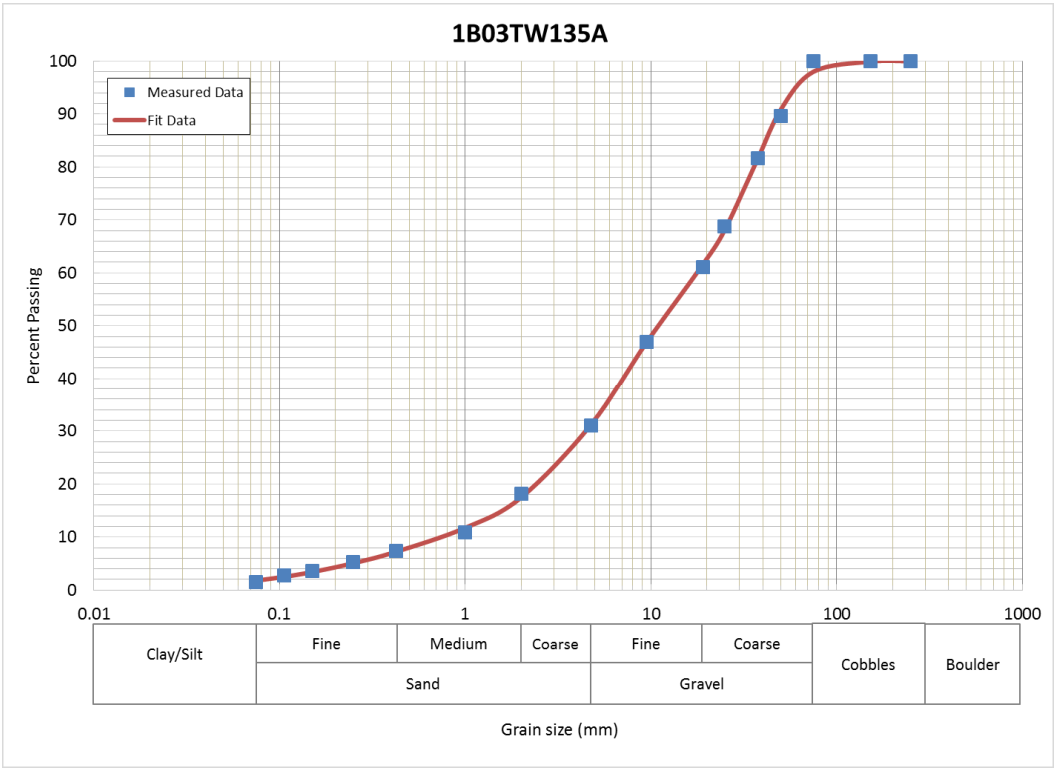
1B03TW135A
Measured Data
Fit Data
Percent Passing
100
90
80
70
60
50
40
30
20
10
0
0.01
0.1
1
10
100
1000
Clay/Silt
Fine
Medium
Coarse
Fine
Coarse
Cobbles
Boulder
Sand
Gravel
Grain size (mm)

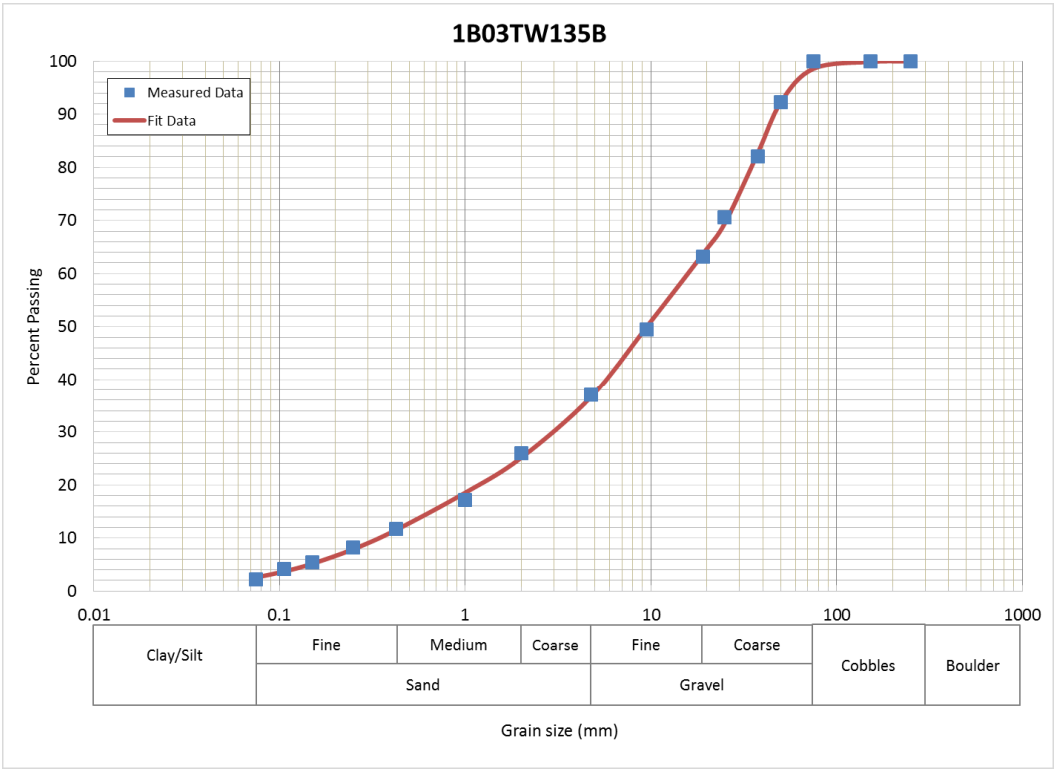
1B03TW135B
Measured Data
Fit Data
Percent Passing
100
90
80
70
60
50
40
30
20
10
0
0.01
0.1
1
10
100
1000
Clay/Silt
Fine
Medium
Coarse
Fine
Coarse
Cobbles
Boulder
Sand
Gravel
Grain size (mm)

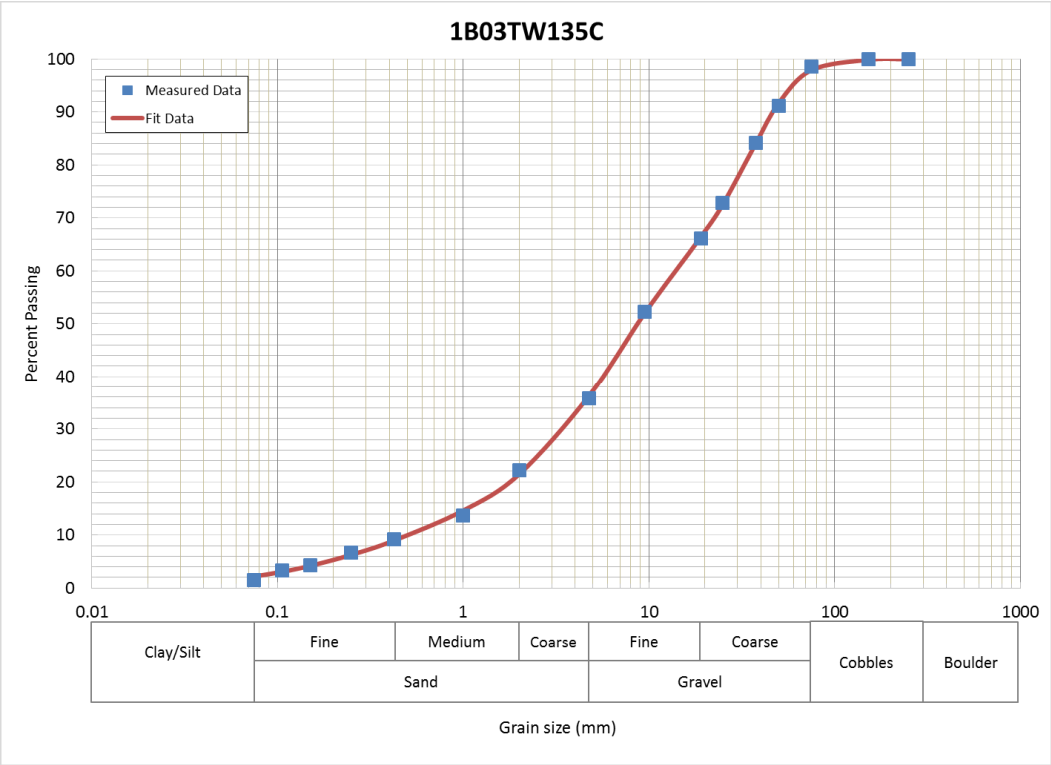
1B03TW135C
Measured Data
Fit Data
Percent Passing
100
90
80
70
60
50
40
30
20
10
0
0.01
0.1
1
10
100
1000
Clay/Silt
Fine
Medium
Coarse
Fine
Coarse
Cobbles
Boulder
Sand
Gravel
Grain size (mm)

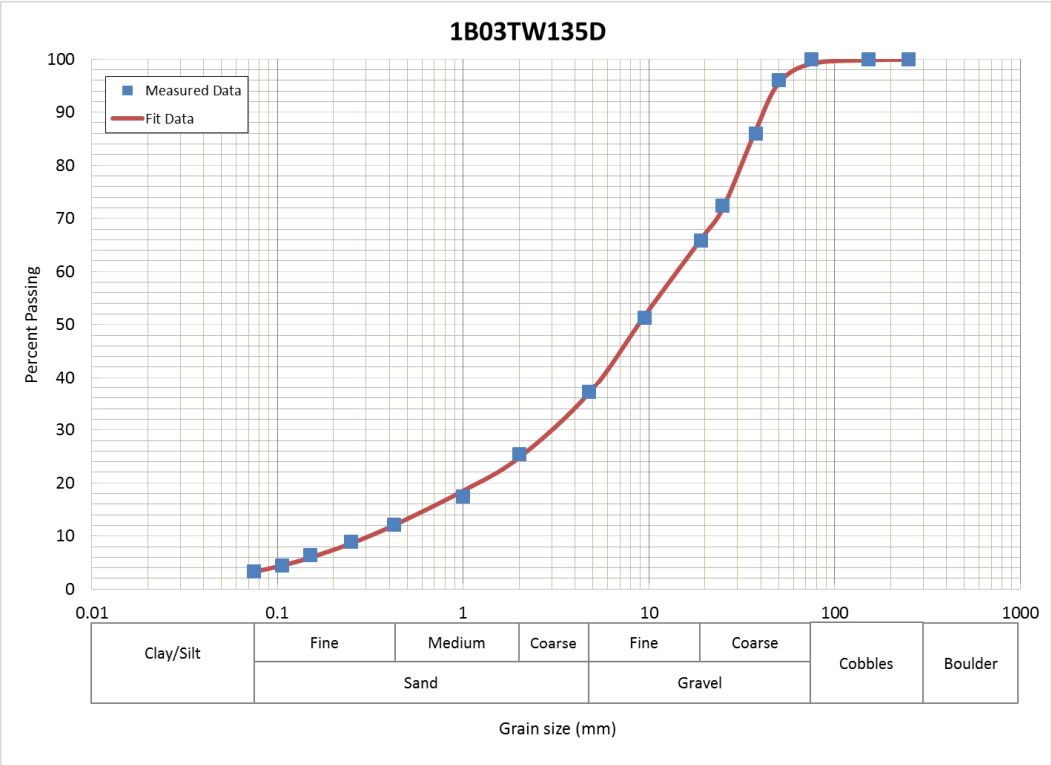
1B03TW135D
Measured Data
Fit Data
Percent Passing
100
90
80
70
60
50
40
30
20
10
0
0.01
0.1
1
10
100
1000
Clay/Silt
Fine
Medium
Coarse
Fine
Coarse
Cobbles
Boulder
Sand
Gravel
Grain size (mm)

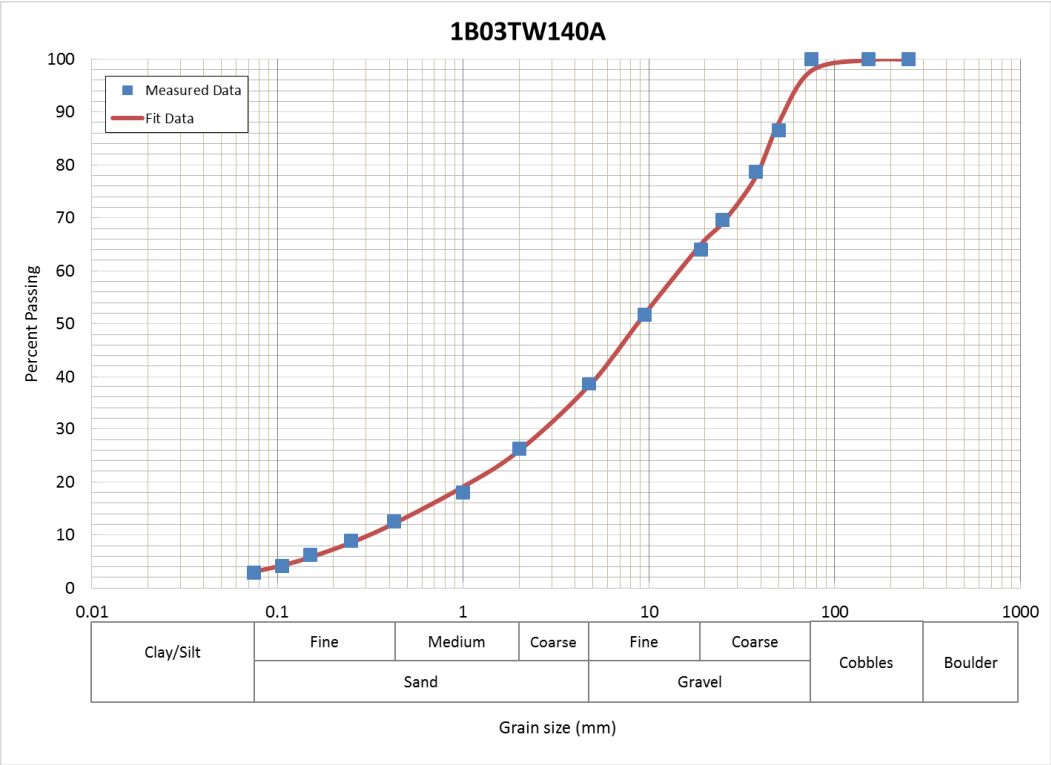
1B03TW140A
Measured Data
Fit Data
Percent Passing
100
90
80
70
60
50
40
30
20
10
0
0.01
0.1
1
10
100
1000
Clay/Silt
Fine
Medium
Coarse
Fine
Coarse
Cobbles
Boulder
Sand
Gravel
Grain size (mm)

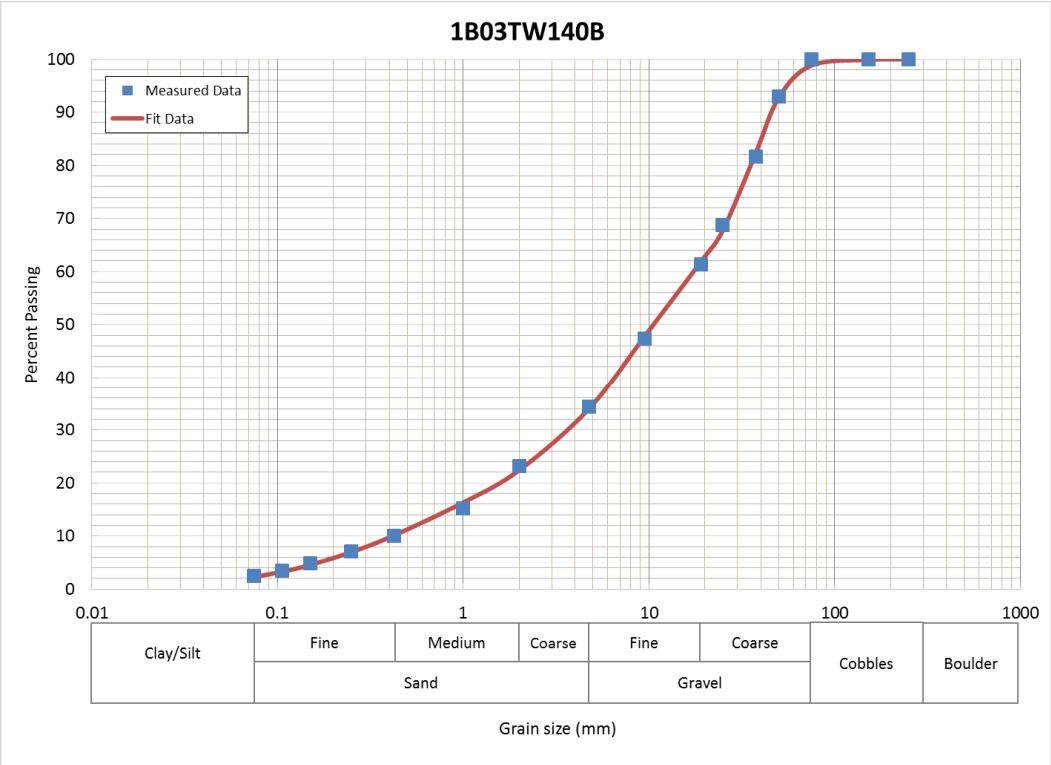
1B03TW140B
Measured Data
Fit Data
Percent Passing
100
90
80
70
60
50
40
30
20
10
0
0.01
0.1
1
10
100
1000
Clay/Silt
Fine
Medium
Coarse
Fine
Coarse
Cobbles
Boulder
Sand
Gravel
Grain size (mm)

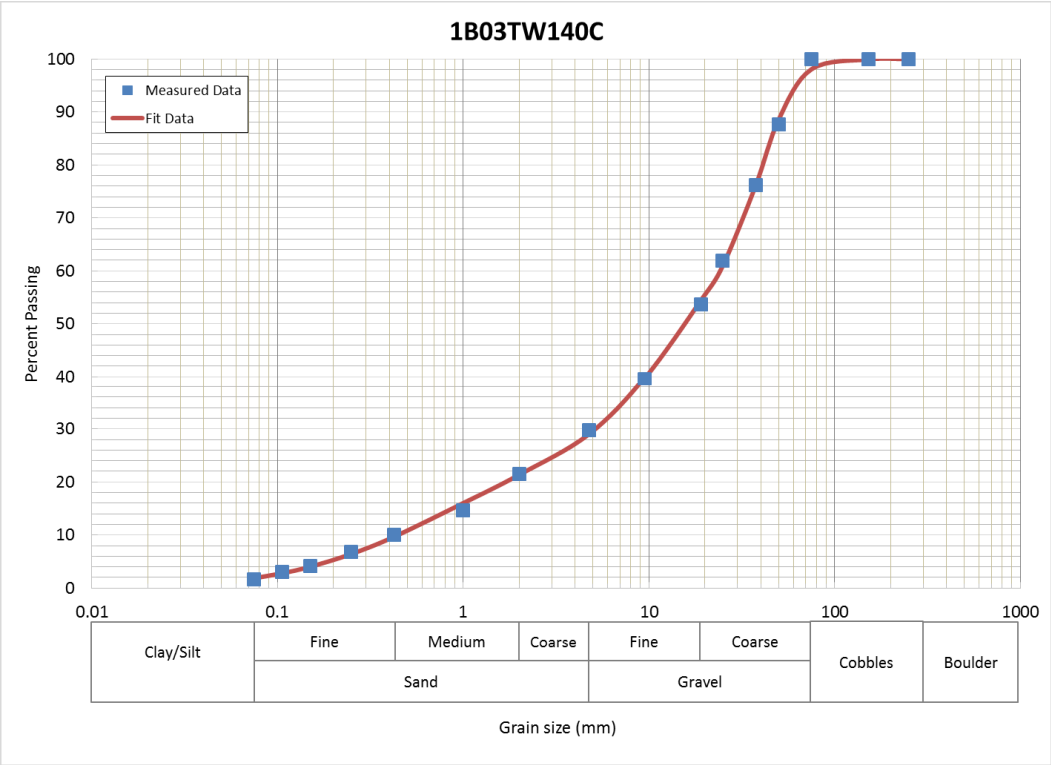
1B03TW140C
Measured Data
Fit Data
Percent Passing
100
90
80
70
60
50
40
30
20
10
0
0.01
0.1
1
10
100
1000
Clay/Silt
Fine
Medium
Coarse
Fine
Coarse
Cobbles
Boulder
Sand
Gravel
Grain size (mm)

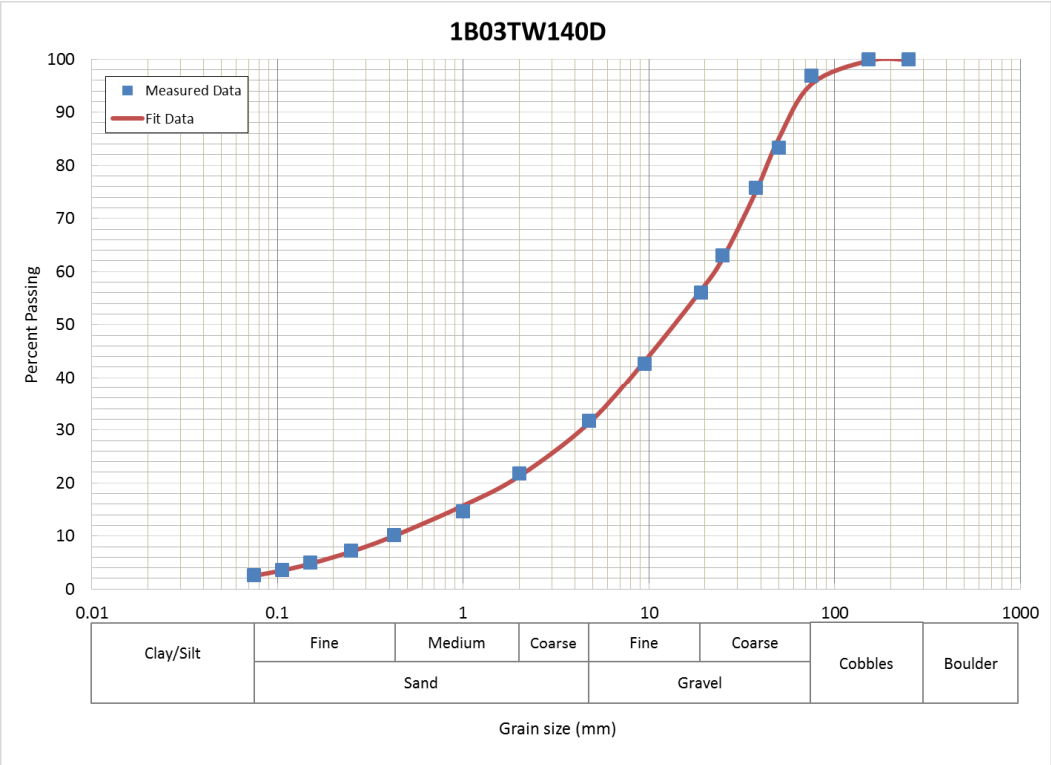
1B03TW140D
Measured Data
Fit Data
Percent Passing
100
90
80
70
60
50
40
30
20
10
0
0.01
0.1
1
10
100
1000
Clay/Silt
Fine
Medium
Coarse
Fine
Coarse
Cobbles
Boulder
Sand
Gravel
Grain size (mm)

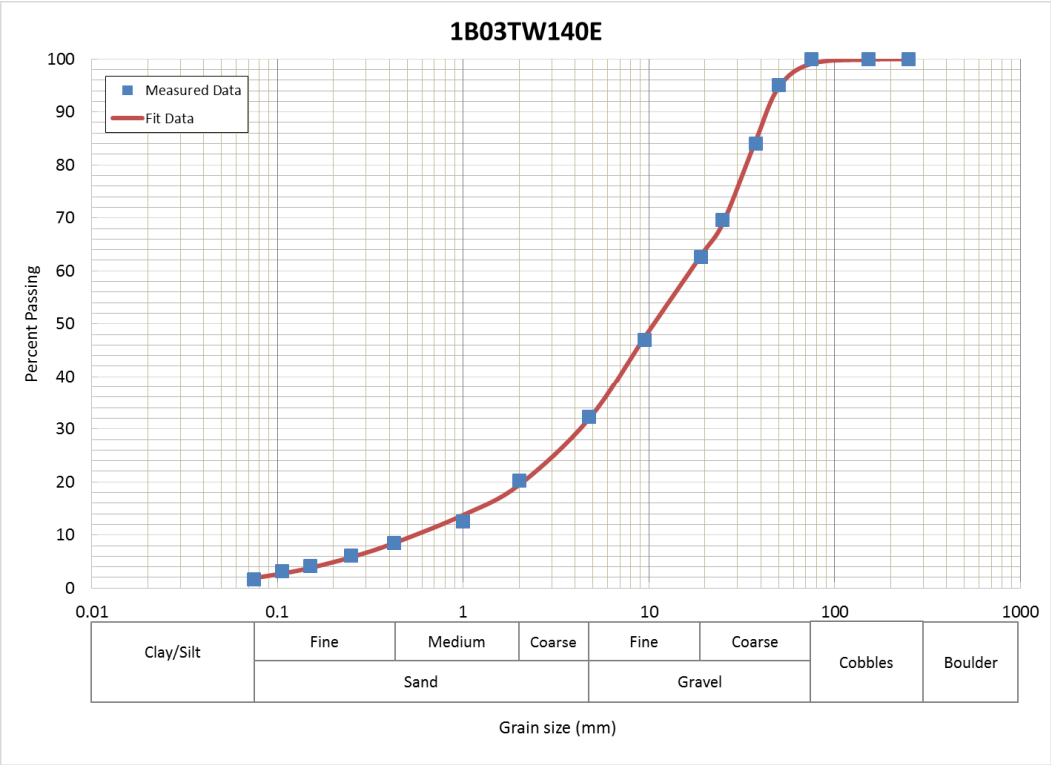
1B03TW140E
Measured Data
Fit Data
Percent Passing
100
90
80
70
60
50
40
30
20
10
0
0.01
0.1
1
10
100
1000
Clay/Silt
Fine
Medium
Coarse
Fine
Coarse
Cobbles
Boulder
Sand
Gravel
Grain size (mm)

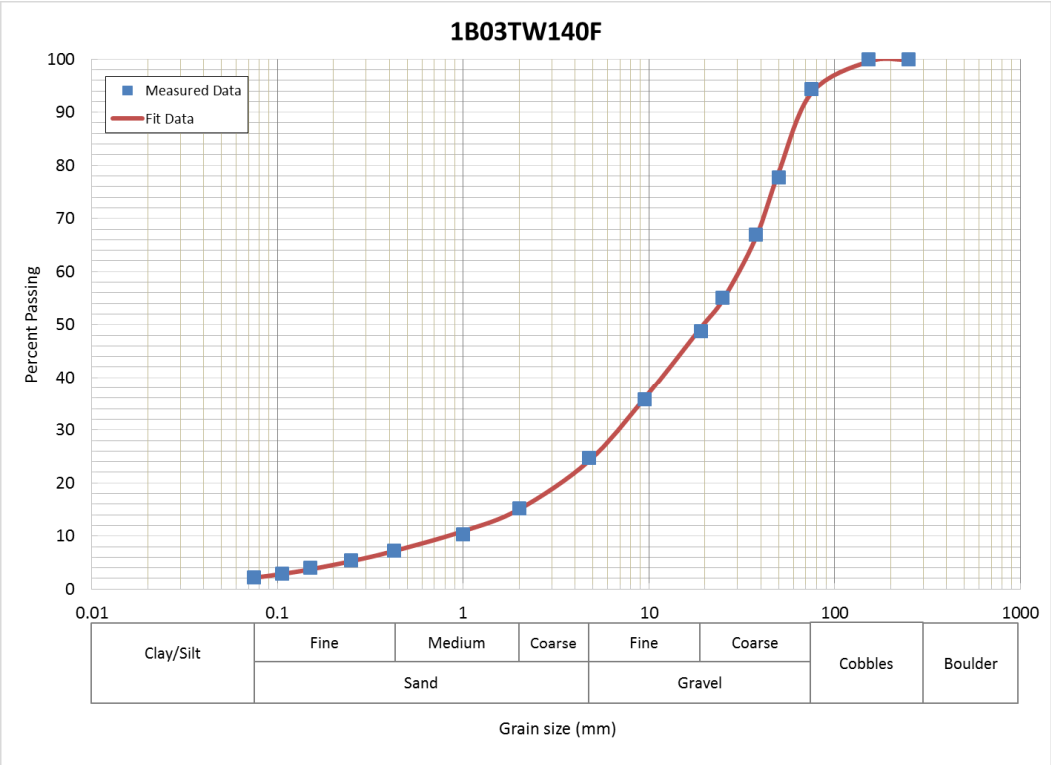
1B03TW140F
Measured Data
Fit Data
Percent Passing
100
90
80
70
60
50
40
30
20
10
0
0.01
0.1
1
10
100
1000
Clay/Silt
Fine
Medium
Coarse
Fine
Coarse
Cobbles
Boulder
Sand
Gravel
Grain size (mm)

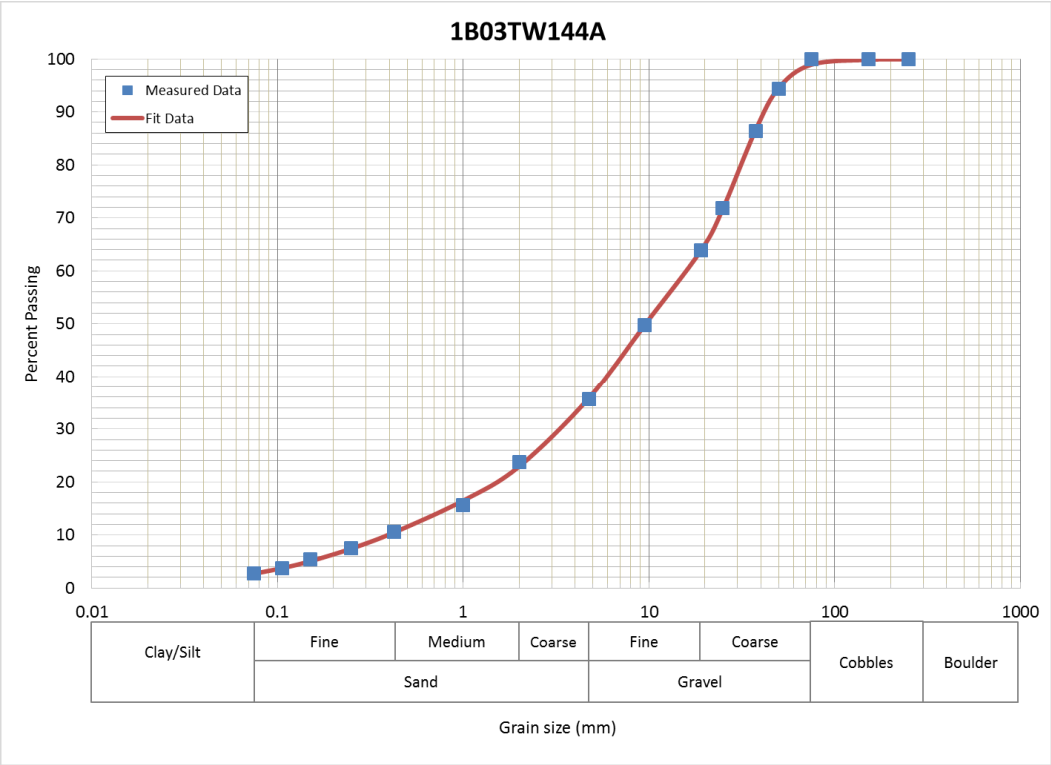
1B03TW144A
Measured Data
Fit Data
Percent Passing
100
90
80
70
60
50
40
30
20
10
0
0.01
0.1
1
10
100
1000
Clay/Silt
Fine
Medium
Coarse
Fine
Coarse
Cobbles
Boulder
Sand
Gravel
Grain size (mm)

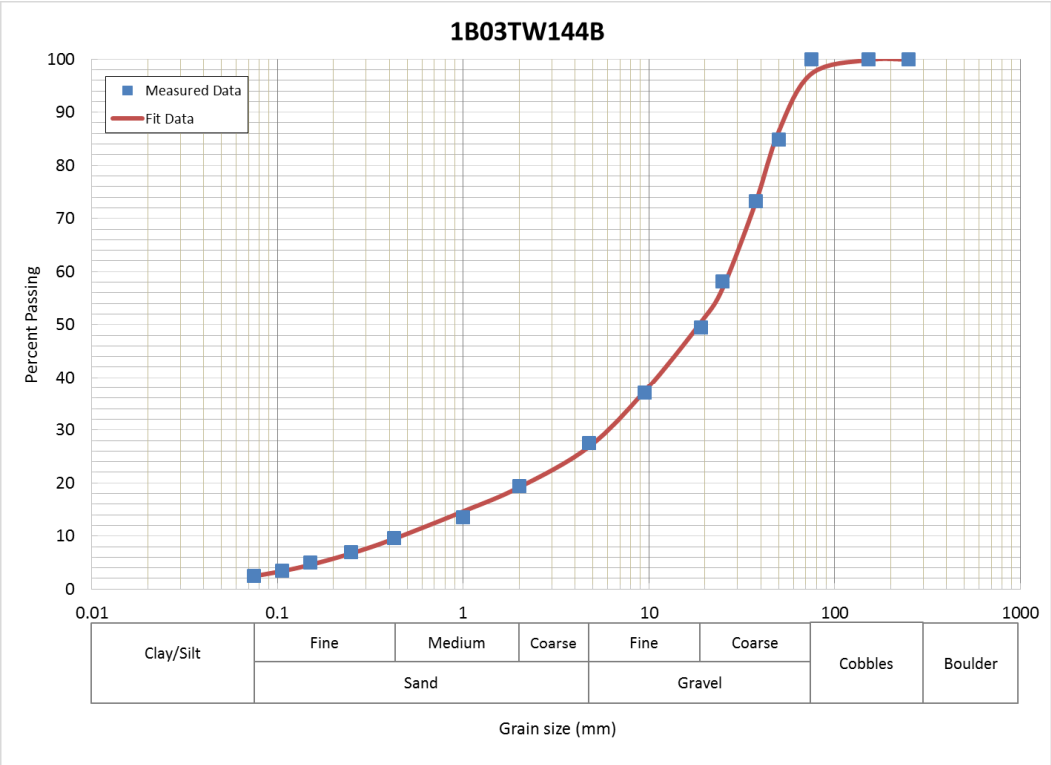
1B03TW144B
Measured Data
Fit Data
Percent Passing
100
90
80
70
60
50
40
30
20
10
0
0.01
0.1
1
10
100
1000
Clay/Silt
Fine
Medium
Coarse
Fine
Coarse
Cobbles
Boulder
Sand
Gravel
Grain size (mm)

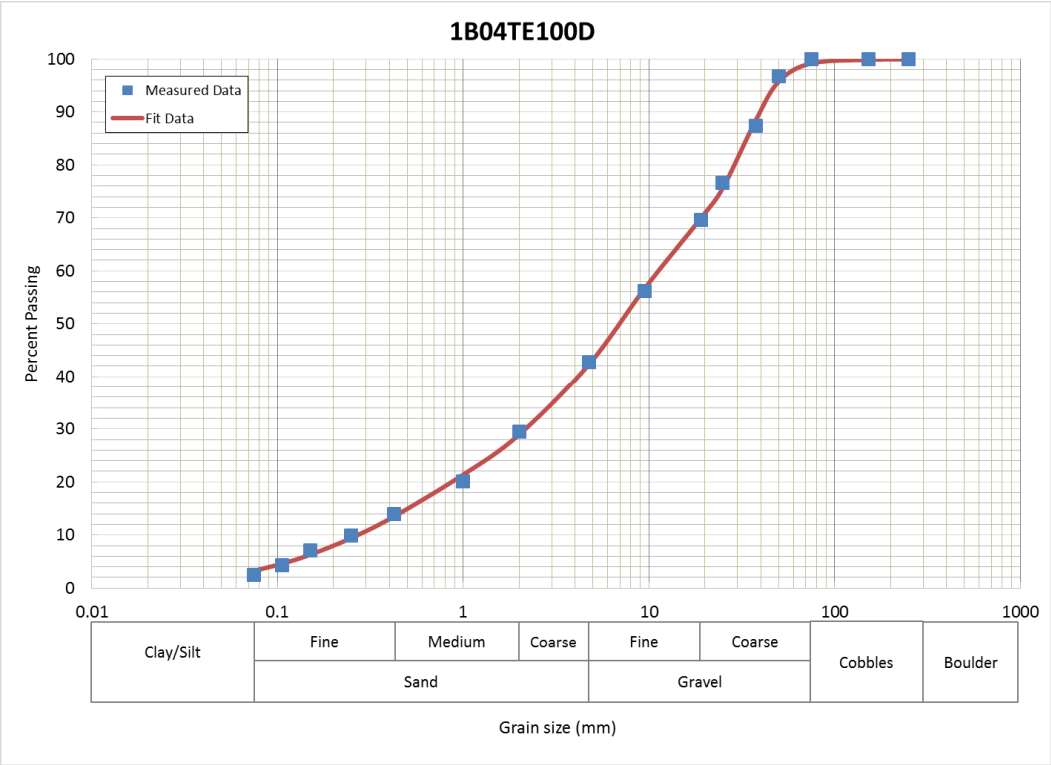
1B04TE100D
Measured Data
Fit Data
Percent Passing
100
90
80
70
60
50
40
30
20
10
0
0.01
0.1
1
10
100
1000
Clay/Silt
Fine
Medium
Coarse
Fine
Coarse
Cobbles
Boulder
Sand
Gravel
Grain size (mm)

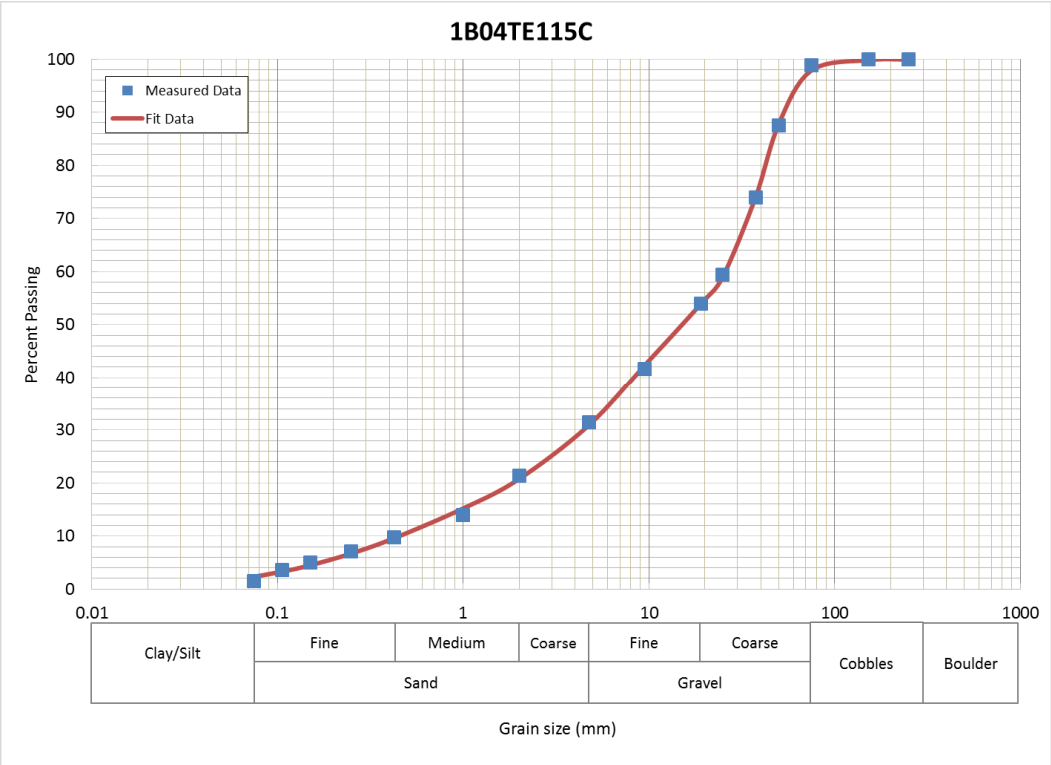
1B04TE115C
Measured Data
Fit Data
Percent Passing
100
90
80
70
60
50
40
30
20
10
0
0.01
0.1
1
10
100
1000
Clay/Silt
Fine
Medium
Coarse
Fine
Coarse
Cobbles
Boulder
Sand
Gravel
Grain size (mm)

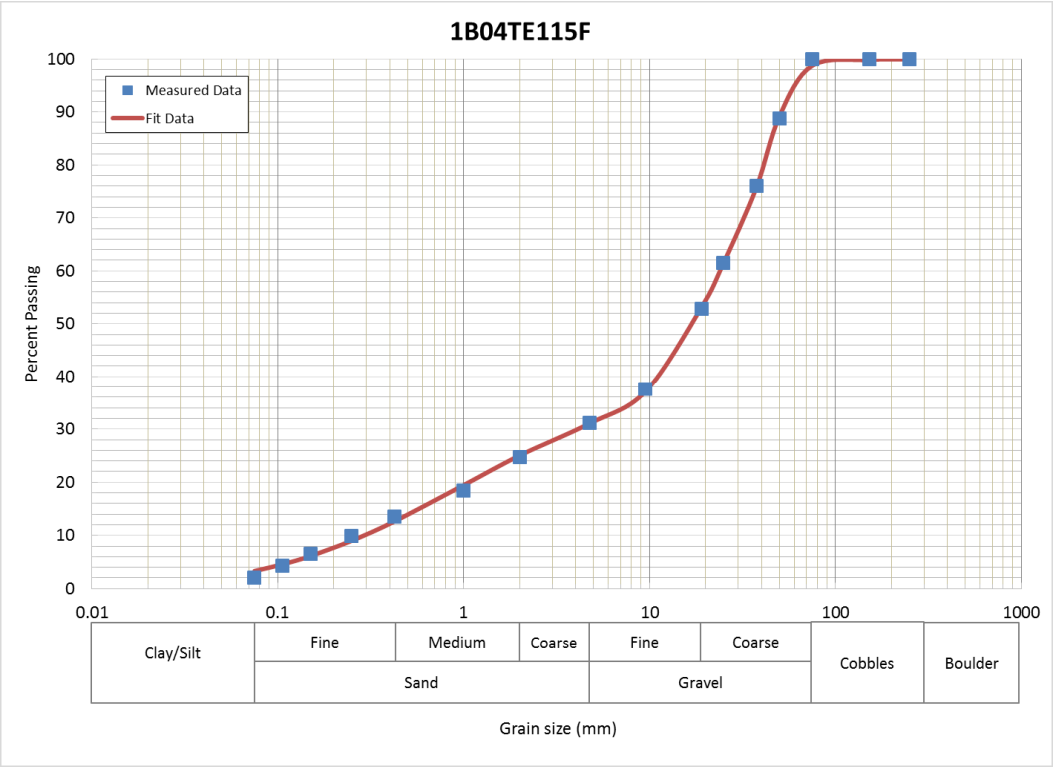
1B04TE115F
Measured Data
Fit Data
Percent Passing
100
90
80
70
60
50
40
30
20
10
0
0.01
0.1
1
10
100
1000
Clay/Silt
Fine
Medium
Coarse
Fine
Coarse
Cobbles
Boulder
Sand
Gravel
Grain size (mm)

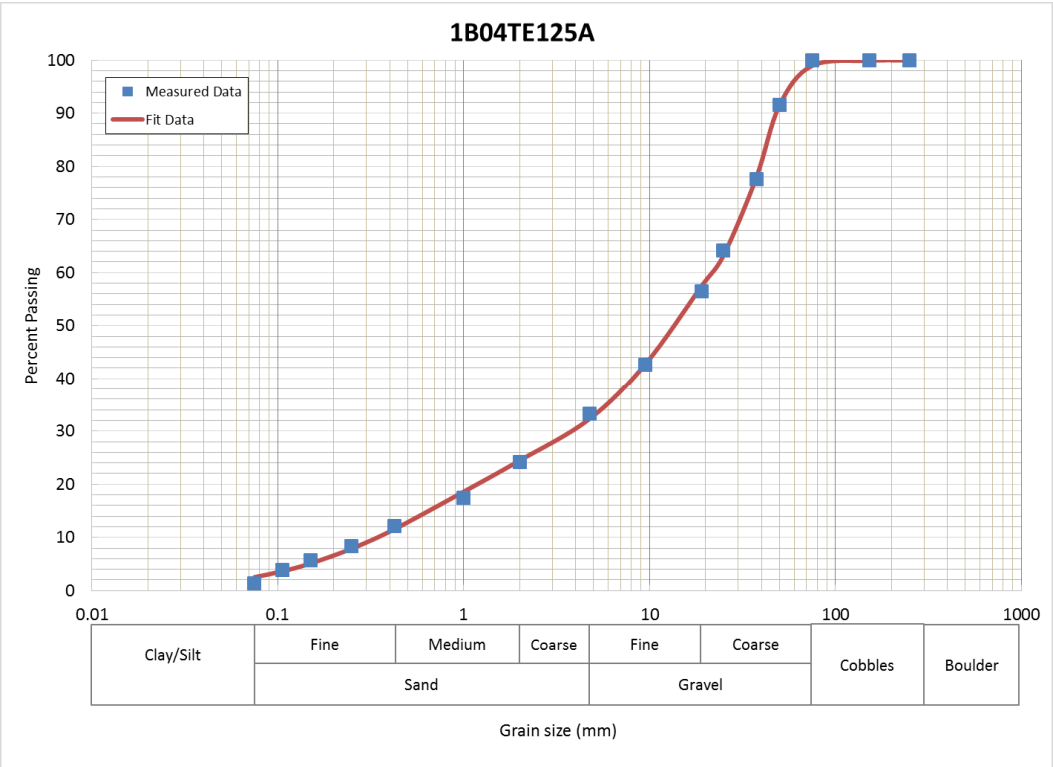
1B04TE125A
Measured Data
Fit Data
Percent Passing
100
90
80
70
60
50
40
30
20
10
0
0.01
0.1
1
10
100
1000
Clay/Silt
Fine
Medium
Coarse
Fine
Coarse
Cobbles
Boulder
Sand
Gravel
Grain size (mm)

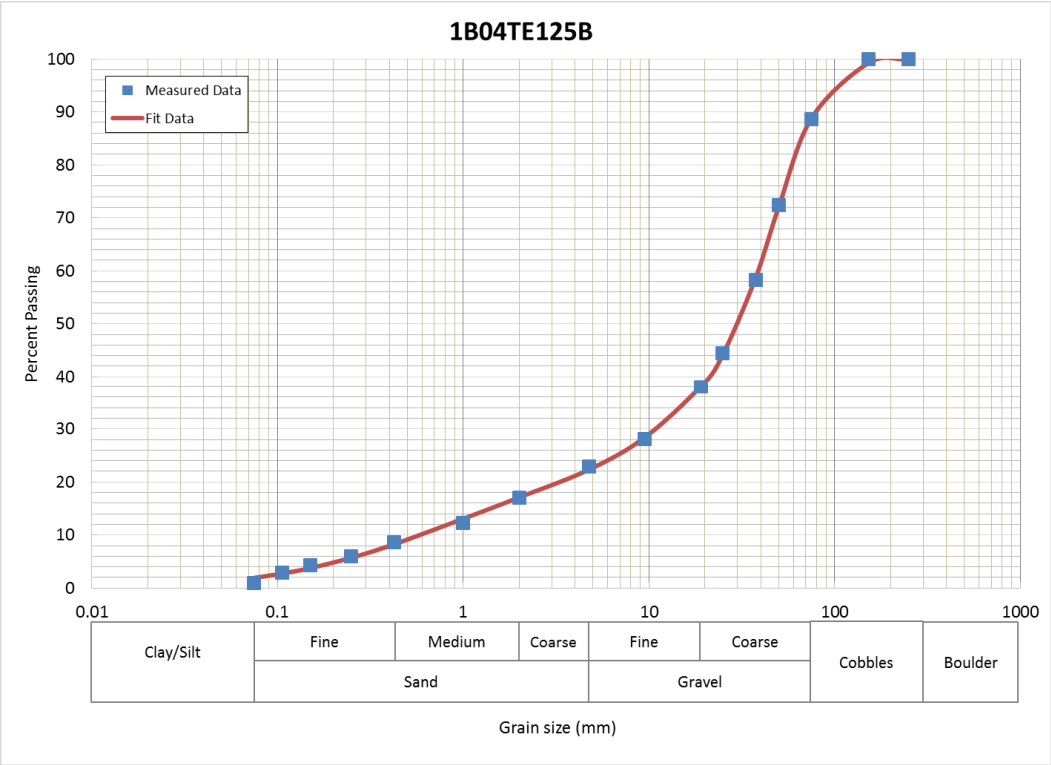
1B04TE125B
Measured Data
Fit Data
Percent Passing
100
90
80
70
60
50
40
30
20
10
0
0.01
0.1
1
10
100
1000
Clay/Silt
Fine
Medium
Coarse
Fine
Coarse
Cobbles
Boulder
Sand
Gravel
Grain size (mm)

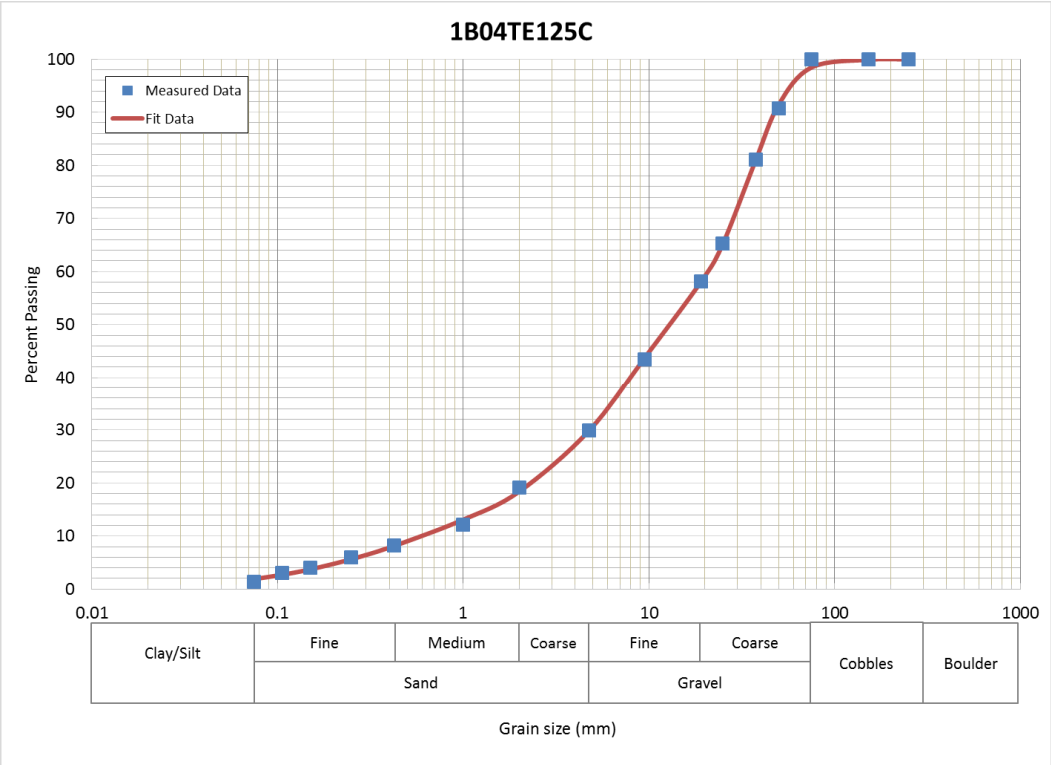
1B04TE125C
Measured Data
Fit Data
Percent Passing
100
90
80
70
60
50
40
30
20
10
0
0.01
0.1
1
10
100
1000
Clay/Silt
Fine
Medium
Coarse
Fine
Coarse
Cobbles
Boulder
Sand
Gravel
Grain size (mm)

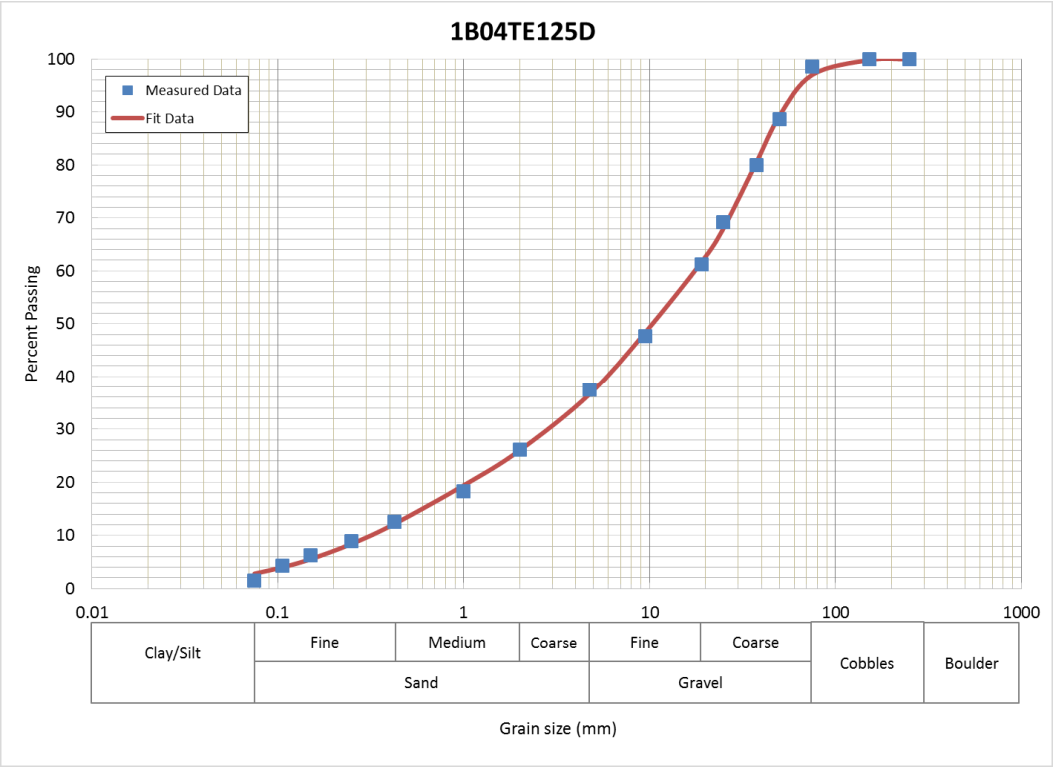
1B04TE125D
Measured Data
Fit Data
Percent Passing
100
90
80
70
60
50
40
30
20
10
0
0.01
0.1
1
10
100
1000
Clay/Silt
Fine
Medium
Coarse
Fine
Coarse
Cobbles
Boulder
Sand
Gravel
Grain size (mm)

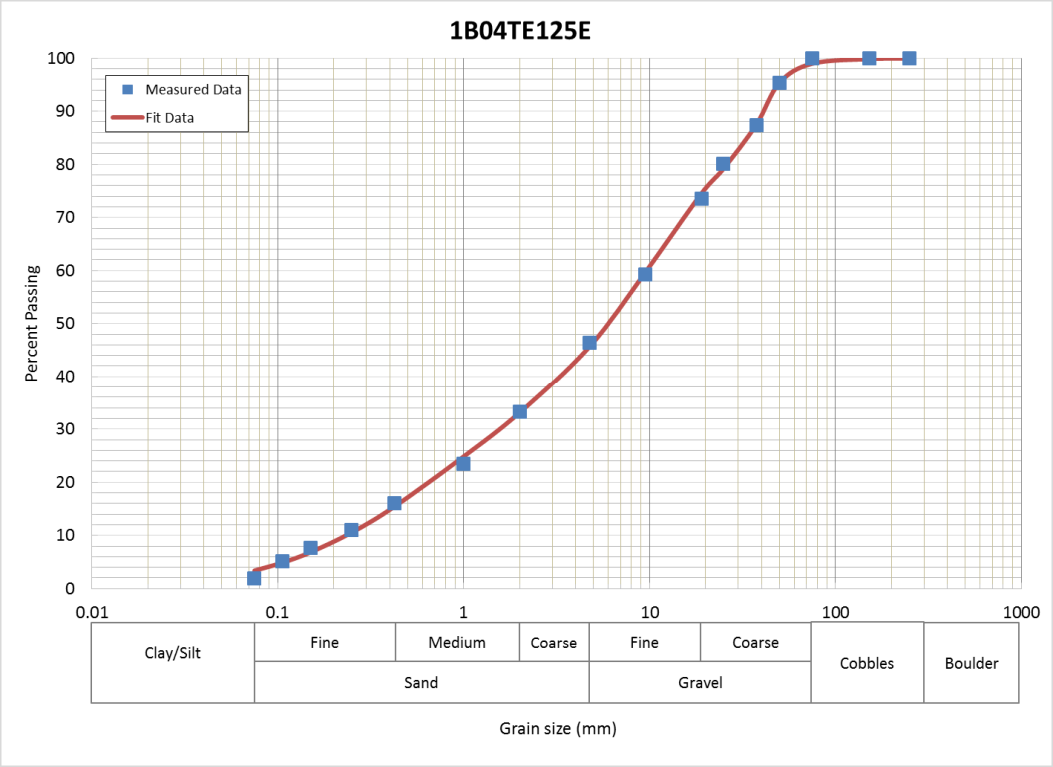
1B04TE125E
Measured Data
Fit Data
Percent Passing
100
90
80
70
60
50
40
30
20
10
0
0.01
0.1
1
10
100
1000
Clay/Silt
Fine
Medium
Coarse
Fine
Coarse
Cobbles
Boulder
Sand
Gravel
Grain size (mm)

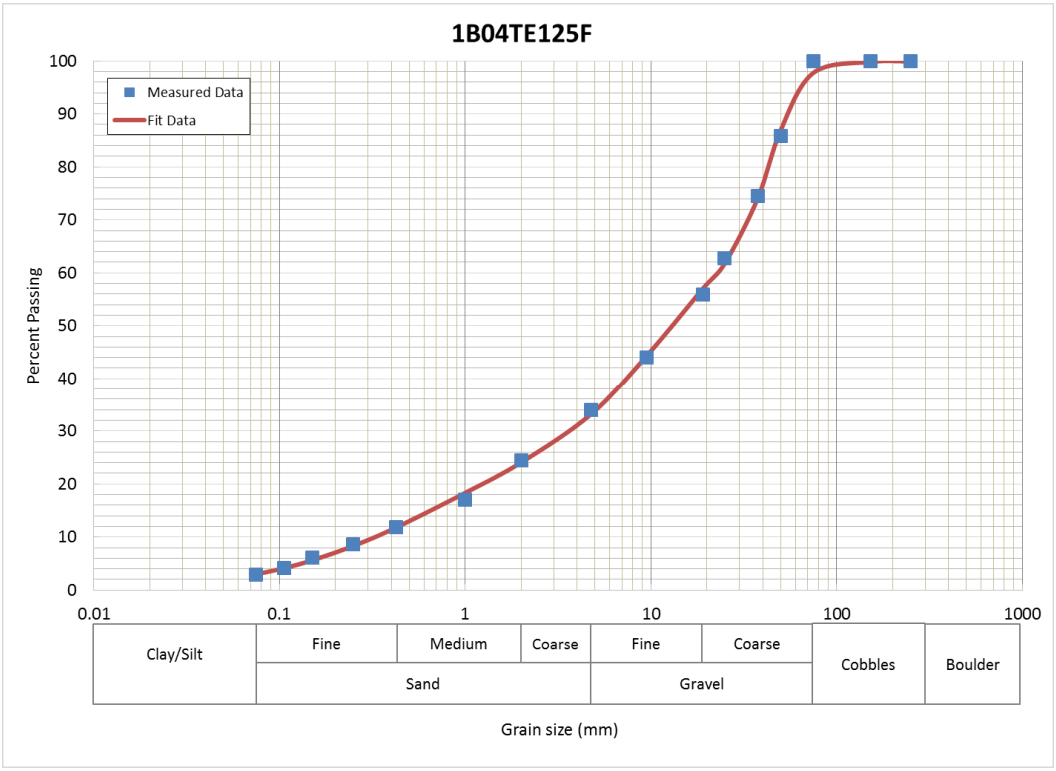
1B04TE125F
Measured Data
Fit Data
Percent Passing
100
90
80
70
60
50
40
30
20
10
0
0.01
0.1
1
10
100
1000
Clay/Silt
Fine
Medium
Coarse
Fine
Coarse
Cobbles
Boulder
Sand
Gravel
Grain size (mm)

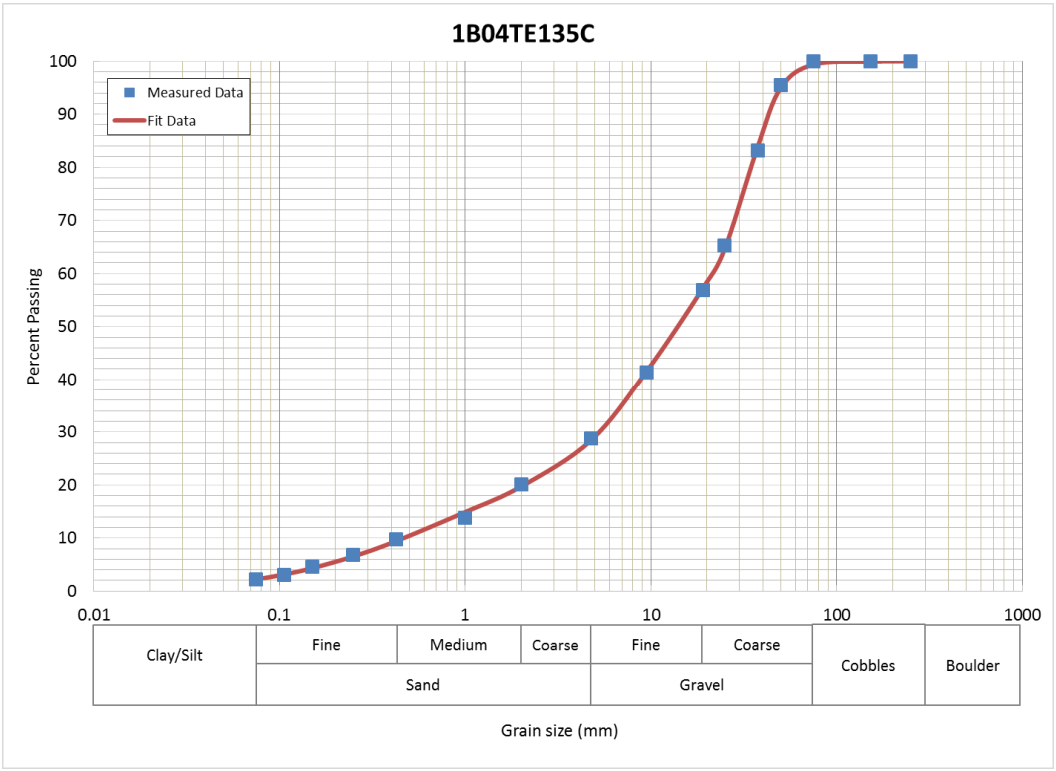
1B04TE135C
Measured Data
Fit Data
Percent Passing
100
90
80
70
60
50
40
30
20
10
0
0.01
0.1
1
10
100
1000
Clay/Silt
Fine
Medium
Coarse
Fine
Coarse
Cobbles
Boulder
Sand
Gravel
Grain size (mm)

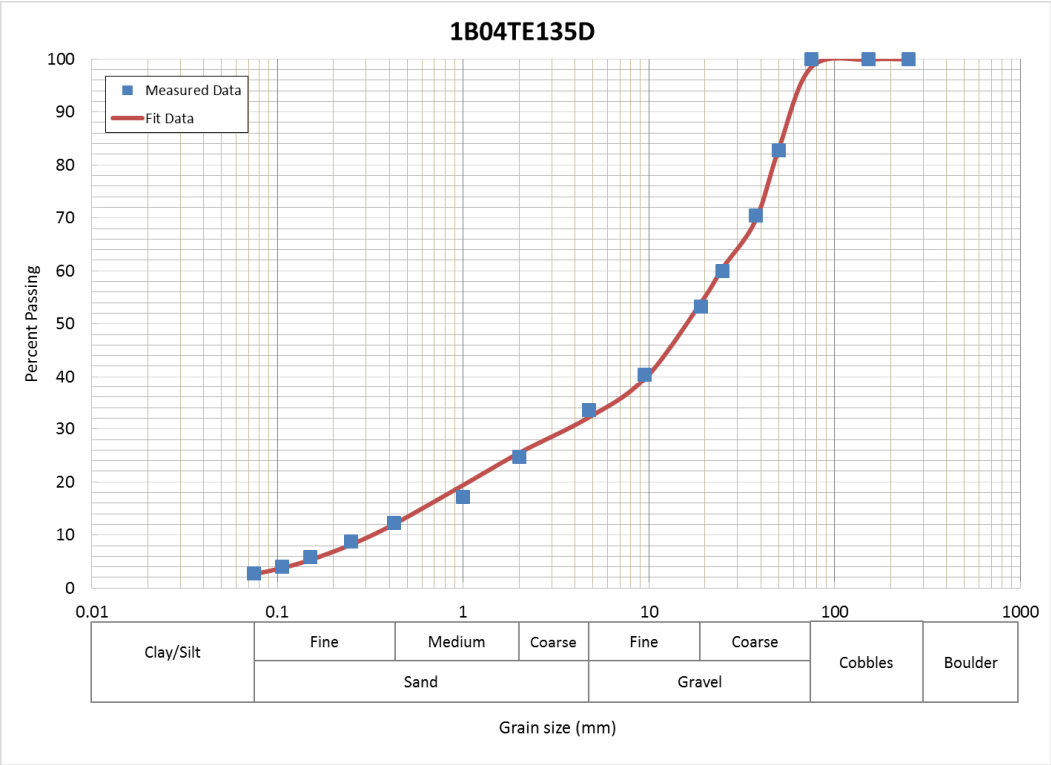
1B04TE135D
Measured Data
Fit Data
Percent Passing
100
90
80
70
60
50
40
30
20
10
0
0.01
0.1
1
10
100
1000
Clay/Silt
Fine
Medium
Coarse
Fine
Coarse
Cobbles
Boulder
Sand
Gravel
Grain size (mm)

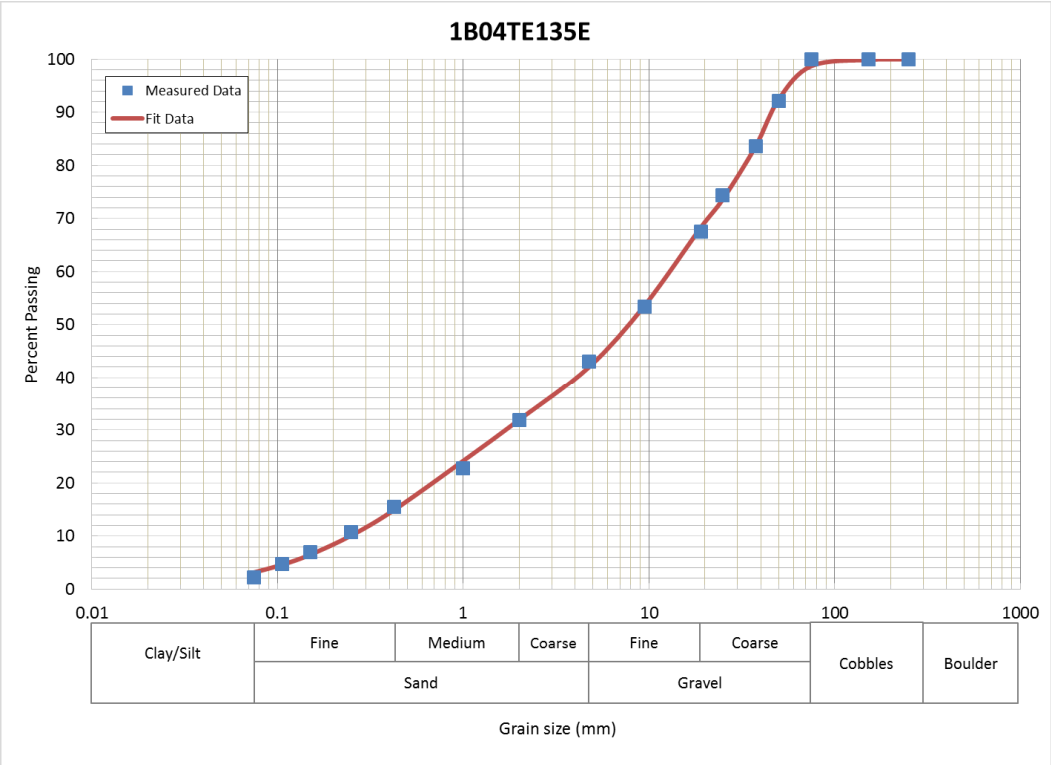
1B04TE135E
Measured Data
Fit Data
Percent Passing
100
90
80
70
60
50
40
30
20
10
0
0.01
0.1
1
10
100
1000
Clay/Silt
Fine
Medium
Coarse
Fine
Coarse
Cobbles
Boulder
Sand
Gravel
Grain size (mm)

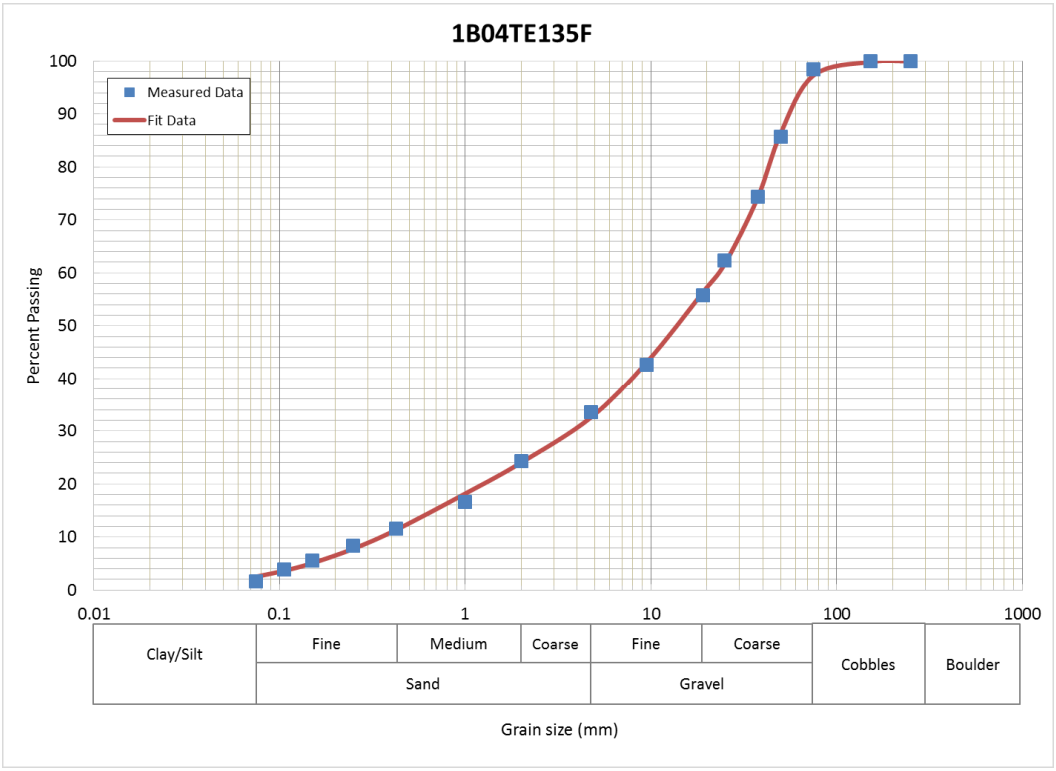
1B04TE135F
Measured Data
Fit Data
Percent Passing
100
90
80
70
60
50
40
30
20
10
0
0.01
0.1
1
10
100
1000
Clay/Silt
Fine
Medium
Coarse
Fine
Coarse
Cobbles
Boulder
Sand
Gravel
Grain size (mm)

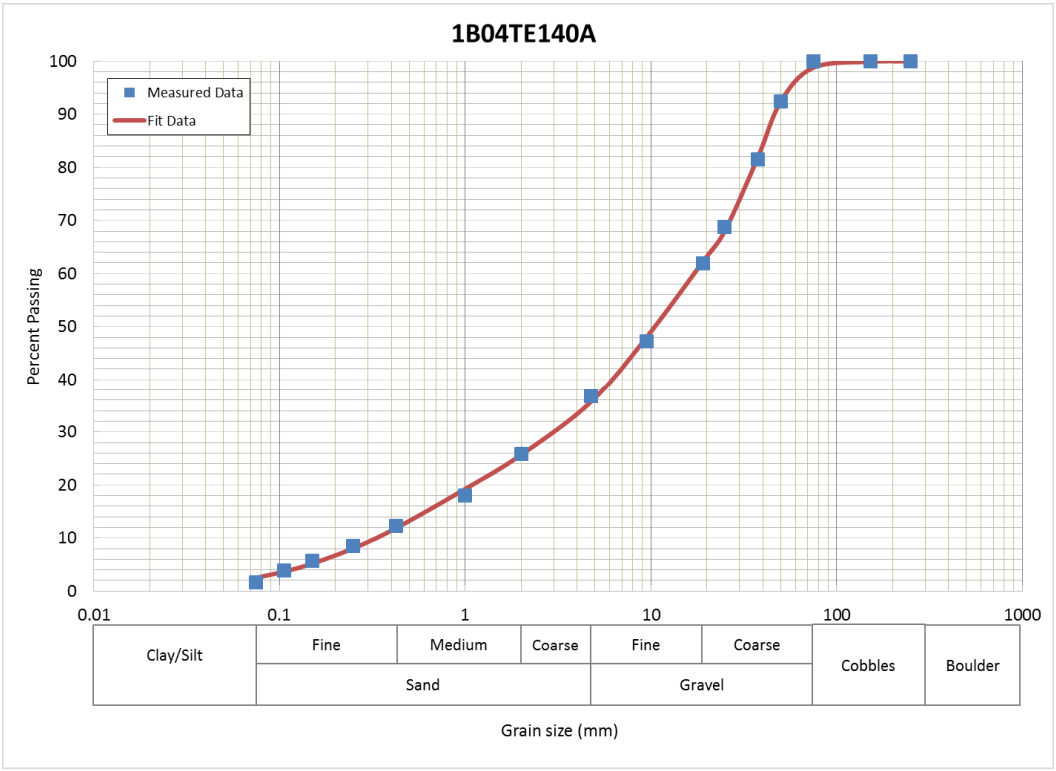
1B04TE140A
Measured Data
Fit Data
Percent Passing
100
90
80
70
60
50
40
30
20
10
0
0.01
0.1
1
10
100
1000
Clay/Silt
Fine
Medium
Coarse
Fine
Coarse
Cobbles
Boulder
Sand
Gravel
Grain size (mm)

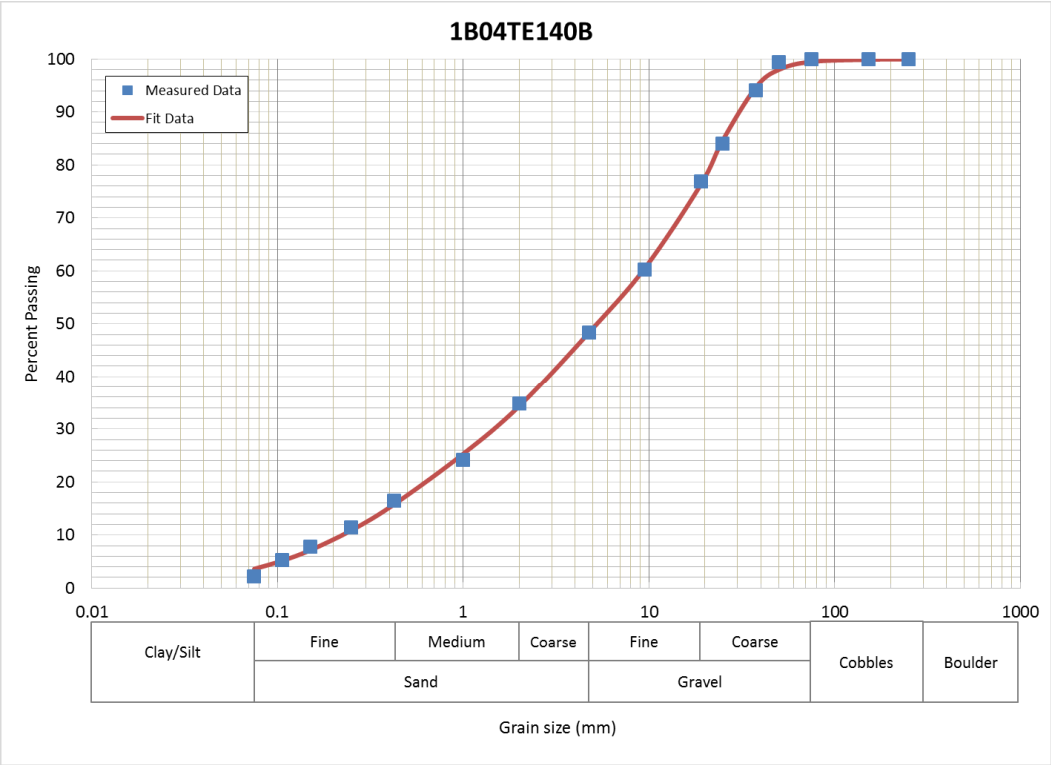
1B04TE140B
Measured Data
Fit Data
Percent Passing
100
90
80
70
60
50
40
30
20
10
0
0.01
0.1
1
10
100
1000
Clay/Silt
Fine
Medium
Coarse
Fine
Coarse
Cobbles
Boulder
Sand
Gravel
Grain size (mm)

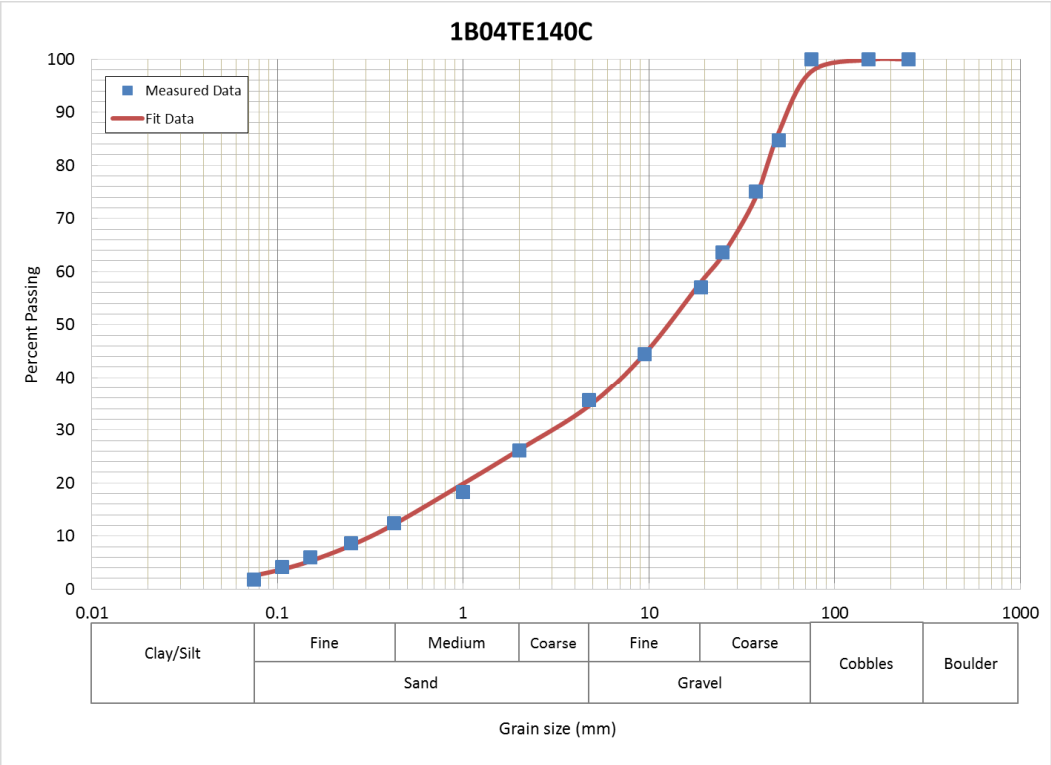
1B04TE140C
Measured Data
Fit Data
Percent Passing
100
90
80
70
60
50
40
30
20
10
0
0.01
0.1
1
10
100
1000
Clay/Silt
Fine
Medium
Coarse
Fine
Coarse
Cobbles
Boulder
Sand
Gravel
Grain size (mm)

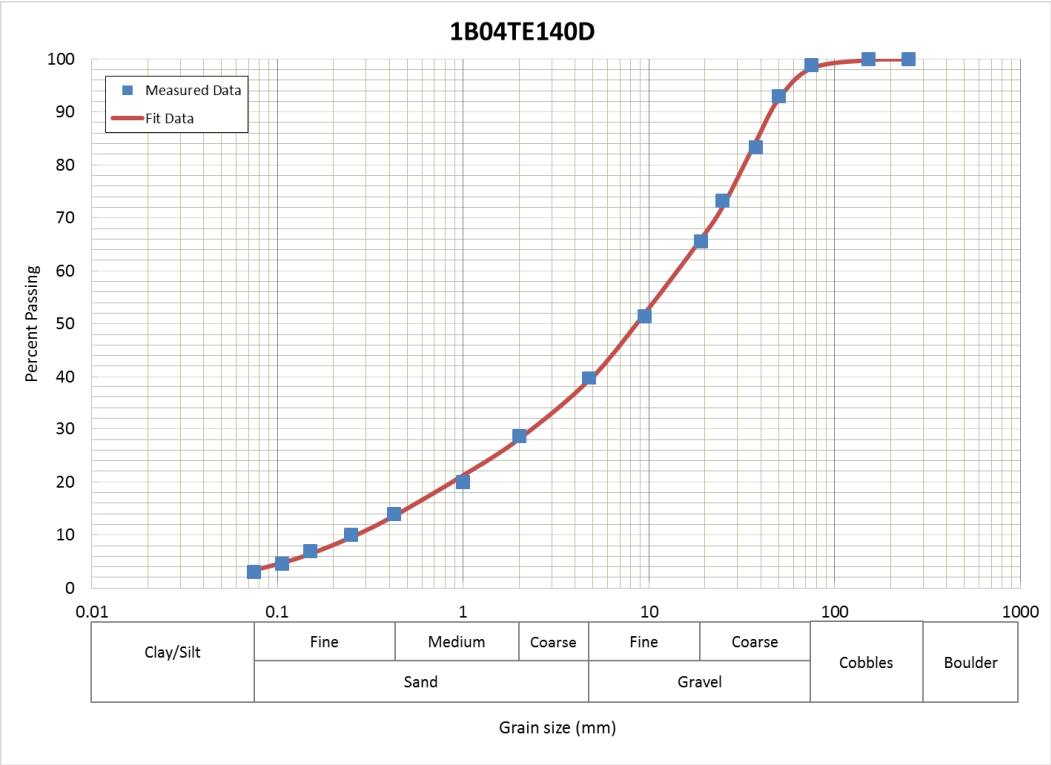
1B04TE140D
Measured Data
Fit Data
Percent Passing
100
90
80
70
60
50
40
30
20
10
0
0.01
0.1
1
10
100
1000
Clay/Silt
Fine
Medium
Coarse
Fine
Coarse
Cobbles
Boulder
Sand
Gravel
Grain size (mm)

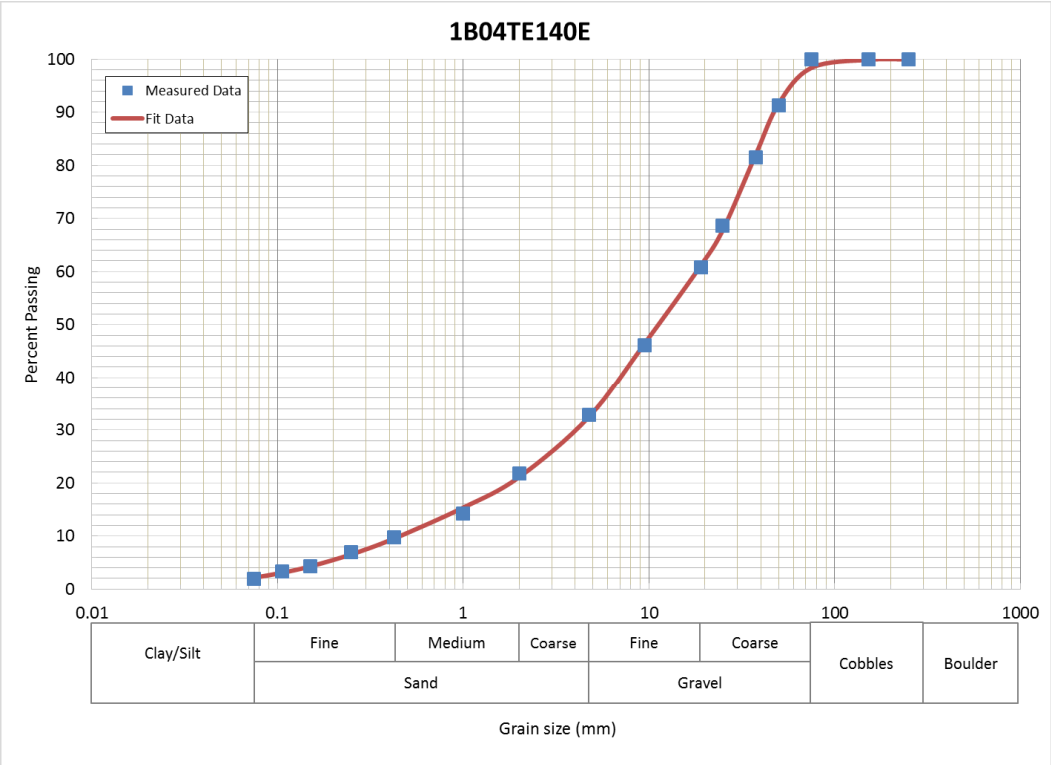
1B04TE140E
Measured Data
Fit Data
Percent Passing
100
90
80
70
60
50
40
30
20
10
0
0.01
0.1
1
10
100
1000
Clay/Silt
Fine
Medium
Coarse
Fine
Coarse
Cobbles
Boulder
Sand
Gravel
Grain size (mm)

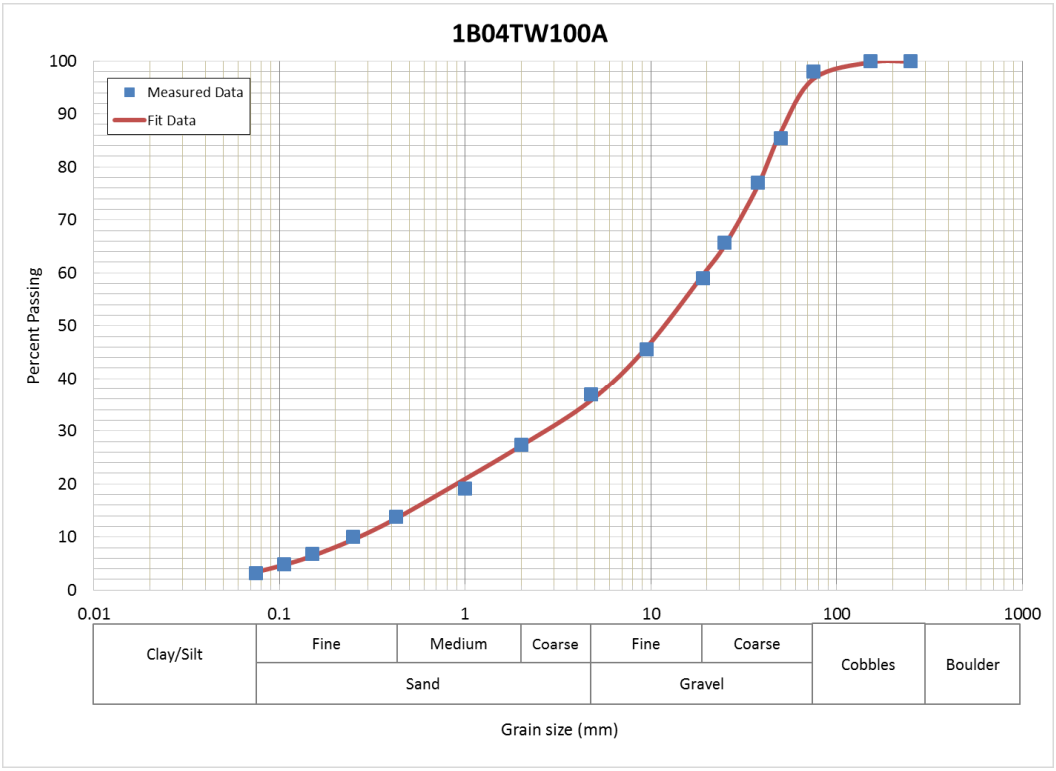
1B04TW100A
Measured Data
Fit Data
Percent Passing
100
90
80
70
60
50
40
30
20
10
0
0.01
0.1
1
10
100
1000
Clay/Silt
Fine
Medium
Coarse
Fine
Coarse
Cobbles
Boulder
Sand
Gravel
Grain size (mm)

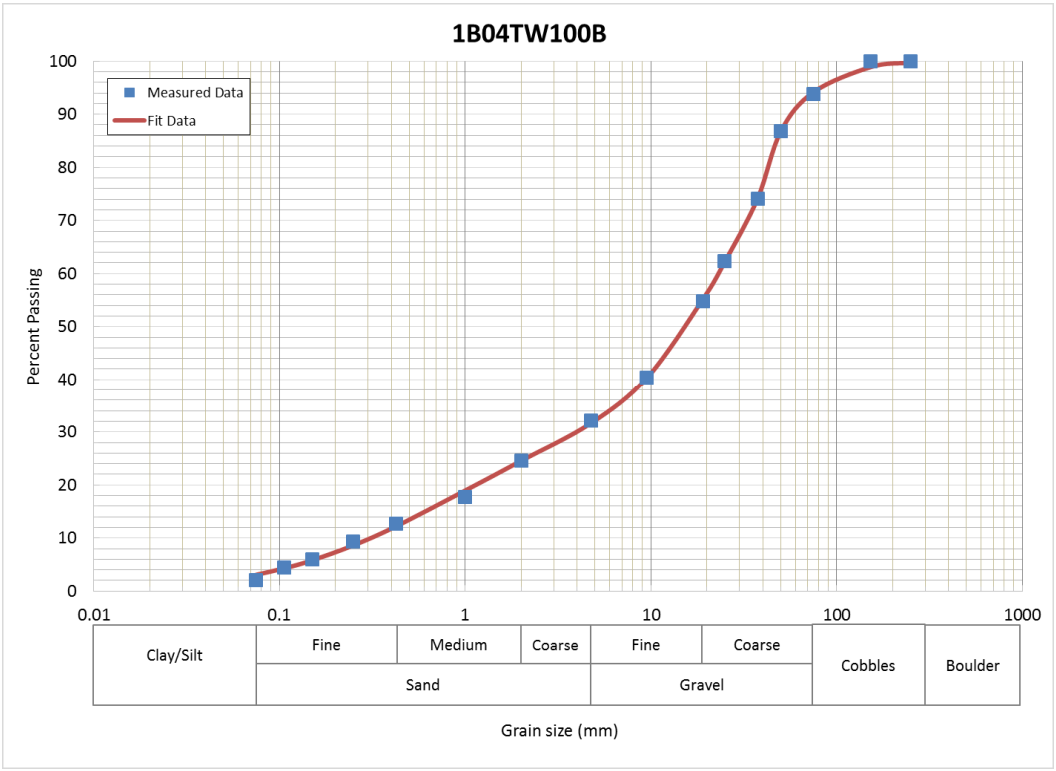
1B04TW100B
Measured Data
Fit Data
Percent Passing
100
90
80
70
60
50
40
30
20
10
0
0.01
0.1
1
10
100
1000
Clay/Silt
Fine
Medium
Coarse
Fine
Coarse
Cobbles
Boulder
Sand
Gravel
Grain size (mm)

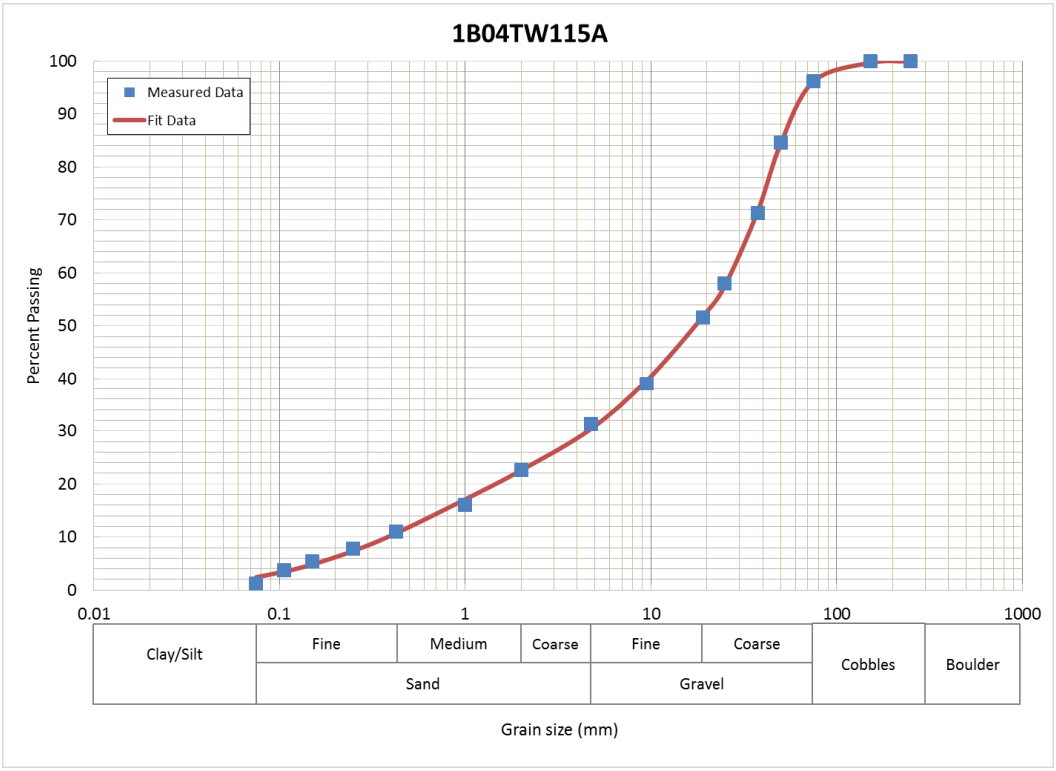
1B04TW115A
Measured Data
Fit Data
Percent Passing
100
90
80
70
60
50
40
30
20
10
0
0.01
0.1
1
10
100
1000
Clay/Silt
Fine
Medium
Coarse
Fine
Coarse
Cobbles
Boulder
Sand
Gravel
Grain size (mm)

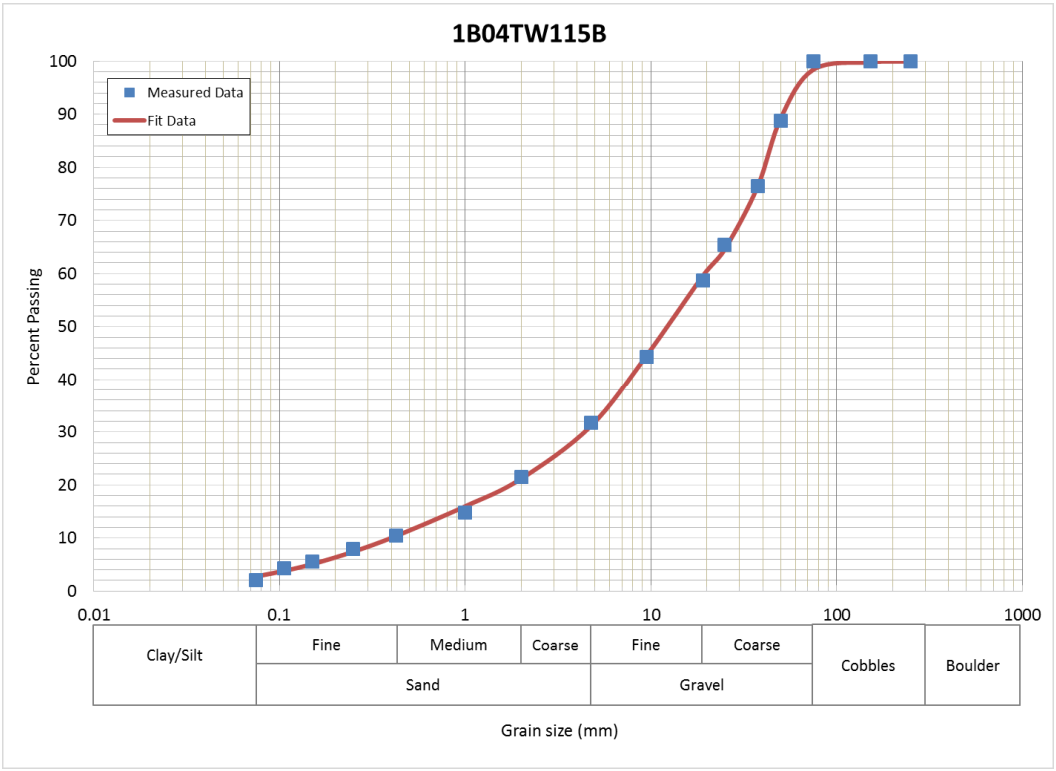
1B04TW115B
Measured Data
Fit Data
Percent Passing
100
90
80
70
60
50
40
30
20
10
0
0.01
0.1
1
10
100
1000
Clay/Silt
Fine
Medium
Coarse
Fine
Coarse
Cobbles
Boulder
Sand
Gravel
Grain size (mm)

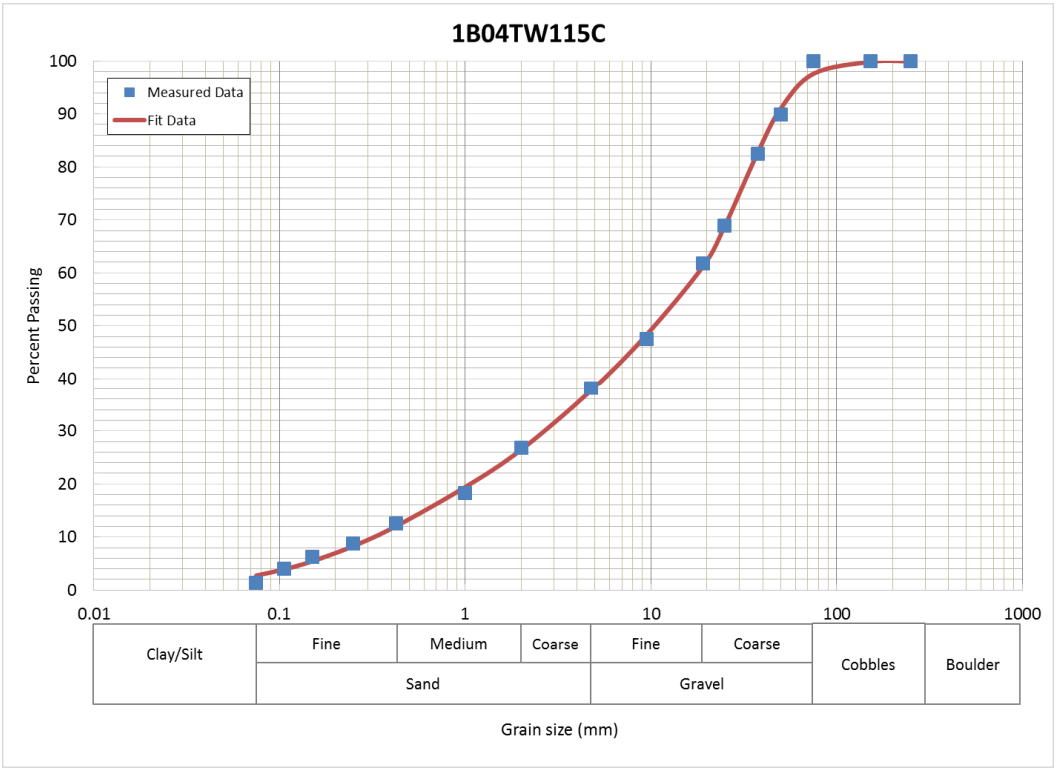
1B04TW115C
Measured Data
Fit Data
Percent Passing
100
90
80
70
60
50
40
30
20
10
0
0.01
0.1
1
10
100
1000
Clay/Silt
Fine
Medium
Coarse
Fine
Coarse
Cobbles
Boulder
Sand
Gravel
Grain size (mm)

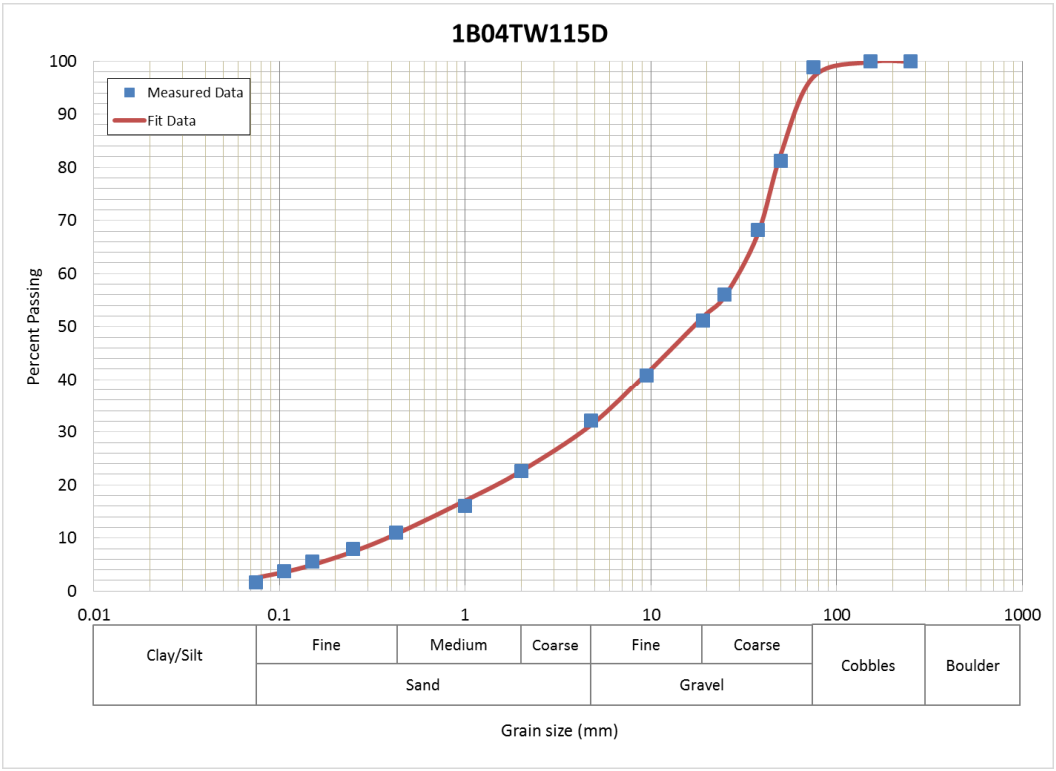
1B04TW115D
Measured Data
Fit Data
Percent Passing
100
90
80
70
60
50
40
30
20
10
0
0.01
0.1
1
10
100
1000
Clay/Silt
Fine
Medium
Coarse
Fine
Coarse
Cobbles
Boulder
Sand
Gravel
Grain size (mm)

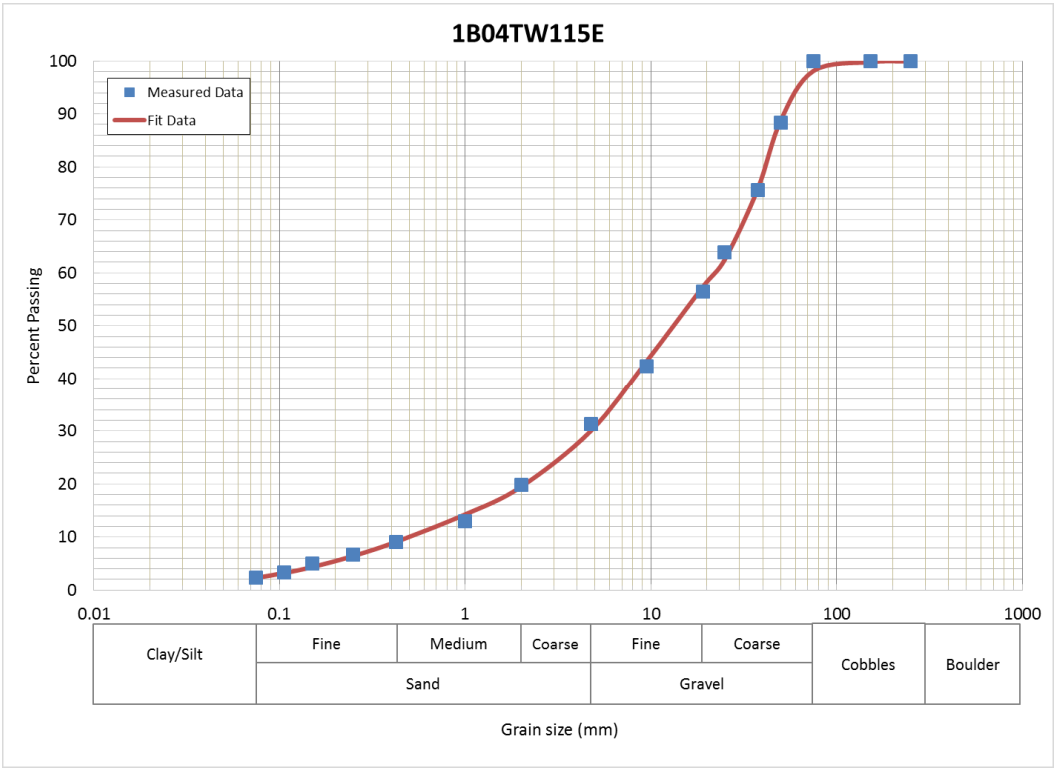
1B04TW115E
Measured Data
Fit Data
Percent Passing
100
90
80
70
60
50
40
30
20
10
0
0.01
0.1
1
10
100
1000
Clay/Silt
Fine
Medium
Coarse
Fine
Coarse
Sand
Gravel
Cobbles
Boulder
Grain size (mm)

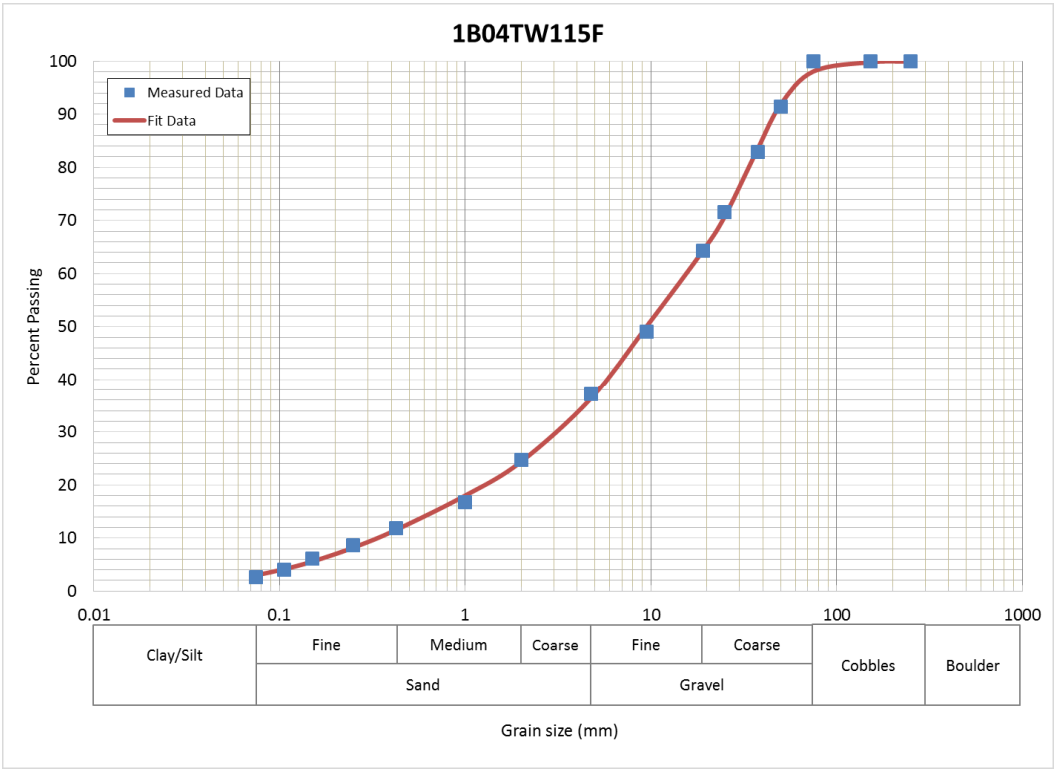
1B04TW115F
Measured Data
Fit Data
Percent Passing
100
90
80
70
60
50
40
30
20
10
0
0.01
0.1
1
10
100
1000
Clay/Silt
Fine
Medium
Coarse
Fine
Coarse
Sand
Gravel
Cobbles
Boulder
Grain size (mm)

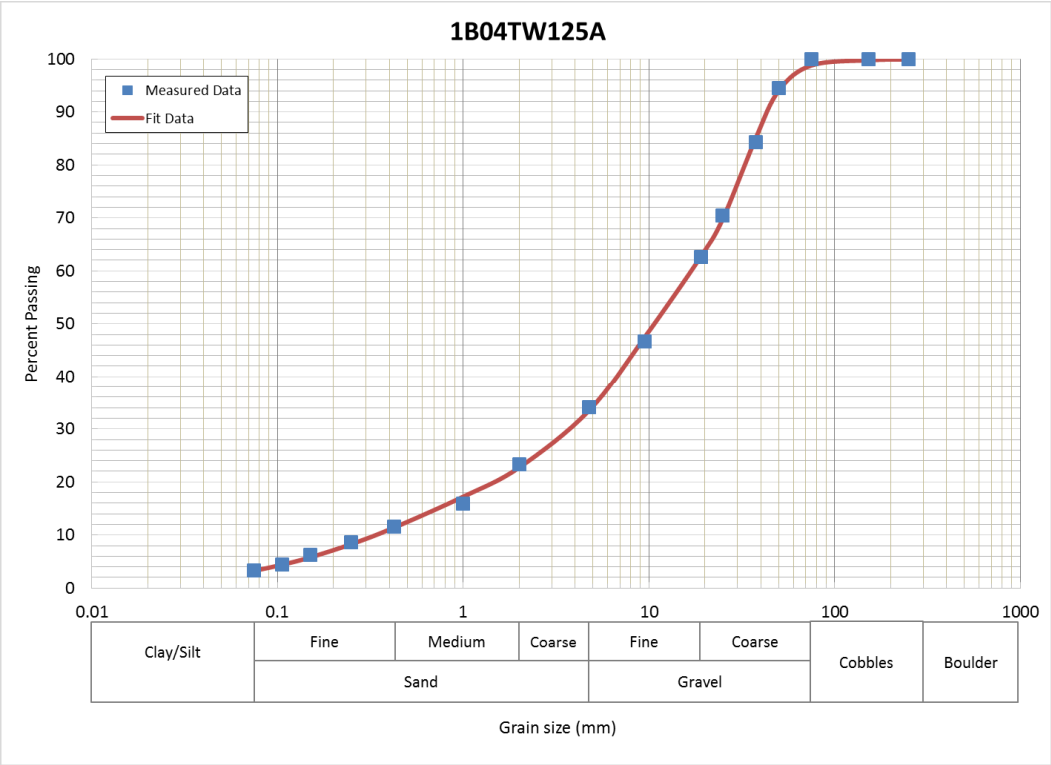
1B04TW125A
Measured Data
Fit Data
Percent Passing
100
90
80
70
60
50
40
30
20
10
0
0.01
0.1
1
10
100
1000
Clay/Silt
Fine
Medium
Coarse
Fine
Coarse
Sand
Gravel
Cobbles
Boulder
Grain size (mm)

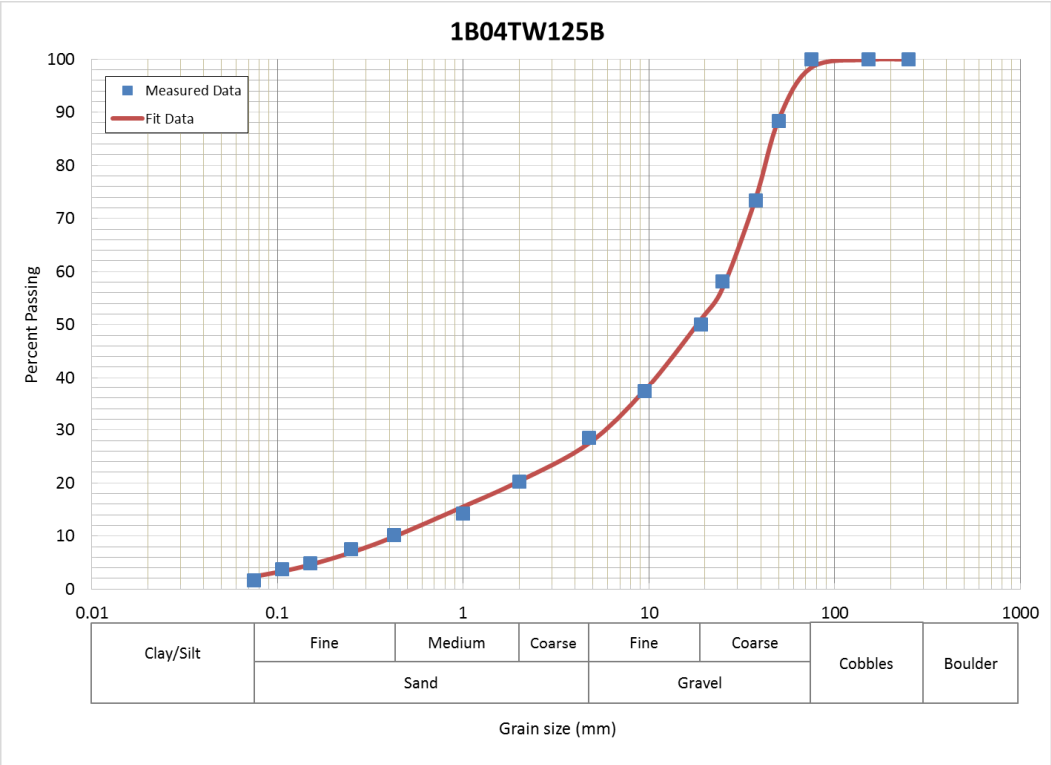
1B04TW125B
Measured Data
Fit Data
Percent Passing
100
90
80
70
60
50
40
30
20
10
0
0.01
0.1
1
10
100
1000
Clay/Silt
Fine
Medium
Coarse
Fine
Coarse
Sand
Gravel
Cobbles
Boulder
Grain size (mm)

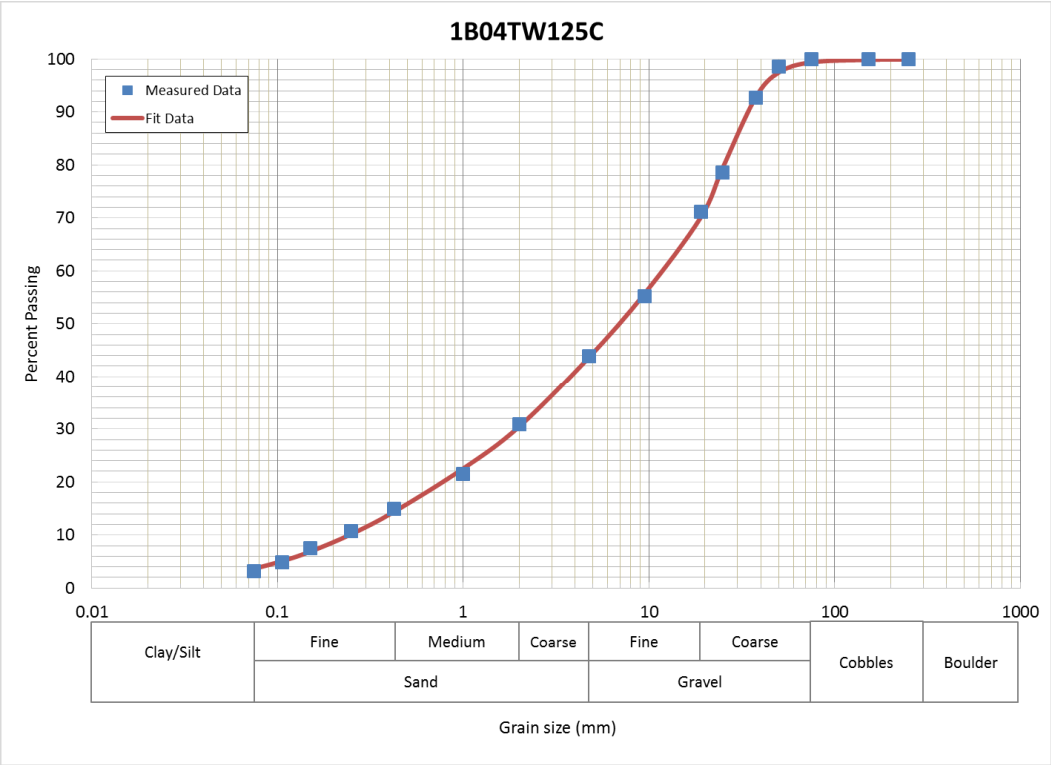
1B04TW125C
Measured Data
Fit Data
Percent Passing
100
90
80
70
60
50
40
30
20
10
0
0.01
0.1
1
10
100
1000
Clay/Silt
Fine
Medium
Coarse
Fine
Coarse
Cobbles
Boulder
Sand
Gravel
Grain size (mm)

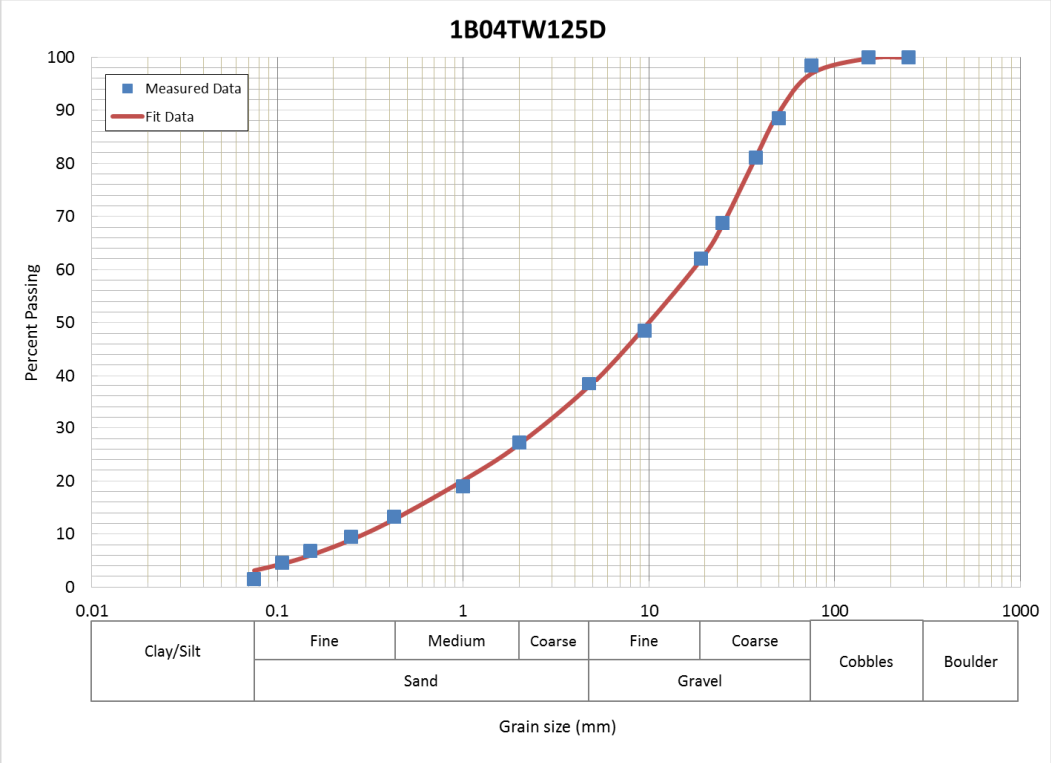
1B04TW125D
Measured Data
Fit Data
Percent Passing
100
90
80
70
60
50
40
30
20
10
0
0.01
0.1
1
10
100
1000
Clay/Silt
Fine
Medium
Coarse
Fine
Coarse
Cobbles
Boulder
Sand
Gravel
Grain size (mm)

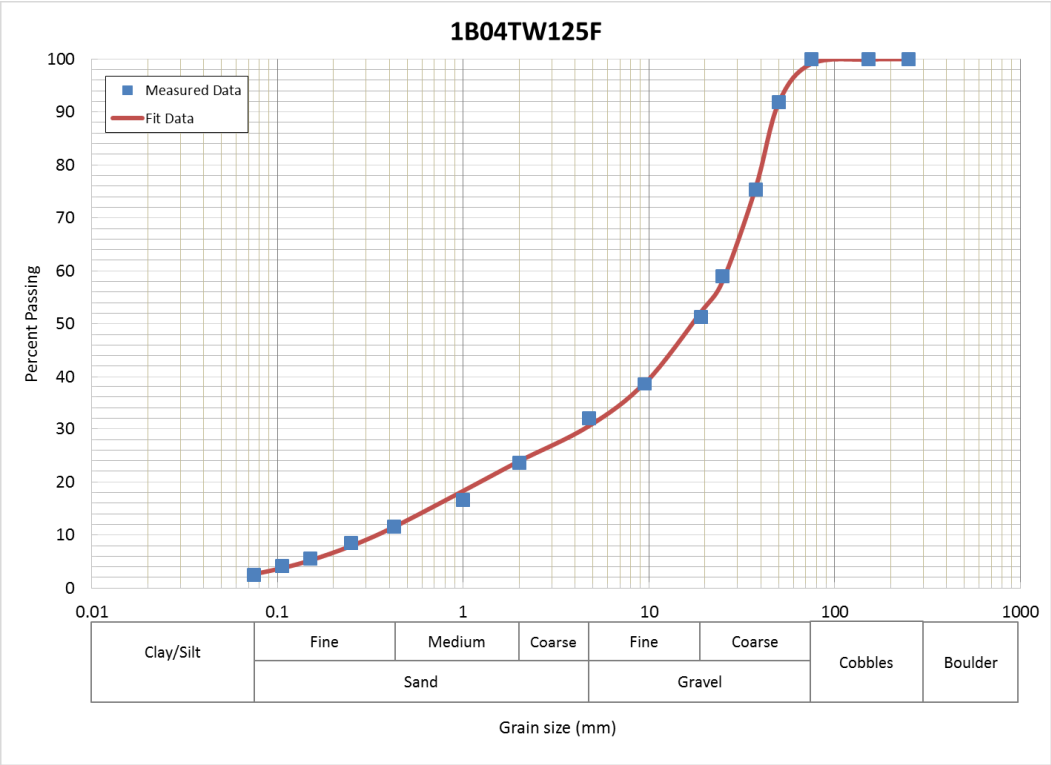
1B04TW125F
Measured Data
Fit Data
Percent Passing
100
90
80
70
60
50
40
30
20
10
0
0.01
0.1
1
10
100
1000
Clay/Silt
Fine
Medium
Coarse
Fine
Coarse
Cobbles
Boulder
Sand
Gravel
Grain size (mm)

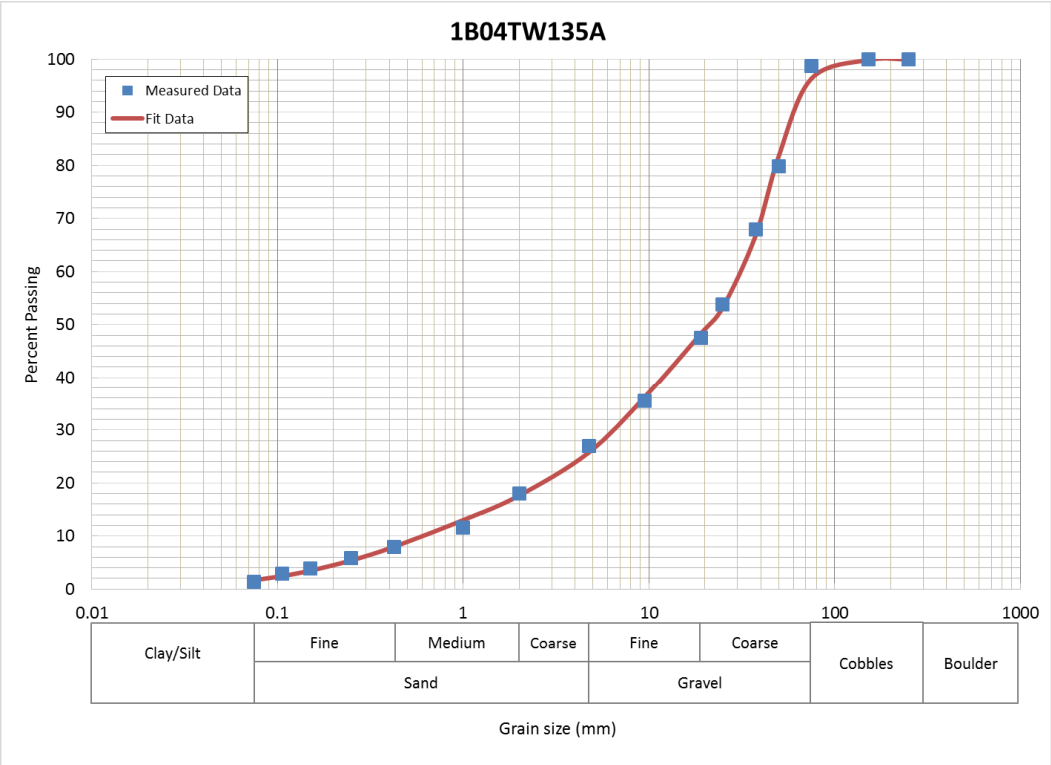
1B04TW135A
Measured Data
Fit Data
Percent Passing
100
90
80
70
60
50
40
30
20
10
0
0.01
0.1
1
10
100
1000
Clay/Silt
Fine
Medium
Coarse
Fine
Coarse
Cobbles
Boulder
Sand
Gravel
Grain size (mm)

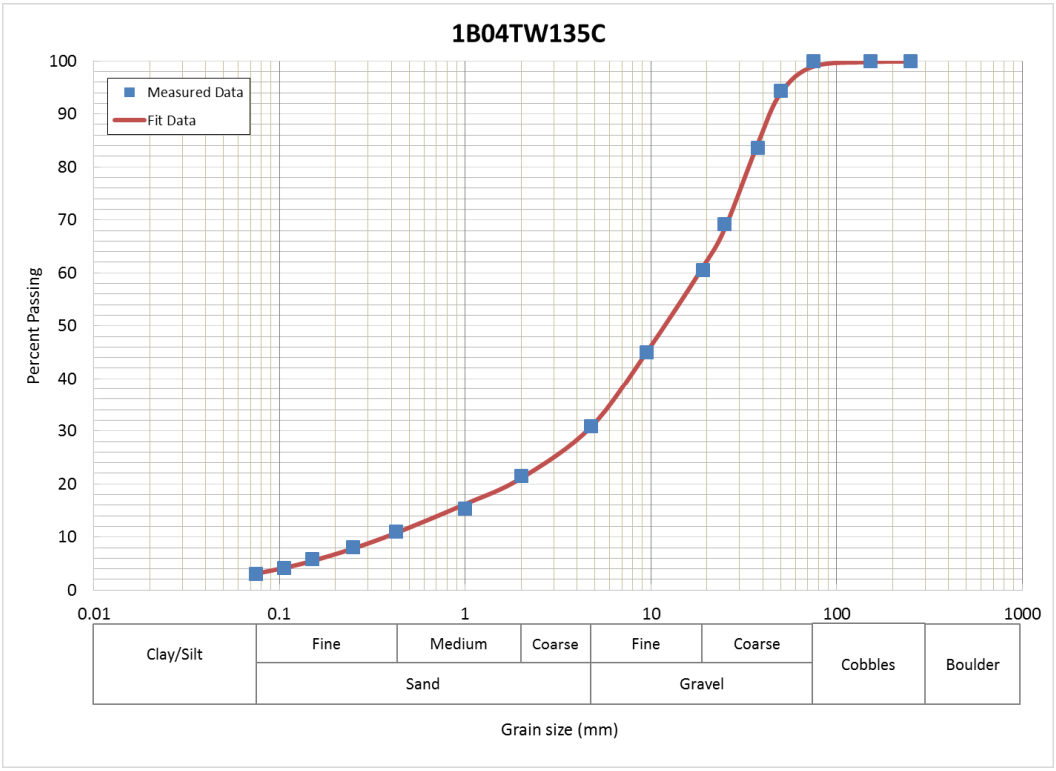
1B04TW135C
Measured Data
Fit Data
Percent Passing
100
90
80
70
60
50
40
30
20
10
0
0.01
0.1
1
10
100
1000
Clay/Silt
Fine
Medium
Coarse
Fine
Coarse
Cobbles
Boulder
Sand
Gravel
Grain size (mm)

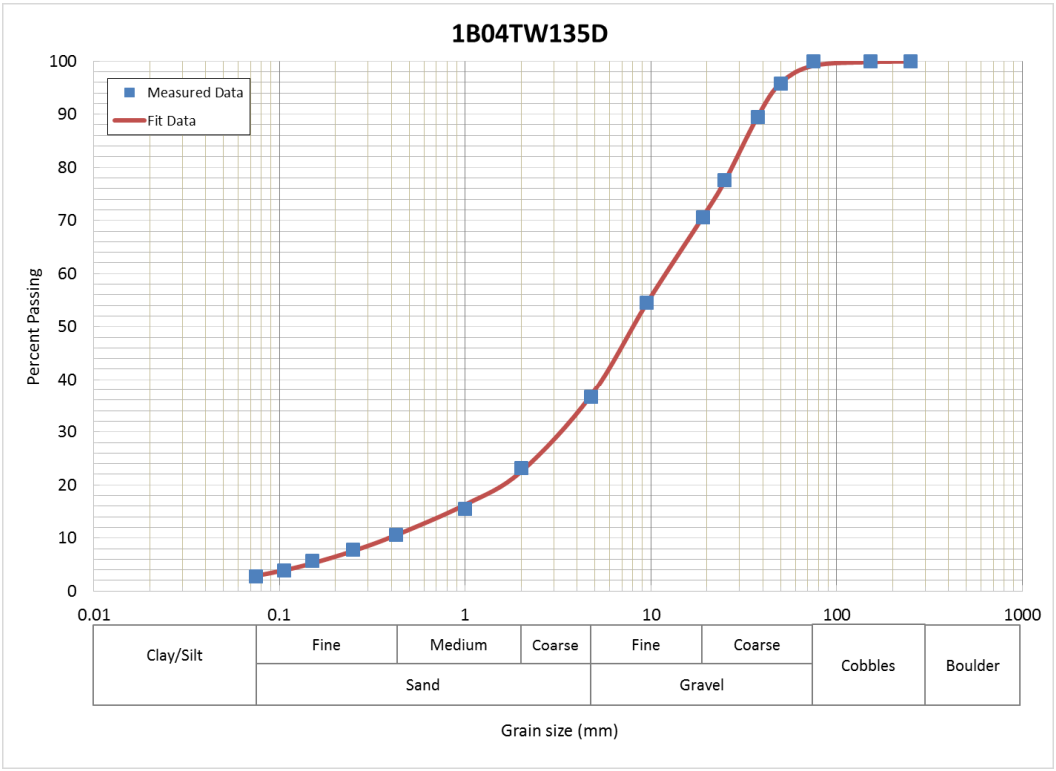
1B04TW135D
Measured Data
Fit Data
Percent Passing
100
90
80
70
60
50
40
30
20
10
0
0.01
0.1
1
10
100
1000
Clay/Silt
Fine
Medium
Coarse
Fine
Coarse
Cobbles
Boulder
Sand
Gravel
Grain size (mm)

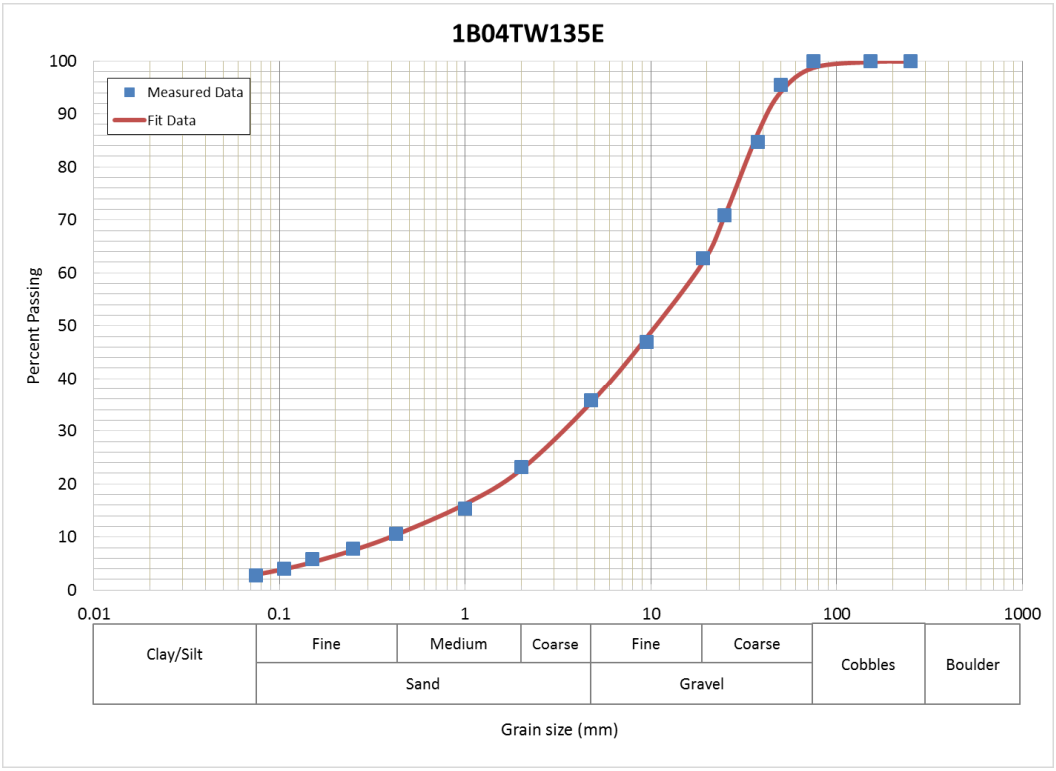
1B04TW135E
Measured Data
Fit Data
Percent Passing
100
90
80
70
60
50
40
30
20
10
0
0.01
0.1
1
10
100
1000
Clay/Silt
Fine
Medium
Coarse
Fine
Coarse
Cobbles
Boulder
Sand
Gravel
Grain size (mm)

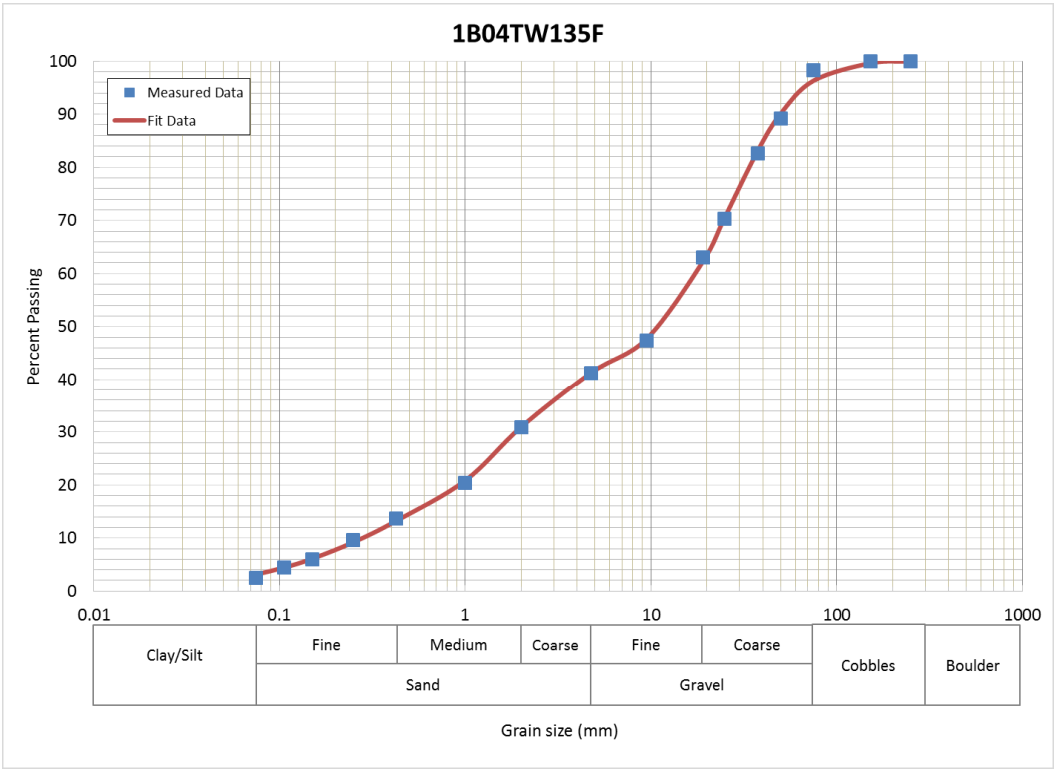
1B04TW135F
Measured Data
Fit Data
Percent Passing
100
90
80
70
60
50
40
30
20
10
0
0.01
0.1
1
10
100
1000
Clay/Silt
Fine
Medium
Coarse
Fine
Coarse
Cobbles
Boulder
Sand
Gravel
Grain size (mm)

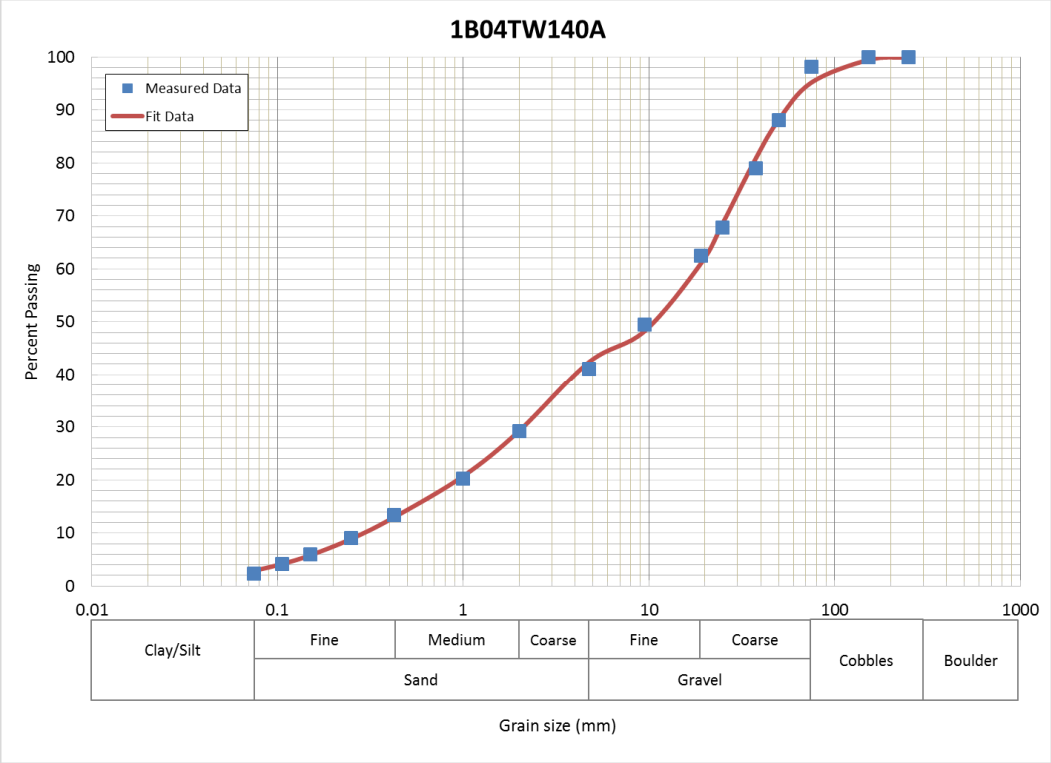
1B04TW140A
Measured Data
Fit Data
Percent Passing
100
90
80
70
60
50
40
30
20
10
0
0.01
0.1
1
10
100
1000
Clay/Silt
Fine
Medium
Coarse
Fine
Coarse
Cobbles
Boulder
Sand
Gravel
Grain size (mm)

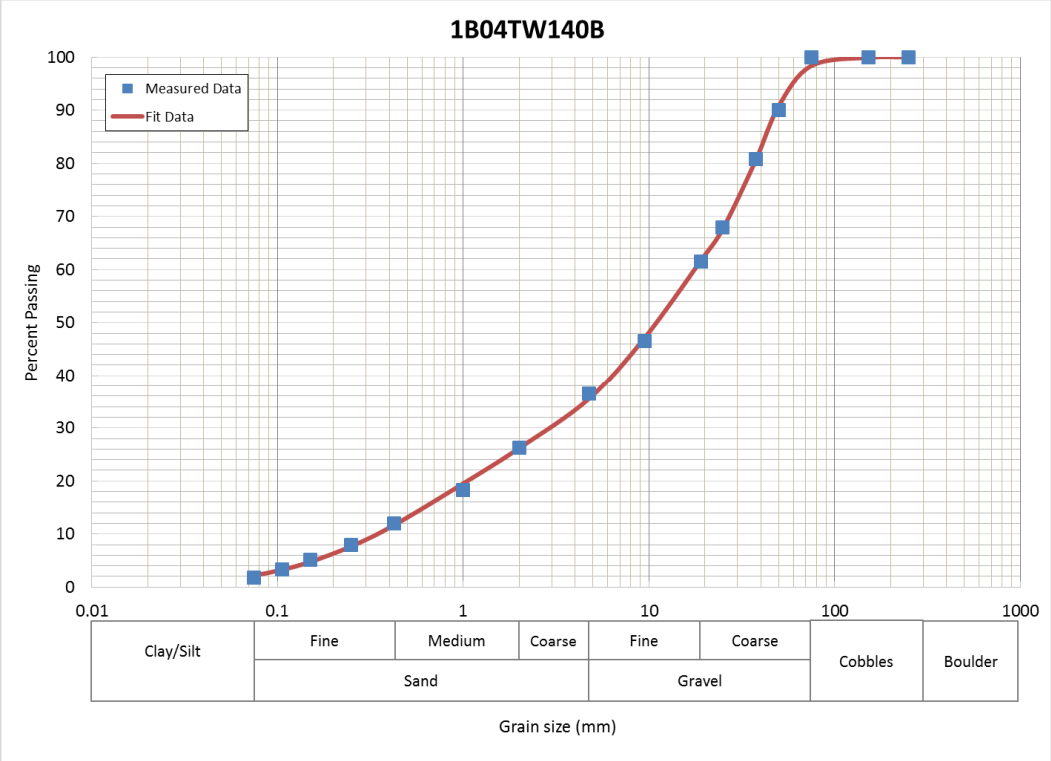
1B04TW140B
Measured Data
Fit Data
Percent Passing
100
90
80
70
60
50
40
30
20
10
0
0.01
0.1
1
10
100
1000
Clay/Silt
Fine
Medium
Coarse
Fine
Coarse
Cobbles
Boulder
Sand
Gravel
Grain size (mm)

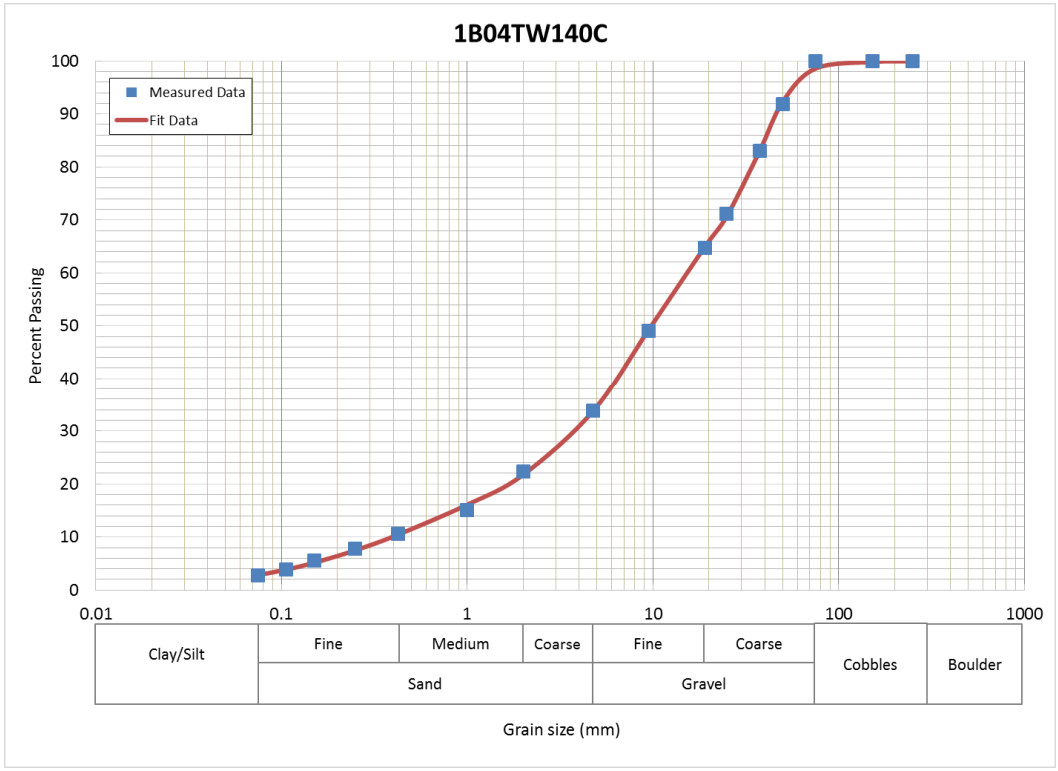
1B04TW140C
Measured Data
Fit Data
Percent Passing
100
90
80
70
60
50
40
30
20
10
0
0.01
0.1
1
10
100
1000
Clay/Silt
Fine
Medium
Coarse
Fine
Coarse
Cobbles
Boulder
Sand
Gravel
Grain size (mm)

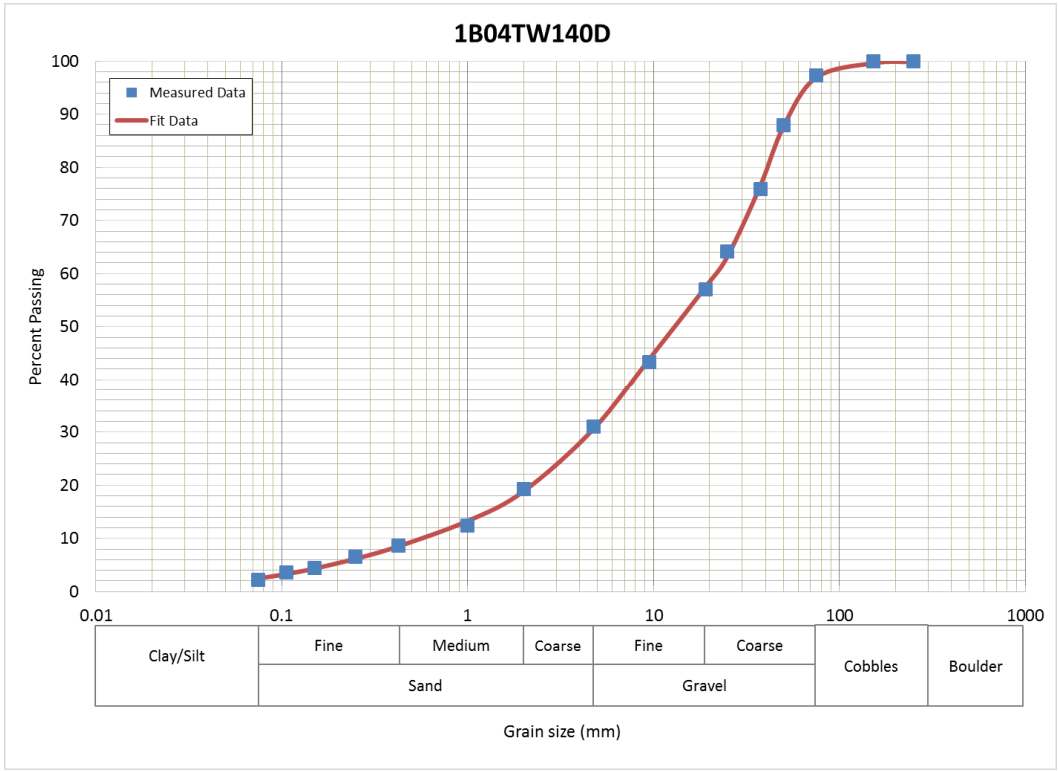
1B04TW140D
Measured Data
Fit Data
Percent Passing
100
90
80
70
60
50
40
30
20
10
0
0.01
0.1
1
10
100
1000
Clay/Silt
Fine
Medium
Coarse
Fine
Coarse
Cobbles
Boulder
Sand
Gravel
Grain size (mm)

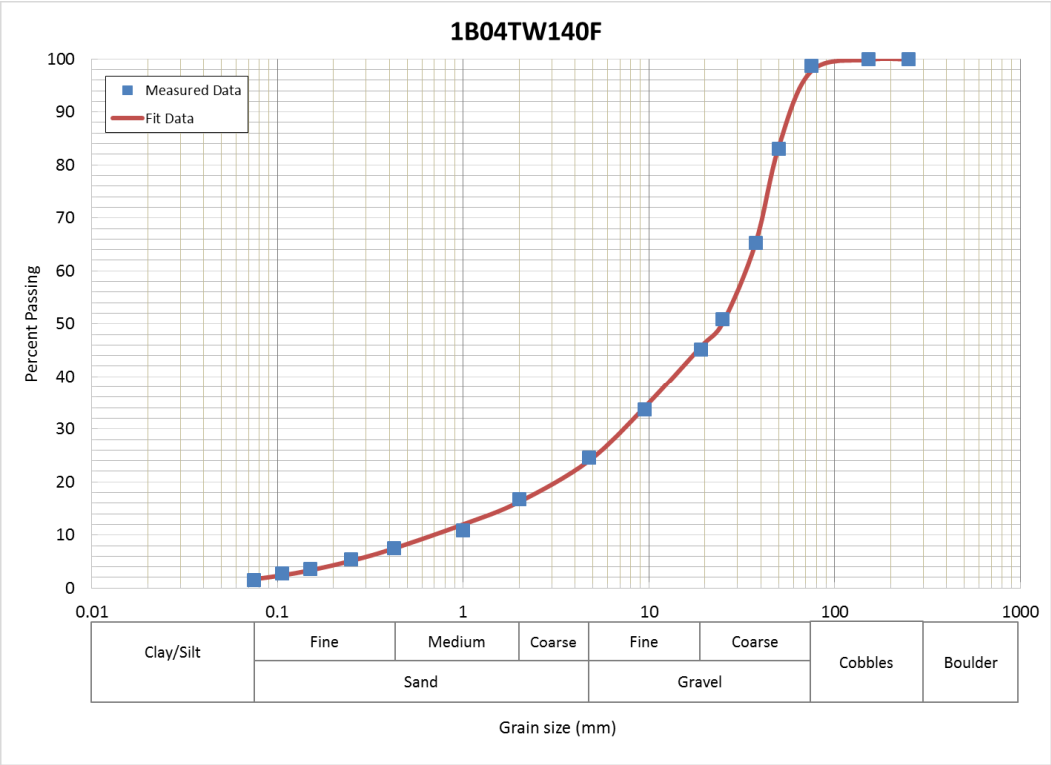
1B04TW140F
Measured Data
Fit Data
Percent Passing
100
90
80
70
60
50
40
30
20
10
0
0.01
0.1
1
10
100
1000
Clay/Silt
Fine
Medium
Coarse
Fine
Coarse
Cobbles
Boulder
Sand
Gravel
Grain size (mm)

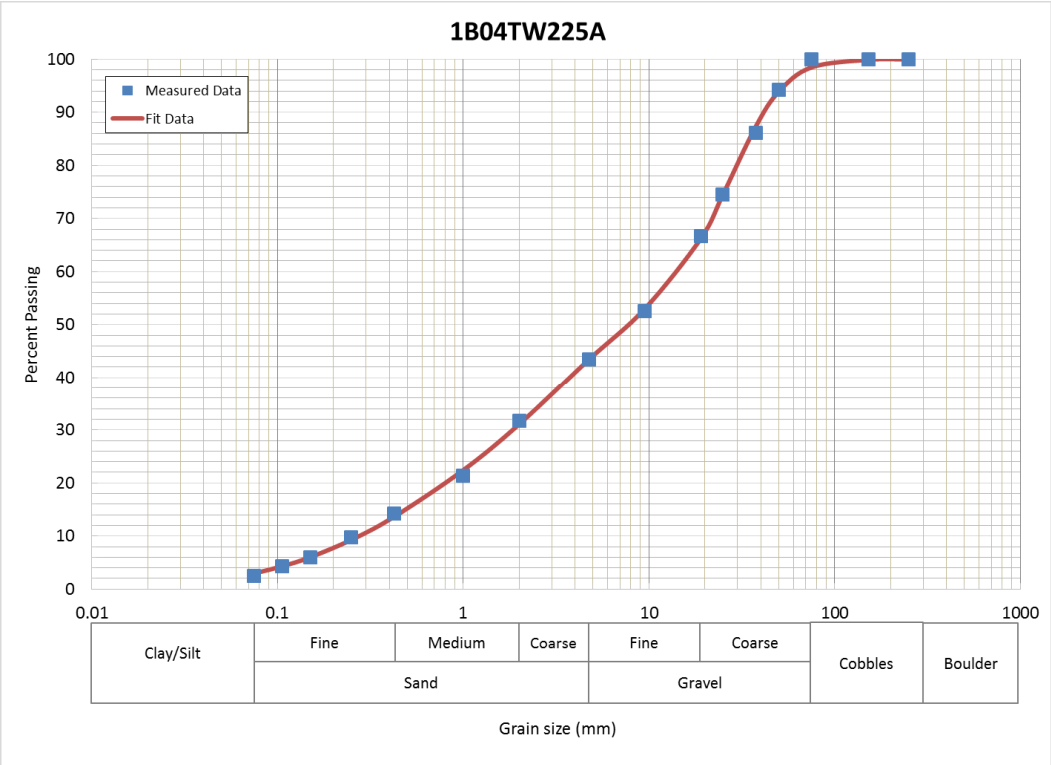
1B04TW225A
Measured Data
Fit Data
Percent Passing
100
90
80
70
60
50
40
30
20
10
0
0.01
0.1
1
10
100
1000
Clay/Silt
Fine
Medium
Coarse
Fine
Coarse
Cobbles
Boulder
Sand
Gravel
Grain size (mm)

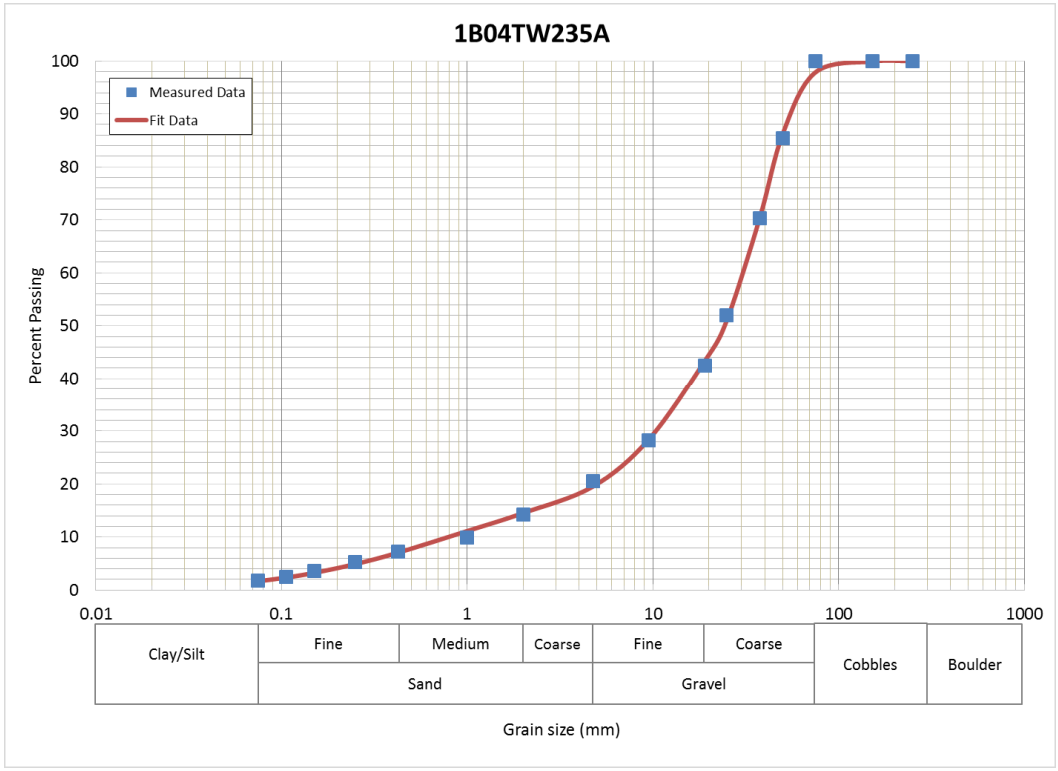
1B04TW235A
Measured Data
Fit Data
Percent Passing
100
90
80
70
60
50
40
30
20
10
0
0.01
0.1
1
10
100
1000
Clay/Silt
Fine
Medium
Coarse
Fine
Coarse
Cobbles
Boulder
Sand
Gravel
Grain size (mm)

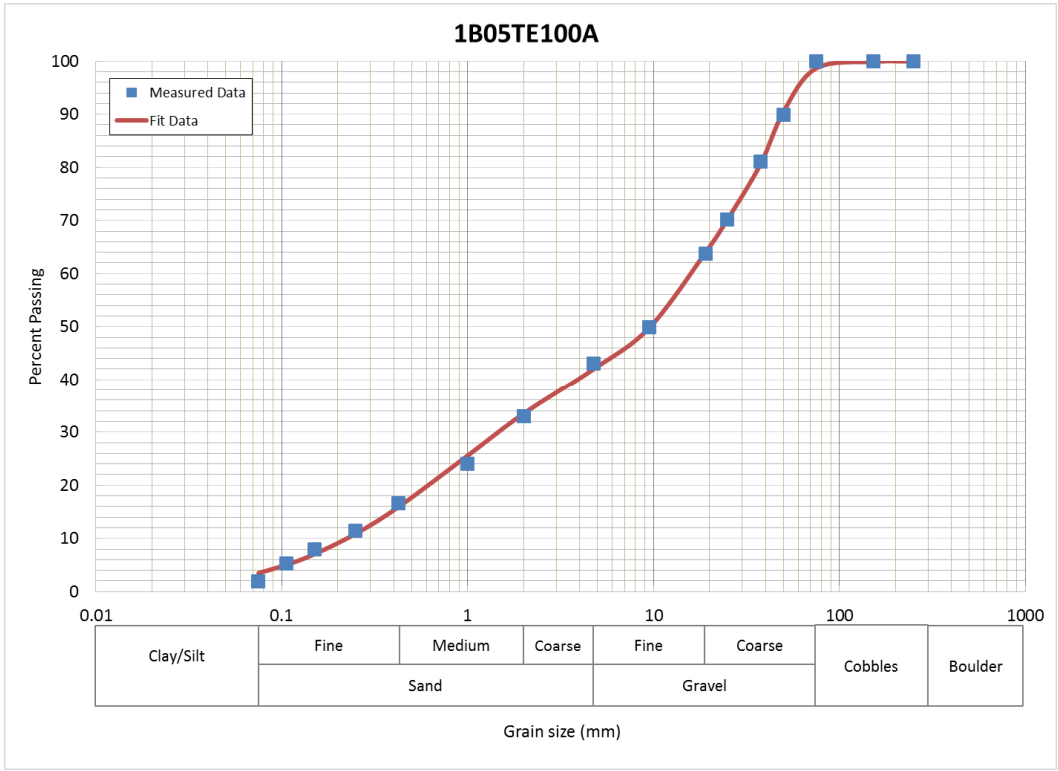
1B05TE100A
Measured Data
Fit Data
Percent Passing
100
90
80
70
60
50
40
30
20
10
0
0.01
0.1
1
10
100
1000
Clay/Silt
Fine
Medium
Coarse
Fine
Coarse
Cobbles
Boulder
Sand
Gravel
Grain size (mm)

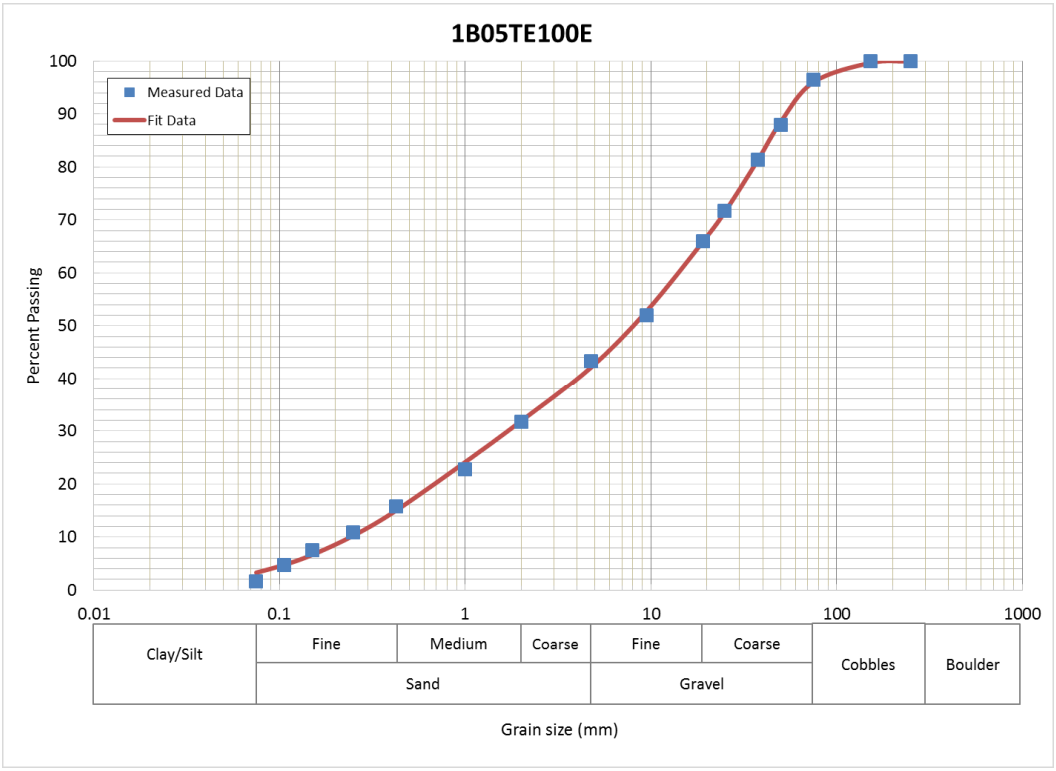
1B05TE100E
Measured Data
Fit Data
Percent Passing
100
90
80
70
60
50
40
30
20
10
0
0.01
0.1
1
10
100
1000
Clay/Silt
Fine
Medium
Coarse
Fine
Coarse
Cobbles
Boulder
Sand
Gravel
Grain size (mm)

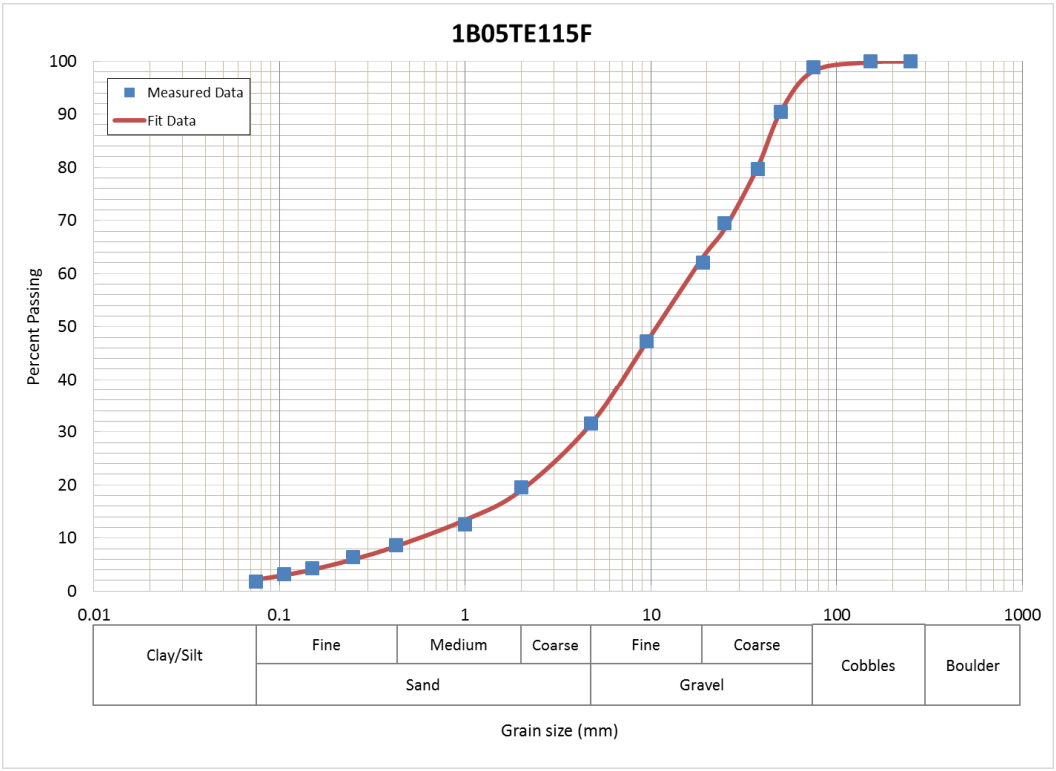
1B05TE115F
Measured Data
Fit Data
Percent Passing
100
90
80
70
60
50
40
30
20
10
0
0.01
0.1
1
10
100
1000
Clay/Silt
Fine
Medium
Coarse
Fine
Coarse
Cobbles
Boulder
Sand
Gravel
Grain size (mm)

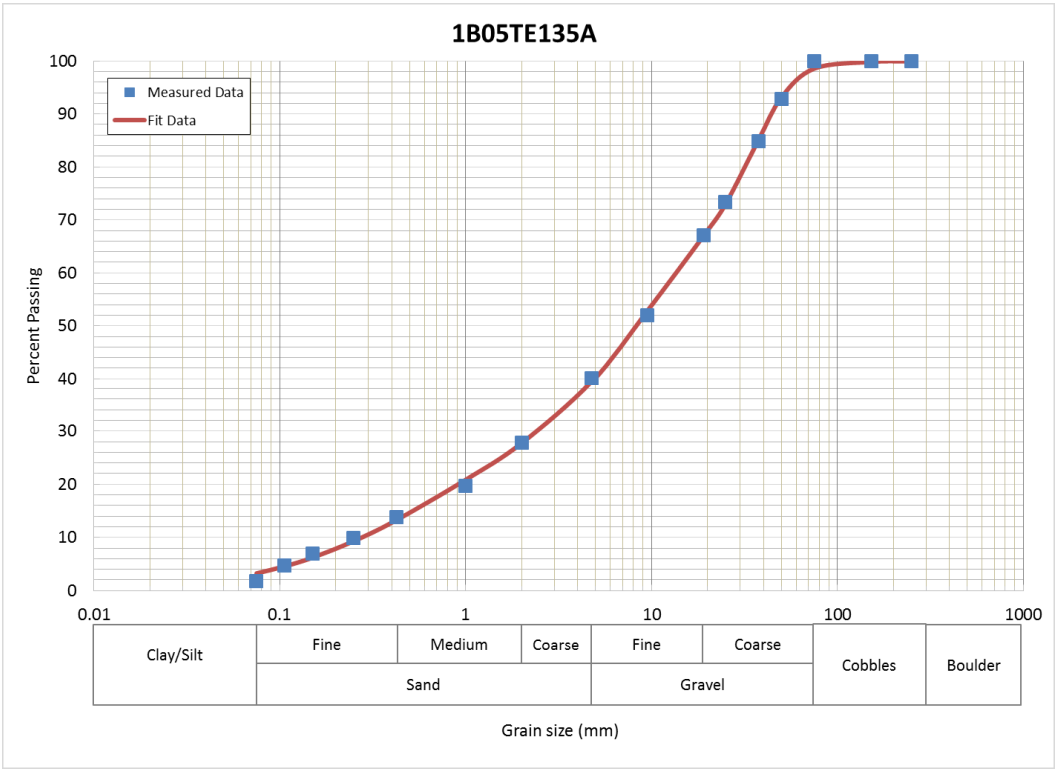
1B05TE135A
Measured Data
Fit Data
Percent Passing
100
90
80
70
60
50
40
30
20
10
0
0.01
0.1
1
10
100
1000
Clay/Silt
Fine
Medium
Coarse
Fine
Coarse
Cobbles
Boulder
Sand
Gravel
Grain size (mm)

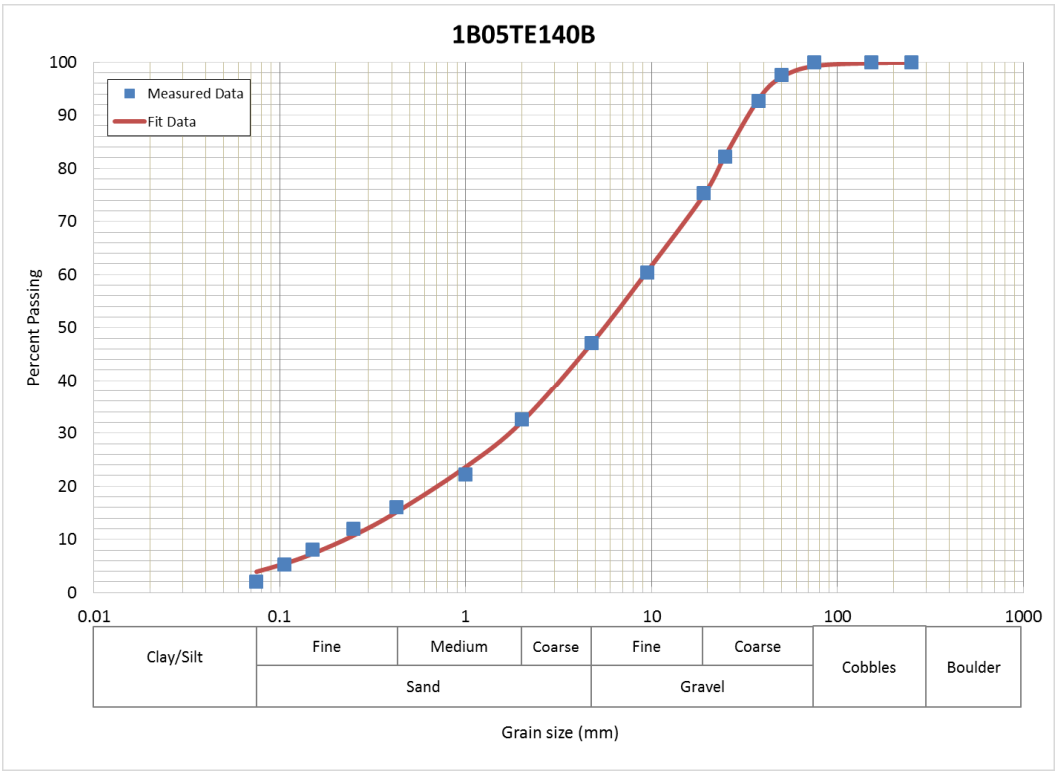
1B05TE140B
Measured Data
Fit Data
Percent Passing
100
90
80
70
60
50
40
30
20
10
0
0.01
0.1
1
10
100
1000
Clay/Silt
Fine
Medium
Coarse
Fine
Coarse
Cobbles
Boulder
Sand
Gravel
Grain size (mm)

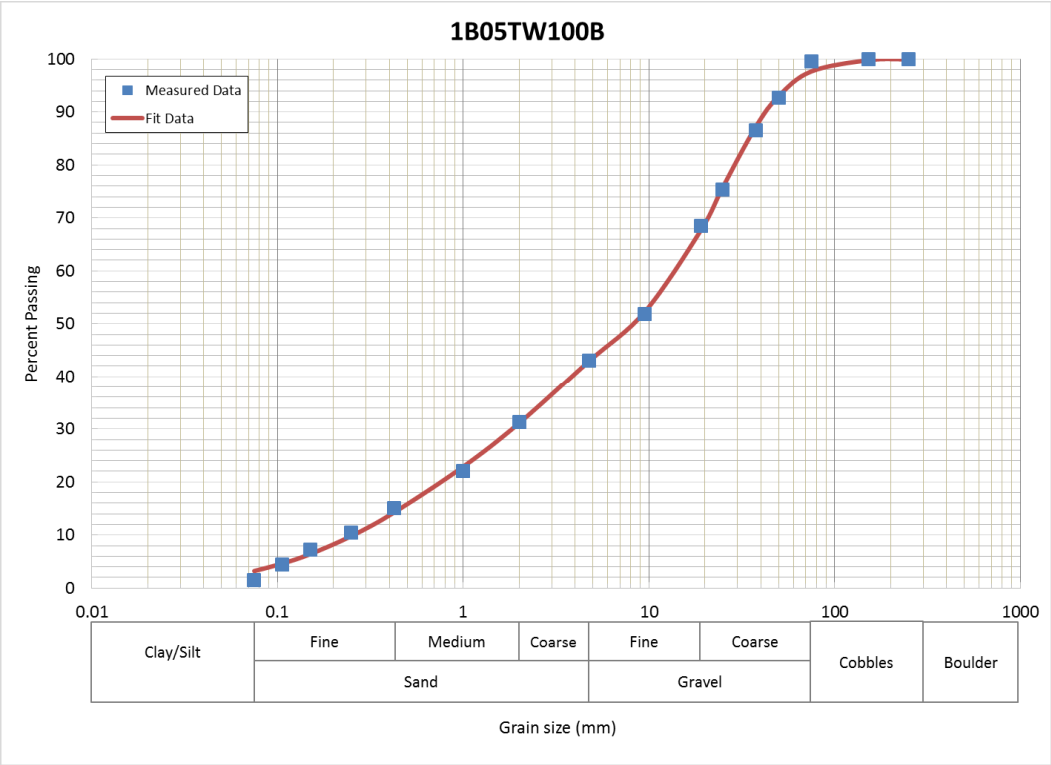
1B05TW100B
Measured Data
Fit Data
Percent Passing
100
90
80
70
60
50
40
30
20
10
0
0.01
0.1
1
10
100
1000
Clay/Silt
Fine
Medium
Coarse
Fine
Coarse
Cobbles
Boulder
Sand
Gravel
Grain size (mm)

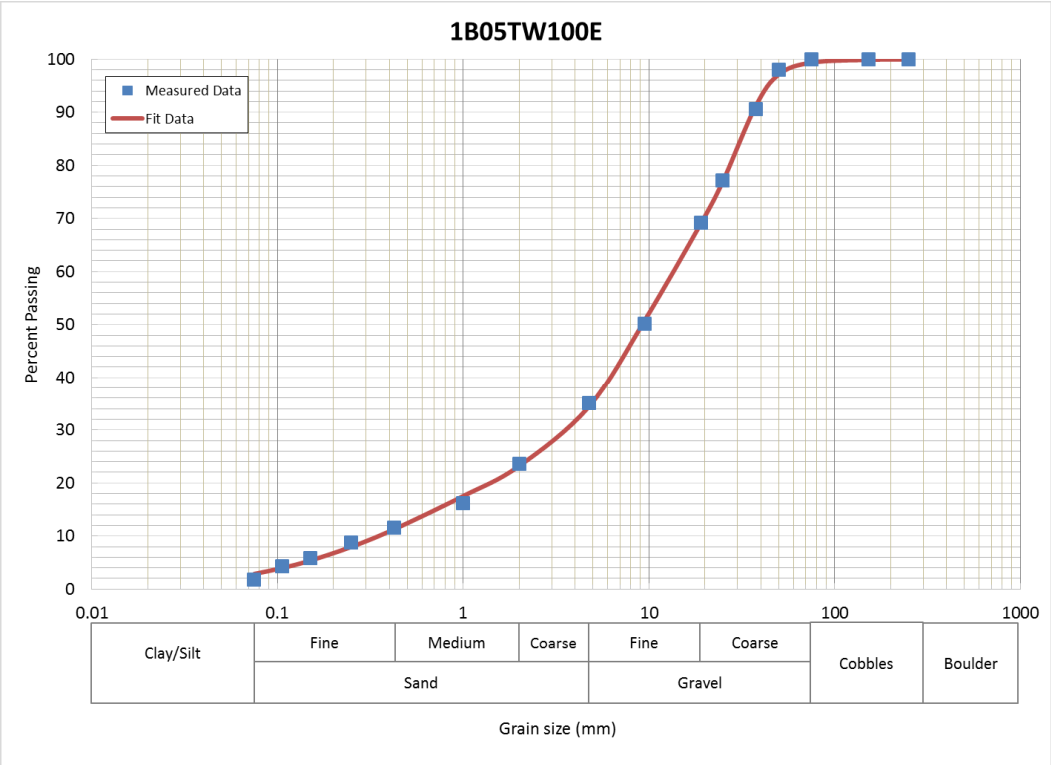
1B05TW100E
Measured Data
Fit Data
Percent Passing
100
90
80
70
60
50
40
30
20
10
0
0.01
0.1
1
10
100
1000
Clay/Silt
Fine
Medium
Coarse
Fine
Coarse
Cobbles
Boulder
Sand
Gravel
Grain size (mm)

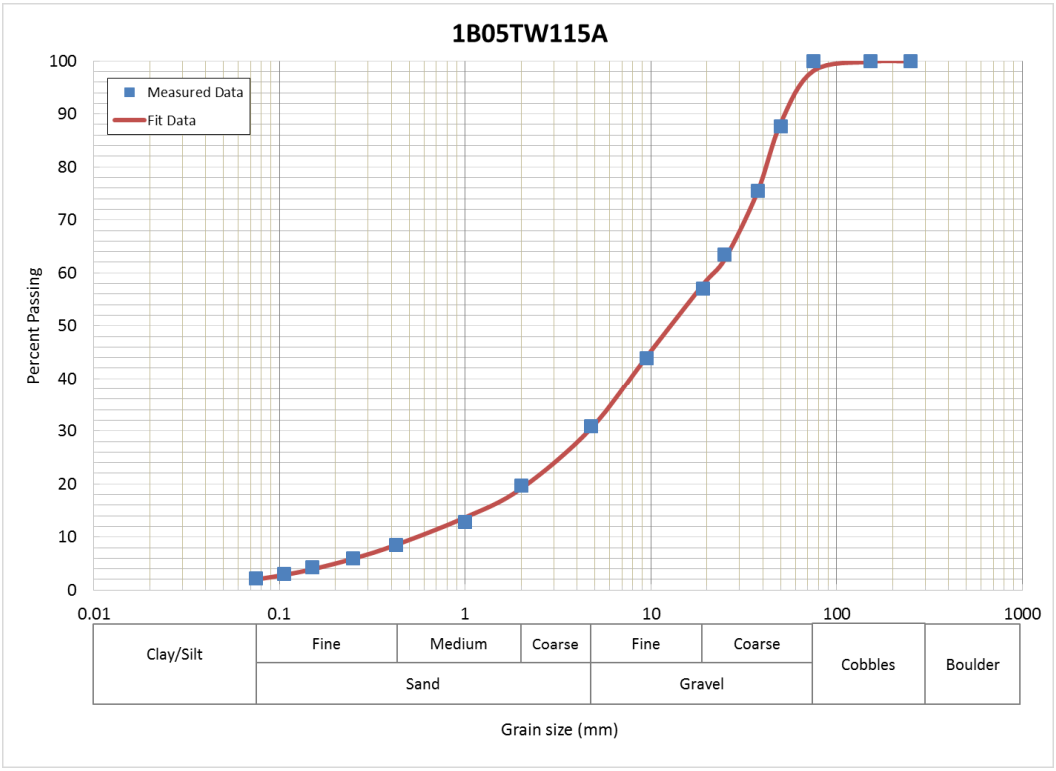
1B05TW115A
Measured Data
Fit Data
Percent Passing
100
90
80
70
60
50
40
30
20
10
0
0.01
0.1
1
10
100
1000
Clay/Silt
Fine
Medium
Coarse
Fine
Coarse
Cobbles
Boulder
Sand
Gravel
Grain size (mm)

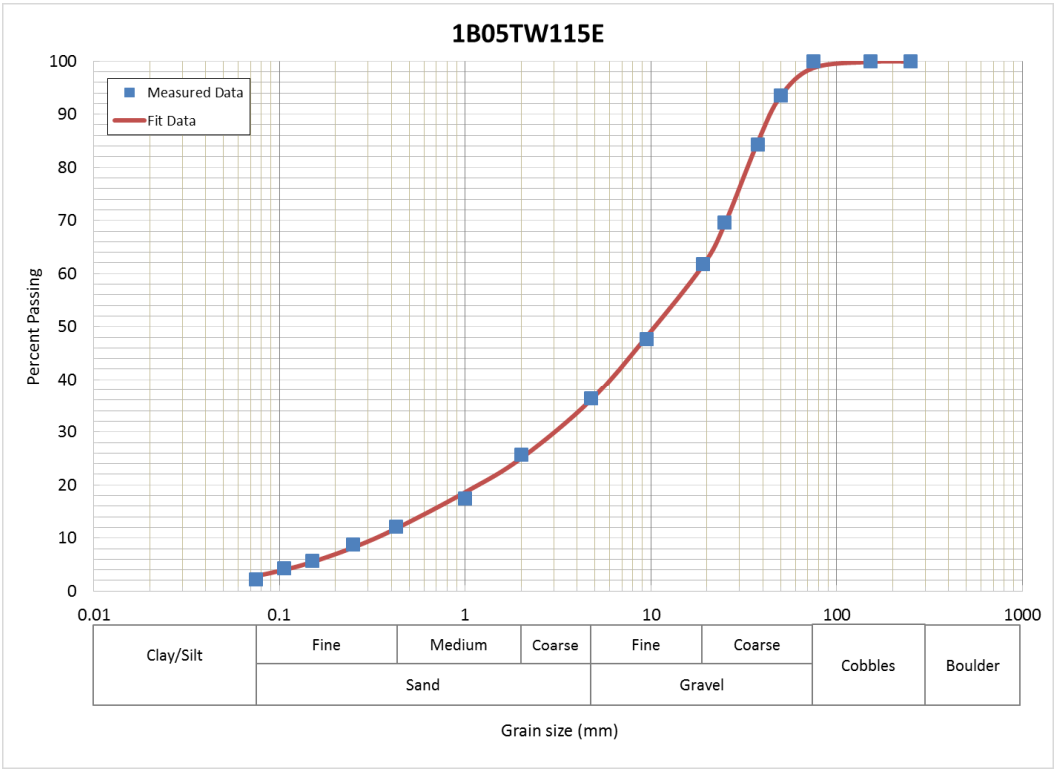
1B05TW115E
Measured Data
Fit Data
Percent Passing
100
90
80
70
60
50
40
30
20
10
0
0.01
0.1
1
10
100
1000
Clay/Silt
Fine
Medium
Coarse
Fine
Coarse
Cobbles
Boulder
Sand
Gravel
Grain size (mm)

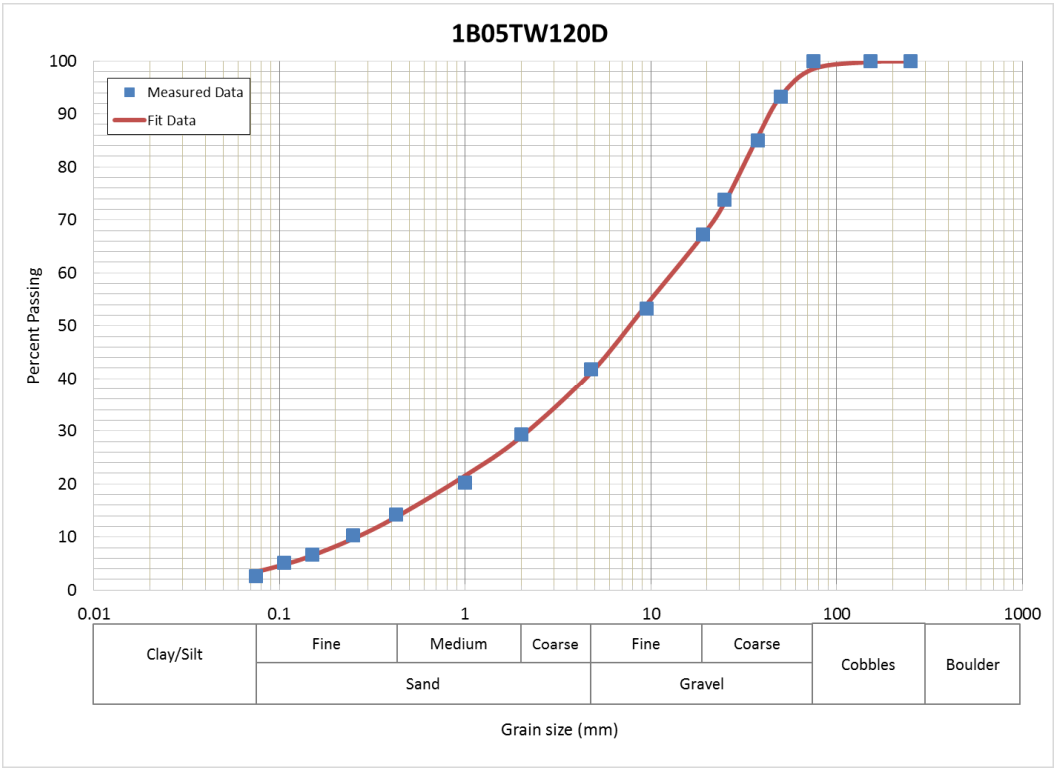
1B05TW120D
Measured Data
Fit Data
Percent Passing
100
90
80
70
60
50
40
30
20
10
0
0.01
0.1
1
10
100
1000
Clay/Silt
Fine
Medium
Coarse
Fine
Coarse
Cobbles
Boulder
Sand
Gravel
Grain size (mm)

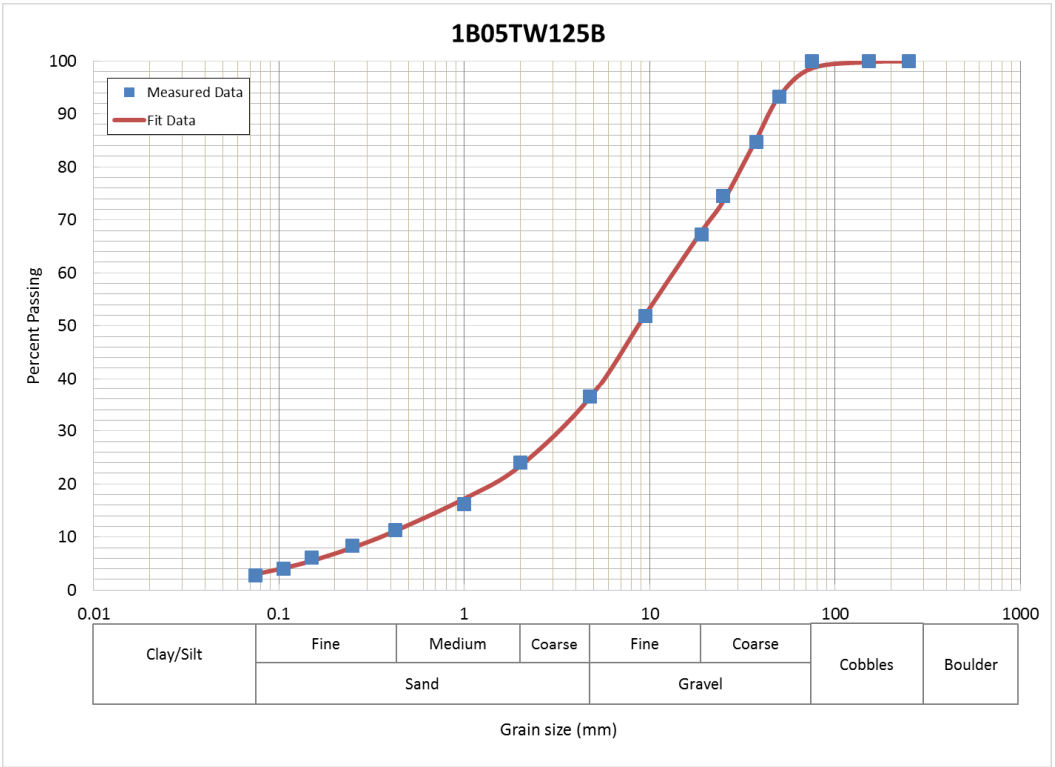
1B05TW125B
Measured Data
Fit Data
Percent Passing
100
90
80
70
60
50
40
30
20
10
0
0.01
0.1
1
10
100
1000
Clay/Silt
Fine
Medium
Coarse
Fine
Coarse
Cobbles
Boulder
Sand
Gravel
Grain size (mm)

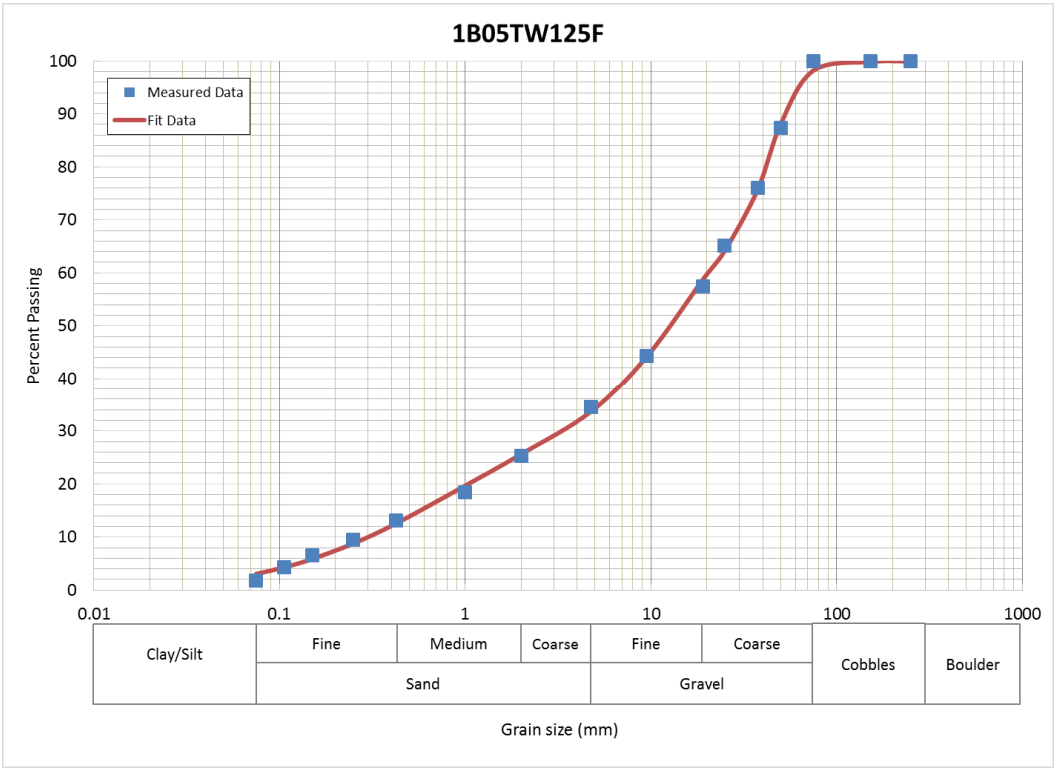
1B05TW125F
Measured Data
Fit Data
Percent Passing
100
90
80
70
60
50
40
30
20
10
0
0.01
0.1
1
10
100
1000
Clay/Silt
Fine
Medium
Coarse
Fine
Coarse
Cobbles
Boulder
Sand
Gravel
Grain size (mm)

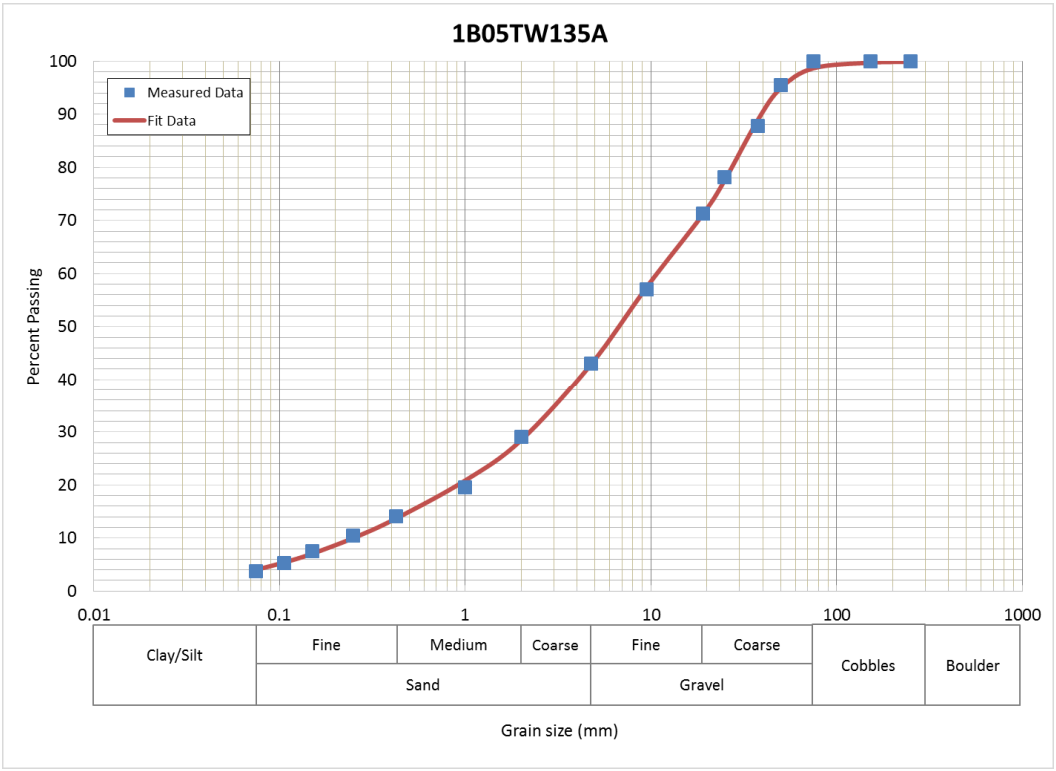
1B05TW135A
Measured Data
Fit Data
Percent Passing
100
90
80
70
60
50
40
30
20
10
0
0.01
0.1
1
10
100
1000
Clay/Silt
Fine
Medium
Coarse
Fine
Coarse
Cobbles
Boulder
Sand
Gravel
Grain size (mm)

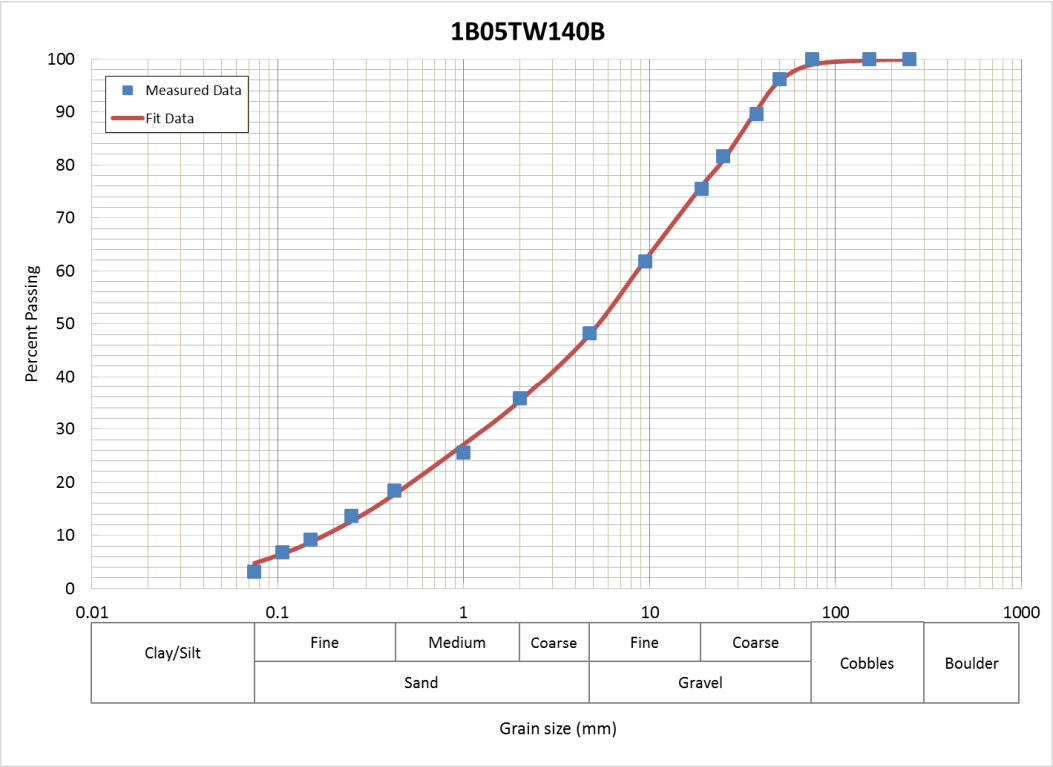
1B05TW140B
Measured Data
Fit Data
Percent Passing
100
90
80
70
60
50
40
30
20
10
0
0.01
0.1
1
10
100
1000
Clay/Silt
Fine
Medium
Coarse
Fine
Coarse
Cobbles
Boulder
Sand
Gravel
Grain size (mm)

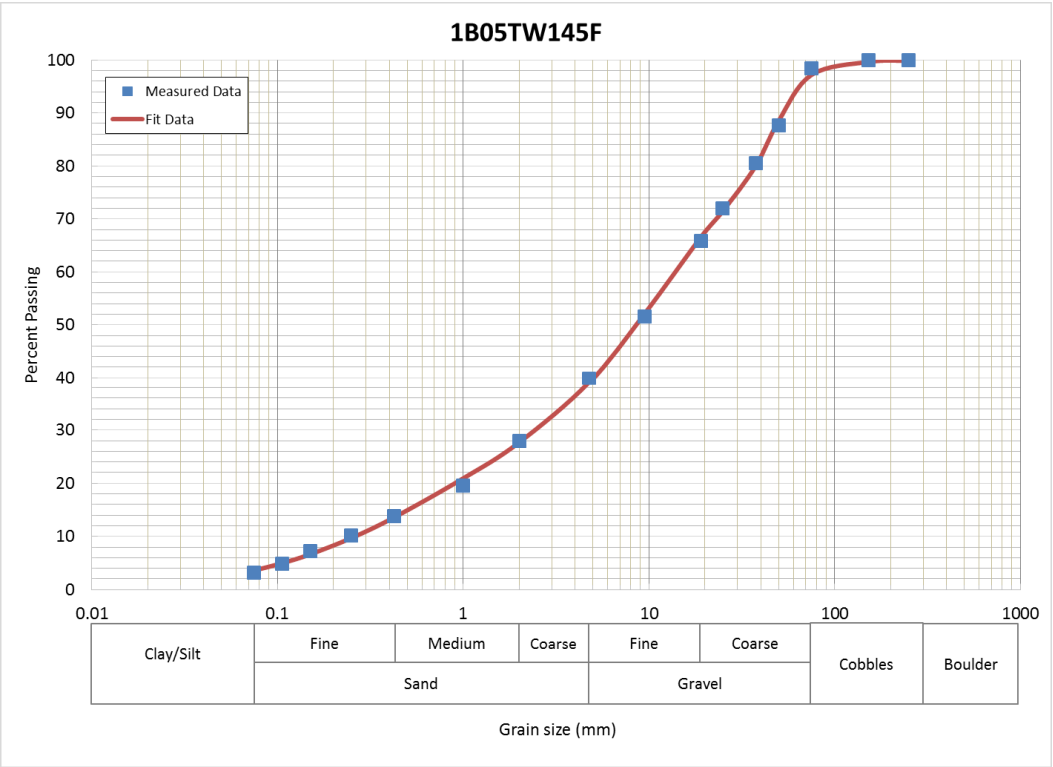
1B05TW145F
Measured Data
Fit Data
Percent Passing
100
90
80
70
60
50
40
30
20
10
0
0.01
0.1
1
10
100
1000
Clay/Silt
Fine
Medium
Coarse
Fine
Coarse
Cobbles
Boulder
Sand
Gravel
Grain size (mm)

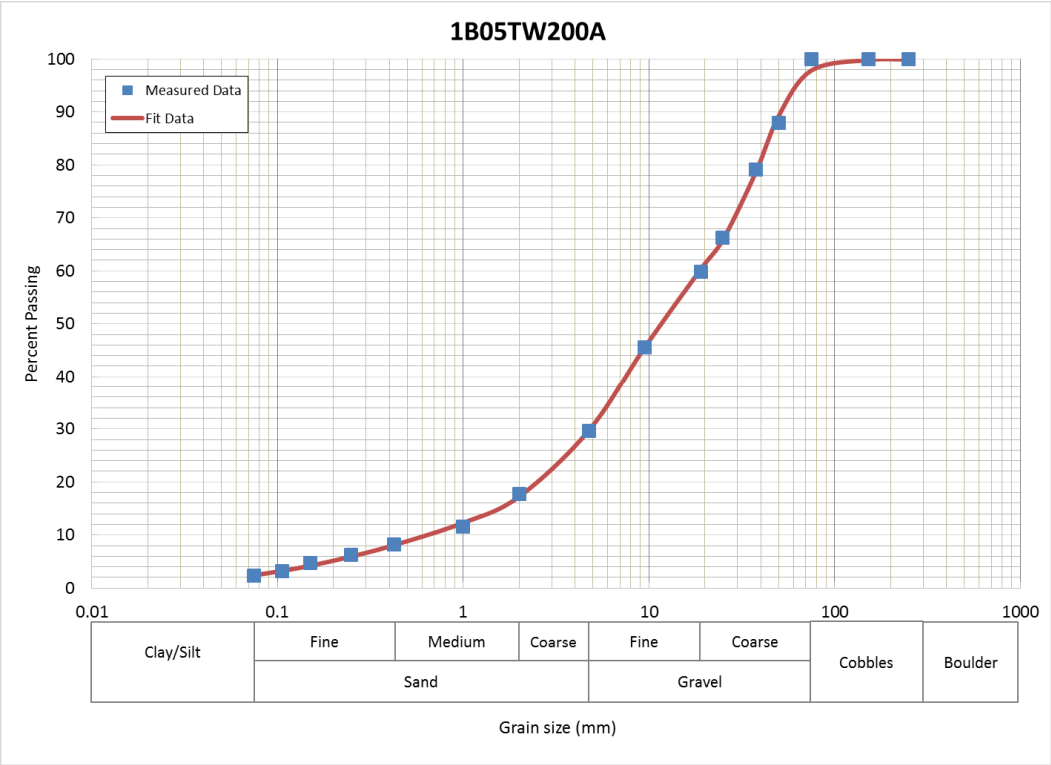
1B05TW200A
Measured Data
Fit Data
Percent Passing
100
90
80
70
60
50
40
30
20
10
0
0.01
0.1
1
10
100
1000
Clay/Silt
Fine
Medium
Coarse
Fine
Coarse
Cobbles
Boulder
Sand
Gravel
Grain size (mm)

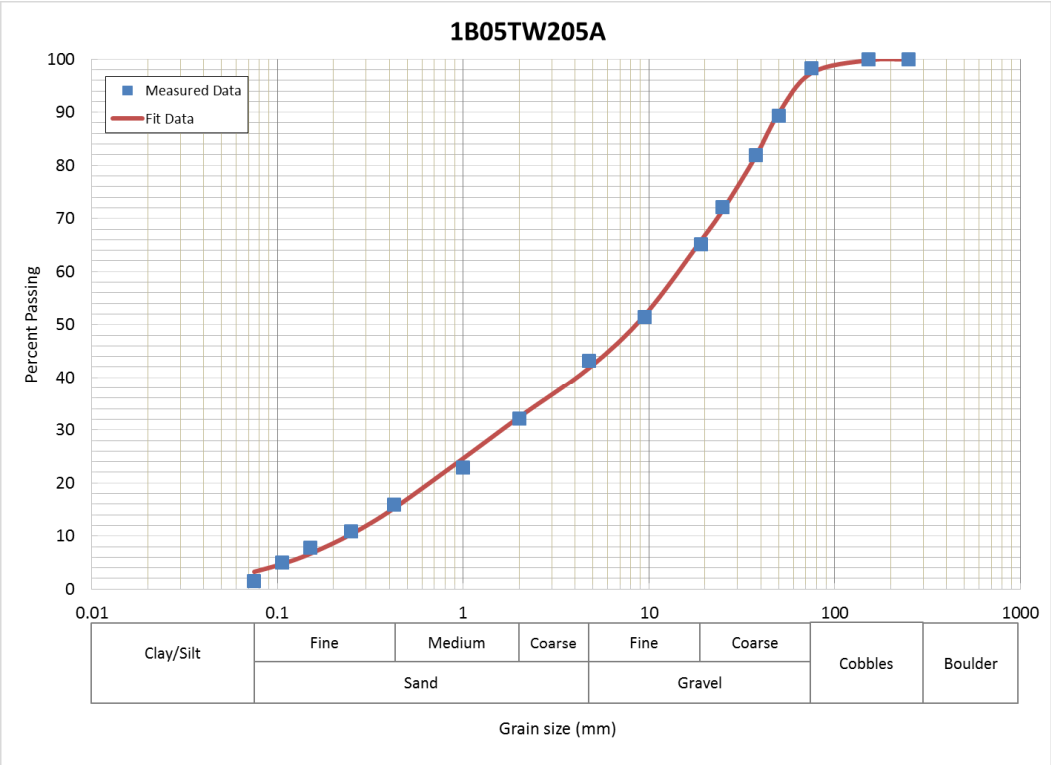
1B05TW205A
Measured Data
Fit Data
Percent Passing
100
90
80
70
60
50
40
30
20
10
0
0.01
0.1
1
10
100
1000
Clay/Silt
Fine
Medium
Coarse
Fine
Coarse
Cobbles
Boulder
Sand
Gravel
Grain size (mm)

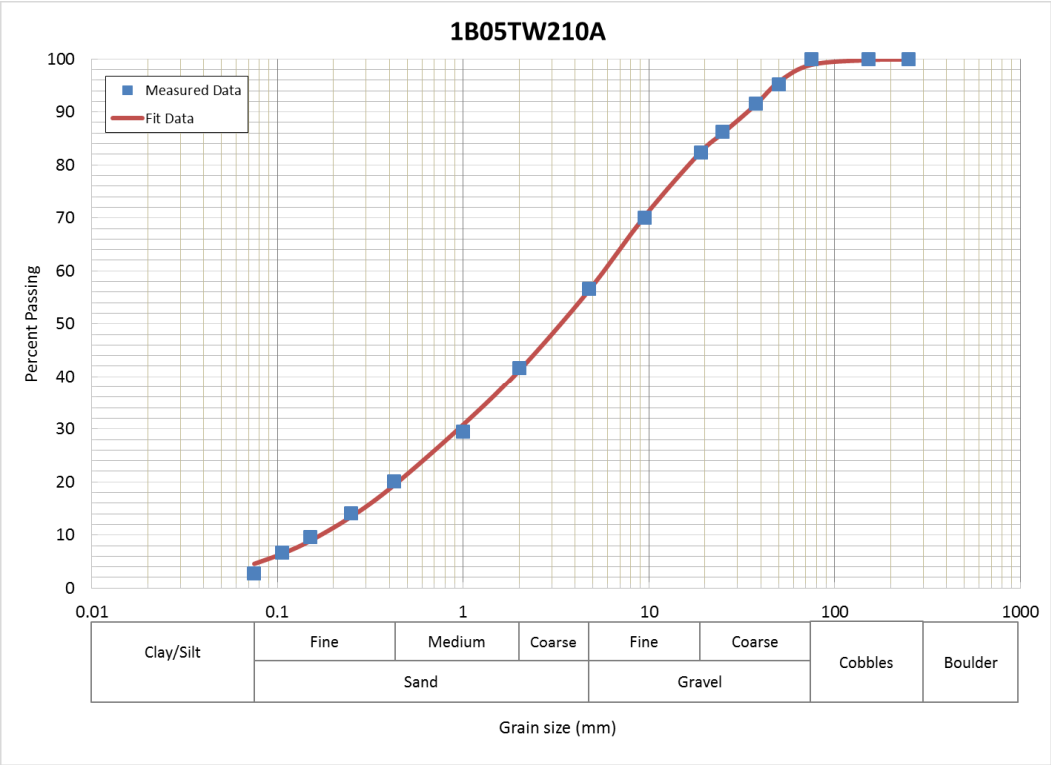
1B05TW210A
Measured Data
Fit Data
Percent Passing
100
90
80
70
60
50
40
30
20
10
0
0.01
0.1
1
10
100
1000
Clay/Silt
Fine
Medium
Coarse
Fine
Coarse
Cobbles
Boulder
Sand
Gravel
Grain size (mm)

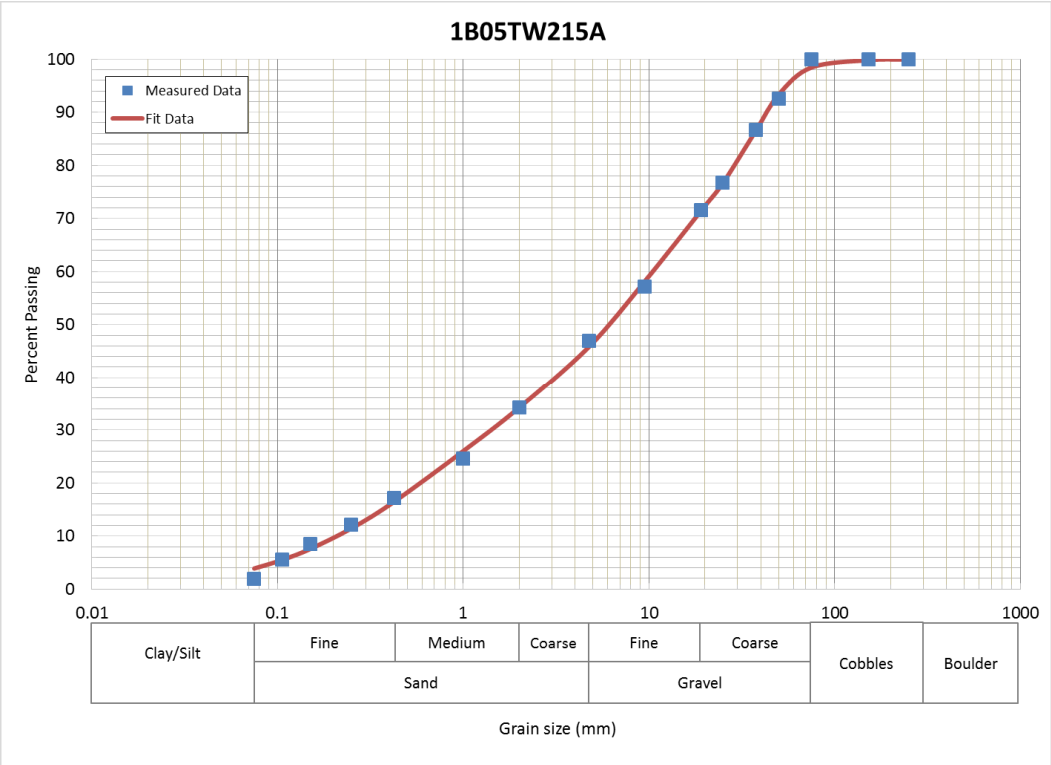
1B05TW215A
Measured Data
Fit Data
Percent Passing
100
90
80
70
60
50
40
30
20
10
0
0.01
0.1
1
10
100
1000
Clay/Silt
Fine
Medium
Coarse
Fine
Coarse
Cobbles
Boulder
Sand
Gravel
Grain size (mm)

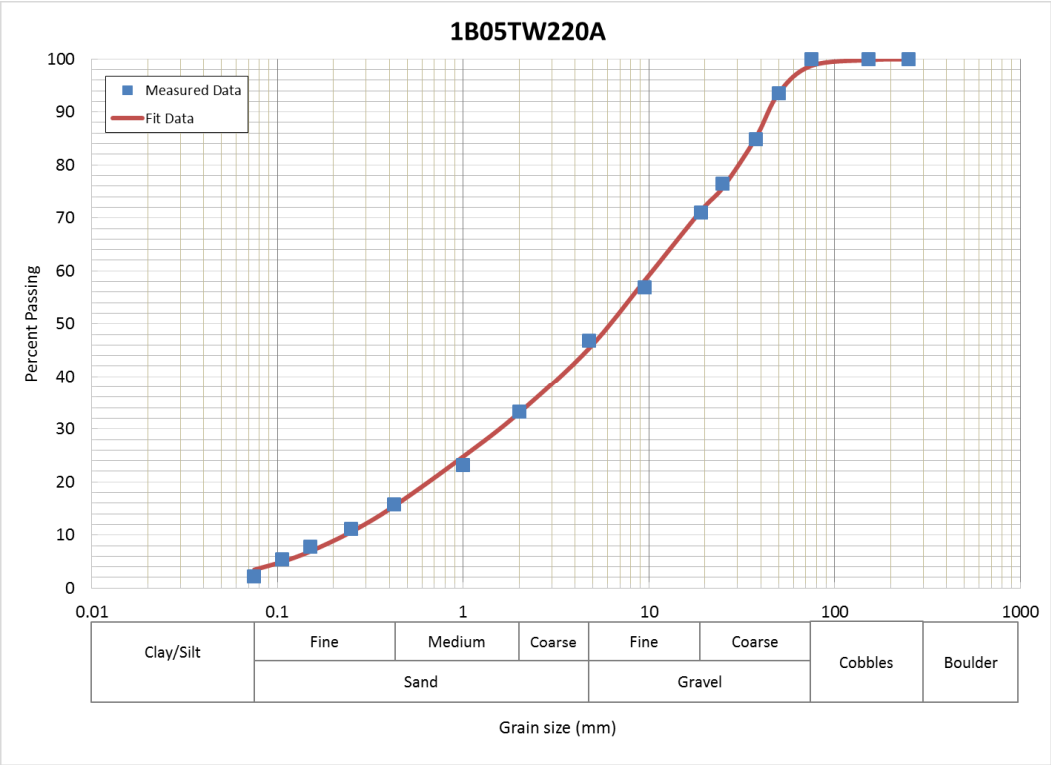
1B05TW220A
Measured Data
Fit Data
Percent Passing
100
90
80
70
60
50
40
30
20
10
0
0.01
0.1
1
10
100
1000
Clay/Silt
Fine
Medium
Coarse
Fine
Coarse
Cobbles
Boulder
Sand
Gravel
Grain size (mm)

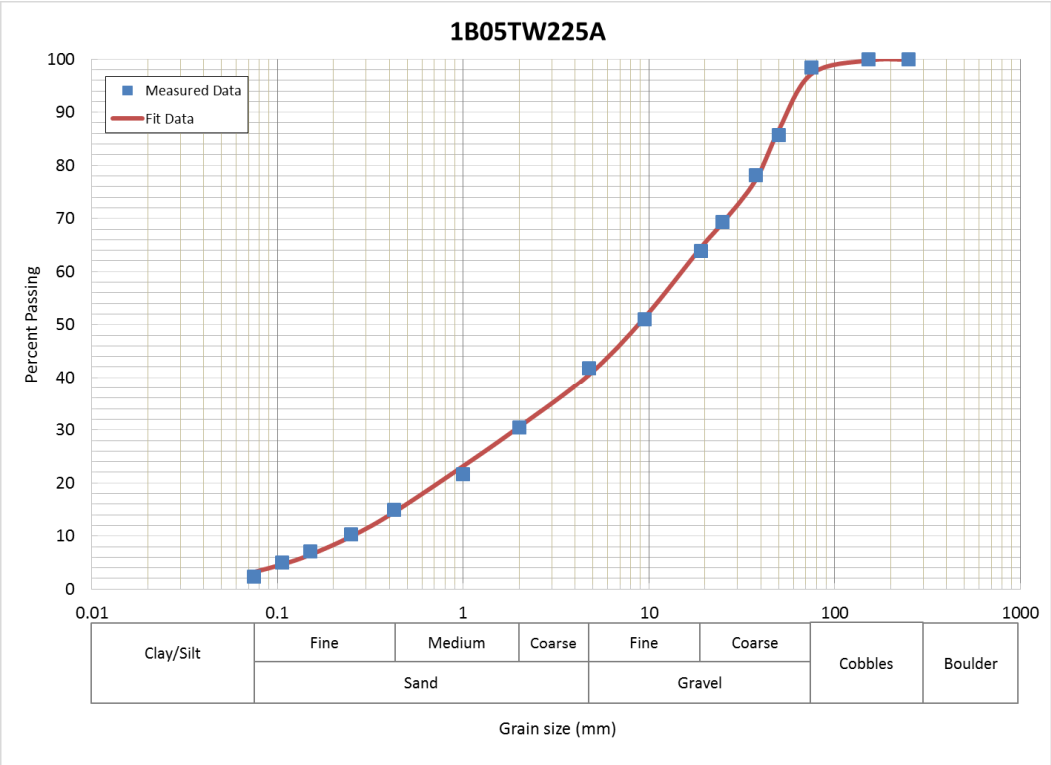
1B05TW225A
Measured Data
Fit Data
Percent Passing
100
90
80
70
60
50
40
30
20
10
0
0.01
0.1
1
10
100
1000
Clay/Silt
Fine
Medium
Coarse
Fine
Coarse
Cobbles
Boulder
Sand
Gravel
Grain size (mm)

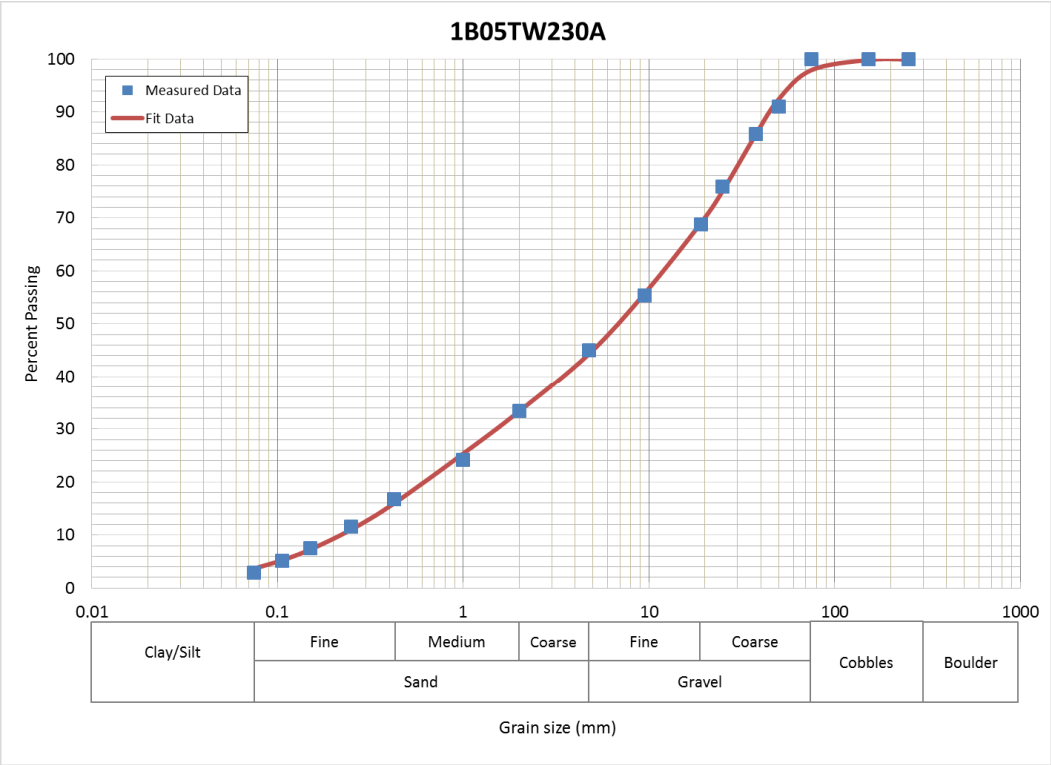
1B05TW230A
Measured Data
Fit Data
Percent Passing
100
90
80
70
60
50
40
30
20
10
0
0.01
0.1
1
10
100
1000
Clay/Silt
Fine
Medium
Coarse
Fine
Coarse
Sand
Gravel
Cobbles
Boulder
Grain size (mm)

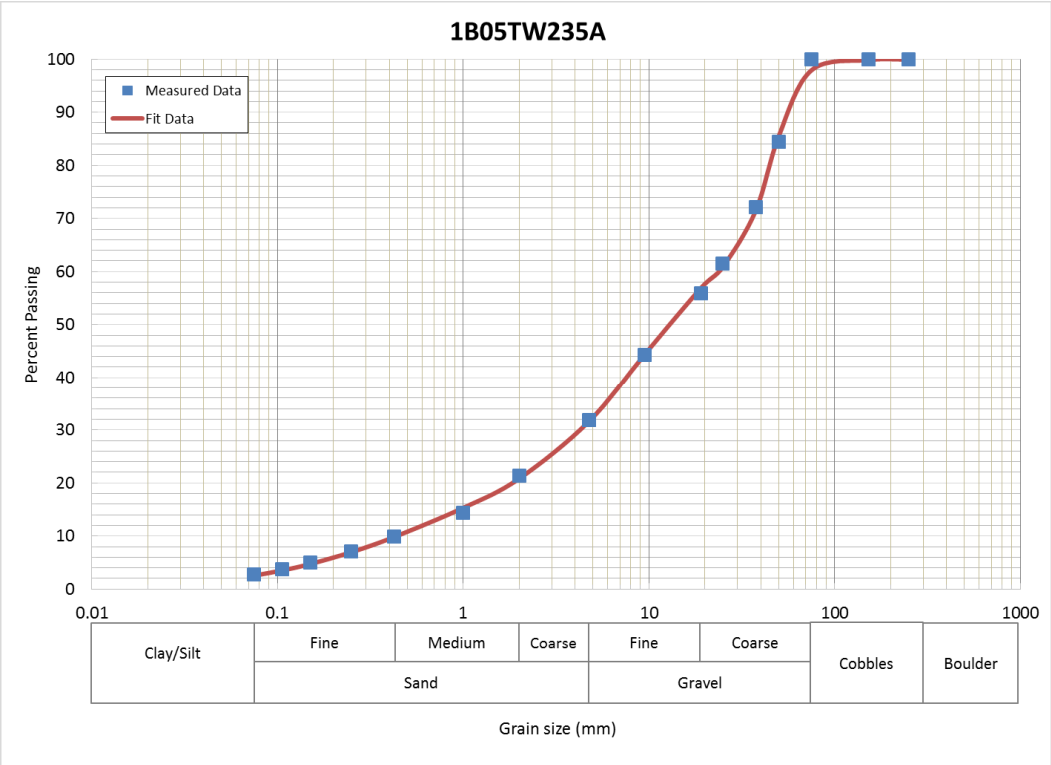
1B05TW235A
Measured Data
Fit Data
Percent Passing
100
90
80
70
60
50
40
30
20
10
0
0.01
0.1
1
10
100
1000
Clay/Silt
Fine
Medium
Coarse
Fine
Coarse
Sand
Gravel
Cobbles
Boulder
Grain size (mm)

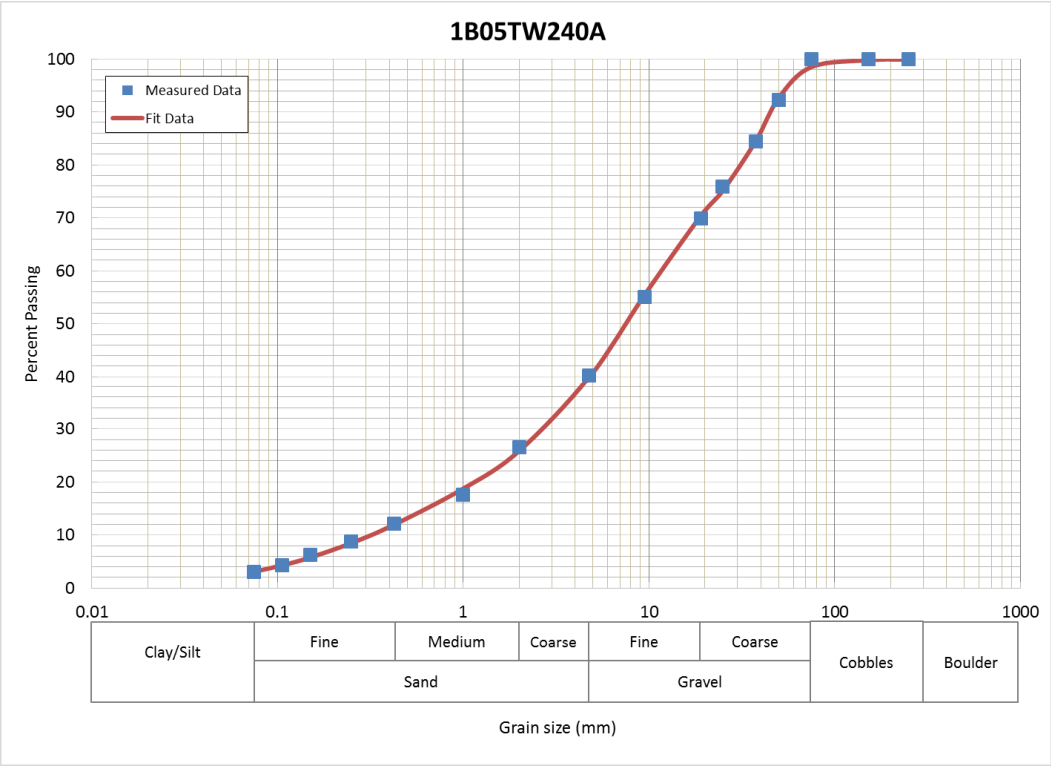
1B05TW240A
Measured Data
Fit Data
Percent Passing
100
90
80
70
60
50
40
30
20
10
0
0.01
0.1
1
10
100
1000
Clay/Silt
Fine
Medium
Coarse
Fine
Coarse
Cobbles
Boulder
Sand
Gravel
Grain size (mm)